Thèse de Doctorat

UNIVERSITE BRETAGNE LOIRE

UNIVERSITÉ DE NANTES

Sikandar Ali CHANNA

Mémoire présenté en vue de l'obtention du
grade de Docteur de l'Université de Nantes
sous le sceau de l'Université Bretagne Loire

École doctorale : *SPIGA*

Discipline : *Science pour l'ingénieur*
Spécialité : Thermique et *Energétique*
Unité de recherche : *LTEN UMR CNRS 6607*

Soutenance prévue le 02/10/2017

Synthesis of Ti-based nanoparticles in continuous flow microreactors

JURY

Rapporteurs :	**Hasna LOUAHILA**	Professeur des universités	LUSAC, Université de Caen-Basse Normandie
	Florence RAZAN	Maître de conférences	SATIE, École Normale Supérieure de Rennes
Examinateurs :	**Graziella GOGLIO**	Professeur des universités	ICMB, Université de Bordeaux
	Hassan PEERHOSSAINI	Professeur des universités	Université Paris Diderot
	Mireille RICHARD-PLOUET	Chargée de recherche	CNRS, IMN - Nantes
	Bertrand GARNIER	Chargé de recherche	CNRS, LTEN - Nantes
Invité(s) :	**Ahmed OULD EL MOCTAR**	Maître de conférences	LTEN, Université de Nantes
	Hélène TERRISSE	Maître de conférences	IMN, Université de Nantes
Directeur de Thèse :	**Bertrand GARNIER**	Chargé de recherche	CNRS, LTEN - Nantes
Co-directeur de Thèse :	**Mireille RICHARD-PLOUET**	Chargée de recherche	CNRS, IMN - Nantes
	Ahmed OULD EL MOCTAR	Maître de conférences	LTEN, Université de Nantes

Acknowledgement

Table of contents :

Résumé 5 pages en français

«Synthèse en microréacteur de nanoparticules d'oxydes de titane »

Introduction

Dans le domaine de l'énergie d'origine photovoltaïque, un des grands challenges actuels concerne la conception et la mise au point de dispositif capable de produire efficacement de l'énergie mais aussi capable de la stocker. Une des pistes très prometteuses est la photobatterie, ce sont des systèmes photochimiques qui utilisent directement l'énergie solaire pour produire des réactions électrochimiques, les charges photogénéréesautorisant ainsi le stockage de l'énergie. Leur réversibilité permet de les extraire à la demande comme dans une batterie traditionnelle. Il existe très peu d'exemples de matériaux au sein desquels les deux fonctions peuvent avoir lieu.Les sols à base de clusters de Ti présentent une telle possibilité. Cependant, la nanostructuration des objets dispersés dans ces solsest fortement liée aux conditions expérimentales lors de sa synthèse et constitue un des point-clés dans l'obtention de matériaux performants du point de vue photochimique. Il s'agit de réactions acido-basiques qui nécessitent un contrôle précis du mode opératoire (température, temps, concentration des réactifs…). Cette nanostructuration est traditionnellement réalisée par des techniques «batch» en utilisant un bain de glace (0°C) en raison de l'exothermicité des réactions[1]. Une des alternatives testée dans ce travail est l'usage de microréacteur qui comporte un certain nombre d'avantages. En effet, les faibles dimensions des microcanaux (largeur et hauteur typiquement inférieures à 1mm) permettent de limiter les gradients de température dans les fluides et de contrôler plus facilement les conditions thermiques de la synthèse par exemple en contrôlant la température des parois. Par ailleurs le confinement des fluides au sein des microcanaux limite les phénomènes parasites rencontrés en atmosphère ambiante (hydrolyse au contact de l'air ambiant humide).

Les travaux qui sont présentés dans ce mémoire de thèse ont concerné essentiellement les trois aspects suivants :

- le suivi de la synthèse de nanoparticules par la mise en œuvre de microréacteurs pour examiner l'effet des conditions opératoires telles que le débit, la concentration des réactifs, le taux de dilution avec un solvant qui s'avérera nécessaire pour obtenir des écoulements stables, et par ailleurs,

- la mesure de l'enthalpie de réaction pour améliorer la connaissance de la synthèse de nanoparticules d'oxyde de titane,

- l'effet de l'usage d'un champ électrique pour intensifier le mélange de réactifs, l'ajout d'un procédé actif de mélange étant nécessaire en raison du caractère laminaire des écoulements en microfluidique.

Chapitre 1

Ce chapitre est dédié à l'étude bibliographique sur la production de nanoparticules notamment de l'oxyde de titane, il se termine par une revue des différents procédés de mélange de fluides.

Il existe plusieurs procédés de synthèse des nanoparticules:mécanique (mécanosynthèse…) ou physique (pyrolyse, évaporation/condensation d'atomes..) ou chimique (dépôt CVD, procédé sol-gel…). Le procédé sol-gel est en fort développement en raison de son faible coût, de sa faible consommation en énergie et car il permet une production de masse.C'est ce procédé qui a été utilisé lors de travaux précédents à l'IMN à Nantes pour la production de nanoparticules d'oxyde de titane. La technique « batch » c'est à

dire le maintien dans un bain de glace à 0°C de la solution réactive ne permet pas alors un bon contrôle de la réaction. C'est ce constat qui a motivé l'utilisation de microréacteurs. Un certain nombre de travaux relatifs à la réalisation de nanoparticules d'oxydes de titane à l'aide de microréacteur, tout en évitant la formation d'agglomérats ont été répertoriés dans la littérature depuis 2002. Ainsi, Wang [2] a produit des nanoparticules d'oxyde de titane de taille inférieure à 10 nm à l'interface entre deux réactifs insolubles. Par ailleurs, Takagi[3]a inséré un capillaire au sein d'un tube permettant la réalisation de nanoparticules de TiO_2 de taille 100 à 140 nm en utilisant un précurseur à faible viscosité, contrairement à celui utilisé dans notre étude.

En ce qui concerne l'intensification du mélange, il existe dans la littérature de nombreux procédés de type passif (par l'utilisation de géométries particulières) ou actif (débits modulés, procédé acoustique, électrique…), ces derniers étant en général plus efficace lorsqu'ils sont applicables [5,6]

Chapitre 2

Dans notre travail, des microréacteurs ont été utilisés pour effectuer la synthèse de sol à base d'oxyde de titane. Ce solest obtenu par l'hydrolyse de $TiOCl_2 \bullet 1.4\ HCl \bullet 7H_2O$en présence de N, N-dimethylformamide (($CH_3)_2NCOH$, noté DMF).En fonction du temps de vieillissement, cette hydrolyse conduit à l'obtention de sols constitués de nanoparticules d'oxyde de titane dispersées dans le solvant [4].

La synthèse de sols pour la production de nanoparticules à base d'oxydede titane étant fortement exothermique, l'effet des conditions opératoires a été étudié en relevant la distribution de températureà l'aide d'une caméra infrarouge, sur un couvre lame de microscope constituant la 4ème paroi du microcanal du microréacteur. Ainsi notre dispositif expérimental comporte un microcanal en Y de section carrée $0,6x0,6\ mm^2$ et de longueur 32 mm recouvert d'un couvre lame de microscope en verre d'épaisseur 100μm, deux pousses seringues Nemesys et une caméra infrarouge Flir modèle Titanium. Le microcanal a été réalisé dans du polytetrafluorethylene (PTFE ou Téflon) en raison de la forte acidité de l'un des réactifs utilisés ($TiOCl_2 \bullet 1.4\ HCl \bullet 7H_2O$).

Deux effets ont été particulièrement analysés: celui du débit des réactifs ainsi que celui du taux de diluant dans le précurseur.

Chapitre 3

Les essais réalisés nous ont permis de réaliser les principales observationssuivantes :

Avec du $TiOCl_2$ pur et des débits entre 0.1 mLh^{-1} et 15 mL h^{-1} pour $TiOCl_2$ et entre 0.1 mL h^{-1} et 15 mL h^{-1} pour le DMF en maintenant un ratio de 2.4 entre eux correspondant à un rapport stoïchiométrique DMF/Ti égal à 6.4, les écoulements dans le microcanal principal sont apparus systématiquement instables et oscillatoires. Une simulation numérique des écoulements à l'aide de Fluent a montré que ces instabilités n'étaient pas dues à la grande différence de viscosité entre les deux réactifs 73 mPa.s pour $TiOCl_2$ et 0.92 mPa.s pour le DMF), ceci semblant plutôt lié à la faible solubilité du $TiOCl_2$ dans le DMF.

Le changement de ratio de débit (entre 2.3 et 2.5) ou de la section des microcanaux à l'entrée (de 0,6 x 0,6 mm^2 à 0,9 x 0,9 mm^2) ne nous a pas permisde stabiliser l'écoulement dans le canal principal.

Les tests avec des solvants comme l'eau, 1-propanol, 1,2-propanediol, 1-octanol supplémentaire avec une fraction volumique de 17 % dans le précurseur $TiOCl_2$ n'ont pas permis de stabiliser l'écoulement. De plus l'utilisation de tels solvants soulèverait un problème de manque de connaissance concernant les réactions entre ce solvant et l'oxychlorure de titane $TiOCl_2$; en effet le travail précédent sur des réacteurs batch a porté essentiellement sur l'étude des réactions entre DMF et $TiOCl_2$[1,4].

Une alternative à l'usage de solvants rendant plus complexe l'analyse a consisté à prédiluer le précurseur $TiOCl_2$ avec du DMF ainsi un ratio volumique de prédilution avec le DMF entre 0 et 20 % a été utilisé, les réactifs étant injectés dans le microréacteur 10 à 15 min après la dilution réalisée en effectuant le mélange DMF/$TiOCl_2$à température ambiante pendant 30 min. En microréacteur, le ratio de pré-dilution ci-dessus (16.7%vol. DMF) s'est avéré induire une stabilisation des écoulements, ce taux de dilution a été retenu pour les travaux dans ce qui suit. On a pu montrér expérimentalement que la distribution de température obtenue témoignait de la stabilité des écoulements et ce pour des débits pas trop élevés (débit $TiOCl_2$ prédilués inférieurs à 5mL.h^{-1}). On a également constaté que dans ces essais, le microcanal n'était pas assez long pour réaliser complètement la synthèse ainsi seulement une partie du profil de température a pu être relevée, il a cependant permis d'observer la stabilité ou non stabilité des écoulements. Pour des mesures quantitatives, des microcanaux beaucoup plus longs seront utilisés.

Les résultats montrent que des débits inférieurs (moins de 7mL h^{-1}) devraient être choisis pour obtenir un mélange suffisant dans le microcanal.

Au cours des expériences,nous avons remarqué que la température maximale a été observée à la sortie du microcanal, ce qui indique que la synthèse n'a pas été complètement réalisée dans le microcanal. En effet, comme très souvent dans les dispositifs microfluidiques, les écoulements sont laminaires. Dans ce cas, le mélange est essentiellement assuré par la diffusion moléculaire qui est très lente. Ainsi, pour réaliser la synthèse de nanoparticules, un très long microcanal est a priori nécessaire, une alternative est l'utilisation d'un procédé d'intensification du mélange.

Suite à ce constat, des microcanaux beaucoup plus longs (294 et 234 mm de long) ont été utilisés. Sans champ électrique, l'écoulement avec les deux réactifs $TiOCl_2$+ 16,7% de DMF et DMF était moins stable que ce qui avait été observé avec un microcanal plus court (32 mm).

Par ailleurs, afin de mieux connaitre la réaction de synthèse des nanoparticules, des mesures quantitatives d'enthalpie de réaction ont été réalisées. Le principe des mesures d'enthalpie de réaction a été précédemment développée par Hany[7] : un microréacteur a été moulé dans du PDMS (poly-dimethylsiloxane), le microcanal principal ayant une longueur de 216 mm pour permettre la caractérisation de la synthèse du sol jusqu'à son achèvement. Le microréacteur PDMS recouvert d'un bloc de Plexiglas a été fermé avec une plaque de silicium et en contact successivement avec une plaque d'aluminium et une cellule Peltier de dimension 30 x 30mm.

Lorsque le microréacteur est alimenté en réactifs, un régime thermique permanent s'établit progressivement et le flux de chaleur ϕdégagé par la réaction de synthèse est obtenu par la mesure de la tension de sortie de la cellule Peltier, celle-ci étant préalablement étalonnée à l'aide d'un film chauffant flexible (Minco).

Ainsi, les flux de chaleur mesurés $\phi(W)$ augmentent avec le débit d'entrée puisque plus de réactifs sont impliqués. Connaissant le débit Q (m^3 s^{-1}) et la concentration de réactifs C (mol m^{-3}), on peut déduire l'enthalpie de réactionΔH (J mol^{-1}) en utilisant la relation :

$$\Delta H = \phi/(Q\ C) \qquad\qquad (1)$$

Il faut noter que la relation précédente est valable pour une conversion de 100 %, ceci est obtenu dans nos essais car le microcanal principal est suffisamment long (216 mm) pour réaliser cette condition.

L'enthalpie de réaction diminue lorsque le taux de DMF utilisé pour la pré-dilution du précurseur augmente. En effet avec du TiOCl$_2$ pur, la valeur de ΔHest de 12.08 kJ mol^{-1} et avec du TiOCl$_2$ pré-dilué avec 15% vol. de DMF, il diminue à 7 kJ mol^{-1}.

Chapitre 4

Les méthodes permettant l'amélioration du mélange sont nombreuses et peuvent être de nature passive ou active [5], [6]. Actuellement, on sait que l'interface entre deux fluides de propriétés diélectriques différentes peut être déstabilisée en appliquant un champ électrique [6]. Ceci entraîne un flux secondaire qui améliore le mélange entre les deux liquides. Comme les deux réactifs utilisés dans notre travail (TiOCl$_2$et DMF)ont des propriétés diélectriques très différentes, des tests ont été conduits avec un tel procédé actif de mélange, c'est à dire basé sur l'utilisation d'un champ électrique.

Un microréacteur dédié à l'étude de l'intensification du mélange a été réalisé. Le microcanal principal (294 mm) est plus long que le précédentpour permettre la réalisation complète de la réaction avant que les réactifs ne sortent du microréacteur.

La première partie du canal principal a été équipée d'une paire d'électrodes enplatine. La distribution de température a été relevée par caméra infrarouge dans les cas avec et sans champ électrique et pour différents débits de réactifs.

À l'aide d'un champ électrique à courant continu, les débits sont devenus stables pour une tension de 1,5 à 4 V, mais on a remarqué l'existence de la formation de gaz provoquée par l'électrolyse de l'eau et la formation de Ti^{3+}. Ces problèmes qui nuisent à la production de nanoparticules de TiO$_2$ ont été surmontés en utilisant un champ électrique à courant alternatif. Les fréquences de 0,1 et 0,5 MHz avec une tension de 5 V ont été définies comme étant trop faibles.

En optimisant les conditions expérimentales, le choix s'est porté sur une tension électrique de 7 V AC avec une fréquence de 1 MHz. Une telle fréquence élevée s'est avérée nécessaire pour éviter l'électrolyse de l'eau et la formation de Ti^{3+} tout en fournissant suffisamment de mélange. Ces résultats ont été obtenus pour duTiOCl$_2$ dilué avec 16,7% de DMF. Pour le TiOCl$_2$ pur, les conditions de fonctionnement c'est-à-dire une tension alternative de 7 V et une fréquence de 1 MHz ont également permis l'amélioration du mélange sans l'électrolyse de l'eau et la formation de Ti3+. Pour le TiOCl$_2$ pré-dilué, le débit de ce précurseur ne doit pas dépasser 3 mL h^{-1}; tandis que pour le TiOCl$_2$ pur, le débit ne doit pas dépasser 2mL h^{-1}. En effet, pour des débits plus élevés, l'écoulement devient instable et la réaction n'est généralement pas complètement réalisée avant la sortie des réactifs du microcanal principal.

Il apparaît que le mélange électrique actif améliore la cinétique de réaction pour de faibles débits. En fait, deux effets combinés peuvent affecter la réaction : (i) le mélange induit par le champ électrique et (ii) la dissipation de chaleur par effet Joule. En effet, en plus de la dissipation de chaleur due à l'exothermicité de la réaction de synthèse, s'ajoute une dissipation par effet Joule due au champ électrique appliqué au liquide agissant comme une résistance électrique. Une évaluation de cet effet Joule a mené à une puissance de l'ordre de 1372 mW qui peut être comparée à l'enthalpie de réaction mesurée qui a impliqué des flux de chaleur de l'ordre de 350 mW. L'effet de la présence du champ électrique est ainsi quatre fois : en plus de l'intensification du mélange, un surcroît de chaleur augmente la cinétique de synthèse de nanoparticules.

Chapitre 5

Des mesures additionnelles sur plusieurs échantillons de sols collectés à la sortie du microréacteur ont été réalisées par la technique de diffusion dynamique de la lumière -DLS-(Malvern Zetasizer NanoZS) afin d'analyser la distribution de taille des nanoparticules synthétisées en fonction des conditions operatoires pertinentes dans le microréacteur.

Par ailleurs, en raison des évolutions constatées, la distribution de taille des nanoparticules a été suivie pendant plusieurs jours.

Les mesures avec la technique DLS(dispersion dynamique de la lumière), pour le microcanal en Y de 32 mm(i.e. sans champ électrique)et pour des débits de 5 et 12mL h^{-1}ont montré une distribution de taille étroite de nanoparticules (5 nm - 40 nm) dans des échantillons pré-dilués avec 16.7% vol. La taille de nanoparticules indiquée est cellecorrespondant au pic de la distribution volumique en considérant des lois log-normales. Après 77 jours, la distribution d'intensité révèle qu'en plus des petites nanoparticules (15 nm), de plus grandes particules (52nm) sont détectées représentant moins de 1% dans la distribution volumique.

Juste en changeant la longueur du microcanal (234 mm), des résultats très similaires ont été obtenus avec une distribution de taille étroite de nanoparticules (3 nm - 38 nm) pour des débits bas (1 et 2.4 mL h^{-1}) et de 4 – 45nm pour des débits plus élevés (5 et 12 mL h^{-1}).

En utilisant un champ électrique alternatif (7 V, 1MHz) dans un microcanal de 234mm, on a constaté une distribution de taille étroite de nanoparticules (3 nm - 50 nm) pour des débits de 1 et 2.4 mL h^{-1}toujours avec des échantillons de TiOCl$_2$ pré-dilués avec 16.7 % vol.

En passant à du TiOCl$_2$ pur (i..e. non dilué) tout en gardant les conditions précédentes, on a obtenu une distribution de taille légérement plus large (5 nm - 70 nm) pour des débits de 1 et 2.4 mL h^{-1} .

Les résultats DLS montrent que la taille des nanoparticules diminue avec le temps puis augmente brusquement avant de se transformer en gel. L'augmentation du débit s'accompagne d'une augmentation de la taille des nanoparticules.Une meilleure répartition des tailles et une accélération de l'hydrolyse du DMF ont été obtenues grâce à la solution pré-diluée.

Conclusion

Les principales observations réalisées dans notre étude sont les suivantes:

- la signature thermique de la synthèse de sols a révélé la formation d'instabilités de l'écoulement à l'intérieur du microréacteur. La dilution de $TiOCl_2$ par certains solvants a résolu ce problème menant à des écoulements continus et stables. La prédilution de $TiOCl_2$ avec du DMF, à hauteur de 16.7 % en vol. a permis d'éviter des instabilités en maintenant le processus de synthèse principalement dans le microréacteur.

- L'enthalpie de réaction de la synthèse du sol peut être mesurée facilement dans un microréacteur équipé d'une cellule Peltier.

- L'usage d'un champ électrique AC permet un mélange actif des réactifs et une dissipation de chaleur par effet Joule. Ces phénomènes combinés accélèrent la réaction de synthèse de nanoparticules qui ne nécessite alors pas de longs microcanaux.

- L'analyse de la distribution de taille de nanoparticules de TiO_2 en utilisant la technique DLS a montré un effet de la vitesse d'écoulement et de l'âge des échantillons.

- Sans procédé d'intensification du mélange, la distribution de taille des nanoparticules est assez étroite avec du $TiOCl_2$ prédilué - typiquement 5- 40 nm.

-La présence de champ électrique (7 V AC, 1MHz) augmente légérement la taille des nanoparticules (jusqu'à 50nm pour le $TiOCl_2$ prédilué à hauteur de 17% en vol. avec du DMF et 70 nm pour le $TiOCl_2$ pur).

Réferences:

[1]   T. Cottineau *et al.*, "Photosensitive Titanium Oxo-polymers: Synthesis and Structural Characterization," *Chem. Mater.*, vol. 20, no. 4, pp. 1421–1430, Feb. 2008.

[2]   H. Wang, H. Nakamura, M. Uehara, M. Miyazaki, and H. Maeda, "Preparation of titania particles utilizing the insoluble phase interface in a microchannel reactor," *Chem. Commun.*, no. 14, pp. 1462–1463, Jul. 2002.

[3]   M. Takagi, T. Maki, M. Miyahara, and K. Mae, "Production of titania nanoparticles by using a new microreactor assembled with same axle dual pipe," *Chemical Engineering Journal*, vol. 101, no. 1, pp. 269–276, Aug. 2004.

[4]   C.-E. Liu *et al.*, "Low Temperature Synthesis of Nanocrystallized Titanium Oxides with Layered or Tridimensional Frameworks, from $[Ti_8O_{12}(H_2O)_{24}]Cl_8. 7H_2O$ Hydrolysis," *Chem. Mater.*, vol. 20, no. 14, pp. 4739–4748, Jul. 2008.

[5]   N.-T. Nguyen and Z. Wu, "Micromixers—a review," *Journal of Micromechanics and Microengineering*, vol. 15, pp. R1–R16.

[6]   A. O. El Moctar, N. Aubry, and J. Batton, "Electro-hydrodynamic micro-fluidic mixer," *Lab Chip*, vol. 3, no. 4, pp. 273–280, Nov. 2003.

[7]   C. Hany, C. Pradere, J. Toutain, and J.-C. Batsale, "A millifluidic calorimeter with InfraRed thermography for the measurement of chemical reaction enthalpy and kinetics," 2012.

General Introduction

Energy is the basic need for all the human being and energy demand keeps increasing with time. Despite the depletion of fossil fuels (oil, coal and natural gas etc) the overall energy consumption is increasing with increase of population. Currently, most of the energy utilized is produced by fossil fuels, which also leave adverse environmental effects like pollution and greenhouse effect. Therefore, it is very necessary to develop renewable energy sources to fulfill the energy needs.Amongst renewable sources, solar energy is very feasible solution, its high cost can be brought down by higher efficiencies without creating any adverse effects on environment.

For energy harvesting of solar energy, photovoltaic is a very interesting process which converts directly light energy into electricity. In this field, one of the big current challenges concerns the design and the development of energy storage devices. One of the very innovative device may be the photobattery, it is a photochemical system which directly uses the solar energy to promote electrochemical reactions. Then the photogenerated charge carriers are stored as chemical energy. The reversibility of the electrochemical processes allows one to recover charge carriers when requested as in a traditional battery. In our approach, one of the important points in the development of successful photobatteries is to optimise the nanostructuration of photosensitive titanium-based materials exhibiting photochemical properties. However, this nanostructuring is strongly dependent on the experimental conditions during synthesis and this constitutes one of the key points to obtain controlled and powerful materials from the photochemical point of view. Indeed, it involves acido-basic reactions which require a precise control of the modus operandi (temperature, time, concentration of reactants). Due to the exothermal nature of the reactions, the mixing of the reactants is usually performed at low temperature (0°C) using an ice-bath [1], this method being known as "batch technique".

One interesting alternative tested in this work is the use of microreactor. Indeed, the use of small lateral size microchannels (less than 1mm) allows one to limit the temperature gradients, and easily control the thermal conditions of the synthesis [2]. Microchannels have also higher surface over volume ratio which is very essential for better heat transfer in microreactors[3,4]. Moreover the confinement of the reactants within microchannels reduces parasitic phenomena occurring in ambient atmosphere such as hydrolysis due to prolonged contact with the relative humidity of air. Finally such strategy allows producing continuously.

However, one drawback of using microreactor is the difficulty to ensure mixing of the reactive fluids. Indeed in microfluidic devices, the flows are laminar so that the mixture is essentially insured by molecular diffusion which is very slow. To achieve the nanoparticle synthesis, a very long microchannel would be needed involving large pressure drop for highly viscous fluids, a convenient alternative is the use of a mixing process. The methods allowing the improvement of the mixture are numerous and can be of passive or active nature [5, 6]. Actually, it is known that the interface between two fluids with different electrical properties can be destabilized by an electric force [6]. This causes a secondary flow which improves the mixing between both fluids. In our work, as the two involved reactants show different relative permittivities, an electric field will be tested for mixing enhancement.

Since 2002, several works were dedicated to titanium oxide nanoparticles production by means of microreactors, while avoiding the formation of agglomerates. So, Wang *et al*. [7] produced TiO_2nanoparticles with a size less than 10 nm at the interface between two insoluble reactants. Afterwards, Takagi [8] has implemented a capillary within a tube allowing the generation of TiO_2 nanoparticles with a 100-140 nm size by using a precursor of low viscosity. The literature review did not show papers dealing with the implementation of an active mixing for TiO_2 nanoparticle production.

In our work, a microreactor is used to perform the synthesis of titanium-based sol which we aim at implementing in photobatteries, as thin film. These sols are obtained by the hydrolysis of $TiOCl_2 \bullet 1.4\ HCl \bullet 7H_2O$ in the presence of N,N-dimethylformamide $((CH_3)_2NCOH$, denoted DMF). Depending on the time of ageing, this hydrolysis leads to the production of sols and then gels composed of nanoparticles dispersed in a solvent [1].Our experiments will be based on the use of an infrared camera to study the thermal signature of the flow inside the microreactor since mixing both reactants is a highly exothermic reaction. Actually the usual method involves mixing reactants in a close vessel at 0°C and then controlling the advancement of the reaction by drying at 70°C for several hours. The idea here is to advantageously exploit the temperature elevation to accelerate the hydrolysis and propose a one-step process, by mixing in microchannels. Diffusion light scattering technique (DLS) and Raman spectroscopy will be carried out to study the size of the nanoparticles, the chemical composition and the complexion of the Ti^{4+} cation by the organic part as a function of time.

The three main objectives of our work are: (i) the follow-up of the nanoparticles synthesis by mean of microreactors to investigate the effect of the operating conditions such as flow rate, concentration, dilution with solvent as will be required, (ii) the characterization of the variation of enthalpy to improve the knowledge of the synthesis and (iii) the effect of applying an electric field in order to enhance the mixing of reactants inside the microreactors. Finally, some optimized experimental conditions should be identified to lead to sols with a known composition and a duration over which the latter does not evolve.

This workwas carried out with the collaboration of two different laboratories:Institut des MatériauxJean Rouxel (IMN) in Nantes which is active in the development of synthesis of nanomaterials in solutionand Laboratoire de ThermiqueetEnergie de Nantes (LTEN) which has developed research in microfluidic and active mixing. This PhD program was supported by the government of Pakistan and the "CNRS-Cellule Energie" through the project entitled "NP TiO_2microréacteur" obtained in 2013.

The manuscript of thesis is divided intofive chapters:

The 1st chapter is dedicated to the literature review on our research topic. Various types of techniques are reviewed for the synthesis of nanoparticles (physical, mechanical and chemical processes). Then a focus is realized on the synthesis of titaniananoparticles by batch technique and also using a microreactor. Finally passive and active mixing methods are reviewed for mixing improvement in order to overcome the previously mentioned drawback of using microreactors.

The 2nd chapter describes the materials and methods. The precursor and the organic solvents involving nanoparticle production and their properties are presented including also the experimental conditions using the traditional batch process. Then we show our experimental setups composed of several microreactors with different inlet shapes, microchannel lengths, whether or not equippedwith Peltier cell or electrodes. Finally the main instruments, their characteristics, calibration procedures and use protocols are described. It concerns the infrared camera and the specific methods for nanoparticles analysissuch as the Dynamic light scattering and Raman scattering.

The 3rd chapter presents the thermal signature of several experiments of nanoparticle synthesis reaction using our microreactors. As for pure $TiOCl_2$ precursor, one have noticed unstable and discontinuous flows, we have then performed several tests for the pre dilution of

TiOCl$_2$using various solvents such as water,1-propanol, 1,2-propanediol, 1-octanol,2-propanol and DMF.

The 4th chapter provides the result obtained when using an electric field just after the inlets of both reactants in the microreactor. Tests are performed using various DC voltages then AC voltages are used with several values of the frequency. The study starts with prediluted TiOCl$_2$ precursor and then is pursued using pure TiOCl$_2$.

The 5th chapter focuses on the analysis of the produced sols in the experiments of the previous two chapters. The size distribution of nanoparticles is analysed by using DLS technique and the chemical composition of solution by using Raman spectroscopy. The effect of operating conditions such as flow rate of reactants and ageing of the solution are finally presented until the sol becomes gel. Some experimental conditions were identified to produce sols with dedicated composition, which remains stable over a reasonable length of time.

References:

[1]   T. Cottineau *et al.*, "Photosensitive Titanium Oxo-polymers: Synthesis and Structural Characterization," *Chem. Mater.*, vol. 20, no. 4, pp. 1421–1430, février 2008.

[2]   M. Luther, J. J. Brandner, K. Schubert, A. Renken, and L. Kiwi-Minsker, "Novel design of a microstructured reactor allowing fast temperature oscillations," *Chem. Eng. J.*, vol. 135, Supplement 1, pp. S254–S258, Jan. 2008.

[3]   D. Hamadi, B. Garnier, H. Willaime, F. Monti, and H. Peerhossaini, "A novel thin-film temperature and heat-flux microsensor for heat transfer measurements in microchannels," *Lab. Chip*, vol. 12, no. 3, pp. 652–658, 2012.

[4]   E. V. Rebrov, J. C. Schouten, and M. H. J. M. de Croon, "Single-phase fluid flow distribution and heat transfer in microstructured reactors," *Chem. Eng. Sci.*, vol. 66, no. 7, pp. 1374–1393, avril 2011.

[5]   J. B. Edel, R. Fortt, J. C. deMello, and A. J. deMello, "Microfluidic routes to the controlled production of nanoparticles," *Chem. Commun.*, no. 10, pp. 1136–1137, May 2002.

[6]   A. O. E. Moctar, N. Aubry, and J. Batton, "Electro-hydrodynamic micro-fluidic mixer," *Lab. Chip*, vol. 3, no. 4, pp. 273–280, 2003.

[7]   H. Wang, H. Nakamura, M. Uehara, M. Miyazaki, and H. Maeda, "Preparation of titania particles utilizing the insoluble phase interface in a microchannel reactor," *Chem. Commun.*, no. 14, pp. 1462–1463, Jul. 2002.

[8] M. Takagi, T. Maki, M. Miyahara, K. Mae, Production of titania nanoparticles by using a new microreactor assembled with same axle dual pipe, Chem. Eng. J. 101, 269-276, 2004

Chapter 1

Literature review on nanoparticles production and mixing process.

1.1 Introduction

Nanoparticles are defined as microparticles with at least one dimension between 1 nm and 100 nm [1]. Importance of nanomaterials is rapidly increasing because of their unique properties. Indeed nanoparticles are intermediate between bulk materials and molecular or atomic structures and contrary to bulk material, the physical properties at the nanoscale depend on the size and shape of particles. Some of the specific properties of nanoparticles are:

- very high surface area to volume ratio (increased surface activity)
- spectral behavior of light scattering and absorption depending on particle size
- increased hardness and fracture strength
-suspension of nanoparticle possible in fluids since the density mismatch can be overcomed by the interaction with the solvent.

Due to these specific behaviors, nanoparticles are widely used in many area such as medicine, materials, electronic, environment, energy as shown in Table 1.1.

Table 1.1: Applications of nanoparticles in various fields[1]

Applied field	Application
Medicines	Drugs
Chemical	Nanoscale chemicals, paints, coatings
Cosmetics	Filteration of ultraviolet radiation, anti aging skin
Materials	Nanoparticles, carbon nanotubes, biopolymers, points, coatings
Food Sciences	Nutracetical food, nanocapsules.
Environment	Purification filters for water and air
Energy	Energy storage, solar cells, Photovoltaic
Military	Weapons
Electronics	Semiconductors chips, memory storage, photonica, optoelectronics

1.2 Synthesis of nanoparticles

1.2.1 Various techniques for nanoparticles production

The shape and size of nanoparticles and therefore their properties are strongly dependent on the production method, so the preparation of nanoscale particles is an important field in nanomaterials science. As shown on Figure 1.1, one can identified three groups for the classification of the main methods to produce nanoparticles: physical, mechanical and chemical methods.

The production methods can are also classified either as "Top down" or "Bottom up". Top down production is breaking large substances into required nanostructured substances and in the Bottom up approach, nanostructures are built up using atoms or molecules. Bottom –up approaches are chemical processes based on transformations in solution e.g. sol-gel processing, chemical vapor deposition (CVD), plasma or flame spraying synthesis, laser pyrolysis, atomic or molecular condensation. Top-down approaches are mechanical milling, laser ablation, sputtering and etching or photolithography.
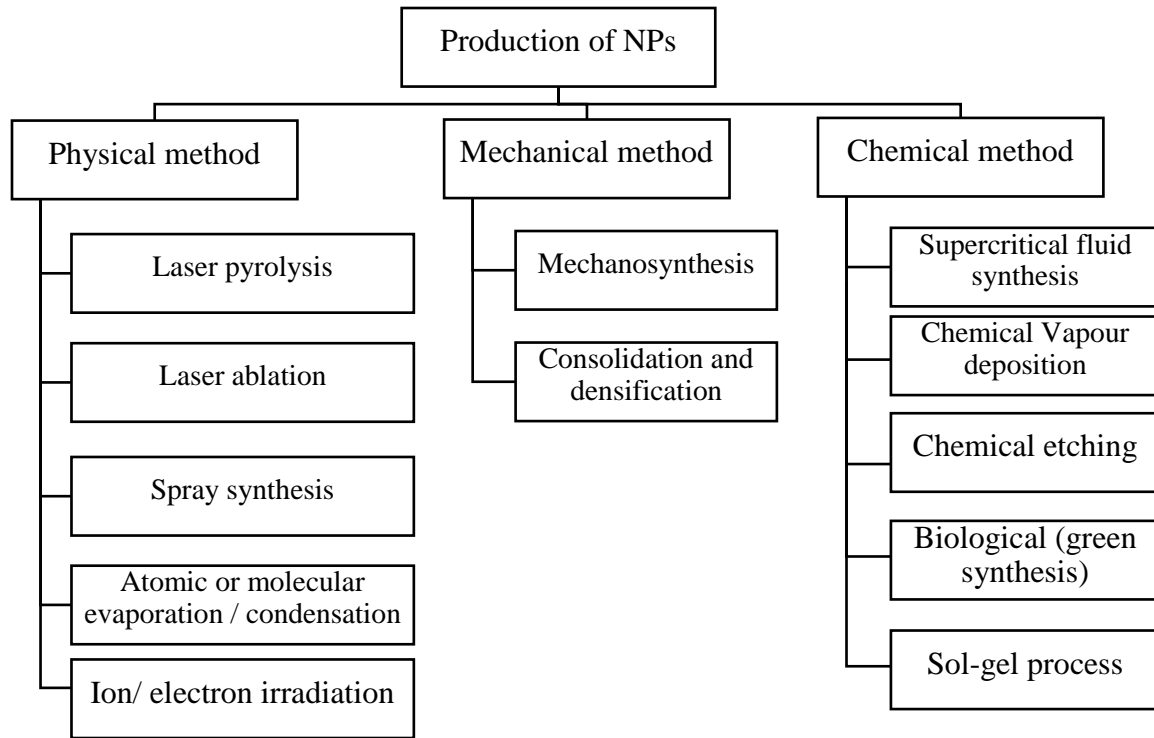
Figure 1.1: Production of nanoparticles through various methods

Table 1.2 shows the types of nanoparticle produced according to various manufacturing methods.

Table 1.2: Nanoparticles synthesis with various existing production methods and related works

Production method	Nanoparticles (size)	Ref.
Laser pyrolysis	SiC(20 – 50nm), SiO_2 (10 - 40 nm), TiO_2 (10 -15 nm)	D'Amato et al. [2]
Spray synthesis	ZnO (10 - 25 nm)	Saiedi et al.[3]
Atomic evaporation/ condensation	Cu (4 – 50nm)	Förster et al.[4]
Mechanosynthesis technique	$CoFe_2O_4$ (cobalt ferrite) Oleic acid coated iron ferrite-magnetite Fe_3O_4 (30nm)	Manova et al.[5] Marince et al.[6]
Supercritical fluid technique	$Li_4Ti_5O_{12}$ Lithium titanate(4 -5 nm)	Nugroho et al.[7]
Chemical vapour deposition	Si-SiOx nanowires (20 – 50 nm) MoS_2 Molybdenum disulfide (60 – 90 nm)	Yue et al.[8] Gao et al.[9]
Sol-gel technique	$Ag_{3(2+x)}Al_xTi_{4-x}O_{11+\delta}$ (17 – 48nm) TiO_2 (4 - 35 nm)	Ramesh [10] Su et al.[11]
Biological method (green synthesis)	Ag (2 – 5 nm)	Jha et al.[12]

1.2.2. Titanium oxide nanoparticles production using sol-gel with batch techniques

As in this work, we will produce titanium based nanoparticles using sol-gel technique, a specific bibliographic study on this topic is provided here. Batch technique will be considered in this section and the case using microreactor will be presented in the following section.

The sol-gel technology is widely used since it is an effective process to produce nanoparticles. This is due to its advantages of low processing cost, energy efficiency, high production rate, and rapid productivity of fine homogeneous powder [13,14].

Table 1.3 shows the production of titanium dioxide nanoparticles by using sol-gel processing with batch technique.

The sol-gel technique is wet chemical technique. This technique is based on the transformation of sol (colloidal suspension of particles in form of liquid) into a network inserting or entangling a liquid phase (gel) [15]. Sol-gel formation occurs in four steps: 1 - hydrolysis, 2-condensation and polymerization, 3-growth of particles and 4- gel. Basic sol-gel process for nanoparticles synthesis is shown in Figure 1.2 [15]. These mentioned steps for the sol-gel process are dependent on several input conditions like water amount, pH value of sol, reaction temperature, concentration of reactant, reaction time, time for gel formation [16].

Table 1.3: Production of titanium dioxide nanoparticles by sol-gel with batch technique

Solvent	Size	Applications and comments	Ref
Precursor : Solution of Titanium (IV) n-butoxide ($Ti(O\text{-}Bu)_4$) and isopropyl alcohol (i-PrOH)+ acetylacetone (as a chemical additive to control the reaction rate)	4-35 nm	photocatalytic	Su *et al.*[11]
Titanium isopropoxide ($Ti(OCH(CH_3)_2)_4$) , ammonium hydroxide (NH_4OH), nitric acid ($HN0_3$) and citric acid monohydrate ($C_3H_5O(COO)_3H_3.H_20$)	0.1-0.5μm	solar cells, chemicals sensor, Photocatalytic etc	Pookmanee *et al.*[17]
Titanium oxychloride ($TiOCl_2\bullet 1.4$ $HCl\bullet 7H_2O$, denoted $TiOCl_2$),and N, N-dimethylformamide (($CH_3)_2NCHO$, denoted DMF)	~ 10 nm	solar cells, photocatalysis, cosmetics products etc	Cottineau *et al.*[18]
Titanium oxychloride ($TiOCl_2\bullet 1.4$ $HCl\bullet 7H_2O$, denoted $TiOCl_2$), N, N-dimethylformamide (($CH_3)_2NCHO$, denoted DMF) and water.	1-2.3 nm	energy storage and conversion, optics and electronics	Terrisse *et al.*[19]
Extract of Moringa oleifera, water and Titanium dioxde (TiO_2)	100 nm	wound healing (Medicine), antibacterial agent against bacteria	Sivaranjani *et al.*[20]

Reaction in the sol-gel process generally involves metal alkoxides $M(OR)_n$ or metal salts based hydrolysis and condensation. Reaction scheme can be written as follows: [11]

1. Hydrolysis
    In hydrolysis, the addition of water into the precursor breaks the molecule and MOH bond is formed as shown in equation below
    $$M(OR)_n + H_2O \rightarrow M(OR)_{n-1}(OH) + ROH$$
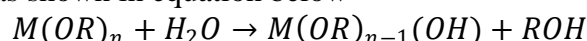
2. Condensation

Olation: $M - OH - M$ bonds

Alcoxalation: $M(OR)_n + M(OR)_{n-1}(OH) \rightarrow M_2O(OR)_{2n-2} + ROH$

Oxolation: $2M(OR)_{n-1} + (OH) \rightarrow M_2O(OR)_{2n-2} + H_2O$

The sol is treated according to the final desired product as shown in Figure 1.2, like thin film coating can be achieved via spinning and dipping technique and in order to get powders, sol is treated using various surfactants. The gel can be converted into aerogel and xerogel by rapidly drying process and by slow drying process respectively. Furthermore to achieve dense ceramic material xerogel is treated by calcinations process [16]
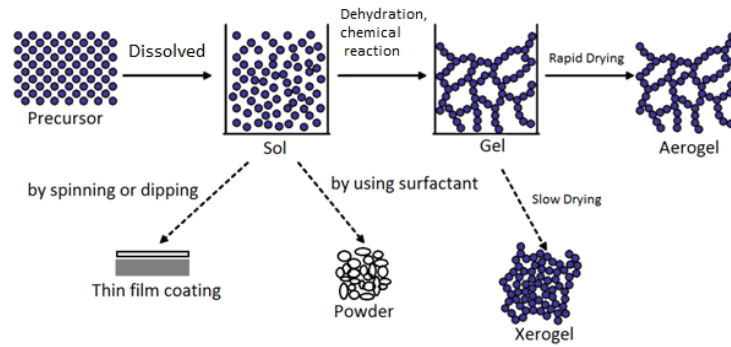

Figure 1.2: Basic sol-gel process flow diagram [15]

Cottineau *et al.*[18]reported synthesis of titanium oxide via sol-gel process using batch technique in an ice bath to control the exothermic reaction. Hydrolysis was initiated by injecting DMF into the precursor of titania solution for 30 minutes under stirring at 25°C. In order to get rapid gelation rate, a thermal treatment was used by placing the solution in an oven (70°) for 24 hours. Gel can be obtained by keeping the sample at room temperature for several months.

In the study of Terrisse *et al.*[19]the addition of water in titania solution and DMF allows the control of the particles size, accelerates the hydrolysis and condensation rate and it also helps to increase the miscibility of titania precursor.

Su *et al.*[11] reported the sysnthesis of Titaniam dioxide via sol-gel process by using solution of Titanium (IV) n-butoxide (Ti(O-Bu)$_4$) and isopropyl alcohol (i-PrOH) and acetylacetone as a chemical additive to control the reaction rate. They observed phase transformation from anatase to rutile with the increase of calcination temperature. It was also concluded that increase of calcination temperature results the increase in size of TiO_2 nanoparticles, as it increases from 4 to 35 nm as temperature was increased to 700°C.

Sivaranjai *et al.*[20]reported the synthesis of titanium nanoparticles using Moringa Oleifera leaves which were used as wound healing and antibacterial agent against gram positive and gram negative bacteria. They tested samples on male albino rats. Titanium nanoparticles were obtained by stirring and centrifugation of the mixture of Moringa powder dissolved in water and titanium dioxide in Erlenmeyer flask. An average size of 100nm of the spherical nanoparticles were recorded by Scanning Electron microscopic (SEM).

There are many reviews available on the synthesis of Titanium dioxde (TiO_2). This issue provides the importance of controlled synthesis to have high performance materials [21].

In batch reactors, all the materials are loaded at once for the reaction and the product is collected at the end of process. Batch reactors are still frequently used to produce nanoparticles, however they have many drawbacks like, time consuming process, non-uniform heating, reproducibility problem of nanoparticles, large area for installation of reactor and sometimes post synthesis needed for purification [22,23].

1.3 Nanoparticles production via a continuous process using microreactors

Over the year, microfluidics is a multidisciplinary field of interest and its development is particularly important in the field of molecular biology, analytical chemistry and microelectronics [24]. In the last few years there has been an explosion of work in this area.Microfluidic devices have microchannel with cross section dimensions ranging from millimeters to micrometers involving flow rates from nano to microliters. For chemical process, the use of microreactors has many advantages. In addition to continuous production, it can provide enhancement of reagent mixing, reduction in the volume of chemicals neededand improvement in temperature control. For nanoparticles production, these features will result in a better control of the size of nanoparticles with increased homogeneity [25,26].

Reactive process in microreactors depends on the flow rate or Reynolds number (flow rate) residence time and reaction throughput. In the fundamental theory of fluid dynamics there are three flow regimes characterized by the Reynolds number which compares the inertial and viscous effects. It is expressed by the following equation:

$$\text{Re} = \frac{\rho V D_h}{\mu} \, or \, \frac{Q D_h}{\nu A} \qquad\qquad 1.1$$

Where ρ (kg m^{-3}) is the density of the fluid, μ (Pa s) its dynamic viscosity, ν(m^2 s^{-1}) its kinematic viscosity, V (m s^{-1}) the average velocity, Q (m^3 s^{-1}) the volumetric flow rate, A isthe cross sectional area of the channel and D_h is the hydraulic diameter of the duct[27]. For a flow of fluid in a closed channel, the hydraulic diameter of the channel is often used as the characteristic length in the Reynolds number calculation. For a Reynolds number less than 2300, the flow is generally considered laminar. For a Reynolds number greater than 4000, the flow rate is considered turbulent. For a Reynolds number between 2300 and 4000, the flow is in a transitional regime between laminar and turbulent. The Reynolds number rarely exceeds 2000 for moderate pressures between 1 and 10 bar. The flows are predominantly laminar and dominated by the viscous effects, therefore rapid mixing by turbulence cannot be carried out in this pressure range. This leads in particular to mixing problems.

Residence time is the average time reaction mixture stays inside the microchannel which can be calculated by this formula:

$$\tau = V/Q \qquad\qquad 1.2$$

Where$V$ (m^3) is the total volume of the solution collected at the outlet of the channel and Q (m^3 s^{-1}) is the inlet or outlet flow rate (reaction mixture volume passes per unit time) from the channel. If there are multi inlet or outlet flows, then Q will be sum of inlet flow rates or sum of outlet flow rates.

Throughput is related to the productivity of the reaction which is measured in moles per minutes and it is directly proportional to the flow rate and concentration of the solution.

Following Table 1.4, shows several works presenting the various types of nanoparticles produced using microreactors.

Table 1.4: Nanoparticle production using microreactors

NPs	Reactants	Size of NPs	Microreactor	Application	Ref.
Titania	1-Titanium tetraisoproxide with Water and formamide , 2-Titanium tetraisoproxide with water	<10nm	Y-shape 9 cm long ceramic microchannel	drugs - medicine	Wang *et al.*[24]
Titania	isopropanol/water	100nm and 4.9nm after ripening and calcining	coaxial dual tubular reactor	medicine, solar cells	Takagi *et al.* [28]
Gold Silver Copper	chloroauric acid $HAuCl_4$ with Potassium carbonate K_2CO_3 and Water and Sodium borohydride $NaBH_4$	<4nm	8 split and recombines units of modular microreactor	chemistry and bioscience	Wagner *et al.* 2008 [29]
Silver	silver nitrate with extract of cacumenplatycladi dispersed in water	3.4nm ± 0.3	microtubular reactor		Liu *et al.* [30,31] and Hung *et al.*[32]
Gold	aqueous solution of gold chloride tetrahydrate $HAuCl_4.4H_2O$ with aqueous solution of alkaline NaOH	star like NPs 4-40nm	double Y-shape microchannel	chemistry and bioscience	Ishizaka *et al.* [33]
Silver, Platinum , Iron oxide	silver nitrate with diethylene	20.9nm	2 phases micro tube reactor		Arndt *et al.* [34]
Cobalt	cobalt(II) chloride hexahydrate dissolved in ethanol with hydrazine alkaline mixture	30 ± 10nm	stainless steel Modular microreactor	magnetic sensors, ferrofluids, contrast agents	Clifford *et al.* [35]
Copper chromite	mixture of copper and chromium nitrate solution with aqueous solution of citric acid	192-300nm	0.2 m long polyethylene tube microreactor	Supporting catalyst in space vehicles and weapon industries	Appalakut ti *et al.*[36]

Appalakutti *et al*. [36]used 200cm long and 0.8mm diameter polythylene tube as a continuous flow microreactor to mix copper and chromium nitrate solution with aqueous solution of citric acid. The objective was to study the effect of flow rate, surfactants and copper and chromite ratio on the size distribution of copper chromite nanoparticles. They used polyvinylpyrrolidone, polyethylene glycol and cetyl trimethyl ammonium bromide as surfactants which were mixed in the solution of copper nitrate and chromium nitrate. Then they were injected in the microchannel to control the size distribution of nanoparticles and size ranging from 192 to 300nm were found using a zeta potential analyzer (Malvern Zetasizer nano ZS 90). The study showed that the flow rate, surfactants and Cu/Cr ratio have important role for controlling the size of the nanoparticles. The particle size increases with increasing flow rate at low Cu/Cr concentrations, this being due to increased interactions between particles involving their agglomeration. On the contrary at high Cu/Cr concentrations, the particle size decreases with increasing flow rate because of the decrease of the residence time. Otherwise, adding the surfactants has helped to decrease the size of nanoparticles by inhibiting their growth and agglomeration.

Clifford *et al*. [35]used stainless steel continuous flow microreactor to improve the quality of nanoparticles in reduced time for production of cobalt nanoparticles. A 30 ± 10nm average size of nanoparticles was recorded by transmission electronic miscroscopy (TEM) technique.

Arndt *et al*. [34] showed that quality of nanoparticles can be improved by using biphasic micro tube reactor for their synthesis. They used ethylene glycol and hexadecaneat temperatures about 160°C, in a two phases micro tube reactor avoiding the typical disadvantages arising from fouling or clogging of micro tube reactors, a problem which can be observed if ethylene glycol is used as a single phase. Silver nitrate with diethylene was used as reactants. Hexadecane, oleic acid and oleylamine were added in the nitrate solution before their mixing in the microchannels. Micro tube reactor (MTR) system was found to provide a fast, continuous and reproducible production of nanoparticles. Indeed, the speed for nanoparticle formation was found 4 times higher than the one with batch reactor and the size distribution was narrowed with a 15% relative standard deviation compared to 24% with batch reactor. Using this MTR system, silver nanoparticles with a 20.9nm size were produced with a 1:5 ratio of silver nitrate ($AgNO_3$) to polyvinylpyrrolidone (PVP). They also showed that by using this type of microreactor, platinum and iron oxide nanoparticles could be also produced.

Another approach for nanoparticle production is the use of a coaxial dual tubular reactor involving annular laminar flows [27]. Tetraisopropoxide (TTIP) and isopropanol/water were used in respectively the inner and outer tubes. TEM and SEM analysis have been performed to understand the crystallographic structure and size distribution. A nanoparticle size of 100nm was recorded and after ripening for 24h and calcining for 2h, a 4.9nm size was evaluated from XRD analysis.

When two different insoluble or immiscible liquids are injected into the microreactor, it appears that the mixing is not done properly due to their different viscosities and densities. A lot of research has been done to solve this issue. Wang *et al*. [24] showed that to obtain stable interface it was very important to use appropriate flow rates and similar viscosities. Two insoluble liquid systems were tested in their study. For the first one, titanium tetraisoproxide was dissolved in1-Hexanol and injected along with distilled water plus formamide solution. In the second liquid system, titanium tetraisoproxide was dissolved in cyclohexane and injected with water solution. These liquid systems were used to control the nanoparticle size distribution in a Y-shape 9cm long ceramic microchannel (width 360µm and

depth 200µm) and flow rate was provided by syringe pump. In comparison with microemulsion method here no surfactant was needed. Microfluidic system was carried out to produce titaniananoparticles exhibiting size less than 10nm recorded by Transmission Electron Microscopy (TEM) on the interface in the microchannel.

Ishizaka *et al*. [33] reported the control of the morphology of gold nanoparticles by mixing aqueous solution of $HAuCl_4.4H_2O$ and aqueous solution of alkaline NaOH in Y-shaped microreactor with another Y-shape microreactor connected at the end to add the aqueous solution of glucose. Glucose is a reduction agent for alkaline aqueous solution used here to provide the control in stability of gold nanoparticles production. They obtained star like nanoparticles which changed to round form with time. Feed rate of NaOH provides control in size, morphology and optical properties of gold nanoparticles.

Another approach reported by Wagner *et al*. [29] by using 8 split and recombine units of mixer for production of gold nanoparticles with sodium borohydride ($NaBH_4$) used as reduction agent. They tested successfully this microsystem for other metal nanoparticles generation like silver, copper and complex particles.

1.4 Mixing enhancement in microreactors

In a microfluidic system, fluidic mixing is difficult because the scale of the channel involves laminar flow at Reynolds number less than 100. The liquid is thus mixed only by molecular diffusion, which is too slow for many applications. In recent years, several mechanisms have been proposed and patented to improve microfluidic mixing efficiency. Interesting review about micromixers have been provided by Chen *et al*. [37] and Nguyen *et al*. [38].

In his review, Nguyen *et al*. [38] proposed a classification scheme for the different types of micromixers as shown in Figure 1.3.
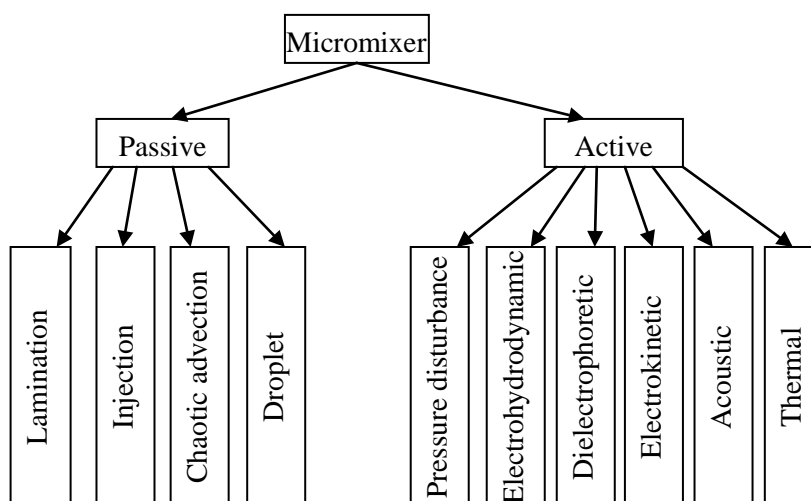

Figure 1.3: Classification scheme for micromixers according to Nguyen *et al*. [38]

There are generally two categories of mixing methods in microfluidics: passive and active ones. In the following, a review on these two methods is provided.

1.4.1 Passive mixing

Passive methods requires longer channel [39] with special geometry of the microchannels that generates cross-flows, generating a chaotic flow obstacles or 3D configurations or zigzag flow drop. Passive mixing does not need any external source to agitate or stir the fluid flow streams so it is very difficult to get proper mixing due to absence of turbulence and low Reynolds number [40].

Among the simplest design for the micromixers are Y or T-shaped microchannels as shown in Figure 1.4 [41]. A simple Y or T-shaped micromixer consists of two inlets by which the fluids are entering inside the main channel where mixture and reaction take place.In such channels mixing and reaction fully depend on the diffusion at the interface of two reactants which involves a slow mixing.
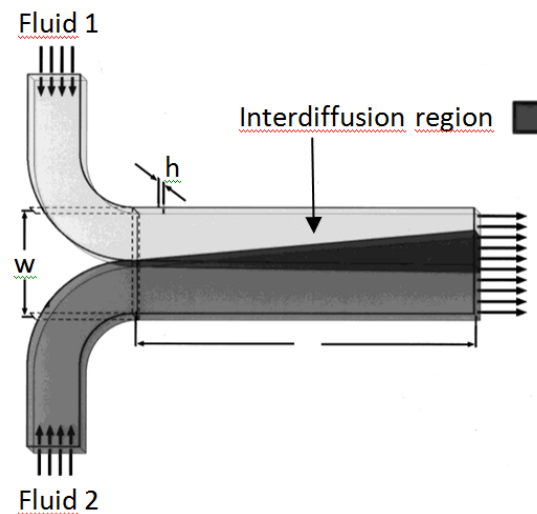

Figure 1.4: Simple design of T-shape microchannel (Kamhols *et al*. [41])

In such channels mixing can be improved by adding obstacles in fluid flow path or by roughening the microchannel walls [41,42] .

Compared to T shape microchannel, Y shape microchannel provides sligthly better mixing as shown by Rudyak *et al*. [44]. In their work, two identical liquids were mixed to compare mixing efficiency of T shape microchannel and Y shapemicrochannel and it has been found that T shape microchannel has 17.6% mixing efficiency and Y shapemicrochannel has 18.2% mixing efficiency. Gobby *et al*. [42] simulated fluid mixing in different micromixer configurations and reported that the Y-angle has a negligible effect on mixing length and pressure gradient. The only marginal effect observed is the appearance of a dead zone (in which the fluid velocity is almost zero) when the angle is -45 ° (Figure 1.5).
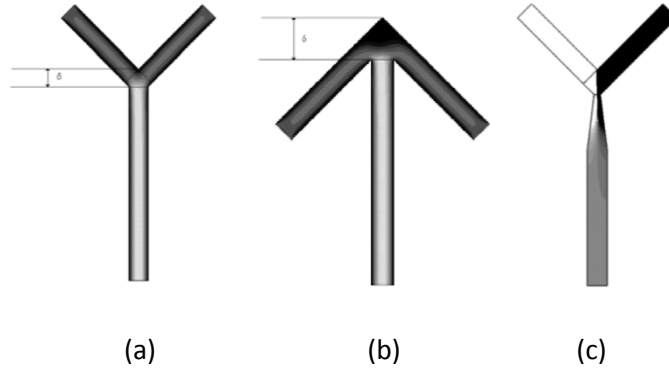
Figure1.5: Different models for mixing (a) +45° oriented Y-mixer (b) -45 oriented Y-mixer (c) Venturi type Y-mixer Gobby *et al*. [42]

Furthermore, providing high dissymmetric flow rates at the inlet of microchannels can decrease the time of mixing by generating secondary flow, swirling flow or vortices in the micromixer[44,45]. Another way proposed by Veenstra *et al*. is to narrow the mixing path in T-type microchannel to minimize the diffusion distance [47].

The alternative injection combined with a pulsating flow is another mean of intensifying mixing. Mao *et al*. [48] developed a T-type microchannel in which they used pulsating flow at both inlets. Their study focused on the effect of the Reynolds number, the Strouhal number and the amplitude of the perturbations so as to reach a uniform species concentration at the exit of the microchannels.Glasgow *et al*. [49] studied numerically and experimentally the mixture in a T-type channel by pumping two reagents with variable rates of sinusoidal signal type. During their tests, the best result was obtained when the two inputs are pulsed and in phase opposition. Using thermal signature of the neutralization reactionof NaOH with HCl,Ammar *et al*. [50]showed that the mixing efficiency was improved by increasing the ratio amplitude to mean value of flow rates and in a less extent by increasing the pulsation frequency.

Another way to improve mixing was reported by Cha *et al*. [51] for Y or T- type microchannel by developing complicated design which separates inlet main stream into number of sub streams which join at the end (called as chessboard) as shown in Figure1.6 [51]. Such types of micromixers are decreasing the diffusion length and increasing contact interface between two fluids.
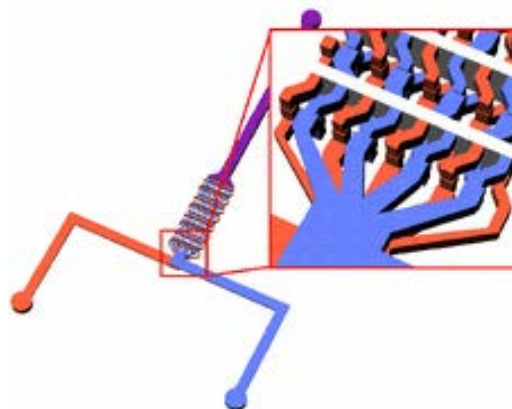

Figure1.6: Chessboard mixer for improved mixing (Cha *et al*. [51])

1.4.2 Active mixing

In active mixing, an external force is applied to mix the fluids by stirring or agitating the flow streams. These external forces can be electric field, pneumatic or mechanical vibration.

Oddy *et al*. [52] reported electrokinetic instability force (EKI) to improve the mixing inside the channel. When two fluids of different conductivities are mixed in the microchannel under electric field then electrokinetic instability occurs as shown in Figure 1.7 [40]. In this work, using aY-shape microchannel, Jin *et al*. have shown that an increase electric field results in an increase in the electrokinetic instability waves which shows that fluid mixing can be improved by adjusting the electric field.
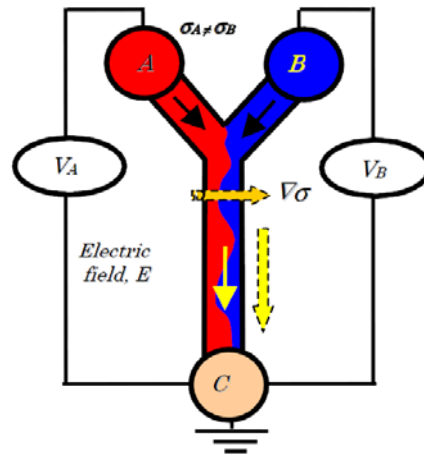

Figure1.7: Y shape microchannel with EKI system (Jin *et al*.[40])

Ould El Moctar *et al*. [53]reported the use of electro-hydrodynamic (EHD) force to enhance mixing inside a T-shape micro channel. They mixed two liquids of identical viscosity and density but with dissimilar electrical properties (conductivity/permittivity) inside a microchannel in presence of electrodes as shown in Figure1.8 [53]. When both liquids are mixed without electric field the mixing is very slow. The presence of electric field destabilizes the interface of both liquids which involves a fast mixing.
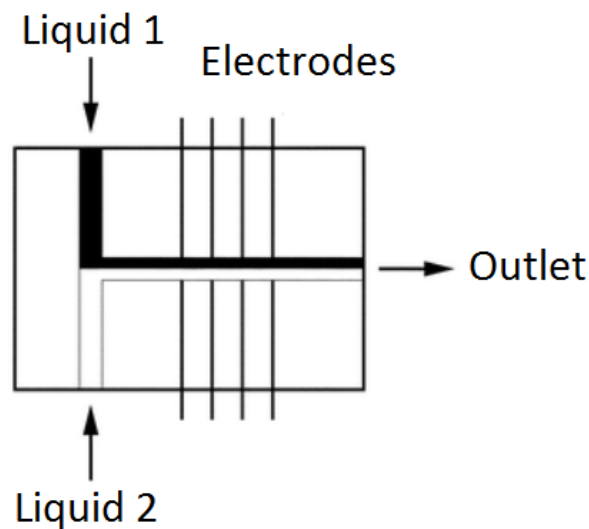

Figure1.8: T shape microchannel with electrodes (Ould El Moctar *et al*.[53])

1.5 Conclusion

Titania nanoparticles have wide variety of applications in different fields and photobattery is one of them. Solar energy storage is a current challenge and the presence of titania nanoparticles would improve the performance of photobatteries because of their high photochemical property. In this chapter, a literature review is dedicated to nanoparticle production with a focus on titania nanoparticles synthesis using microreactors. Various methods have been reported in this chapter. Mainly the synthesis of nanoparticles through batch process and continuous process using microreactors are discussed. Synthesis of nanoparticles through continuous process have various advantages like it has better control over temperature, concentration and time and better control of the size distribution of nanoparticles. Proper mixing is very essential for homogeneous, smaller and narrow distributed nanoparticles. At the end of this chapter, various passive and active methods are reviewed for mixing improvement in order to overcome one drawback of using microreactors which is the lack of transversal flows resulting in a poor mixing of reactive fluids.

References:

[1]   S. L. Pal, U. Jana, P. K. Manna, G. P. Mohanta, and R. Manavalan, "Nanoparticle: An overview of preparation and characterization (2000-2010).," *http://www.japsonline.com/counter.php?aid=159*, Aug. 2011.

[2]   R. D'Amato *et al.*, "Synthesis of ceramic nanoparticles by laser pyrolysis: From research to applications," *J. Anal. Appl. Pyrolysis*, vol. 104, pp. 461–469, Nov. 2013.

[3]   H. R. Saiedi, M. Sayyadnejad, M. Ali, and R. A. Morad, *Synthesis of ZnO Nanoparticles by Spray Pyrolysis Method. .*

[4]   H. Förster, C. Wolfrum, and W. Peukert, "Experimental study of metal nanoparticle synthesis by an arc evaporation/condensation process," *J. Nanoparticle Res.*, vol. 14, no. 7, pp. 1–16, Jul. 2012.

[5]   E. Manova *et al.*, "Mechano-Synthesis, Characterization, and Magnetic Properties of Nanoparticles of Cobalt Ferrite, $CoFe_2O_4$," *Chem. Mater.*, vol. 16, no. 26, pp. 5689–5696, Dec. 2004.

[6]   T. F. Marinca *et al.*, "Mechanosynthesis, structural, thermal and magnetic characteristics of oleic acid coated Fe_3O_4 nanoparticles," *Mater. Chem. Phys.*, vol. 171, pp. 336–345, Mar. 2016.

[7]   A. Nugroho, D. Yoon, O.-S. Joo, K. Y. Chung, and J. Kim, "Continuous synthesis of $Li_4Ti_5O_{12}$ nanoparticles in supercritical fluids and their electrochemical performance for anode in Li-ion batteries," *Chem. Eng. J.*, vol. 258, pp. 357–366, Dec. 2014.

[8]   Y. Yu, R. Luo, and H. Shang, "Growth and photoluminescence of Si-SiOx nanowires by catalyst-free chemical vapor deposition technique," *Appl. Surf. Sci.*, vol. 368, pp. 325–331, Apr. 2016.

[9]   B. Gao and X. Zhang, "Synthesis of MoS_2 Inorganic Fullerene-like Nanoparticles by a Chemical Vapour Deposition Method," *South Afr. J. Chem.*, vol. 67, no. 1, pp. 6–11, Jan. 2014.

[10]   S. Ramesh, "Sol-Gel Synthesis and Characterization of Nanoparticles," *J. Nanosci.*, vol. 2013, Jan. 2013.

[11]   C. Su, B.-Y. Hong, and C.-M. Tseng, "Sol-gel preparation and photocatalysis of titanium dioxide," *Catal. Today*, vol. 96, no. 3, pp. 119–126, Oct. 2004.

[12]   A. K. Jha, K. Prasad, K. Prasad, and A. R. Kulkarni, "Plant system: Nature's nanofactory," *Colloids Surf. B Biointerfaces*, vol. 73, no. 2, pp. 219–223, Oct. 2009.

[13]   H. Dislich, "New Routes to Multicomponent Oxide Glasses," *Angew. Chem. Int. Ed. Engl.*, vol. 10, no. 6, pp. 363–370, Jun. 1971.

[14]   B. J. J. Zelinski and D. R. Uhlmann, "Gel technology in ceramics," *J. Phys. Chem. Solids*, vol. 45, no. 10, pp. 1069–1090, 1984.

[15]   M. J. Madou, "Pattern Transfer with additive techniques," in *Fundamentals of Microfabrication: The Science of Miniaturization, Second Edition*, CRC Press, 2002, pp. 156–157.

[16]   C. Daraio and S. Jin, "Synthesis and Patterning Methods for Nanostructures Useful for Biological Applications," in *Nanotechnology for Biology and Medicine*, G. A. Silva and V. Parpura, Eds. Springer New York, 2012, pp. 27–44.

[17]   P. Pookmanee and S. Phanichphant, "Titanium dioxide powder prepared by a sol-gel method," *J. Ceram. Process. Res.*, vol. 10, no. 2, Apr. 2009.

[18]   T. Cottineau *et al.*, "Photosensitive Titanium Oxo-polymers: Synthesis and Structural Characterization," *Chem. Mater.*, vol. 20, no. 4, pp. 1421–1430, février 2008.

[19]   A.-F. B. Hélène Terrisse, "Monodispersed titanium oxide nanoparticles in N,N-dimethylformamide: water solutions," *J. Sol-Gel Sci. Technol.*, vol. 67, no. 2, 2013.

[20]   V. Sivaranjani and P. Philominathan, "Synthesize of Titanium dioxide nanoparticles using Moringa oleifera leaves and evaluation of wound healing activity," *Wound Med.*, vol. 12, pp. 1–5, Mar. 2016.

[21]   G. Liu, H. G. Yang, J. Pan, Y. Q. Yang, G. Q. (Max) Lu, and H.-M. Cheng, "Titanium Dioxide Crystals with Tailored Facets," *Chem. Rev.*, vol. 114, no. 19, pp. 9559–9612, Oct. 2014.

[22]   L. Gutierrez, L. Gomez, S. Irusta, M. Arruebo, and J. Santamaria, "Comparative study of the synthesis of silica nanoparticles in micromixer–microreactor and batch reactor systems," *Chem. Eng. J.*, vol. 171, no. 2, pp. 674–683, juillet 2011.

[23]   C.-H. Chang, B. K. Paul, V. T. Remcho, S. Atre, and J. E. Hutchison, "Synthesis and post-processing of nanomaterials using microreaction technology," *J. Nanoparticle Res.*, vol. 10, no. 6, pp. 965–980, Aug. 2008.

[24]   H. Wang, H. Nakamura, M. Uehara, M. Miyazaki, and H. Maeda, "Preparation of titania particles utilizing the insoluble phase interface in a microchannel reactor," *Chem. Commun.*, no. 14, pp. 1462–1463, Jul. 2002.

[25]   J. B. Edel, R. Fortt, J. C. deMello, and A. J. deMello, "Microfluidic routes to the controlled production of nanoparticles," *Chem. Commun.*, no. 10, pp. 1136–1137, May 2002.

[26]   A. Jahn, J. E. Reiner, W. N. Vreeland, D. L. DeVoe, L. E. Locascio, and M. Gaitan, "Preparation of nanoparticles by continuous-flow microfluidics," *J. Nanoparticle Res.*, vol. 10, no. 6, pp. 925–934, Feb. 2008.

[27]   K. Mishima and T. Hibiki, "Some characteristics of air-water two-phase flow in small diameter vertical tubes," *Int. J. Multiph. Flow*, vol. 22, no. 4, pp. 703–712, Aug. 1996.

[28]   M. Takagi, T. Maki, M. Miyahara, and K. Mae, "Production of titania nanoparticles by using a new microreactor assembled with same axle dual pipe," *Chem. Eng. J.*, vol. 101, no. 1–3, pp. 269–276, août 2004.

[29]   J. Wagner, T. R. Tshikhudo, and J. M. Köhler, "Microfluidic generation of metal nanoparticles by borohydride reduction," *Chem. Eng. J.*, vol. 135, Supplement 1, pp. S104–S109, Jan. 2008.

[30]   H. Liu *et al.*, "Microfluidic biosynthesis of silver nanoparticles: Effect of process parameters on size distribution," *Chem. Eng. J.*, vol. 209, pp. 568–576, Oct. 2012.

[31]   H. Liu, J. Li, D. Sun, T. Odoom-Wubah, J. Huang, and Q. Li, "Modeling of Silver Nanoparticle Formation in a Microreactor: Reaction Kinetics Coupled with Population Balance Model and Fluid Dynamics," *Ind. Eng. Chem. Res.*, vol. 53, no. 11, pp. 4263–4270, Mar. 2014.

[32]   J. Huang *et al.*, "Biogenic Silver Nanoparticles by Cacumen Platycladi Extract: Synthesis, Formation Mechanism, and Antibacterial Activity," *Ind. Eng. Chem. Res.*, vol. 50, no. 15, pp. 9095–9106, août 2011.

[33]   T. Ishizaka, A. Ishigaki, H. Kawanami, A. Suzuki, and T. M. Suzuki, "Dynamic control of gold nanoparticle morphology in a microchannel flow reactor by glucose reduction

in aqueous sodium hydroxide solution," *J. Colloid Interface Sci.*, vol. 367, no. 1, pp. 135–138, février 2012.

[34]   D. Arndt, J. Thöming, and M. Bäumer, "Improving the quality of nanoparticle production by using a new biphasic synthesis in a slug flow microreactor," *Chem. Eng. J.*, vol. 228, pp. 1083–1091, juillet 2013.

[35]   D. M. Clifford, A. A. El-Gendy, A. J. Lu, D. Pestov, and E. E. Carpenter, "Room Temperature Synthesis of Highly Magnetic Cobalt Nanoparticles by Continuous Flow in a Microfluidic Reactor," *J. Flow Chem.*, vol. 4, no. 3, pp. 148–152, août 2014.

[36]   S. Appalakutti, S. Sonawane, B. A. Bhanvase, V. Mittal, and M. Ashokkumar, "Process intensification of copper chromite (CuCr2O4) nanoparticle production using continuous flow microreactor," *Chem. Eng. Process. Process Intensif.*, vol. 89, pp. 28–34, Mar. 2015.

[37]   C.-H. Chen, "Recent Patents on Micromixing Technology and Micromixers," *Recent Pat. Mech. Eng.*, vol. 2, no. 3, pp. 240–247, Nov. 2009.

[38]   N.-T. Nguyen and Z. Wu, "Micromixers—a review," *J. Micromechanics Microengineering*, vol. 15, pp. R1–R16.

[39]   E. A. Mansur, M. YE, Y. WANG, and Y. DAI, "A State-of-the-Art Review of Mixing in Microfluidic Mixers," *Chin. J. Chem. Eng.*, vol. 16, no. 4, pp. 503–516, Jan. 2008.

[40]   Z. Jin, S. Someya, K. Okamoto, and H. Hu, "Mixing Enhancement in a Microfluidic Device," *J. Vis.*, vol. 11, no. 1, pp. 35–36, Jan. 2008.

[41]   A. E. Kamholz, B. H. Weigl, B. A. Finlayson, and P. Yager, "Quantitative Analysis of Molecular Interaction in a Microfluidic Channel: The T-Sensor," *Anal. Chem.*, vol. 71, no. 23, pp. 5340–5347, décembre 1999.

[42]   D. Gobby, P. Angeli, and A. Gavriilidis, "Mixing characteristics of T-type microfluidic mixers," *J. Micromechanics Microengineering*, vol. 11, no. 2, p. 126, 2001.

[43]   T. J. Johnson, D. Ross, and L. E. Locascio, "Rapid Microfluidic Mixing," *Anal. Chem.*, vol. 74, no. 1, pp. 45–51, Jan. 2002.

[44]   V. Rudyak and A. Minakov, "Modeling and Optimization of Y-Type Micromixers," *Micromachines*, vol. 5, no. 4, pp. 886–912, Oct. 2014.

[45]   M. Hoffmann *et al.*, "Experimental and numerical investigations of T-shaped micromixers," *ResearchGate*, Jan. 2003.

[46]   S. H. Wong, M. C. L. Ward, and C. W. Wharton, "Micro T-mixer as a rapid mixing micromixer," *Sens. Actuators B Chem.*, vol. 100, no. 3, pp. 359–379, mai 2004.

[47]   T. T. Veenstra, T. S. J. Lammerink, M. C. Elwenspoek, and A. van den Berg, "Characterization method for a new diffusion mixer applicable in micro flow injection analysis systems," *J. Micromechanics Microengineering*, vol. 9, no. 2, p. 199, 1999.

[48]   W. B. Mao and J. L. Xu, "Micromixing enhanced by pulsating flows," *Int. J. Heat Mass Transf.*, vol. 52, no. 21–22, pp. 5258–5261, Oct. 2009.

[49]   I. Glasgow and N. Aubry, "Enhancement of microfluidic mixing using time pulsing," *Lab. Chip*, vol. 3, no. 2, pp. 114–120, May 2003.

[50]   A. Houssain, B. Garnier, D. Sediame, A. OULD EL MOCTAR, and H. Peerhossaini, "Heat-Transfer Analysis and Improved Mixing in Multifunctional Microreactor Using Sapphire Window and Infrared Thermography." International Journal of Microscale and Nanoscale Thermal and Fluid Transport Phenomena 4, no. 3/4 (2013): 249."

[51]   J. Cha *et al.*, "A highly efficient 3D micromixer using soft PDMS bonding," *J. Micromechanics Microengineering*, vol. 16, no. 9, p. 1778, 2006.

[52]   M. H. Oddy, J. G. Santiago, and J. C. Mikkelsen, "Electrokinetic Instability Micromixing," *Anal. Chem.*, vol. 73, no. 24, pp. 5822–5832, décembre 2001.

[53]   A. O. E. Moctar, N. Aubry, and J. Batton, "Electro-hydrodynamic micro-fluidic mixer," *Lab. Chip*, vol. 3, no. 4, pp. 273–280, 2003.

Chapter 2

Materials and methods

2.1 Reactants and reactions

The sol TiDMF is obtained from an exothermic reaction between a titanium precursor, titanium oxychloride ($TiOCl_2 \bullet 1.4\ HCl \bullet 7H_2O$, denoted $TiOCl_2$), and an organic solvent, N, N-dimethylformamide (($CH_3)_2NCHO$, denoted DMF).

$TiOCl_2 \bullet 1.4\ HCl \bullet 7H_2O$ is a yellow and viscous liquid. Above 35°C, the evaporation of the hydrochloric acid leads to the precipitation of white and amorphous titanium oxohydroxide, although the solution is stable at room temperature in a closed vessel since it may react with the ambient humidity. Its physico-chemical characteristics are summarized in Table 2.1.

Table 2.1: Physical and chemical properties of $TiOCl_2 \bullet 1.4\ HCl \bullet 7H_2O$

Physical state	Liquid
Color	Yellow
Odour	Irritant
pH	< 1
Molar mass	311.6 g mol^{-1}
Crystallization temperature	< - 45 °C
Decomposition temperature	>35°C
Vapor Pressure	15 kPa at 30°C
Density	1.58 kg dm^{-3} at 20 °C
Dynamicviscosity	73 mPa s at 20°C ; 51 mPa s at 30°C

N, N-dimethylformamide is an aprotic and dipolar organic solvent. It is in the form of a colorless, hygroscopic liquid. At room temperature, the DMF is stable. Heated to temperatures above 350°C, it decomposes into dimethylamine and carbon monoxide. Its physico-chemical characteristics are summarized in Table 2.2.

Table 2.2: Physical and chemical properties of N, N-dimethylformamide ((DMF).

Molecular formula	C_3H_7NO
Physical state	Liquide
Color	Colourless
Odour	Amine likeodour
Molar mass	73.1 g mol^{-1}
Boiling point	153 °C
Fusion point	-61°C
Refractive index	1.43
Density	0.9445
Dynamicviscosity	0.802 mPa s at 25 °C
Dipolar moment	3.4D
Dielectric Constant	36.7 at 300 K

2.2 Ti-based nanoparticles production in batch process (at IMN)

Production of Ti-based nanoparticles through batch process is already done at IMN. As in our work we replaced batch technique with microreactor, we used all the experimental conditions as a reference for our work of production of Ti-based nanoparticles through microreactor.

2.2.1 Experimental conditions in batch process

The synthesis of the TiDMF sol is carried out by mixing the precursors TiOCl$_2$ and DMF in a closed vessel to limit the losses of HCl placed in an ice bath to control the exothermic reaction. The mixture is stirred for 30 minutes at a temperature lower than 35 ° C to obtain homogeneous mixture. The sol resulting from this reaction is slightly yellowish and viscous depending on the concentration rate. Annabelle Rouet, during her thesis[1], used different ranges of titanium concentrations from 0 to 2 mol L^{-1} (The initial titanium concentration of $TiOCl_2$ was 4.85 molL^{-1}). All the sols obtained immediately after synthesis were transparent and homogeneous but their evolution over time differed according to the titanium concentration as shown below

- [Ti] <0.2 molL^{-1}: white precipitate of titanium oxide hydrate;

- 0.2 molL^{-1}<[Ti] <0.8 molL^{-1}: opaque TiDMF gel;

- 0.8 molL^{-1}<[Ti] <1.7 molL^{-1}: transparent and homogeneous TiDMF gel;
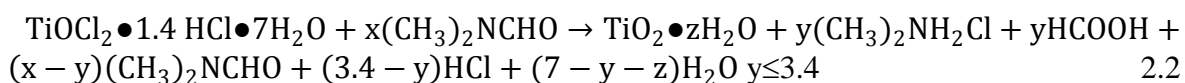
- [Ti]> 1.7 molL^{-1}: white and opaque polymer.

Various works[2,3]carried out were focused on the titanium concentration of 1.42 molL^{-1}in order to obtain a sufficient high titanium concentration and a stable TiDMF gel. At room temperature, it is necessary to wait a few months to obtain a TiDMF gel. However, it is possible to accelerate the reaction by using a heat treatment at 70°C for about twenty hours.

DMF hydrolysedwith water and HCl with time leads to the formation of methanoic acid (HCOOH) and dimethylammonium chloride (DMACl) according to reaction as shown in equation 2.1 [4].

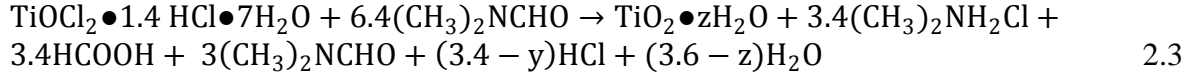$$(CH_3)_2NCHO + HCl + H_2O \rightarrow (CH_3)_2NH_2Cl + HCOOH \qquad 2.1$$
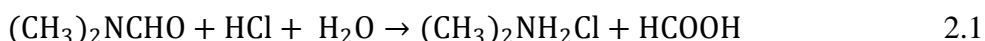
Equation 2.1: Hydrolysis of DMF in the presence of hydrochloric acid

The presence of DMF, DMACl and methanoic acid in TiDMF sol was demonstrated by Infra-Red and Raman spectroscopy[5]. DMF does not only have a solvent role in the formation of the TiDMF sol since its hydrolysis consumes hydrochloric acid which is necessary for the stabilization of $TiOCl_2$. Therefore, $TiOCl_2$will evolve and polymerize via a process of hydrolysis and condensation involving olation and oxolation processes. So, the overall reaction of the solution can be written as below:

$$TiOCl_2 \bullet 1.4\ HCl \bullet 7H_2O + x(CH_3)_2NCHO \rightarrow TiO_2 \bullet zH_2O + y(CH_3)_2NH_2Cl + yHCOOH + (x - y)(CH_3)_2NCHO + (3.4 - y)HCl + (7 - y - z)H_2O\ y{\leq}3.4 \qquad 2.2$$

Equation 2.2: Condensation reaction of TiDMF

In the case of the sol with a titanium concentration equal to 1.42 molL^{-1}, the initial DMF number is 6.4. At the equilibrium, the reaction then becomes:

$$TiOCl_2 \bullet 1.4\ HCl \bullet 7H_2O + 6.4(CH_3)_2NCHO \rightarrow TiO_2 \bullet zH_2O + 3.4(CH_3)_2NH_2Cl +$$
$$3.4HCOOH + 3(CH_3)_2NCHO + (3.4 - y)HCl + (3.6 - z)H_2O \qquad 2.3$$

Equation 2.3: Condensation reaction of TiDMF titanium concentration of 1.42 molL^{-1}

In fact, we also know [2] that part of $HCOO^-$ and DMACl are interacting with the solid part of gels as mentioned below.

2.2.2 Hydrolysis and condensation of TiOCl₂ in N,N-dimethylformamide

Raman spectroscopy is used to quantify the rate of hydrolysis of TiDMFsol and gel by Thomas Cottineau in his thesis[5]. Further, SolèneBéchu[6]completed this analysis by reproducing the experiments and correlating these results with analysis during her thesis. The hydrolysis of the TiDMF sol was evaluated using symmetrical vibrational bands $v_s(C'_2N)$ of DMF at 866cm⁻¹ $v_s(CN)$ Dimethylammonium (DMACl) at $891 cm^{-1}$.

$$DMF_{hydrolysis} = 100 \frac{A_{DMA^+}/J_{DMA^+}}{A_{DMA^+}/J_{DMA^+} + A_{DMF}/J_{DMF}} \qquad 2.4$$

Equation2.4: Calculation of hydrolysis rate of DMF with A_{DMA^+} and A_{DMF} the areas of the peaks at 891 cm^{-1} and 866 cm^{-1} respectively and J_{DMA^+} and J_{DMF} the calibration coefficients, related to

$$A_{species} = J_{species} \times [species]$$

According to equation 2.2, Figure 2.1below shows amount of DMACl estimated by Raman spectroscopy which varies linearly with the DMACl concentration.
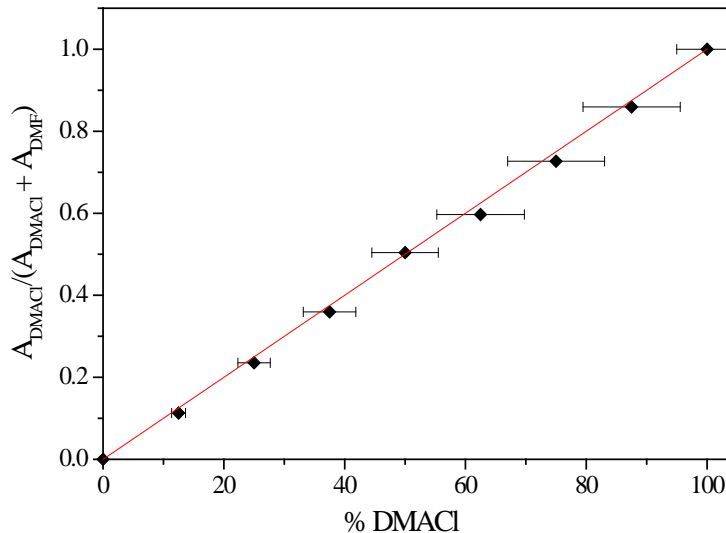

Figure 2.1: Normalized area correlation of peak 891 cm^{-1} / percentage of DMF formed [2]

From the hydrolysis rate, it is then possible to obtain the number of DMF consumed per titanium. According to the overall equation of the polycondensation reaction (Equation

2.2),there are 3.4 HCl atoms available at the start of the reaction. During the reaction, they reactwith DMF to produce DMACl. To obtain the level of DMF consumed by Ti, it is therefore sufficient to multiply the hydrolysis rate by the initial number of DMF per Ti, therefore 6.4 in a sol of titanium concentration of 1.42 molL^{-1}, assuming that the system is considered closed, and that there is no loss of reagent.
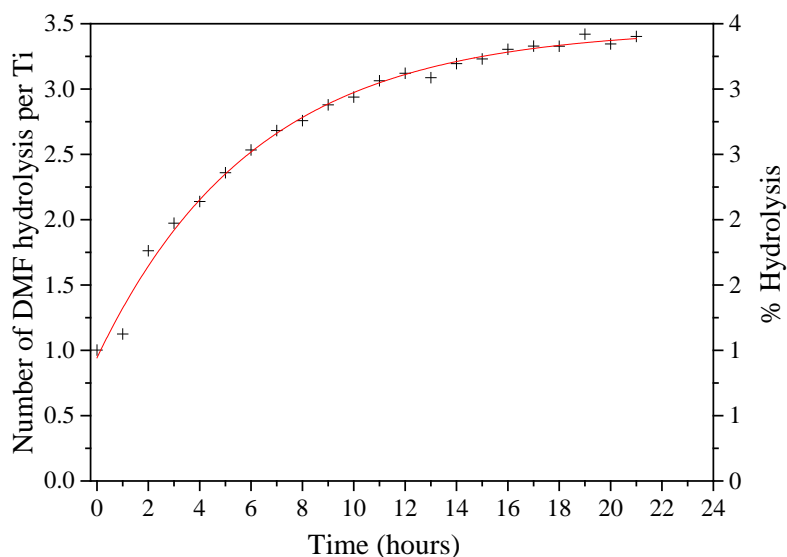

Figure 2.2: Number of DMF hydrolysis per Ti in TiDMF sol with [Ti] = 1.42 molL^{-1}as a function of the drying time at 70°C with refinement carried out on the kinetics hydrolysis[6]

The Raman spectra obtained from the sols also provide other information, especially in the region 500-850 $cm^{-1}$where four peaks are identified. The first band at 630 $cm^{-1}$is attributed to the TiOCl$_2$ precursor of titanium, the band at 663 cm^{-1} corresponds to the bending δ (O = C-N) of the DMF[7]. The bands located at 692 and 710 $cm^{-1}$are also related to the deformation of the δ (O = CN) of the DMF but this time correspond to a deformation of the DMFs linked to Ti (IV) cations (as presented in fresh sols structures and aged sols / gels of the structural evolution). In order to better understand the hydrolysis process within the TiDMF material, the amounts of free DMF in solution and DMF bound to the titanium network can be studied as a function of the rate of hydrolysis of the sol.

To complement this information, it is necessary to couple these Raman data with the proton (^{1}H) and carbon (^{13}C) liquid NMR data realized by Annabelle Rouet during her thesis[1]. Actually since liquid NMR is sensitive to mobile species only, it can be considered that only the free species in the solution are probed. Taking into account the proportion of free DMF, it is possible to evaluate the amount of $HCOO^-$ and DMA^+ in solution (free). By taking the hydrolysis rate (determined by Raman spectroscopy), the total amount of $HCOO^-$ and DMA^+(free and bound) can be calculated as well.By difference with the free values obtained in NMR spectroscopy, the amount of $HCOO^-$ and DMA^+bonded to the titanium network is also accessible. Figure 2.3summarizes the evolution of these species in the hydrolysis reaction [5].
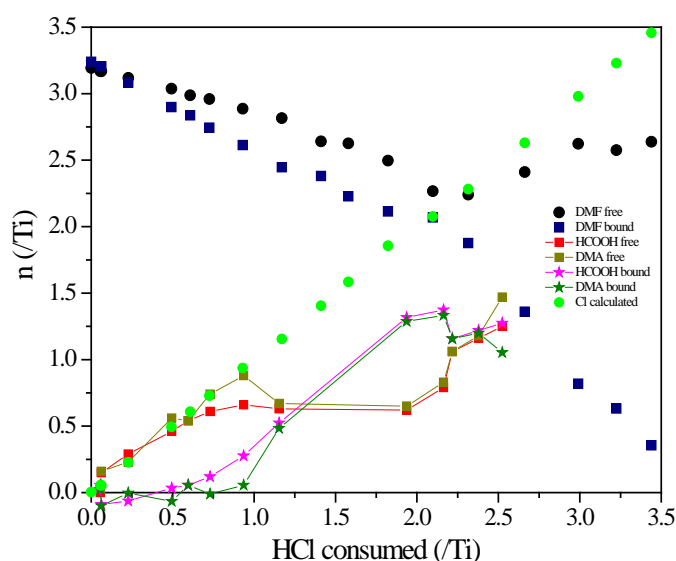
Figure 2.3: Evolution of the different species (free and bound) resulting from the hydrolysis of DMF as a function of the number of HCl consumed by titanium for [Ti] = 1.42 molL^{-1}[5]

Indeed it should be emphasized here that no NMR data of the liquid could be obtained for a HCl content consumed by Ti greater than 2.6 since the species are no longer sufficiently mobile from the liquid NMR point of view.

Different stages of hydrolysis emerge from these evolutions. In order to better interpret them, it is necessary to note that DMF enters into the coordination of titanium from the beginning of the mixture (information available by Raman analyses):

- 0.0-0.5 Hydrolyzed DMF/Ti: the hydrolysis is carried out in equivalent ratio on both the free DMF (~ 3 per Ti) and the bound DMF (~ 3 per Ti), but the resulting species (HCOO$^-$ and DMA $^+$) are released as a free form in solution;

- 0.5-1.0 hydrolyzed DMF/Ti: the hydrolysis here takes place primarily on the solid through the bound DMF (more pronounced decrease) and generates free DMA $^+$ species as in the first step, but unlike the first step, also generates HCOO$^-$linked species;

- 1.0-2.0 hydrolyzed DMF/Ti: the hydrolysis preferentially takes place on the solid from the bound DMF (but both DMF are indeed decreasing) by incorporation of HCOO$^-$in the network. The DMACl which remained in solution in the previous stages interacts with the solid under construction and the quantity of species in solution varies a little bit;

- 2.0-3.4 hydrolyzed DMF/Ti: in this last step, an obvious decrease of bound DMF is observed whereas the amount of hydrolyzed species in the solid is constant. The hydrolysis therefore continues rather in solution, with desorption of the bound DMF during the condensation of the network, allowing the increase of the free HCOOH and DMACl compounds. Indeed, the amount of free DMF remains constant or even slightly increases.

2.3 Microreactor Devices

From the heat transfer and fluid flow point of view, many devices were used in this work in order to study different aspects. First study was about the passive mixing and the stability of the flow. A second device was constructed in order to measure the enthalpy of the reaction. The last device aimed to improve the mixing by using an active mixing system based on the use of electrical field. In this section, we will be describing these devices, the results will be analysed later in the document.

2.3.1 Microchannel's Material

Most often microreactors are designed according to the desired mixing and chemical reaction. We used different materials for fabrication of microchannels like polymethylmethacrylate, polydimethylsiloxane andpolytetrafluoroethylene, denoted hereafter PMMA, PDMS and PTFE, respectively. In previous study [8] there was some damage to PMMAmicroreactor caused by DMF. PDMS has indeed limited chemical compatibility with DMF. Additionally, its low thermal conductivity and mechanical strength limit its application at high temperature and pressure arises[9]. It was concluded from the preliminary tests [8] that PTFE microchannel is recommended for the mixing of $TiOCl_2$and N,N-dimethylformamide $((CH_3)_2NCHO$, denoted DMF) because of its resistance against chemicals and of its wide range of thermal stability between -200°C to +260°C.

2.3.2 Passive mixing experimental setup.

The experimental setup used for the purpose of passive mixing and flow stability study is shown in Figure 2.4. The main components of this setup are:
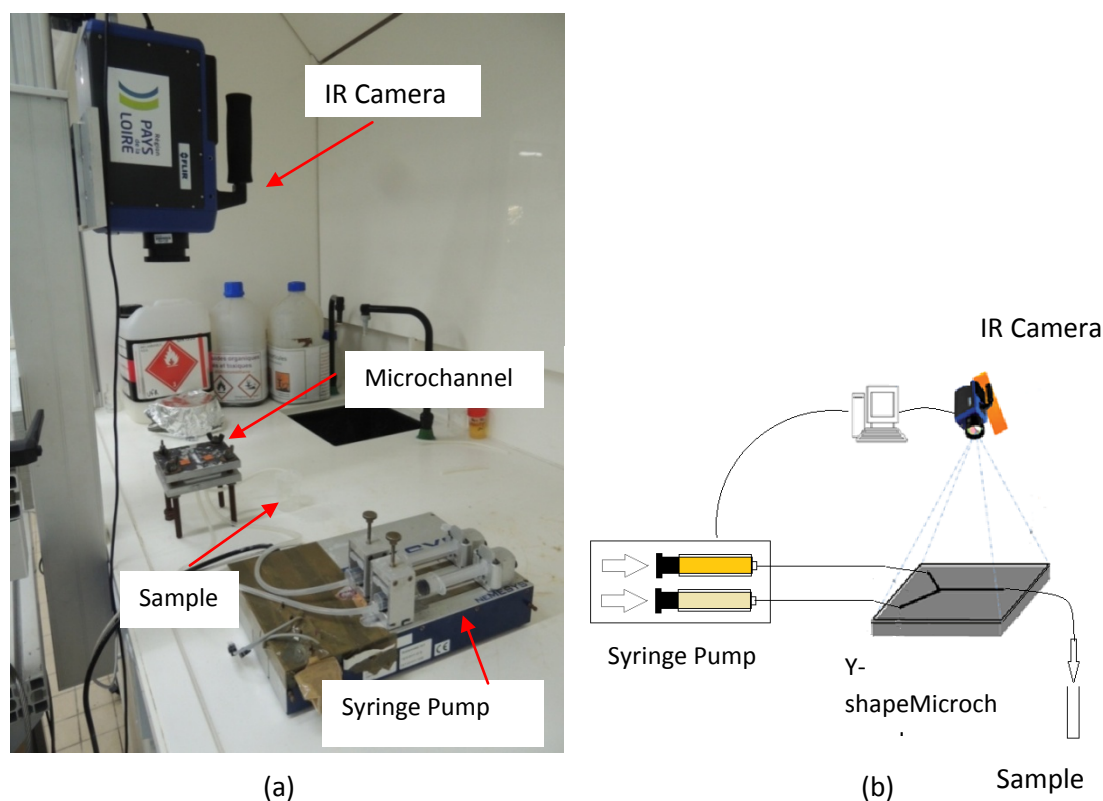

Figure 2.4: (a) Experimental setup (b) Schematic view of experimental setup

2.3.2.1 Microchannel

In our work for passive mixing, we used two inlets and one exit microchannels.These T-type, arrowhead type and Y-type microchannels as shown in Figure 2.5 were fabricated at LTN from the polytetrafluoroethylene (PTFE) piece. T-type, arrowhead type and Y type microchannels are having mixing length of 40mm, 40mm and 32mm respectively with $0.6{\times}0.6\ mm^2$ cross sectional area. Geometry of all the three microchannels are shown in Figure 2.6.

A thin glass sheet of 100μm was placed on the top of the PTFE microreactor and tightened with upper and lower flanges with PTFE sheet and rubber isolation as shown in Figure 2.7.
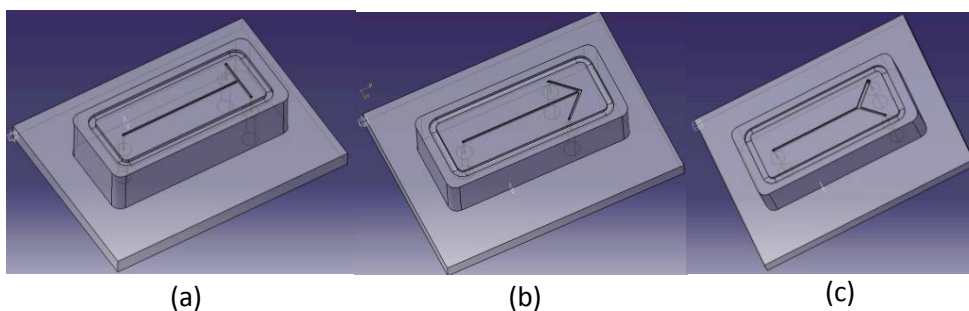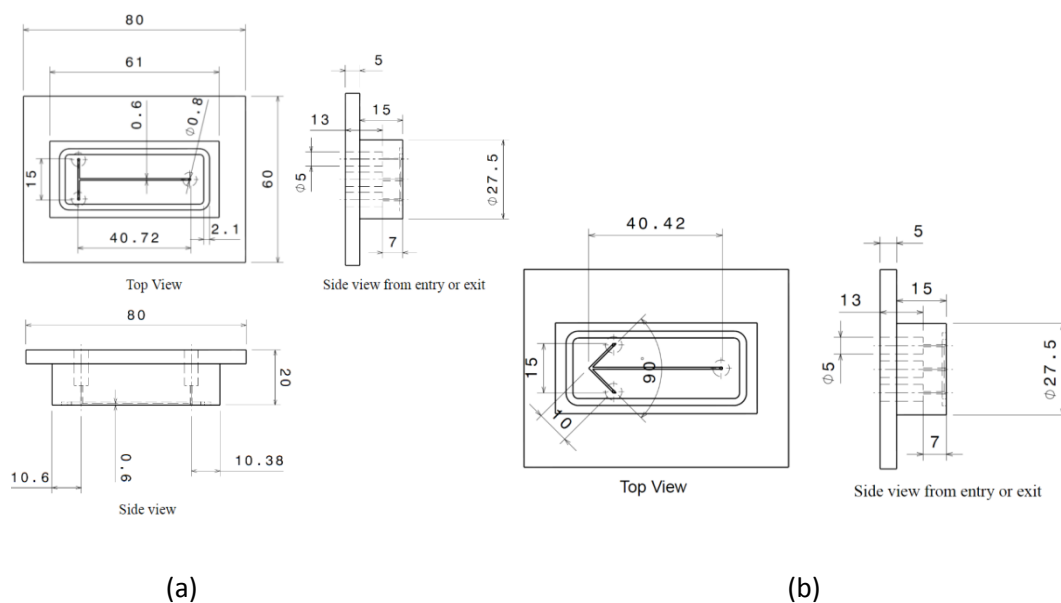

(a) (b) (c)

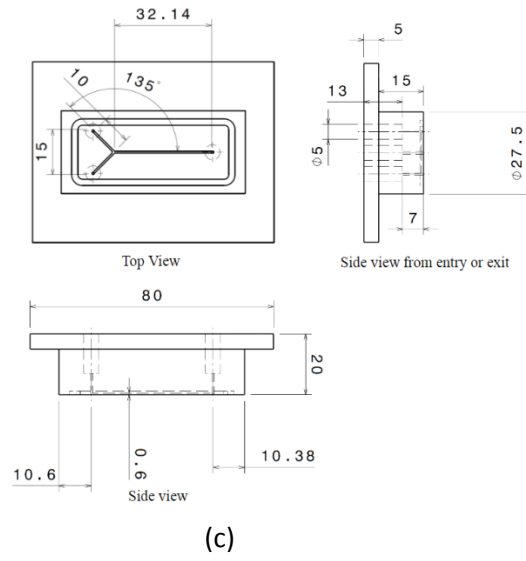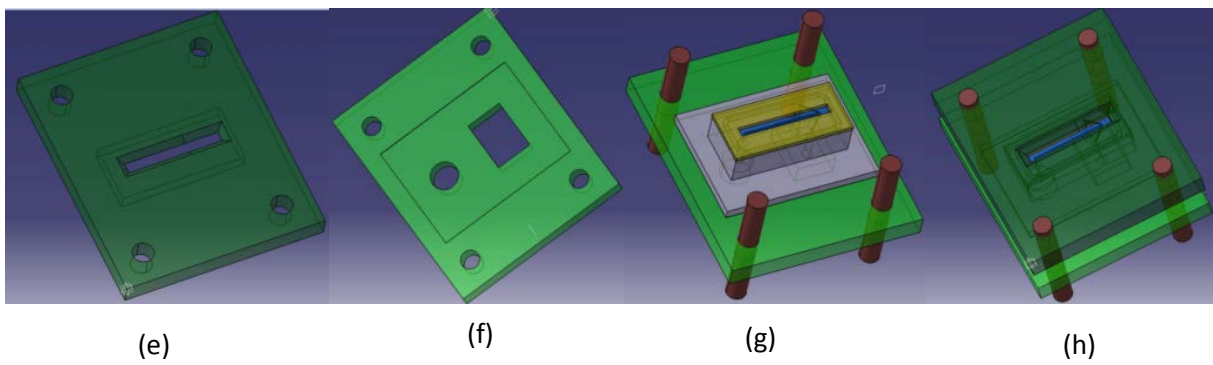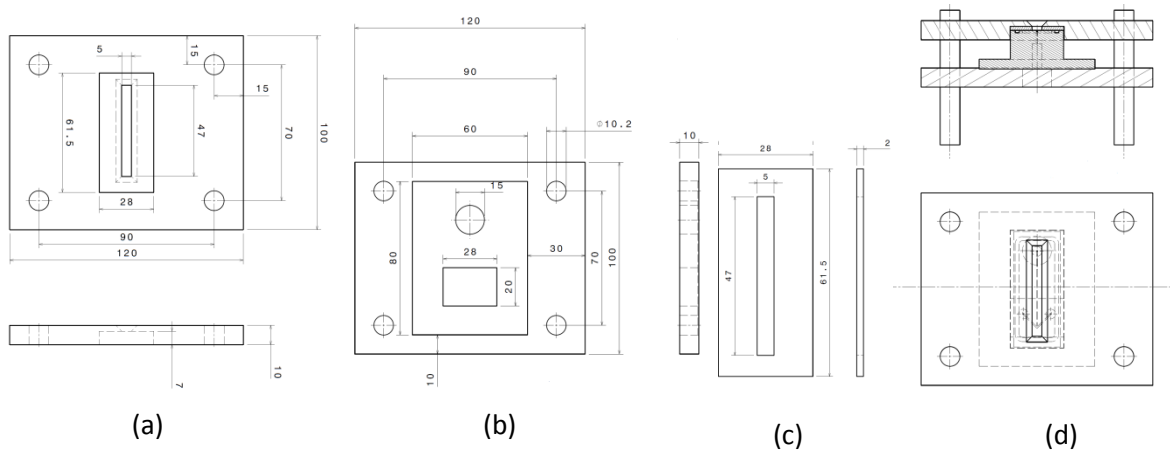Figure 2.5: (a) T-type (b) arrowhead type (c) Y-type microchannels

(a) (b)

(c)

Figure 2.6: (a) Geometry of T-type (b) Geometry of arrowhead type (c) Geometry of Y-type microchannels

(a)   (b)   (c)   (d)

(e)   (f)   (g)   (h)

(i)

Figure 2.7: (a) (e) Upper flange (b) (f)Lower flange (c) (g) PTFE isolation sheet

(d)(h) Assembly (i) Final assembly

We have successfully tested these three microchannels for mixing of titania precursor ($TiOCl_2$) and DMF. We have found in our tests that the Y-shape microreactor leads to better mixing results than the other two. This result is coherent with findings of Valery *et al.* [10] for the two identical liquids at Reynolds number range between 0.01 and 10. So, we selected Y-type microchannel for our further experiments (cf Chapter 3 and Chapter 4).

2.3.2.2 Injection system

NEMESYS low pressure (3 bar) syringe pump was used for injection of reactants in the microchannel. NEMESYS syringe pump provides smooth and pulsation free continuous flow streams. With the help of the user interface software package we used different flow rates for each syringe according to the demand of experiment. Various volumes of liquid can be pumped through this pump. Syringe holder is adjustable according to the diameter of syringe, normally syringe holder allows to hold syringe diameter (outer) from 6mm upto 30mm and piston stroke length is 56mm. In our work we have used onesyringepump for each syringe as shown in Figure 2.8 to pump titanium oxychloride hydrate and DMF.
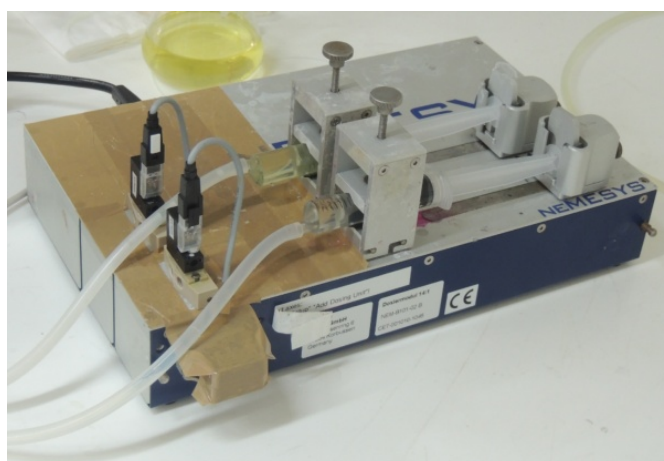

Figure 2.8: NEMESYS low pressure (3 bar) syringe pump

2.3.2.3 IR thermography

FLIR-Titanium SC 7000 was used to analyse the temperature distribution from the top of the microreactor. To monitor the thermal analysis, its user interface Altair package was used which provides thermal video of reaction area throughout the channel. It gives temperature information as a function of pixels. FLIR-Titanium 7000 is equipped with a 50mm lens, 160×128 pixels and a sensitivity of 17 mK. The majority of infrared cameras have a microbolometer type detector, mainly for economical reasons. The one used was equipped with an indium antimonide (InSb) (3-5 μm) matrix photonic detector cooled by a Stirling engine at -196°C (77K). This non-intrusive temperature measurement technique allows us to get thermal analysis information as images or profiles as a function of the distance.The external assembly of the microchannel was black painted. Scale calibration for the distance was performed by capturing one image. In this image two points A and B were selected in the microreactor whose distance is known in millimeters. IR image gives the information between these two points in pixels. We calculated the scaling factor that is needed to convert pixels into millimeters and used for the rest of the calculations.

Figure 2.9: FLIR SC7000 IR Camera

2.3.3 Enthalpy measurement setup

The enthalpy experimental measurement system is shown on Figure 2.10. In addition to the injection system described previously, this setup is composedof the microchannel device and the electrical system (Keithley voltmeter) to measure the voltage of the Peltiercell.

The microreactor was molded in PDMS, the main twisted microchannel having a 216 mm length to allow the characterization of the sol synthesis until its completion (Figure 2.11 a). PDMS is used because it is easy to mold, it is normally chemically neutral with the reagents and is transparent, which allows one to see the solutions. The Figure 2.11 (b) shows the details of elements arrangement to obtain the setup. The PDMS microreactor (2) topped with a Plexiglas block (1) was closed with a silicon plate (4) and then an aluminum one (5) in contact with a 30 x 30 mm^2 Peltier cell (6). The plexiglass (1) the aluminum plates (5) and (7) base allow the system to be tightened and centered.The two aluminum compounds (5) and (7), which are on both sides of the heat flux measuring element (Peltiercell), are equipped with thermocouples. The silicon plate (4) is there for providing the sealing with PDMS while having low thermal resistance. The large steel block (8) serves as a thermal mass. A heat exchanger is cooling this block at 10 ° C. The heater (3), the Peltiercell and the known resistance, are connected to a generator and to a multimeter as shown in Figure 2.10.
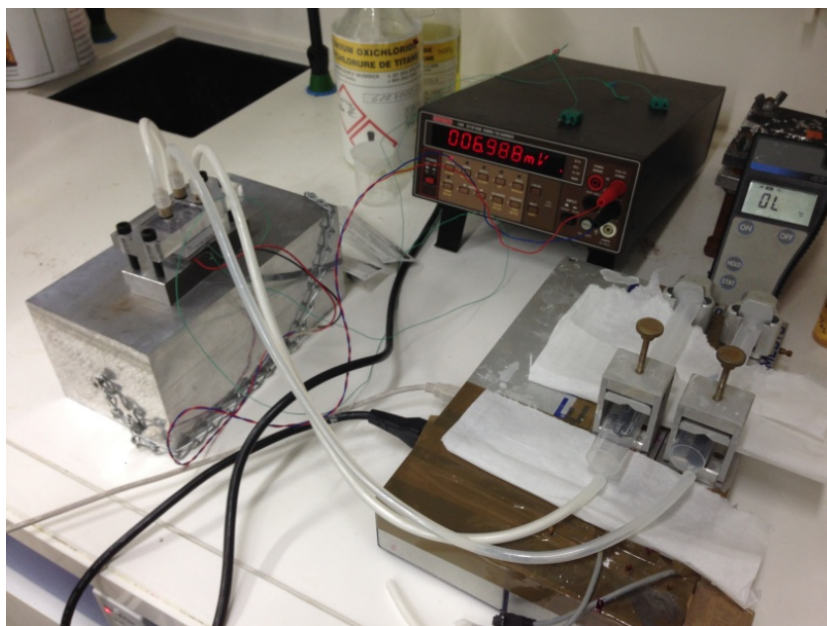
Figure 2.10: Experimental setup for measurement of enthalpy

(a)

PDMS microreactor
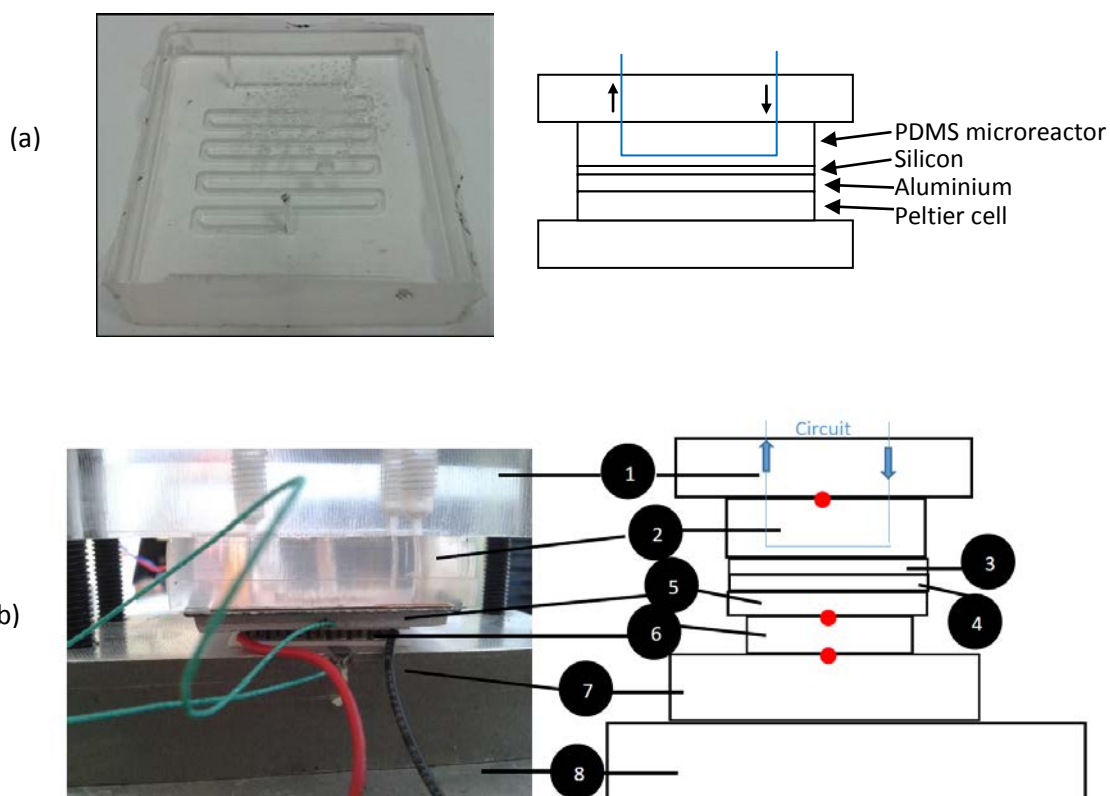Silicon
Aluminium
Peltier cell

(b)

Figure 2.11. (a) 216 mm long microreactor machined inside a PDMS block, (b) experimental setup dedicated to variation of enthalpy measurement: thermocouples (●) (1) Plexiglass (2) PDMS microreactor (3) Heater (4) Silicon plate (5) Aluminum top plate (6) Peltiercell (7) Aluminum base plate (8) Heat exchanger

The calibration of the Peltier cell was performed using a copper etched foil heater. The relationship between heat flux and the voltage of the Peltier cell is shown in Figure 2.12.
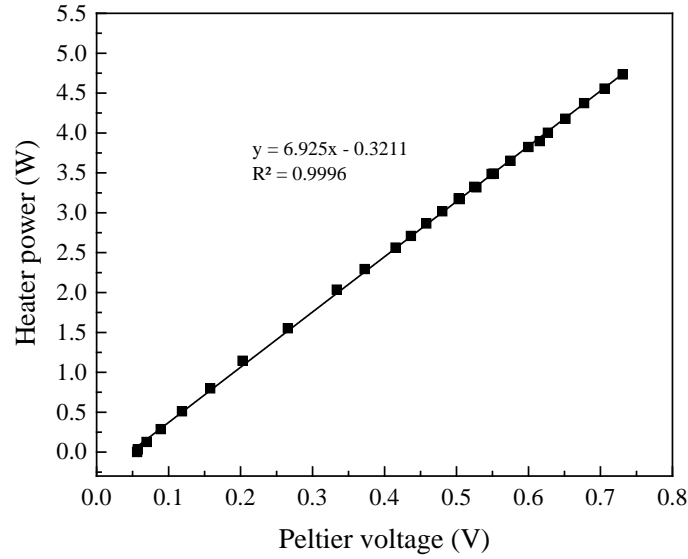

y = 6.925x - 0.3211
R² = 0.9996

Figure 2.12: Calibration of Peltiercell (Power – Voltage correlation)[11]

A correction to the calibration of Figure 2.12 was done because of some heat transferred through PDMS block. The latter was measured thanks to temperature measurement using thermocouples. Actually, given that the thermal conductivity of aluminum and silicon are very large compared to that of PDMS (237 and 14W/mK versus 0.15 W/mK)[11], it is assumed that the temperature of the heater is that measured by the thermocouple above the Peltiercell. The heat losses through the PDMS can be estimated by calculation:

$$\Phi = \frac{\lambda_{PDMS} \times S}{e} \left(T_{top} - T_{PDMS} \right) \qquad\qquad 2.5$$

Then the actual power diffused towards the Peltiercell can be deduced (Figure 2.13).This equation (Φ=6.43xV) will be used to determine the heat flux released by the reaction when we measure the voltage of the Peltiercell.
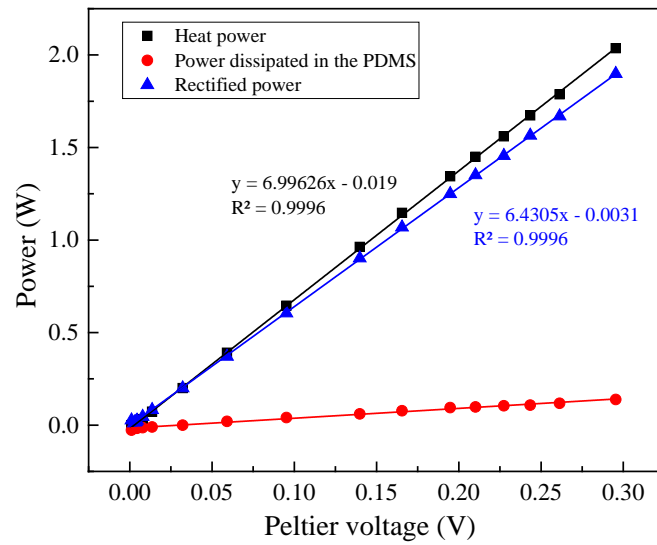
Figure 2.13: Comparison of powers in the system (power-voltage calibration including heat loss)[11]

2.3.4 Active electrical Micromixer

This other experimental setup shown on Figure 2.14 is dedicated to the study of the effect of electrical field on the mixing enhancement and the kinetic of reaction. This system includes the IR Camera and the injection system described previously. A stabilized electrical power supply is used with a function generator to impose an electrical field to the electrodes when they are activated.
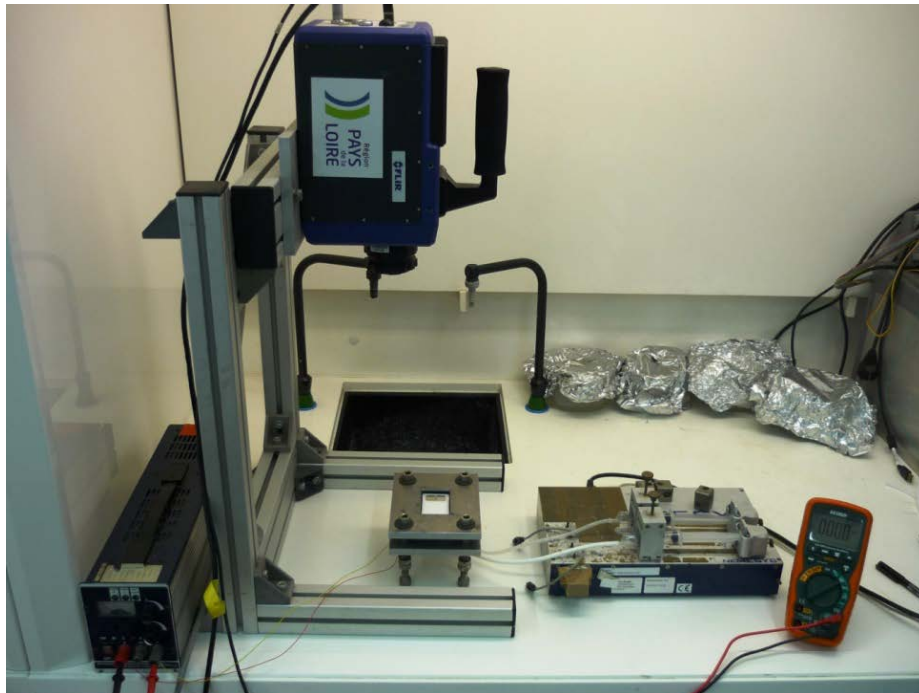

Figure 2.14: Experimental setup of longer microchannel with electrodes.

A long twisted PTFE microchannel allowing to the reaction to be fully completed is constructed. The first one without electrodes has a mixing length of 294 mm as shown in Figure 2.15 (a) and second one with electrodes has a mixing length of 234 mm as shown in Figure 2.15 (b) both with $1\times1mm^2$ cross sectional area.
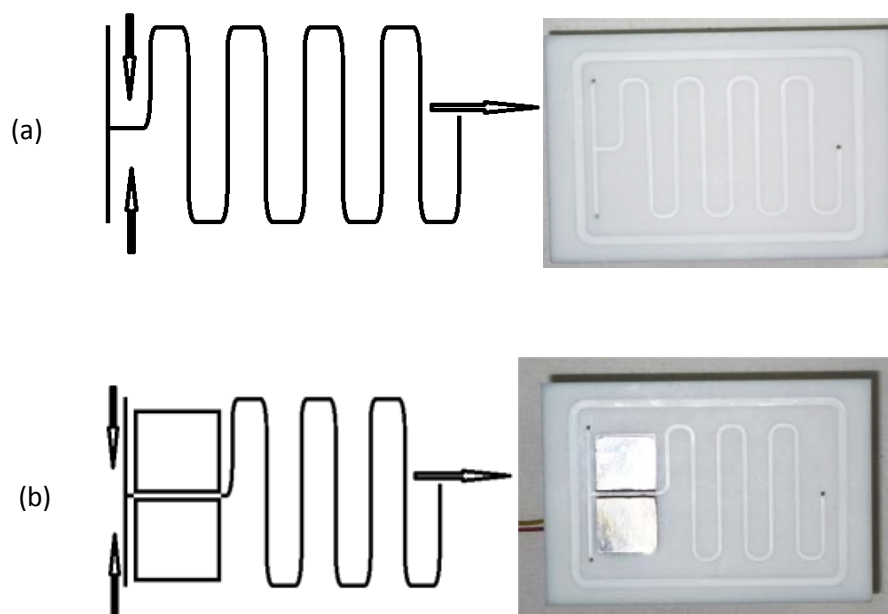

Figure 2.15 (a) 294 mm long microreactor without electrodes (b) 234 mm long microreactor with electrodes.

A 1mm glass sheet was placed on the top of the PTFE microreactor and tightened with upper and lower flanges with rubber isolation as shown in Figure 2.16. The electrodes can be connectedtoa DC or AC voltage generator as shown in Figure 2.14 of experimental setup. In the latter case, frequency and the voltage of the electric field can be varied.
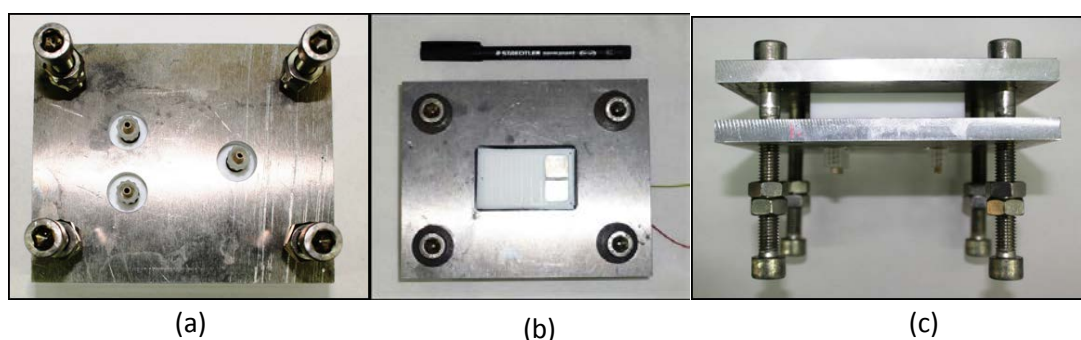

Figure 2.16 (a) Back view of assembly (b) Top view of assembly (c) Side view of assembly

Since the acidity of TiOCl$_2$ is stronger than the acidity of concentrated HCl, a special attention has to be paid to the choice of materials for the electrodes. Due to their insolubility in hydrochloric solution, platinum and gold were selected. Their reactivity was tested by following the weight evolution of pieces of platinum (Pt) and gold (Au) after they were set in

a solution of TiOCl$_2$-DMFfor 1 day. Surprisingly a blue coloration appears in the solution due to the reduction of Ti(IV) to Ti(III) in the presence of gold (Figure 2.17). The associated weight loss remains below 0.10 % and we obtained the values shown in Table 2.3.

Table: 2.3 Mass variations during material test with DMF

Material	Weight Before (g)	Weight After (g)	Difference (g)	% weight
Gold (Au)	45.7487	45.7388	0.0099	0.0022 %
Platinum (Pt)	1.4938	1.4926	0.0012	0.0803 %

Figure 2.17: Platinum (left) and gold (right) during test with DMF

However, according to the image above Figure 2.17, we can see that the gold has reacted with the solution by forming Ti^{+3} (blue), so our decision was to use platinum as electrodes.

2.4 Nanoparticles Analysis

2.4.1 Dynamic Light scattering DLS technique

It is really important to measure size of nanoparticles particles in order to understand and control the product quality and processes. Dynamic light scattering (DLS) is a technique that can be used to measure the size of nanoparticles.

DLSis using the principle of Brownian motion to measure the size of nanoparticles, dispersed in a liquid phase.When the laser beam strikes the suspension, due to the Brownian motion the intensity of scattered light fluctuates and these fluctuations are measured according to time[12].Brownian motion depends on the particle size and viscosity of the solvent. Smaller particles are having faster Brownian motion and large particles are having slower Brownian motion, as demonstrated in Figure 2.18.
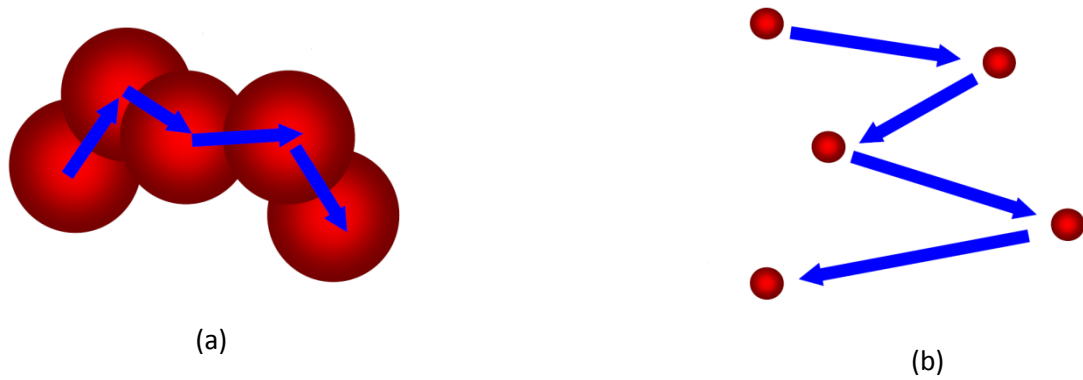
(a)

(b)

Figure 2.18: (a) Small particles - Faster Brownianmotion (b) Large particles-SlowerBrownianmotion[12]

The dynamic information of the nanoparticles are obtained from the autocorrelation function. The correlator is constructing the autocorrelation function, $G(\tau)$, of the scattered intensities of the particles at interval of time and comparing the signals, over a period of time.

$$G(\tau) = \int_0^\infty I(t)I(t+\tau)dt \qquad 2.6$$

where I(t) is the intensity at the moment t, t is the time and τ is the delay time.

This signal is related to the probabilty to find the particle at the same time after the characteristic τ delay time. On certain time when signal correlation starts to decrease it gives information about the mean diameter. When the particles are large and move slowly then the autocorrelation function will decay slowly, as shown in Figure 2.19 (a) . If the particles are smaller and moving quickly then the correlation function will reduce quickly, as shown in Figure 2.19 (b).
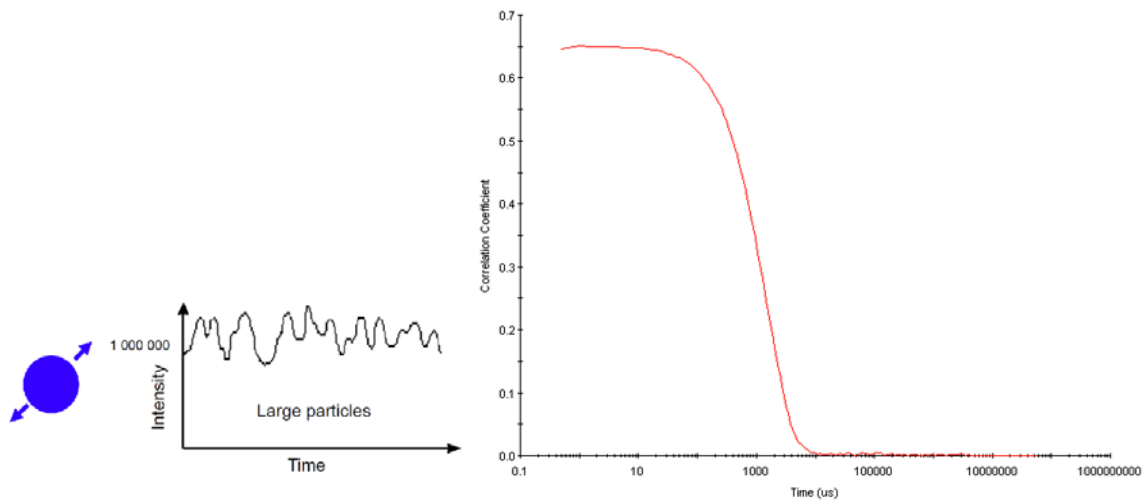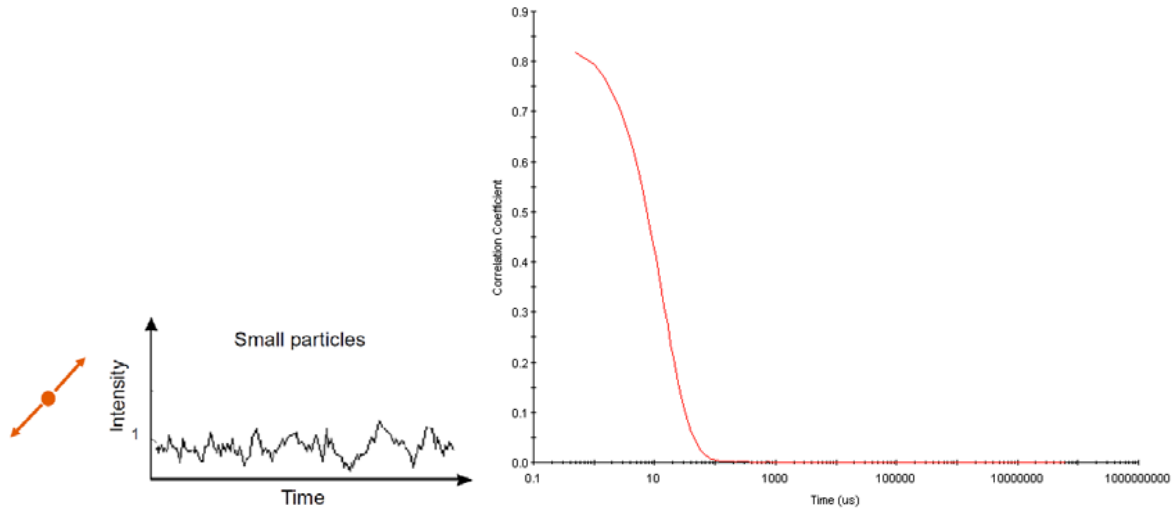
Figure 2.19: (a) Correlogram of large particles (b) Correlogram of small particles

Note that the scattered intensity of large particles may be several orders of magnitude higher that for smaller particles: In Figure 2.19 (a) 6 orders of magnitude larger than in Figure 2.19 (b).

Through various mathematical algorithms in the software fitting the auto-correlation function provides the size distribution of nanoparticles. Mainly there are two fundamental approaches. First one is cumulants analysis and second one is distribution analysis. In cumulants analysis, correlation function is single exponentially fitted with delay time to obtain z-average and polydispersity index, defined by the ISO standards (ISO 13321, ISO 22412). Only initial time delay (short time) of correlogram part is considered in cumulants analysis and larger time delay are totally ignored.

In distribution analysis, correlation function is multiple exponentially fitted with delay time to obtain size distribution of nanoparticles by Non-negative least squares (NNLS). In distribution analysis, both initial decay time (short time) and larger time decay parts of correlogramare considered for the analysis.

From the auto-correlation function fit using algorithm it is possible to have access to the translational diffusion coefficient,D which is linked to the nanoparticles hydrodynamic diameter d_h through the Stokes-Einstein relation (equation 2.6)[12].Once the diffusion coefficient is known then hydrodynamic diameter can be calculated easily according to equation 2.7.

$$D = \frac{kT}{3\pi\eta \, d_h} \qquad\qquad 2.7$$

WhereD is the coefficient of translational diffusion, k is the Boltzmann constant, T is the temperature and η is the dynamic viscosity of solvent of the dispersion (DMF).

The hydrodynamic diameter deduced from DLS measurementstakes into account the double layer surrounding the particles. It is due to the interaction of the particles surface with the ions present in solution. Its thickness is characterizedby the Debye length, 1/K, which can be assessed using the following equation 2.8.

$$K = F\sqrt{\frac{1000 \sum_i \, c_i z_i^2}{\varepsilon\varepsilon_0 RT}} \qquad\qquad 2.8$$

with F the Faraday's constant, c_i the concentration (mol L^{-1}) in the i ion z_i charged, ε and ε_0 the dielectric constant of the solvent and permittivity of vacuum (8.854×10^{-12} C^{2}J^{-1}m^{-1}) respectively and R the constant of perfect gazes. We need to evaluate the dielectric constant of the solvent by taking into account the DMF and water really present in solution. The dielectric constant of mixed DFM-H$_2$O, ε_{mix}, presents a shift with respect to the values deduced from the sum of the dielectric constants of pure solvents weighted by the molar fraction: $\varepsilon_{mix} = xH_2O\varepsilon H_2O + xDMF\varepsilon DMF + \Delta\varepsilon$ with xH_2O and $xDMF$ the molar fractions in water and DMF, respectively, $\varepsilon H_2O = 78.5$ and $\varepsilon DMF = 36.7$, $\Delta\varepsilon$ is extracted from Rohdewald *et al.*[13]. The ionic species present in solution have also to be identified. Similarly to the estimation developed in BoryanaTodorova's PhD[14], we chose to consider that due to polar character of DMF-H$_2$O mixture, the ionic species are coming from the dissociation of hydrochloride acid. In addition here we also considered free dimethylammonium chloride. In the range 1 to 2.5 HCl consumed per Tication, only 0.5 DMACl per Ti were accounted to contribute to the ionic force based on the number of free DMACl for sols prepared in batch (Figure 2.3). Since some of the DMF molecules are complexing the Ti(IV) cation, only the free DMF species were taken into account. Again we also made the assumption that chloride ions are not entering the coordinence of Ti and that the initial formulation of the Ti precursor may be TiO(OH)$_2$, 3.4HCl, 5H$_2$O leading to a final composition of the solvent per Ti close to: 2H$^+$, 2Cl$^-$, 3.6H$_2$O, 2.7DMF, 0.5DMA$^+$, 0.5Cl$^-$ when 1.4 DMF is hydrolysed and 1.4H$^+$, 1.4Cl$^-$, 3H$_2$O, 2.3DMF, 0.5DMA$^+$, 0.5Cl$^-$ when 2 DMF arehydrolysed.Theintermediate calculations are gathered in Table 2.4 for [Ti^{4+}]=1.42 mol L^{-1} and assuming an hydrolysis advancement of 1.4 and 2 hydrolysed DMF/Ti.

Table 2.4: Debye length estimation

xH20	xDMF	eps calc	eps exp	[Ti(IV)] (mol L^{-1})	H+/Ti	Cl-/Ti	DMA+/Ti	2 X ionic force	kappa (m-1)	1/kappa (nm)
0.571	0.429	60.6	51.7	1.42	2.00	2.50	0.50	7.10	7.63E+09	0.13
0.566	0.434	60.4	51.5	1.42	1.40	1.90	0.50	5.40	6.67E+09	0.15

In both cases, it is worth noting that the Debye length is very short and in the following,the size of the particles can and will be assimilated to the hydrodynamic diameter obtained by DLS.

2.4.1.1 Common terms used in DLS analysis.

i. Z-Average

It is also called cumulants mean and it is hydrodynamic parameter, if the sample is monodisperse then it shows only one peak distribution. If the sample is polydisperse then it shows more than one peak distribution in the sample. Therefore, in case of polydisperse sample z-average will be mean of all the peaks distributions available in the sample, which is not very representative of the sample.

ii. Polydispersity Index

Polydispersity index is a dimensionless number which indicates the quality of sample. PDI is calculated from the cumulants analysis of the intensity autocorrelation function. If PDI is greater than 0.7 then it means that distribution is very much wider and not suitable for DLS analysis. PDI values below than 0.7 are much favorable for DLS analysis. In case of highly monodisperse sample PDI value is even lesser than 0.05 which is very rare.

PDI is calculated with this formula

$$PDI = (\frac{\sigma}{d})^2$$

Where σ is standard deviation and d is is diameter of concerned distribution or the z-average value of the hydrodynamic diameter.

iii. Y-Intercept or Intercept

Y-Intercept of the autocorrelation function is used to evaluate the quality of the data. It is the signal to noise ratio from the measured sample. Intercept values lie between 0 and 1. Values between 0.6 and 0.9 are considered for good signals. If the values are between 0.9 and 1 then the signals are considered as best. Lower than 0.6 signals are not considered as good.

iv. Intensity and Volume distribution

Intensity size distributions of the particles are the first order results from DLS experiments. If the intensity distributions show narrow peaks then it can be converted into volume distribution by using MIE theory.Somewhat intensity distribution can be misleading because sometimes of the presence of large particles, aggregation/agglomerations dominate in the size distributions results. Indeed larger particles will diffuse light largely whereas even if more numerous in volume,the intensity diffused by smaller onescan be of severalorder of magnitude lower. In such case,intensity distribution consists of several peaks, as shown in Figure 2.20. Figure 2.20 shows the existence of two different size distribution, one at 20nm size and another at 2610nm size. Volume distribution gives more realistic results with a single peak, as presented in Figure 2.21. Which shows the percentage of volume at certain size, as 17nm size in Figure 2.21. In volume distribution, large particles representing a very low proportion in the solution are infact negligible.
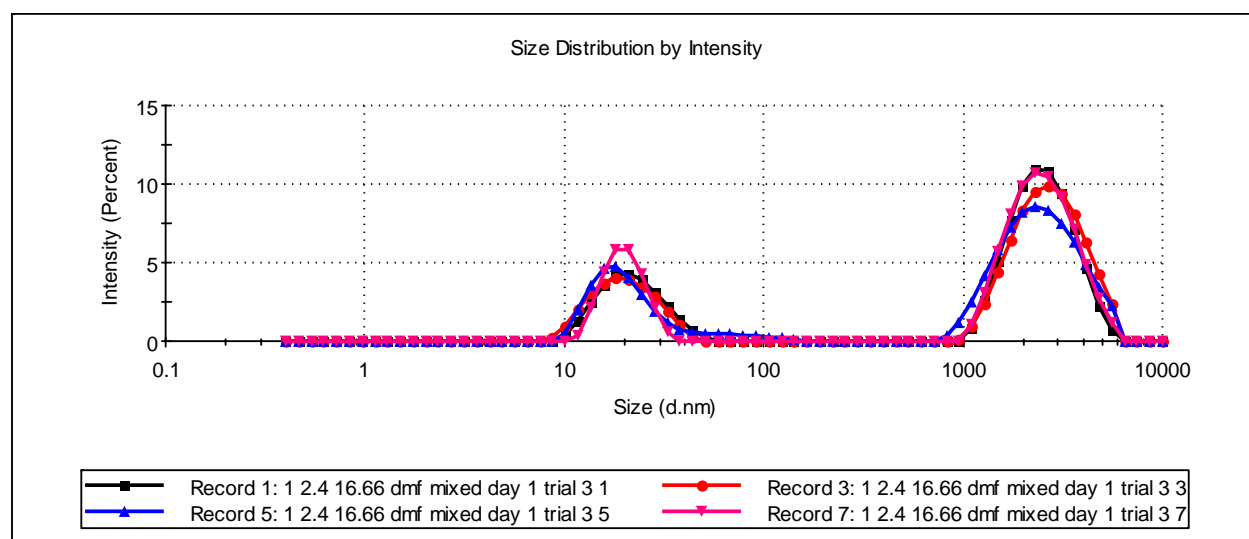

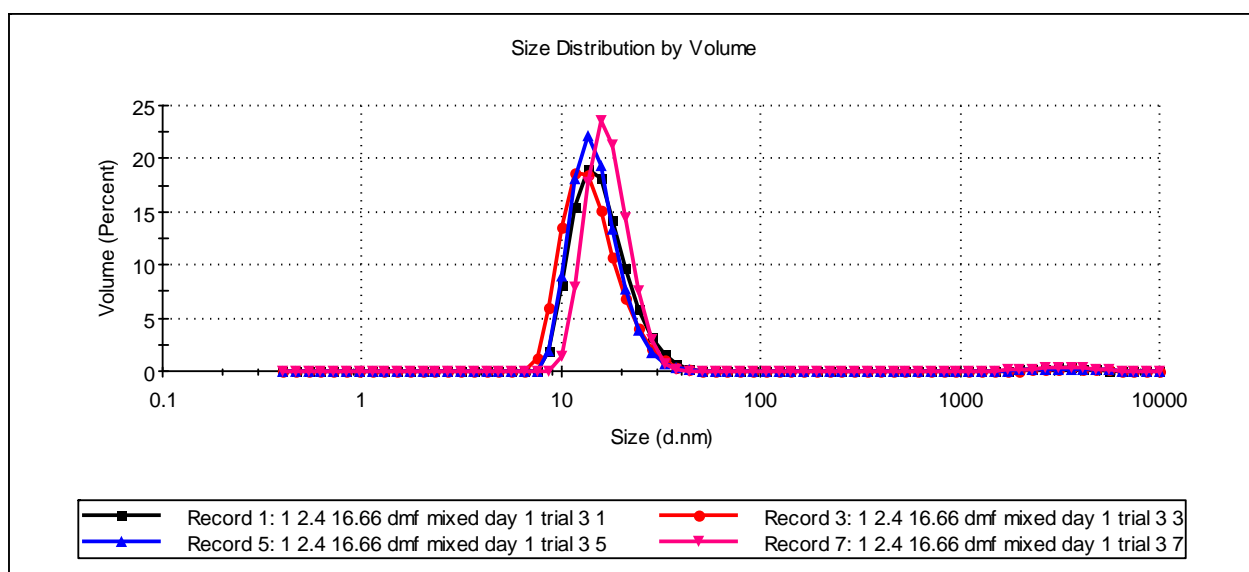Figure 2.20: Size distribution of nanoparticles by Intensity

Figure 2.21: Size distribution of nanoparticles by volume

In order to get the representative size for the volume distribution, the volume distributions were fitted according to a Log normal distribution formula (equation 2.9).

$$y = yo + \frac{A}{\sqrt{2\pi}wx} e(-(ln\,{}^{x}/{}_{xc}))^{\frac{2}{2w^2}} \qquad\qquad 2.9$$

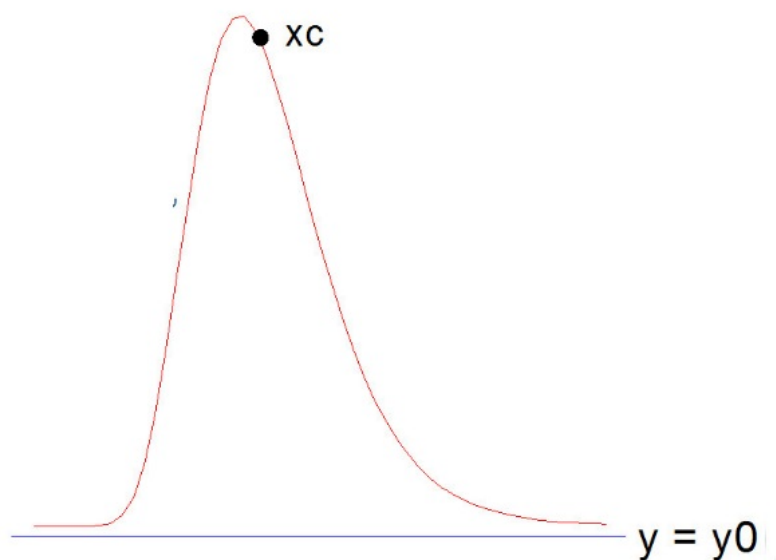with x_c the position of the peak, w the standard deviation, y_0 the baseline.

Figure 2.22: Peak position in Lognormal distribution

2.4.1.2 Sample preparation

Size measurements of nanoparticles were performed using Malvern Zetasizer Nano ZS equipped with He-Ne laser (633nm) with the detection angle of 173°(backscattered diffuse light) shown in Figure 2.22.Solutionswerefiltered with 0.2µm filter to remove dust and large particles. Filtered solutionswerecollected in polystyrene cuvettes (maximum 4 mL) which were let for 3 minutes at the measurement temperature (25°C) to reach equilibrium. In thezetasizer user interface,$TiO_2$was selected as the diffusingmaterial with refractive index equal to 2.750 and absorption at 633 nm equal to 0.DMF was selected as dispersant solvent with refractive index of 1.420 and viscosity of 0.8020 mPa sat 25°C. All the measurement were repeated atleast 6 times on the same sample to check the reproducibility.
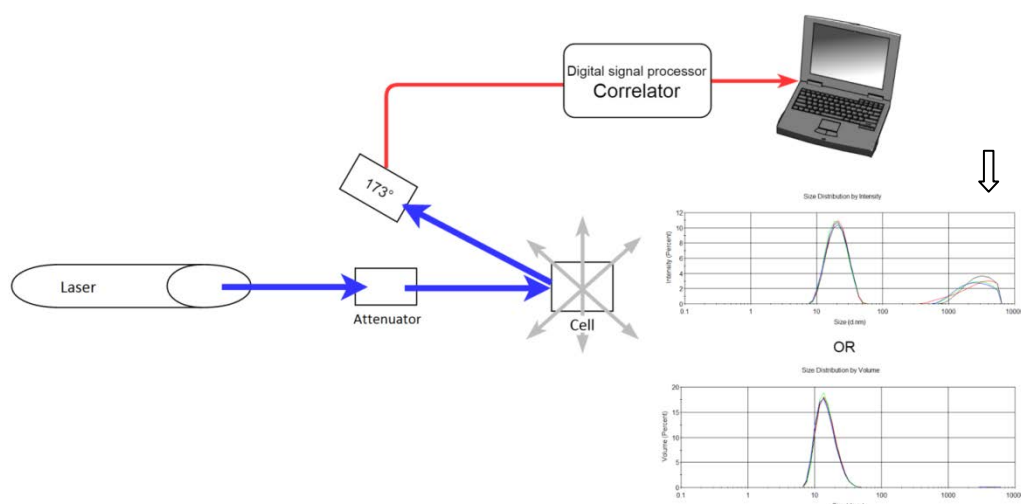

Figure 2.22: Principle of DLS measurement

2.4.2 F.T Raman Spectroscopy

2.4.2.1 Principle of F.T Raman spectroscopy

Raman spectroscopy is a light scattering technique. This technique was named after an Indian physicist Sir Chandrasekhara V. Raman. As mentionedin 2.2.2, FT Raman scatteringis used to study the chemical composition and complexion of the organic part as a function of time.It is non destructive analysis and it is an inelastic light scattering technique. Small volume of sample is needed for the analysis, minimum 5mL volume stored in glass vials. Laser light strikes the solution and the light scattered in all the direction passes through lens to interferometer which converts all the signal into interferogram. Laser excites molecules at virtual electronic level and when they are coming back to theirfundamental level then they are emitting laser light, that's what contributes to the signals. Fourier transform algorithm is used to convert these signals into Raman spectrums as shown in Figure 2.24.

Raman spectroscopy makes it possible to determine the composition of a material by analyzing the photons emitted after the excitation of the atoms of the compound by an incident light ray via vibrational levels. In Raman spectroscopy, the energy of the incident photon is greater than the energy required for the atom to pass into a first excited state (Figure

2.24). In this case, the system reaches a fictitious higher energy level, called a level of dressed material. The system then de-energizes by emitting a photon. It is these photons re-emitted by the material which are collected and used to plot a spectrum representing the intensity of the received signal as a function of the number of waves of the photons detected.

Three different de-excitation modes are possible (Figure 2.23): if the material returns to its initial state, then the photon emitted are identical to the absorbed photon, this corresponds to an elastic light scattering. If the material de-energizes at an energy level lower than the level it occupied before absorption, then the photon emitted has a greater energy than the absorbed photon: it is an inelastic scattering of the Anti-Stokes type. Finally, if the material returns to a more energetic state than that which it initially occupied, then the emitted photon has a lower energy than that of the incident photon. In this case, it is an inelastic scattering of Stokes.
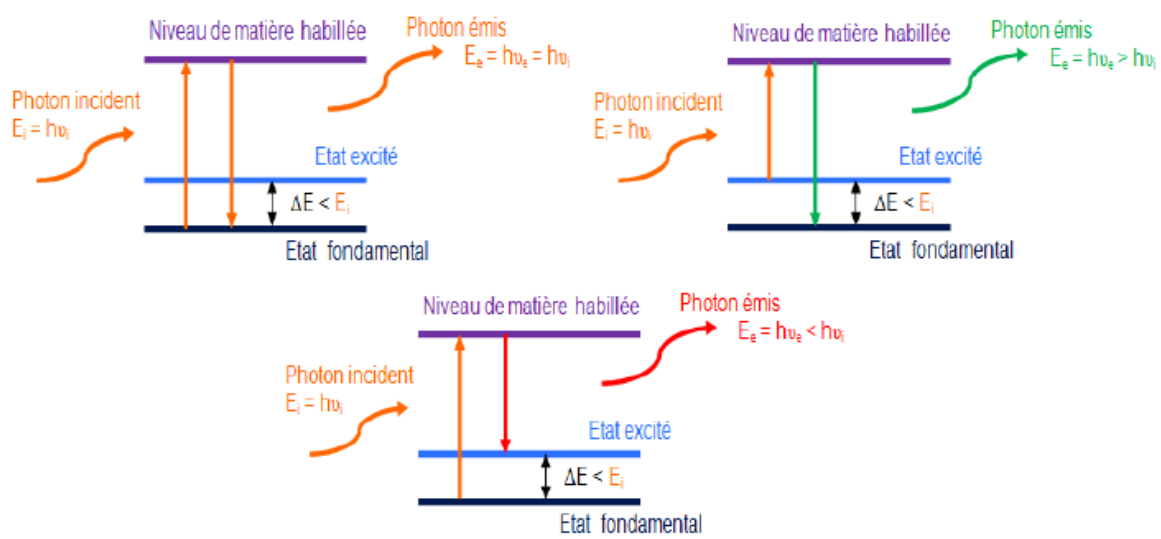

Figure 2.23: Principle of Raman Spectroscopy: After having been excited by a light wave (Ei) more energetic than the energy difference between the ground level and the excited level (ΔE), the system can return to equilibrium according to three Modes of de-excitation, and the energy of the emitted photon (Ee) depends on these modes. At the top left, the diffusion is elastic (Ee = Ei), on the right the diffusion is inelastic Anti-Stokes (Ee>Ei), and at the bottom the diffusion is inelastic Stokes (Ee<Ei) [15].

All theramanspectra were obtained using Bruker Multiram FT Raman spectrometer with a laser wavelength of 1064nm and power of 300mW. All the spectra were decomposed and fitted to extract thedata of the different peaks in CASA XPS (Computer Aided Surface Analysis for X-ray Photoelectron Spectroscopy). The spectra are quantified in terms of areas and positions in the region of interest extending from 450 to 1000 cm^{-1}, according to a procedure previously reported [5].
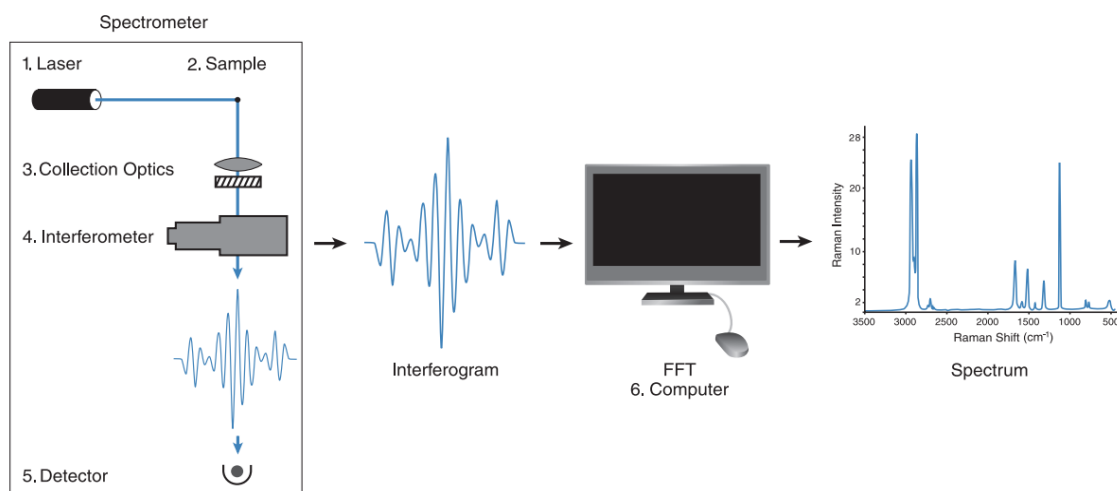
Figure 2.24: Working principle of FT Raman spectroscopy

2.4.2.2 Calibration of selected band area andanalytical method

As explained in previous section 2.2.2 one of the ways to follow the hydrolysis of DMF to DMACl is to focus Raman spectra on the vibrating bands at 866cm^{-1} ($v_s(C'_2N)$ of DMF) and 891 cm^{-1}. ($v_s(CN)$ of DMA^+). The sensitivity factors were determined for Ti/DMF=6.4 by SolèneBéchu[6]. However, it is necessary to get the evolution of the sensitivity factors for the different ratio tested i.e. Ti/DMF=7.9 corresponding to the case of pre-diluted TiOCl$_2$ for which [DMF] is 9.81 molL^{-1}.The calibration solutions for [DMF] ranging from 9.5 to 12 $mol\ L^{-1}$ were prepared and analysed by SolèneBéchu during her PhD, which is demonstrated in Figure 2.25.

Standard pure Titania solution and diluted solution with DMF at various concentrations are shown in Table 2.5. Table 2.5 also shows the concentration of titania and DMF when pre-diluted solution and DMF are mixed in microreactor at 2.4 flow rate ratios.

Table 2.5: Standard concentration (Pure Titania and DMF)

Solution	Reactants	Volume (mL)	Density of the mixture	Conc ($mol\ L^{-1}$)	DMFtot/Ti
Pure Solution	TiOCl$_2$	5	1.1698	1.53	6.2
	DMF	12		9.46	
Pre-diluted solution	TiOCl$_2$ + 16.7% of DMF	20	1.473	4.21	0.52
	DMF	4		2.17	
After mixing	TiOCl$_2$ + 16.7% of DMF	Flow rate ratio = 2.4		1.24	7.9
	DMF			9.81	

Evaluation of the sensitivity factors for the peaks of interest (DMF at 660 and 866 cm^{-1}and DMACl at 890 cm^{-1}) as a function of the concentration in DMF is plotted in Figure 2.26.To follow the exact hydrolysis, we used sensitivity factor from Figure 2.26 which is used in Chapter 5 in Raman analysis section.
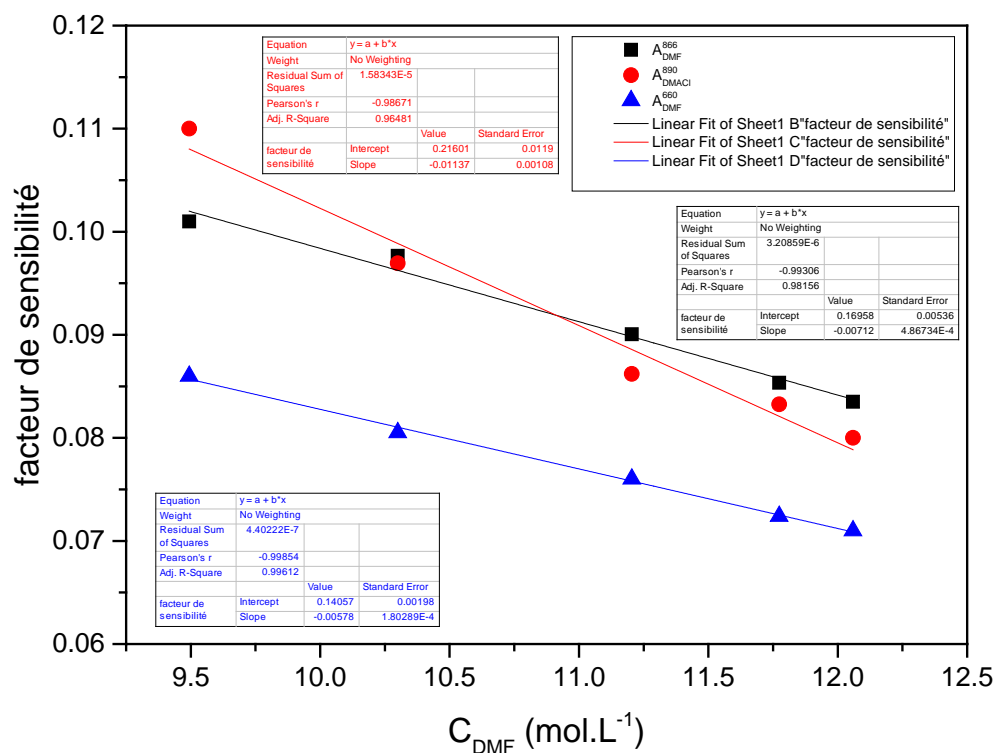
Figure 2.25: Sensibility factors at various DMF concentrations.

Following Table 2.6 shows the sensitivity factor values for pure TiOCl$_2$ and pre-diluted solution.

Table 2.5: Sensitivity factor of various concentrations.

	[DMF]mol L^{-1}	J890 DMA mol L^{-1}	J866DMFmol L^{-1}	J660DMFmol L^{-1}
PureTiOCl$_2$	9.46	0.108	0.101	0.086
Pre-dilutedTiOCl$_2$ (with 16.7% of DMF)	9.81	0.104	0.099	0.084

2.5 Conclusion

In this work, microreactors have been used to perform the synthesis of titanium based sol. Mainly three type of microreactors were used which are Y-shape 32 mm long microchannel, 234 mm long microchannel (without electrodes) and 234 mm long microchannel (with electrodes). Initially Y shape microchannel was selected on the basis of better mixing results than the others two (arrow head microchannel and T shape microchannel), this result is coherent with findings of Valery *et al*. work[10]. 234 mm longer microchannel was used to follow the reaction till the end. Other 234 mm long microchannel with electrodes was used to improve mixing. All the microchannels specifications and components of experimental setup are presented in this chapter. Sol is obtained by the hydrolysis of $TiOCl_2 \bullet 1.4\ HCl \bullet 7H_2O$ in the presence of N, N-dimethylformamide $((CH_3)_2NCOH$, denoted DMF) as a function of the aging time, this hydrolysis leads to obtaining sols consisting of nanoparticles dispersed in the solvent. To analyse the sol characteristics, DLS and Raman techniques were used. Both techniques are also discussed in this chapter with various terms to follow the nanoparticles formation and any evolution of the chemical composition and complexation of the solid part by organic species arising from DMF and the by-products of its hydrolysis.

References:

[1]   A. Rouet, *De la polycondensation des oxydes de titane à la génération d'une photobatterie*. Université de Nantes, 2005.

[2]   T. Cottineau, "Sols et gels photosensibles à base d'oxyde de titane pour applications photovoltaïques," Thèse de doctorat, Université de Nantes, France, 2007.

[3]   G. Guignard, "Vers la réalisation d'un prototype de photo-batterie à base de sols-gels d'oxyde de titane photosensibles," Université de Nantes, Nantes, France, 2014.

[4]   B. G. Challis and J. A. Challis, "Reactions of the carboxamide group," in *Amides (1970)*, J. Zabicky, Ed. John Wiley & Sons, Ltd., 1970.

[5]   T. Cottineau, M. Richard-Plouet, J.-Y. Mevellec, and L. Brohan, "Hydrolysis and Complexation of N,N-Dimethylformamide in New Nanostructurated Titanium Oxide Hybrid Organic–Inorganic Sols and Gel," *J. Phys. Chem. C*, vol. 115, no. 25, pp. 12269–12274, juin 2011.

[6]   S. Béchu, "Etude et caractérisation de couches minces photosensibles organique-inorganique à base de titane pour la conversation de l'energie solaire," Université de Nantes, Nantes, 2017.

[7]   T. C. Jao, I. Scott, and D. Steele, "The vibrational spectra of amides—Dimethyl formamide," *J. Mol. Spectrosc.*, vol. 92, no. 1, pp. 1–17, Mar. 1982.

[8]   A. Bodiguel, "Optimisation de la synthèse de sol-gel nanostructurée dans un microréacteur," Rapport de stage DUT, 2014 2013.

[9]   K. F. Jensen, "Silicon-Based Microreactors," in *Microreactor Technology and Process Intensification*, vol. 914, 0 vols., American Chemical Society, 2005, pp. 2–22.

[10]   V. Rudyak and A. Minakov, "Modeling and Optimization of Y-Type Micromixers," *Micromachines*, vol. 5, no. 4, pp. 886–912, Oct. 2014.

[11]   A. Bodiguel, S. A. Channa, B. Garnier, M. Richard-Plouet, A . Ould el Moctar and L. Brohan "Optimisation de la synthèse de sols-gels d'oxyde de titane nanostructuré pour le stockage photochimique de l'énergie solaire : Intensification du mélange et suivi dans un microréacteur," Université de Nantes, Nov. 2014.

[12]   B. J. Berne and R. Pecora, *Dynamic Light Scattering: With Applications to Chemistry, Biology, and Physics*. Courier Corporation, 2000.

[13]   P. Rohdewald and M. Moldner, "Dielectric constants of amide-water systems," *J. Phys. Chem.*, vol. 77, no. 3, pp. 373–377, Feb. 1973.

[14]   B. Todorova, *Propriétés physico-chimiques de solutions colloïdales photosensibles à base d'oxyde de titane*. Université de Nantes, 2009.

[15]   C. Vaillant, Synthèse et etude des propriétés optiques de couches de TiO_2-SiO_2, mémoire, Université de Nantes, 2017

Chapter 3

Fluid flow and thermal analysis

3.1 Pure Solution

All the measurementswere performedwith the experimental setup described in section 2.3.2 (Figure 2.4) by using the Y-shape microchannelpresented in Figure 2.5. The first experiments were realized with the injection of pure $TiOCl_2$and N,N-dimethylformamide (DMF) into the 32mm long Y shape microchannel.$TiOCl_2$ and DMFwere transferred to the pumping syringes and both syringes were loaded in the syringe pump system. Various experiments were performed as shown in Table 1. A constant flow rate between 0.05 and 0.3 mL $h^{-1}$was used for$TiOCl_2$ and between 0.12 and 0.72 mLh^{-1} for DMF with a flow rate ratio of 2.4. The values of Reynolds number were calculated by using equation 1.1 which was presented in section 1.3. Residence time for each solution was calculated by using equation 1.2, described also in section 1.3.

Temperature elevationdue to the exothermic effect inside the microchannelwas monitored by IR camera. Figure 3.2 (a) shows the IR image (taken from IR video) of the reaction which occurred inside the microchannel when $TiOCl_2$ and DMF were injected at 0.1 mL h^{-1} and 0.24 mL h^{-1} respectively. The flow in the microchannel was systematically discontinuous, pulsating and unstable. An illustration is provided by Figure 3.2 (a) where several hot spots can be observed. Figure 3.2 (b) shows the temperature distribution along the microchannel which is obtained from IR image by selecting a linear line along x-axis in the middle of the channel while y-axis shows the temperature increase. One can see a discontinuous temperature evolution along the main microchannel. The same observation was also noticed for the other flow rates as shown in Figure 3.3 and 3.4

Table 3.1: Experiments performed on pure $TiOCl_2$ and DMF in a Y shape microreactor

Pure $TiOCl_2$		DMF		Residence time for 1 mL Volume (minutes)
Flow Rate (mL h^{-1})	Reynolds Number	Flow Rate (mL h^{-1})	Reynolds Number	
0.05	$49.9\ 10^{-5}$	0.12	$5.7\ 10^{-5}$	352.9
0.075	$74.9\ 10^{-5}$	0.18	$8.5\ 10^{-5}$	235.2
0.1	$99.9\ 10^{-5}$	0.24	$11.4\ 10^{-5}$	176.5
0.2	$199.8\ 10^{-5}$	0.48	$22.8\ 10^{-5}$	88.2
0.3	$299.7\ 10^{-5}$	0.72	$34.3\ 10^{-5}$	58.8

Preliminary numerical simulation of fluid flow in a microreacteor performed by Badri in 2015 (not published) revealed that the instabilities were not due to the viscosity discrepancy of both reactants. One explanation for the instabilities could be the lack of miscibility of both reactants. These instabilities of the flow inside the microreactor does not constitute optimal conditions for nanoparticle production in a well-controlled manner. Therefore it was very important to find a way to overcome this instability problem. For this purpose, $TiOCl_2$ was diluted with various solvents before injection into the microreactor. The results are reported in the next section.

Otherwise, for each experiment, a minimum of 10 mL solution was collected at the outlet of the main microchannel then it was stirred for 2 to 3 minutes before analysis of the nanoparticle by DLS and Raman technique. Results will be presented in chapter 5.
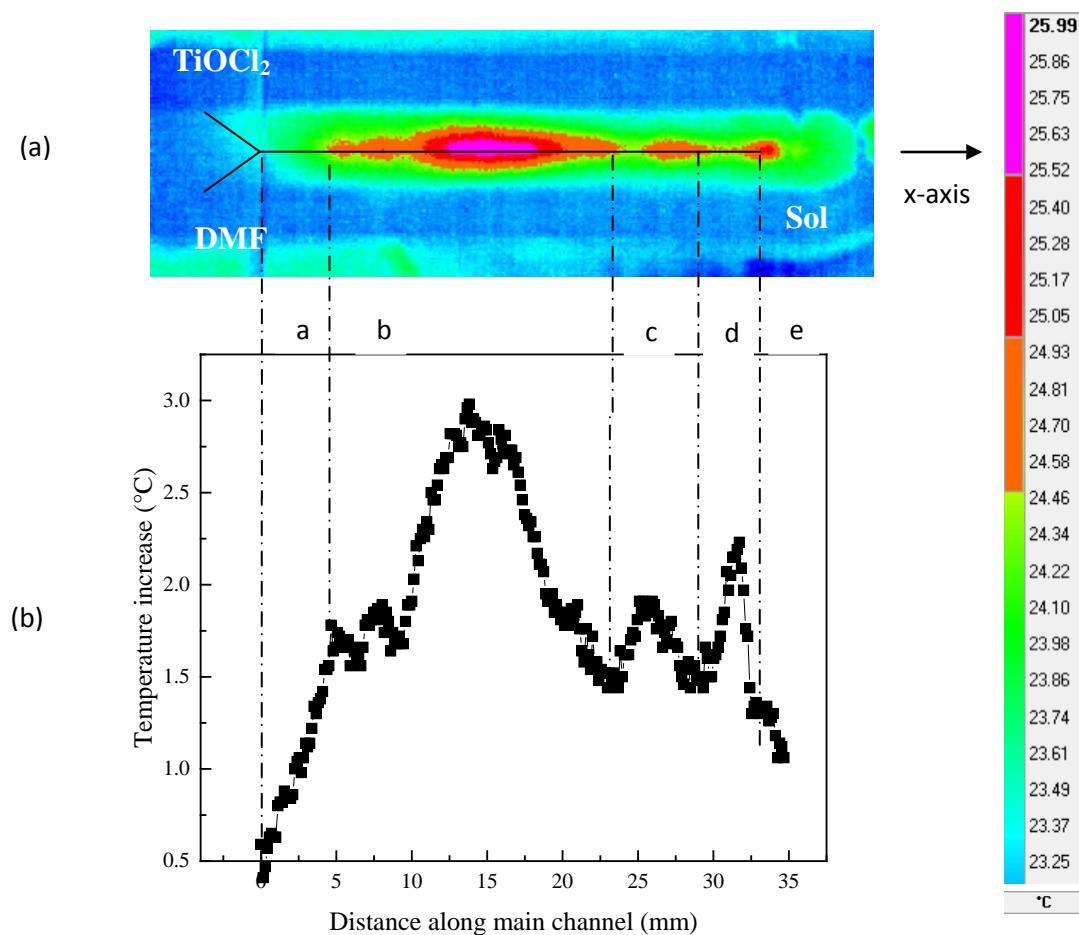
Figure 3.2 Mixing of the pure TiOCl$_2$ (at 0.1 mL h^{-1}) and DMF (at 0.24mL h^{-1}): (a) IR image of the exothermic reaction inside the microreactor and (b) Temperature distribution along the main microchannel (x-axis)
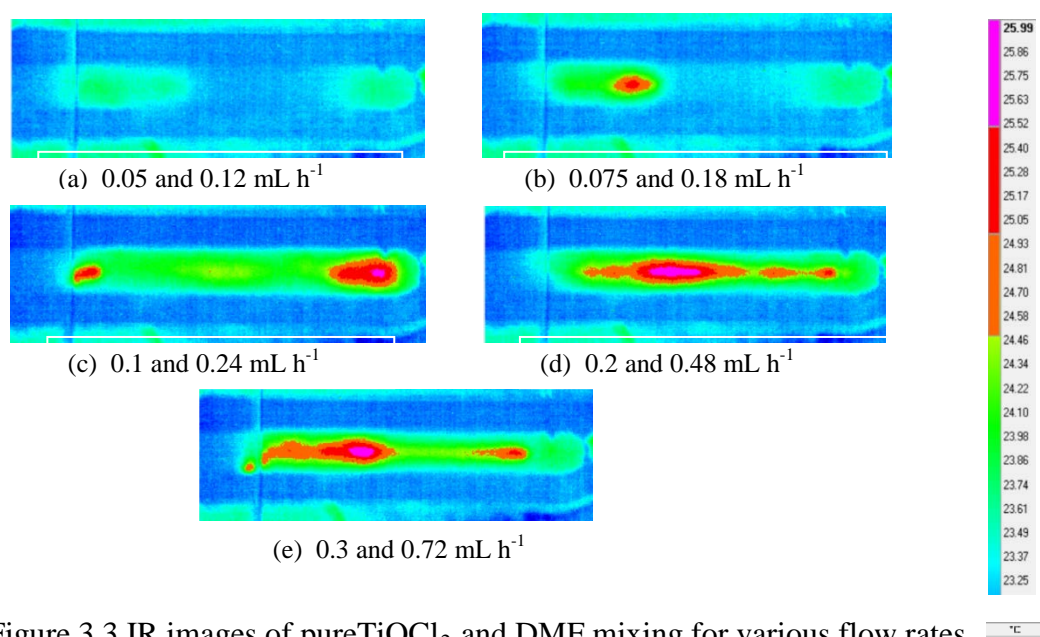

(a) 0.05 and 0.12 mL h^{-1}

(b) 0.075 and 0.18 mL h^{-1}

(c) 0.1 and 0.24 mL h^{-1}

(d) 0.2 and 0.48 mL h^{-1}

(e) 0.3 and 0.72 mL h^{-1}

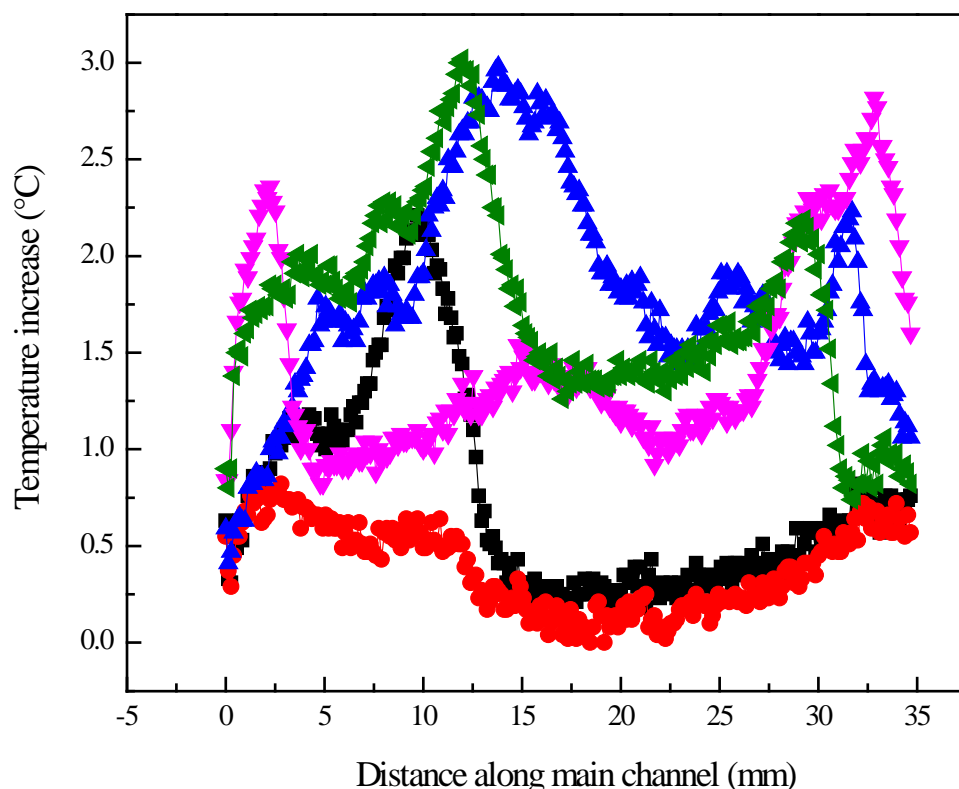Figure 3.3 IR images of pureTiOCl$_2$ and DMF mixing for various flow rates

Figure 3.4 Temperature distribution in the Y- shape microreactor for the mixing of pure TiOCl$_2$ and DMF

Flow rates: 0.05 and 0.12 mL h^{-1} (▬■▬), 0.075 and 0.18 mL h^{-1} (▬●▬), 0.1 and 0.24 mL h^{-1} (▬▲▬), 0.2 and 0.48 mL h^{-1} (▬▼▬), 0.3 and 0.72 mL h^{-1} (▬◄▬)

3.2 Diluted solution with various solvents

To obtain stable and continuous flow, TiOCl$_2$ was diluted before entering in the microchannel with different solvents like water, 1-propanol, 1,2-propanediol, 1-octanol, 2-propanoland N,N-dimethylformamide. Several experiments were performed with these solvents and for different values of reactantflow rates as shown in Table 3.2.

We started our pre-dilution tests by diluting TiOCl$_2$ with 16.7% of water. It was observed by IR images that the fluid flow is still discontinuous, pulsating and unstable as shown in Figure 3.5(a).Figure 3.5 (b) shows the temperature distribution along the microchannel at 0.1 and 0.24mL h^{-1} for diluted TiOCl$_2$ with water and DMF respectively which indicates also the discontinuity of the temperature distribution.

Table 3.2: Different solvents used to pre-dilute $TiOCl_2$ at 16.7 % in volume mixed with DMF and a 2.4 flow rate ratio between both reactant flow rates and various flow rates used in the experiments

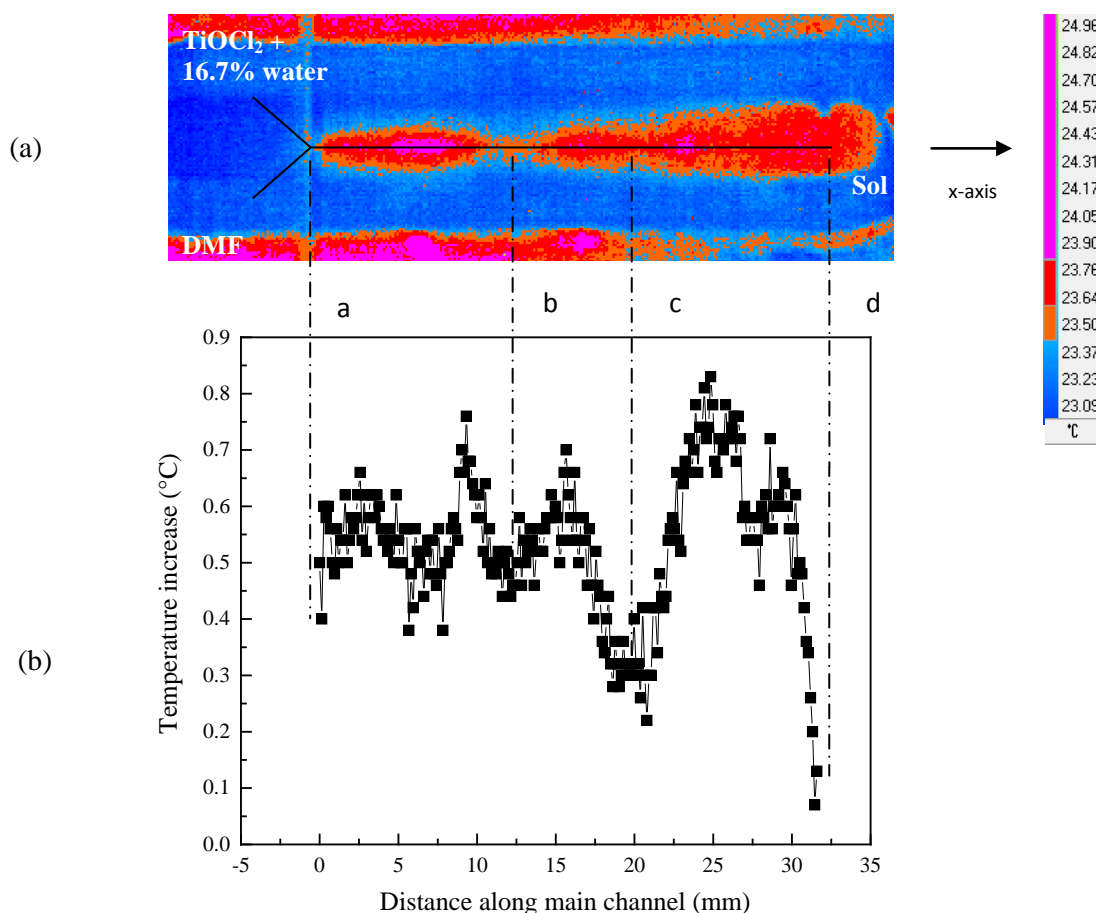| Solvent for $TiOCl_2$ predilution	Flow rates range for $TiOCl_2$ and DMF (mL h^{-1})
Water	$TiOCl_2$ (0.1 – 0.6) and DMF (0.24 – 1.64)
1-propanol	$TiOCl_2$ (3.5 – 7) and DMF (8.4 – 16.8)
1,2-propanediol	$TiOCl_2$ (0.4 – 8) and DMF (0.96 – 19.2)
1-octanol	$TiOCl_2$ (0.4 – 7) and DMF (0.96 – 16.8)
2-propanol	$TiOCl_2$ (1.5 – 12) and DMF (3.6 – 28.8)

Figure 3.5 Mixing of diluted $TiOCl_2$ with water (at 0.1 mL h^{-1}) & DMF (at 0.24mL h^{-1})(a) IR Image of the exothermic reaction inside the microreactor (b) Temperature distribution in the Y- shape microreactor

After that, we havetestedsome other solvents with various flow rates as mentioned in Table 3.2. It was observed by IR images as shown in Figure 3.6 that the fluid flow was still a little bit pulsating and discontinuous except in the case of 2-propanol. Figure 3.7 (a) shows the IR image of the reaction when diluted $TiOCl_2$ with 2-propanol and DMF were injected at 5 mL h^{-1} and 12 mL h^{-1} respectively and it shows that the flow in the channel was very stable and continuous without any pulsating phenomenon.
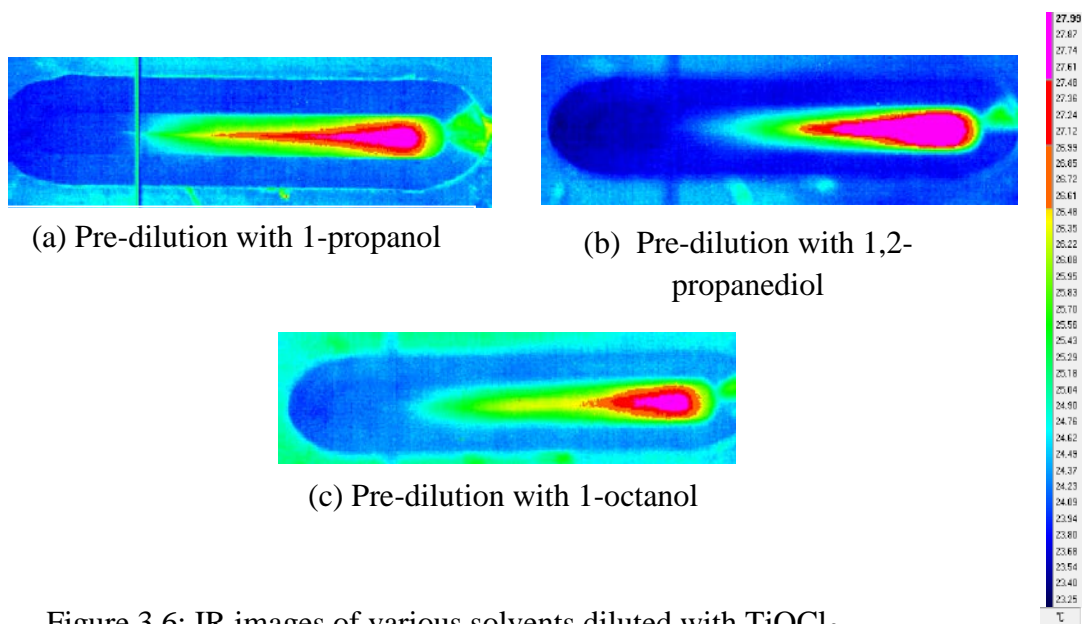
(a) Pre-dilution with 1-propanol

(b) Pre-dilution with 1,2-propanediol

(c) Pre-dilution with 1-octanol

Figure 3.6: IR images of various solvents diluted with $TiOCl_2$
(6 mLh^{-1}flow rates for diluted $TiOCl_2$and 14.4 mLh^{-1} for DMF)

The stability was retained for 2-propanol for all the flow rates from 1.5 to12 mL h^{-1}for diluted $TiOCl_2$ with 2-propanol and 3.6 to28.8mL h^{-1}for DMF with a 2.4 flow rate ratio, as demonstrated in Figure 3.7.Figure 3.8 shows the temperature evolution along the microchannel for various flow rates which exhibits a continuous increase in temperature inside the microchannel due to exothermic reaction. It seems that there is no influence of the reactant flow rates using 2-propanolas solvent, the increase in temperature extends all along the channel to reach +4°C to +5°C approximately.
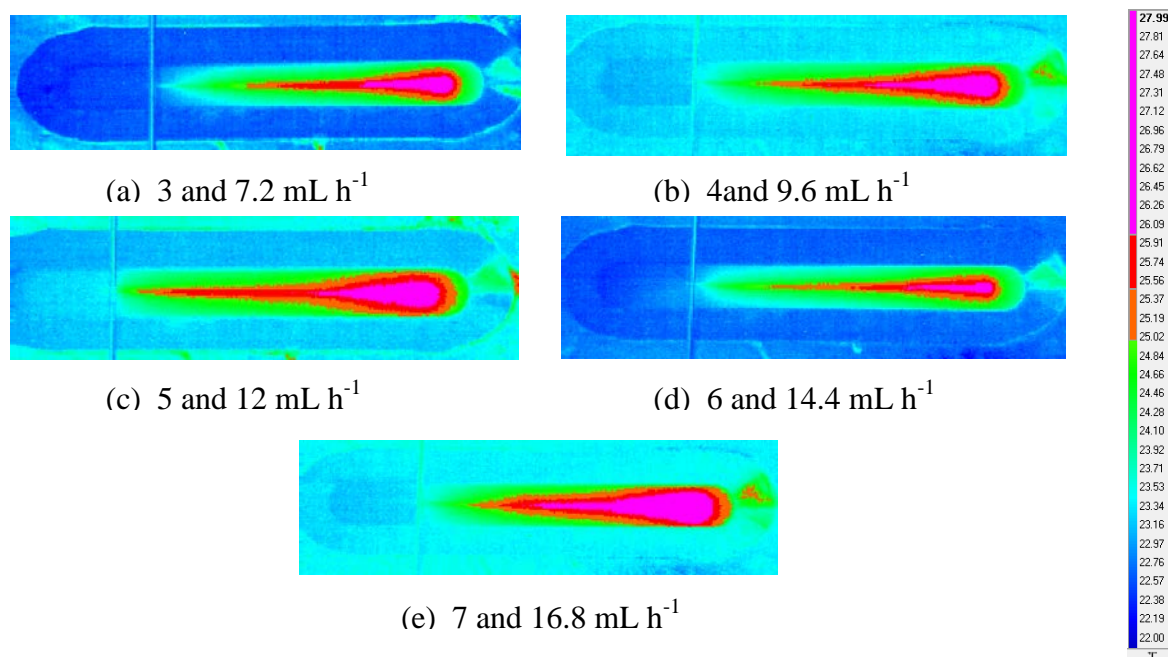

(a) 3 and 7.2 mL h^{-1}

(b) 4and 9.6 mL h^{-1}

(c) 5 and 12 mL h^{-1}

(d) 6 and 14.4 mL h^{-1}

(e) 7 and 16.8 mL h^{-1}

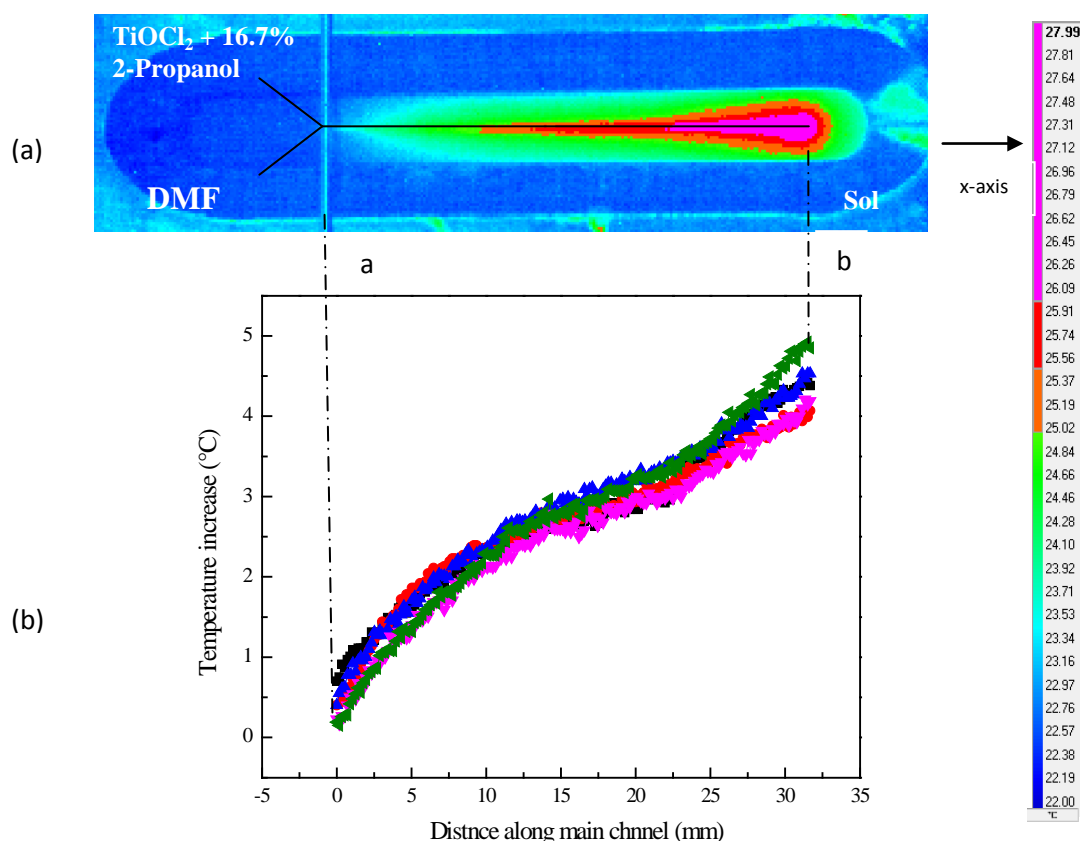Figure 3.7 IR images of $TiOCl_2$ + 16.7% of 2-propanoland DMF for various flow rates

Figure 3.8: Mixing of the $TiOCl_2$ + 16.7% of 2-propanol and DMF:(a) IR Camera image (b) Temperature distribution in the Y- shape microreactor:
Flow rates: 3 and 7.2 mLh^{-1} (—■—), 4and 9.6 mLh^{-1}, (—●—), 5 and 12 mLh^{-1} (—▲—), 6 and 14.4mLh^{-1} (—▼—), 7 and 16.8mLh^{-1}(—◀—)

3.3 Pre-diluted solution with DMF

With the traditional batch process for nanoparticles production, the $TiOCl_2$ precursor is used with DMFonly i.e. without other solvents [1]. In addition the use of solvents involved additional chemical reactions which makes more complex the analysis of reaction products. Therefore we have decided to use DMF as solvent for the predilution of $TiOCl_2$. In the following, the procedure for the dilution of the precursor with DMF is presented, then the results on the behavior of the flow in the main microchannel for various concentrations of DMF and flow rates are shown and discussed.

3.3.1 Dilution

Before injection in the microreactor, 4mL, 8mL or 12 mL of DMF were transferred into a syringe and manually added to 20 mL of the commercial $TiOCl_2$ solution through the cap of a closed flask, leading to volume percentage in DMF of 16.7% (0.52 DMF/Ti), 28.6% (1.03 DMF/Ti) and 37.50%(1.61 DMF/Ti) respectively. While keeping the whole solution in an ice bath at 0°C, the pre-diluted solution was stirred for 30 minutes, before being transferred to one of the pumping syringe. Then, the other syringe was filled with DMF and both syringes were loaded in the syringe pump system and activated with controlled $TiOCl_2$ +DMF and DMF flow rates with a 2.4 flow rate ratio.

3.3.2 Effect of concentration

Tests with our microreactor were performed with three different amounts of DMF for TiOCl$_2$ predilution: 16.7% (0.52 DMF/Ti), 28.6% (1.03 DMF/Ti) and 37.50 % (1.61 DMF/Ti). For all these tests, the flow rate for the TiOCl$_2$ precursor diluted with DMF was ranging from 4 to 8 mLh^{-1} while the flow rate for DMF was varied from 9.6 to 19.2 mLh^{-1} i.e with a 2.4 flowrate ratio. Flow rates were kept constant until the reaction became thermally stable. It was observed with the IR camera that the fluid flows in the microreactor were stable and continuous for all the tests. As expected, adding more amount of DMF during the pre-dilution stage has induced lower temperature increases as shown in Figure 3.9 for a TiOCl$_2$ +DMF flow rate of 5mL h^{-1} and for DMF a 12mL h^{-1} flow rate. It can be seen that the temperature increases was about 13°C for the less pre-diluted solution whereas it was limited to 2°C and 1°C for an amount of DMF of 28.6% and 37.5% respectively.
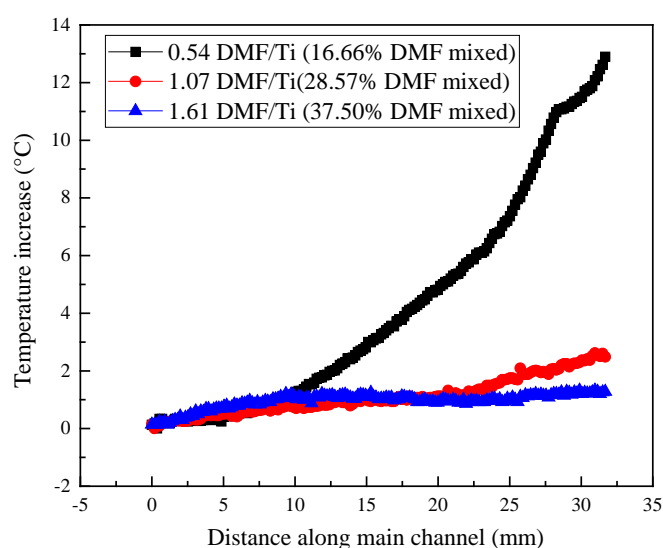

Figure 3.9: Effect of concentration of DMF premixed with TiOCl$_2$ on the temperature distribution inside the main microchannel (5 mLh^{-1} flowrate for TiOCl$_2$+DMF and 12 mL h^{-1} for DMF)
Concentrations: (TiOCl$_2$ + 16.7 % of DMF (0.52 DMF/Ti)), (──■──), (TiOCl$_2$ + 28.6% of DMF (1.03 DMF/Ti))(──●──) and (TiOCl$_2$ + 37.50 % of DMF1.61 DMF/Ti) (──▲──)

The temperature profile of the mixing (TiOCl$_2$ + 16.7% of DMF) and DMF can be compared to the ones previously obtained for the mixing of TiOCl$_2$ + 16.7 % of other solvents and DMF. As shown on Figure 3.10, the increase in temperature is limited to 4°C for solvents such as 1-propanol, 2-propanol, 1-octanol while the increase in temperature is of 8°C for the 1,2-propanediol. If DMF is used as the solvent, the temperature increase is even much higher since it reaches 15°C. This difference may be attributed to the acid-base reaction taking place with DMF as a weak base whereas this is not the case for the other solvents.
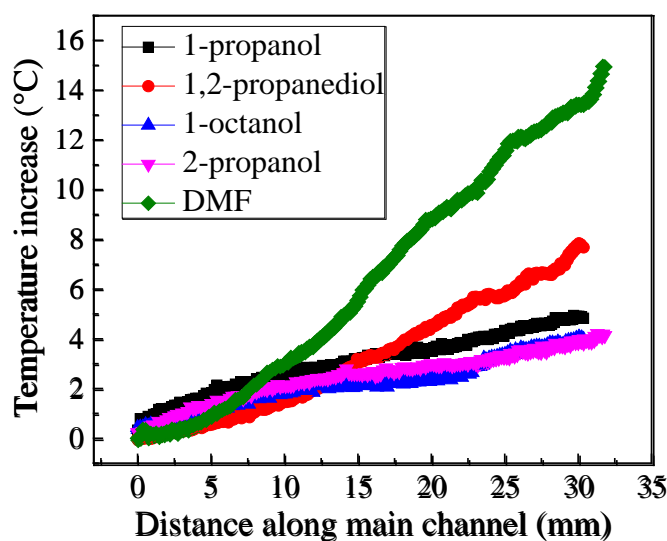
Figure 3.10: Temperature distribution inside the main microchannel for the reaction between $TiOCl_2$ pre-diluted with various solvents and DMF (flow rate 6 and 14.4mL h^{-1} respectively)

For a dilution of $TiOCl_2$ with 16.7 % of DMF, the exothermic effect was larger meaning that the degree of advancement of the reaction is less before the injection of reactants in the microcreactor. Because there is more DMF to react in the case of the less predilution. In addition the flow in the main microchannel figured out to be stable and continuous. So a predilution of 16.7% (0.52 DMF/Ti) was selected for further experiments.

3.3.3 Effect of flow rate

Working with a 16.7 % of DMF for the pre-dilution of $TiOCl_2$, the effect of flow rate on the behavior of the flow was investigated. Both reactants were injected with flow rates ranging from 4 to 8 mL h^{-1} for pre-diluted $TiOCl_2$ and from 9 to 19.2 mLh^{-1} for DMF keeping a 2.4 flow rate ratio between them. Table 3.3 shows the experiments performed with various flow rates and the corresponding low Reynolds numbers. Figure 3.11 shows the IR images of the reaction inside the microreactor for all the studied flow rates. Figure 3.12 (b) shows the obtained temperature distributions on the centerline of the main microchannel. Both Figures show that the flows are continuous and stable. During the experiment, a minimum of 30 mL of reaction product was collected at the outlet of the main microchannel for further analysis by DLS or Raman techniques.

Table 3.3: Experiments performed with pre-dilution $TiOCl_2$ with 16.7% of DMF

0.52 DMF/Ti		DMF		Residence time for 30 mL Volume (minutes)
Flow Rate (mL h^{-1})	Reynolds Number	Flow Rate (mL h^{-1})	Reynolds Number	
4	24.5×10^{-3}	9.6	4.58×10^{-3}	132.35
5	30.7×10^{-3}	12	5.72×10^{-3}	105.88
6	36.8×10^{-3}	14.4	6.86×10^{-3}	88.23
7	42.9×10^{-3}	16.8	8.00×10^{-3}	75.63
8	49.1×10^{-3}	19.2	9.15×10^{-3}	66.17

(a) 4and 9.6 mL h^{-1}

(b) 5 and 12 mL h^{-1}

(c) 6 and 14.4 mL h^{-1}

(d) 7 mL h-1 and 16.8mL h^{-1}

Figure 3.11: IR images of pre-diluted TiOCl$_2$ with 16.7% of DMF and DMF for various flow rates
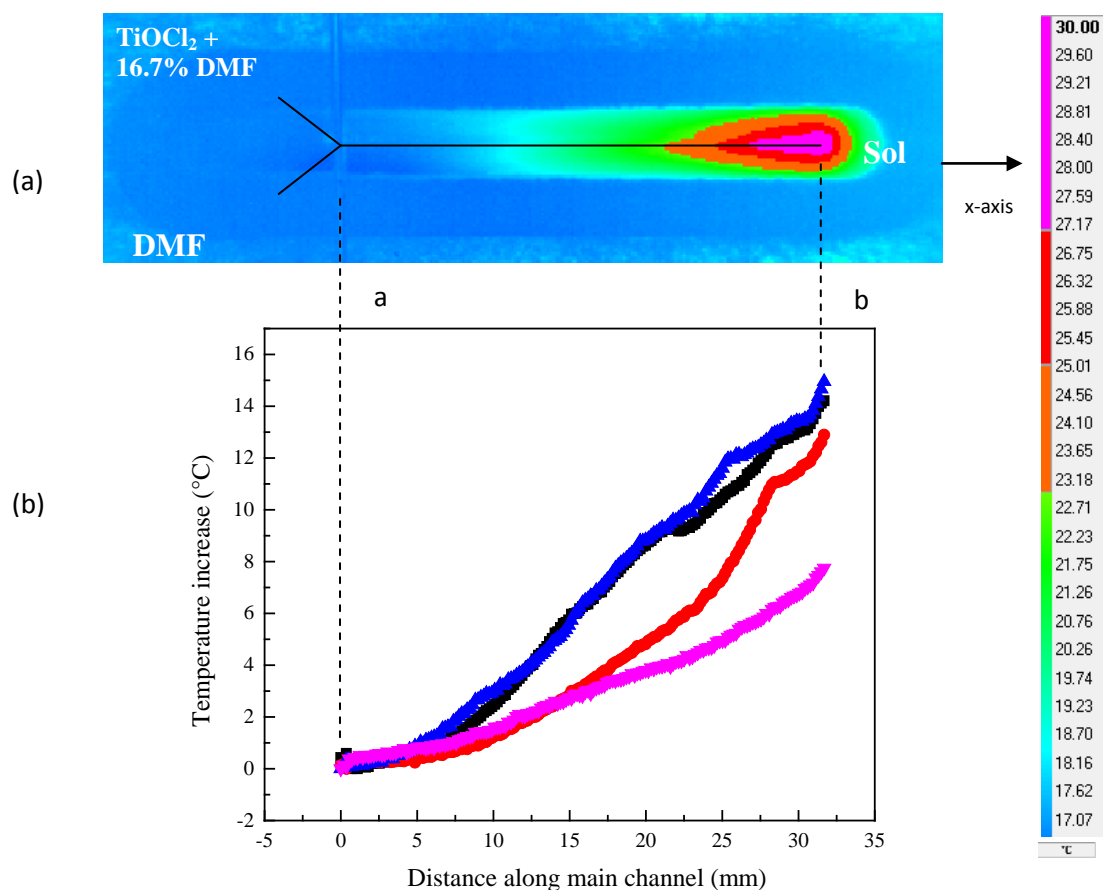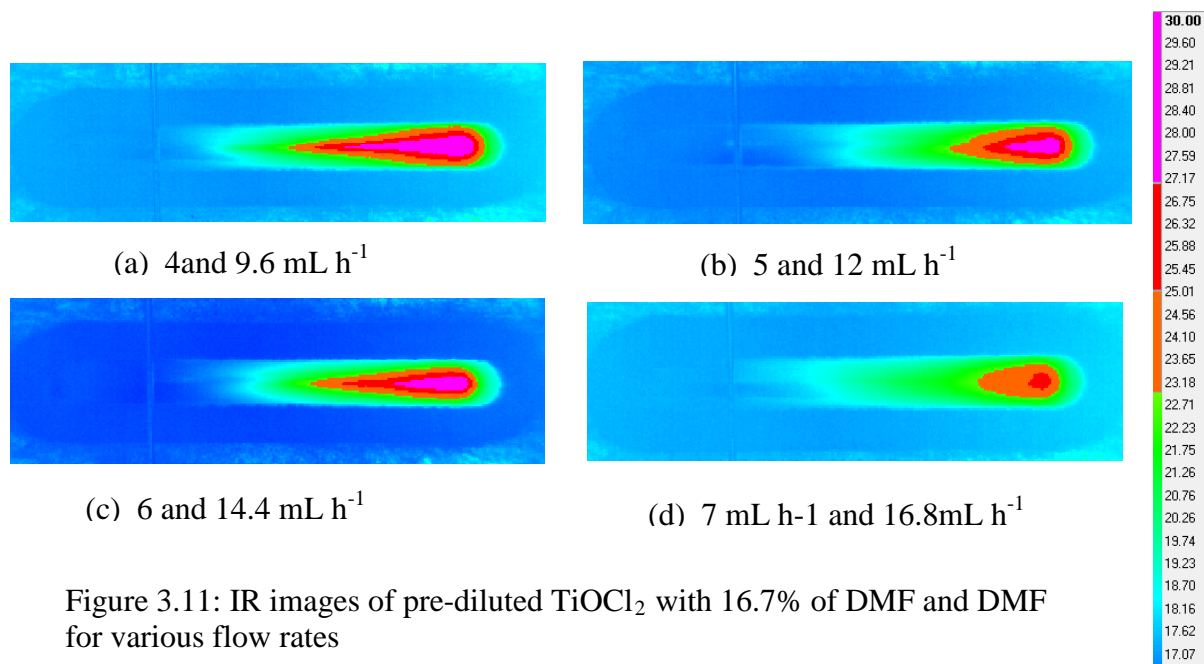

Figure 3.12: Mixing of TiOCl$_2$ + 16.7% DMF and DMFin: (a) IR camera image , (b) Temperature distribution in the Y- shape microreactor

Flow rates: 4mL h^{-1}and 9.6 mL h^{-1}(—■—), 5mL h^{-1}and 12mLh^{-1}, (—●—), 6 mL h^{-1}and 14.4mL h^{-1} (—▲—), 7 mL h^{-1}and 16.8 mL h^{-1}(—▼—)

3.4 Enthalpy measurement

Enthalpy measurements were performed to get more information about the hydrolysis of DMF by $TiOCl_2$ acidic solution. The experimental procedure based on the use of a Peltier cell and a PDMS microchannel was presented in chapter 2, section 2.3.3.

Enthalpy reaction measurements were performed using solvents for $TiOCl_2$ predilution which involves stable, continuous and non pulsating flow in the microchannel. So results will be presented only for solvents such as 2-propanol and DMF. For both solvents, the effects of concentration and flow rate were investigated.

3.4.1 Enthalpy measurement for $TiOCl_2$ prediluted with 2-propanol

Before injection in the microreactor, 3.5 mL, 4 mL, 4.1 mL or 4.4 mL of 2-propanol were loaded into the syringe and manually added to 20 mL of the $TiOCl_2$ solution inside a closed flask, leading to 2-propanol volume percentages of 15%, 16.7%, 17% and 18% respectively. Pre-diluted solutions were stirred for 30 minutes and were kept in an ice bath at 0°C to slow down the progress of the reaction during the transfer of the syringes in the Nemesys pumping system.

In Figure 3.13, the total heat flux (ϕ) measured through the output voltage of Peltier cell is plotted against the $TiOCl_2$+2-propanol flow rate. One can see that the measured total heat fluxes through the Peltier cell increase linearly with the flow rate values. The slopes, ϕ vs. flow rate, divided by the concentration of reactants provide the measured variation of enthalpies. Indeed, the enthalpy can be calculated from the relation:
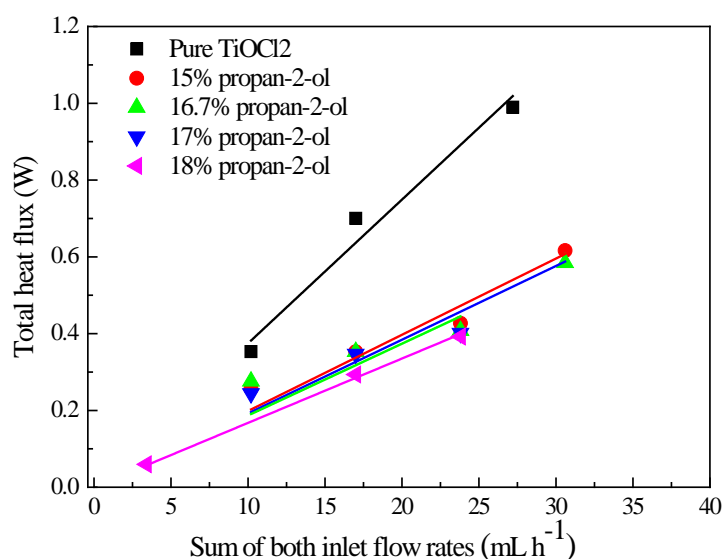
$$\Delta H = \frac{\phi}{Q\ C\ X} \qquad\qquad 3.1$$

Figure 3.13 Total heat flux (ϕ) obtained through the output voltage of Peltier cell as function of $TiOCl_2$+ 2-propanol flow rate

where ΔH(J mol^{-1}) is the enthalpy reaction, Q (m^{3}s^{-1}) the flow rate, C (mol m^{-3}) the concentration of the reactants, ϕ (W) the heat flux and X the reaction conversion [3,4]. For our calculation here, as the microchannel is long enough (216mm), we assume complete reaction($X=1$).

Figure 3.14 shows the obtained variation of enthalpies as function of the concentration of 2-propanolused for the precursor pre-dilution. As expected the enthalpy decreases as the amount of 2-propanol is increased. Indeed for pure TiOCl$_2$, the ΔH value is 12.08 kJ mol^{-1} and for TiOCl$_2$ pre-diluted with 15% vol. 2-propanol, it decreases to 6.2 kJ mol^{-1}.
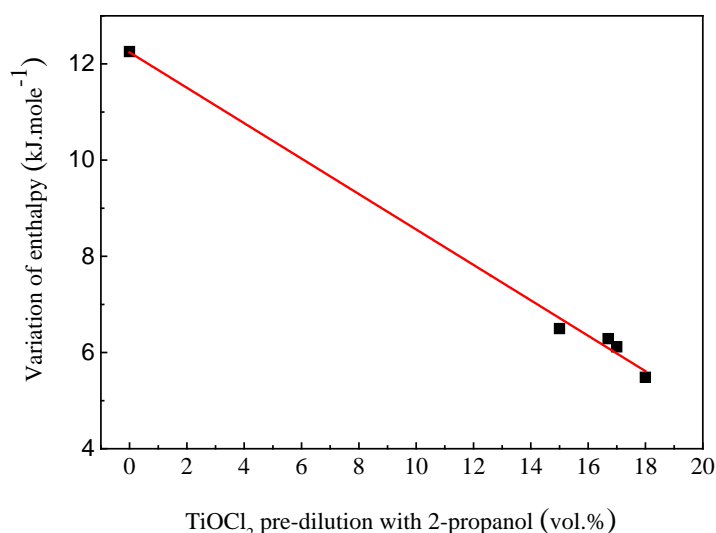

Figure 3.14: Effect on the variation of enthalpy of the concentration of 2-propanolfor the pre-dilution ofTiOCl$_2$

3.4.2 Enthalpy measurement with DMF pre-dilution

Before injection in the microreactor 0.6 mL, 2.2 mL, 3.5 mL or 5 mL of DMF were loaded into the syringe and manually added to 20 mL of TiOCl$_2$ solution through the cap of the closed flask, leading to DMF volume percentages of 3%, 10%, 15% and 20% respectively. Pre-diluted solutions were stirred for 30 minutes and were kept in an ice bath at 0°C. Then pre-diluted TiOCl$_2$ and DMF were loaded successively into the syringe pumps.

In Figure 3.15, total heat flux (ϕ) measured through the voltage of the Peltier cell by are plotted as function of pre-diluted TiOCl$_2$ flow rates. The measured total heat flux increases linearly with the flow rate values. The slopes,ϕ vs. flow rate, divided by the concentration of reactants provide the variation of enthalpies using previous Equation 3.1.
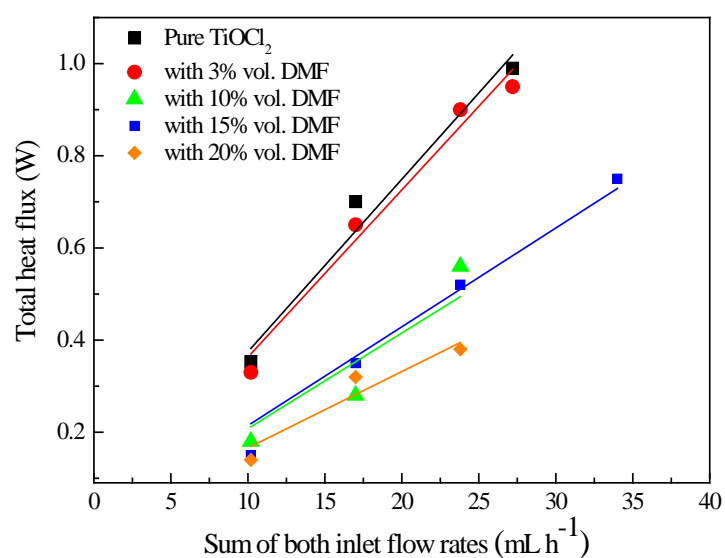
Figure 3.15 Heat flux measured by Peltier cell as function of the flow rate of TiOCl$_2$ pre-diluted with DMF

Figure 3.16 shows the values of variation of enthalpy as function of amount of DMF used for the pre-dilution of TiOCl$_2$. As expected the enthalpy decreases with increasing concentration of DMF for TiOCl$_2$ pre-dilution. Indeed for pure TiOCl$_2$, the ΔH value is 12.08 kJ mol^{-1}, and for TiOCl$_2$ pre-diluted with 15% volume of DMF, ΔH value decreases to 7 kJ mol^{-1}.
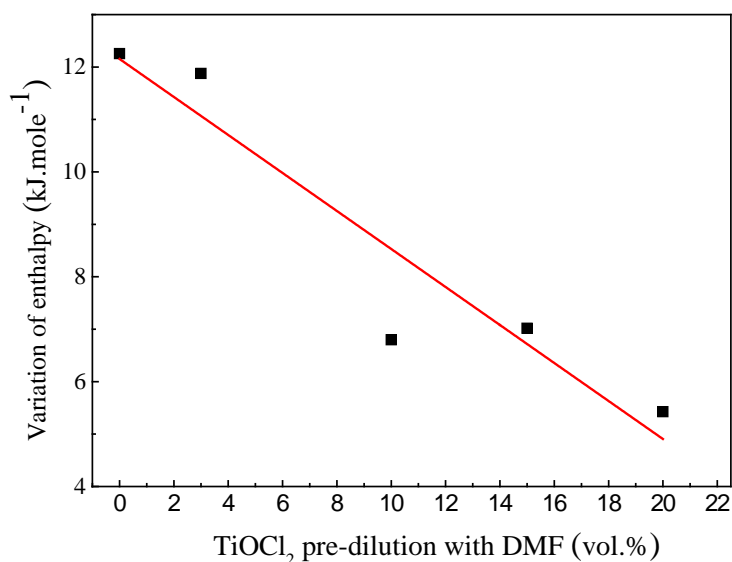

Figure 3.16 Effect of TiOCl$_2$ pre-diluted with DMF on the enthalpy

3.5 Discussion

Enthalpy decreases with increase of predilution of 2-propanol or DMF, as demonstrated in Table 3.4. When enthalpy compared on same amount of predilution in $TiOCl_2$ then enthalpy of predilution with DMF (7 kJ mol^{-1}) was found larger than predilution with 2-propanol (6.2 kJ mol^{-1}). Again this is the signature of mixing strong acid with a weak base.

Table 3.4: Total heat flux of pure $TiOCl_2$, prediluted $TiOCl_2$ with 2-propanol and prediluted $TiOCl_2$ with DMF

Sum of both inlet flow rates (mL h^{-1})	Pure $TiOCl_2$		At 15% predilution with 2-propanol		At 15% predilution with DMF	
	Total heat flux (mW)	Enthalpy (kJ mol^{-1})	Total heat flux (mW)	Enthalpy (kJ mol^{-1})	Total heat flux (mW)	Enthalpy (kJ mol^{-1})
10.2	390		190		210	
17	635	12.06	300	6.2	360	7
27.2	1000		480		530	

3.6 Conclusion

In this 3rd Chapter, the use of continuous flow via a microreactorwas demonstrated as an alternative to the batch technique for performing the hydrolysis of TiOCl$_2$ by DMF. Infrared camera was found as an interesting tool to observe the flows inside the microreactor. When using pure TiOCl$_2$ and DMF, this method has revealed the existence of flow instabilities with discontinuous and pulsating phenomenon. As it is a drawback for producing nanoparticles in a well-controlled manner, it is important to reduce these instabilities. For this purpose, the TiOCl$_2$ precursor waspre-diluted with various solvents. Solvents such as water,1-propanol, 1,2-propanediol, 1-octanol did not provide any significant improvement. Since diluted aqueous TiOCl$_2$ and DMF are miscible, we can conclude that the miscibility is probably not the origin of instabilities. However, continuous and stable flows have been obtained with 2-propanol and DMF.

Finally DMF was preferred to 2-propanol since being already one of the reactant involved in the synthesis, it does not involve additional reactions.Tests with several amounts of DMF for TiOCl$_2$ pre-dilution have shown that a 16.7% volumic amount of DMF was enough to maintain stable flows while preserving the synthesis process mainly within the microreactor.

Moreover, the variation of enthalpy of the sol-gel synthesis was measured in amicroreactor using a Peltier cell. Value of 12.08 kJ mol^{-1}were obtained for pure TiOCl$_2$. As expected decreasing values were obtained for increasing amount of solvent for the TiOCl$_2$ pre-dilution.Smaller values were obtained in case of predilution due to the fact that the reaction has already begun during this first predilution step.

During the experiments one have noticed that the maximum temperature was observed at the outlet of the microchannel, inducing that the synthesis was not fully achieved inside the microchannel. Indeed, the flow in the microchannel is laminar, thus mixing is only provided through molecular diffusion, which is very slow. Therefore a much longer microchannel is required. An interesting alternative which would avoid excessive pressure drop in the microreactor consists in using a passive or active mixing technique. Next chapterwill be focused on this point.

References:

[1]   T. Cottineau *et al.*, "Photosensitive Titanium Oxo-polymers: Synthesis and Structural Characterization," *Chem. Mater.*, vol. 20, no. 4, pp. 1421–1430, février 2008.

[2]   C.-E. Liu *et al.*, "Low Temperature Synthesis of Nanocrystallized Titanium Oxides with Layered or Tridimensional Frameworks, from [Ti8O12(H2O)24]Cl8·HCl·7H2O Hydrolysis," *Chem. Mater.*, vol. 20, no. 14, pp. 4739–4748, Jul. 2008.

[3]   C. Hany, C. Pradere, J. Toutain, and J.-C. Batsale, "A millifluidic calorimeter with infrared thermography for the measurement of chemical reaction enthalpy and kinetics," *Quant. InfraRed Thermogr. J.*, vol. 5, no. 2, pp. 211–229, Dec. 2008.

[4]   H. Ammar, B. Garnier, A. Ould el Moctar, H. Willaime, F. Monti, and H. Peerhossaini, "Thermal analysis of chemical reactions in microchannels using highly sensitive thin-film heat-flux microsensor," *Chem. Eng. Sci.*, vol. 94, pp. 150–155, May 2013.

Chapter 4

Mixing enhancement using an electric field

4.1 Introduction

Currently, it is known that the interface between two fluids of different dielectric properties can be destabilized by applying an electric field [1]. This results in a secondary flow which improves mixing between two liquids. In our case, the two reagents used $TiOCl_2$ and DMFhave very different dielectric properties.Indeed, the static dielectric constant or relative permittivity for DMF is equal to 36.7 whereas the value for $TiOCl_2$ is close to the one of water (ε_r=78.5) as it is an aqueous solution of titanium tetrachloride. Therefore were carried out with such an active mixing method, i.e. based on the use of an electric field.

In the previous study dealing with the observation of the flow of the two reactive fluids, a32mm long microchannel was used showing that the reaction was not achieved as the peak of temperature for stable flows was observed at its outlet. For this new section, we have used two new microchannels with a length of 294mm for the one without electrodes and 234mm for the one with electrodes. Their descriptions are provided in section 2.3.4. One should notice that due to the increased length of the microchannels, a greater surface had to be covered by the glass plate. Therefore to avoid its bending, two solutions were tested. Firstly, a PMMA grid located on a 0.1mm thick glass plate was used as can be observed on Fig 4.1. Secondly a much thicker glass plate (1 mm) was used. Figure 4.1 shows infrared images for the two cases using DMF and $TiOCl_2$prediluted with 16.7%DMF as reactants. Temperature distributions along the main microchannel are presented in Figure 4.2. One can observed that the temperature increases is not seriously affected when changing the glass thickness from 0.1 to 1mm. Indeed, the temperature peak decreases from 7.5°C to 6°C i.e. with only a 1.5°C discrepancy.Furtherexperiments in this chapter were performed with a 1mm thick glass plate since the temperature discrepancy is small and it provides a better observation of thermal effects in the entire microchannel.
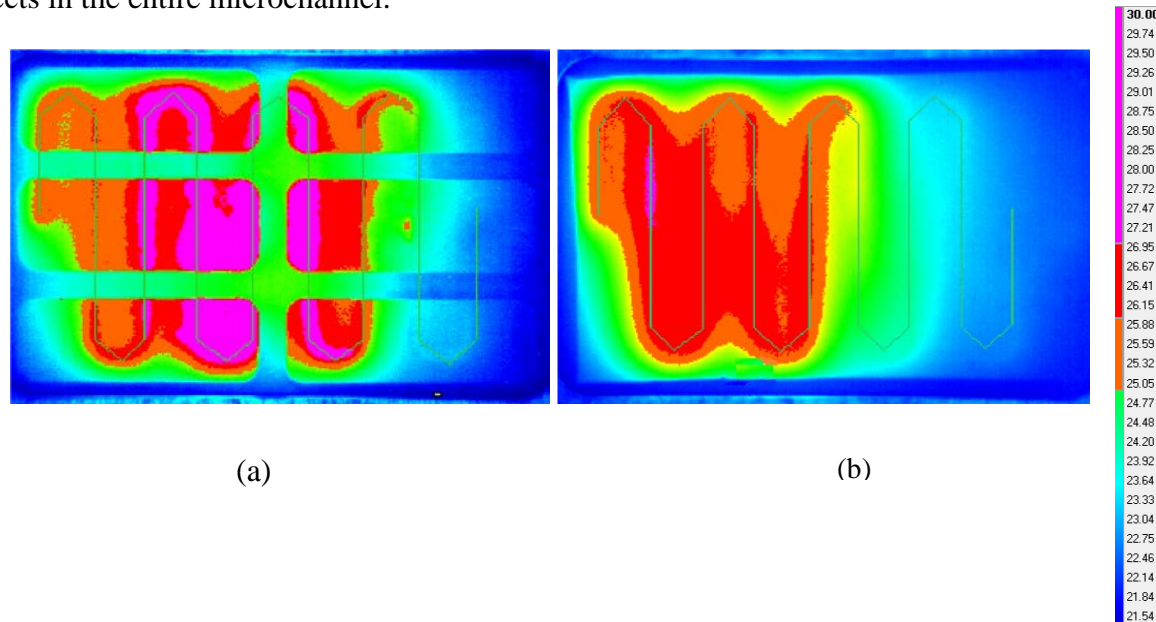

(a)   (b)

Figure 4.1:IR images with two glass plate thicknesses: (a) 0.1mm with a PMMA grid (b) 1mm without grid ($TiOCl_{2+}$ 16.7% DMF with flow rate of 6 ml h^{-1} and DMF at 14.4 mL h^{-1})
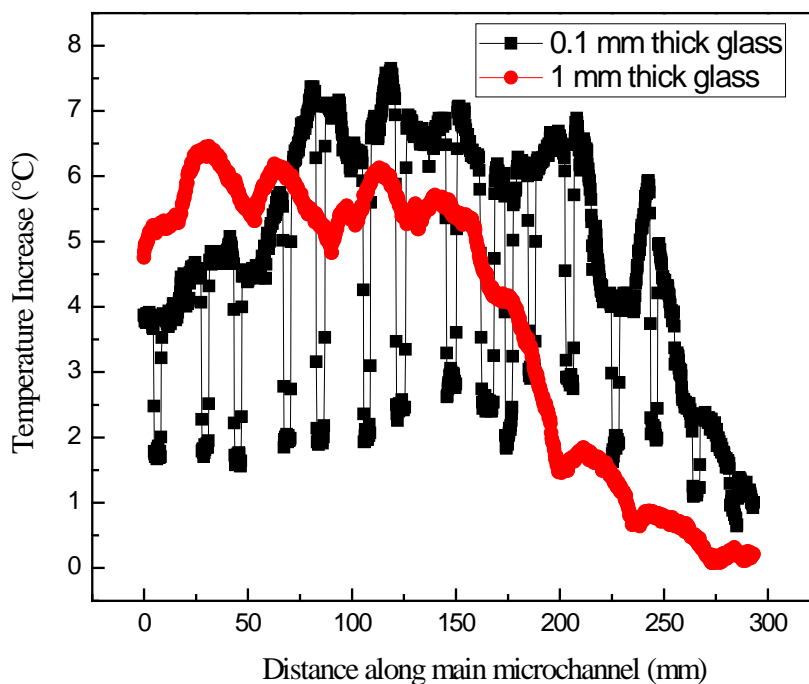
Figure 4.2: Temperature distributions with two glass plate thicknesses (reactants: TiOCl$_2$ +16.7% DMF with flow rate of 6 mL h^{-1} and DMF at 14.4 mL h^{-1})

In this section which is dedicated to the effect of electrical fields, results will be presented for two solutions which were interesting to study: the premixed solution (DMF and TiOCl$_2$ with 16.7%DMF) as it was the one which offers stable flows and the solution with pure TiOCl$_2$ (DMF and TiOCl$_2$). For both solutions, the experiments were performed without the presence of an electric field (for comparison purpose) and then with an electric field.

For each experiment, a minimum of 30 mL solution was collected at the outlet of the main microchannel then it was stirred for 2 to 3 minutes before analysis of the nanoparticle sizeby DLS and Raman technique. Results will be presented in chapter 5.

4.2 Pre-mixed solution

4.2.1 Results without electric field

The experiments performed without electric field are different from the ones of chapter 3 since longer channels are used. They were performed with DMF and predilutedTiOCl$_2$ with 16.7% DMFand this for various flow rates. The two long microchannels (234 and 294 mm) were used.

Figure 4.3showsthe temperature measured with the longer microchannel (294 mm) and flow rate of 6 mL h^{-1}and 14.4 mL h^{-1} for respectively the prediluted TiOCl$_2$ and DMF.

The reaction occurs inside the microchannel and is completed beforeitsoutlet. The flow figures out to be unstable and discontinuous which was not observed with the shorter microchannel (32 mm).Figure 4.4shows the temperature distribution along the microchannel

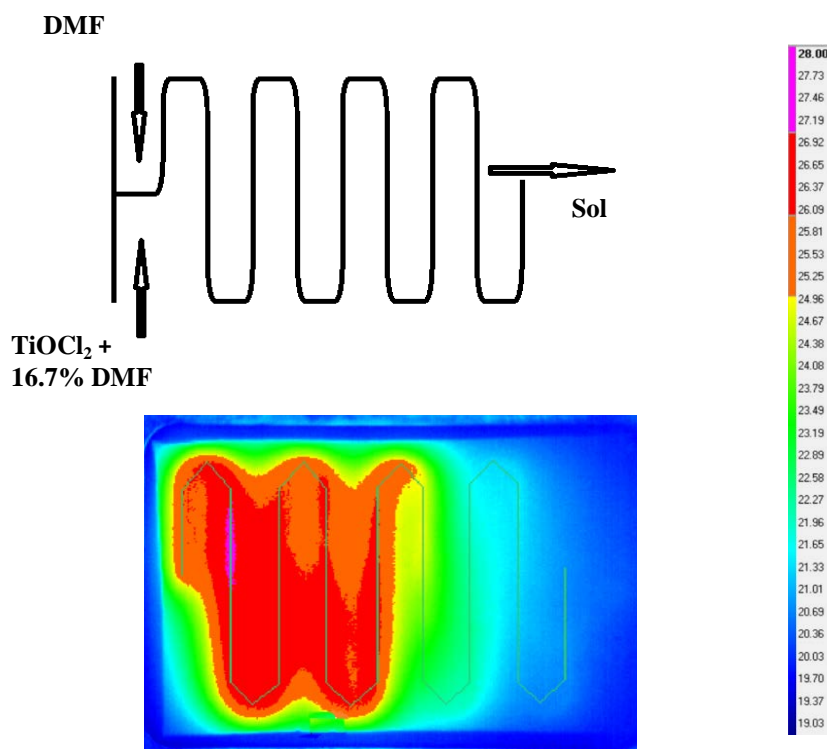which is obtained from IR image by following the middle ofthechannelwhile y-axis shows the temperature increase.

Figure 4.3: IR image of exothermic reaction inside the microreactor (294 mm, 6 and 14.4 mL h^{-1}, TiOCl$_2$+16.7%DMF and DMF)
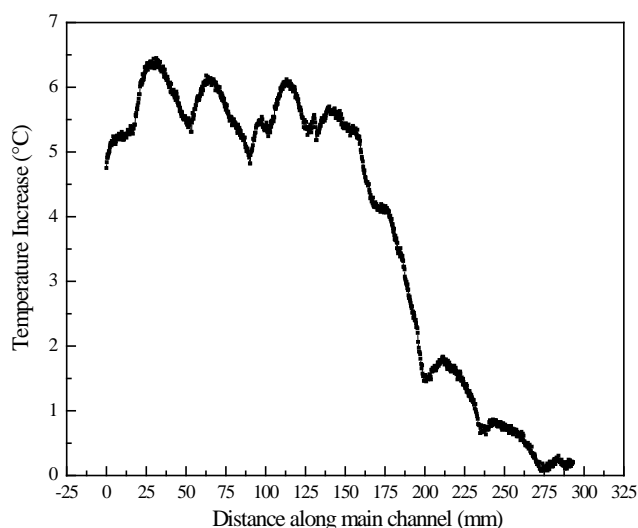

Figure 4.4: Temperature distribution in the 294 mm long microreactor:(TiOCl$_2$ + 16.7% DMF with a flow rate of 6 mL h^{-1}and DMF at 14.4 mL h^{-1})

Moreover, measurements werealsoperformed with the 234 mm long microchannel, the one with electrodes which are not activated in this section.Figure 4.5shows the IR images of the reaction for various flow rates. The same observationwas also made here from the IR imagesthatthe flow was still discontinuous and unstable. However there is an exception for

the flow rate of 5 mL h^{-1} for TiOCl$_2$ and 12 mL h^{-1} for DMF (Figure 4.5c) where it appears stable. Figure 4.6 shows the temperature distribution along the microchannel which is obtained from IR images. It seems that the reaction was not fully achieved at the outlet of the microchannel for the chosen set of flowrates.
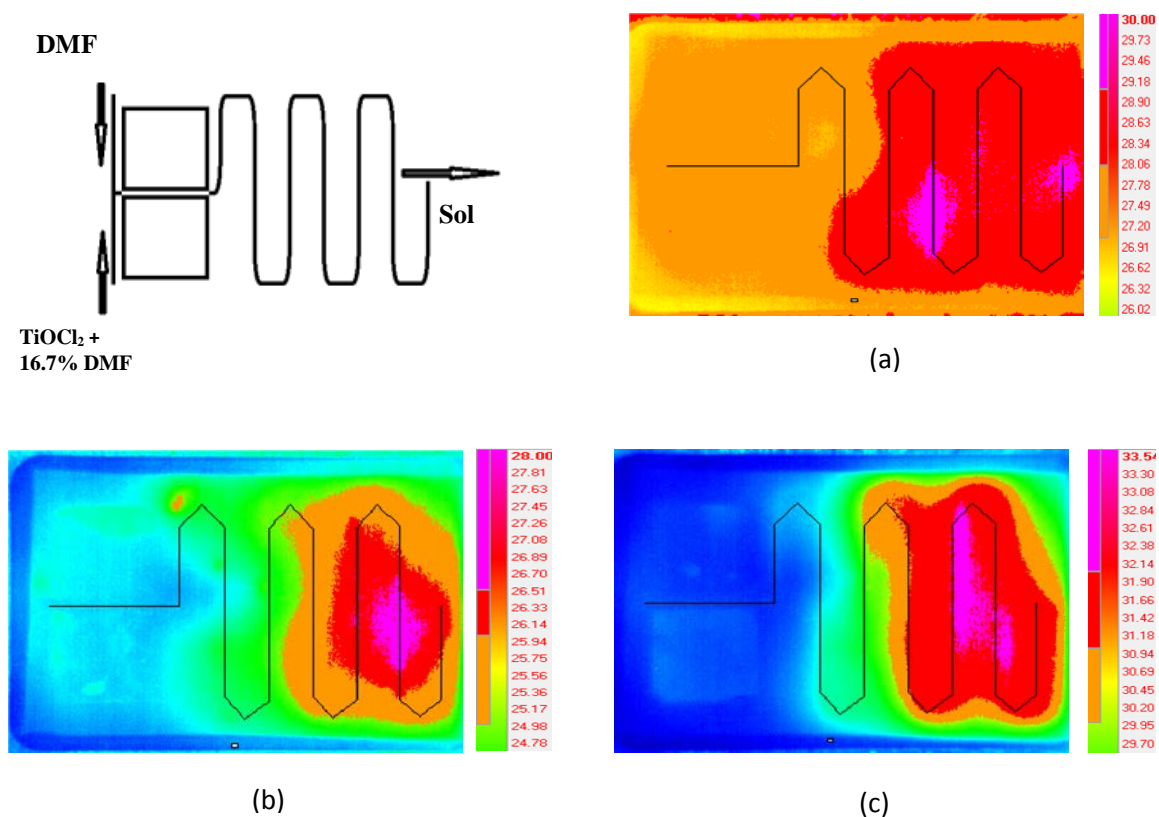

Figure 4.5: IR image of exothermic reaction inside the microreactor for various flow rates of TiOCl$_2$+16.7%DMF and DMFof respectively: (a)1 mL h^{-1}and 2.4 mL h^{-1}(b) 3 mL h^{-1}and 7.2 mL h^{-1}(c) 5mL h^{-1}and 12mL h^{-1}
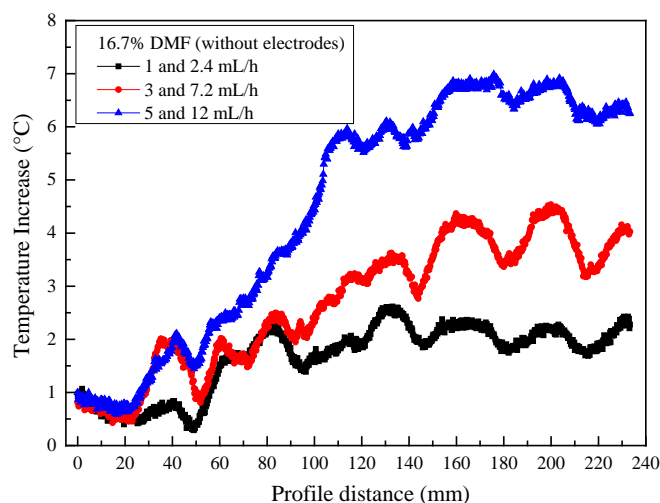

Figure 4.6: Temperature distribution in the 234mm long microreactor with TiOCl$_2$ + 16.7% DMF and DMF

Compared to the results of previous chapter, it appears that increasing the length of the microchannel has led to less stable flows.

Finally Table 4.1 synthetized all the obtained results with TiOCl$_2$prediluted with 16.7%DMF without electric field.

Table 4.1: Experimentsperformed using long microchannels (234 or 294 mm)without electric field (TiOCl$_2$ +16.7% DMF and DMF)

Length ot the used microreactor (mm)	TiOCl$_2$ (diluted with 16.7% DMF)		DMF		Main channel velocity (m s^{-1})	Residual time for 30 mL Volume (minutes)	Stable Flow (⊘) or unstable flow (⊗)
	Inlet flow Rate (1) (mL h^{-1})	Reynolds Number	Inlet Flow Rate (2) (mL h^{-1})	Reynolds Number			
234	1	3.68 10^{-3}	2.4	6.86 10^{-4}	9.42 10^{-4}	529.4	⊗
234	3	11.1 10^{-3}	7.2	20.5 10^{-4}	28.2 10^{-4}	176.5	⊗
234	5	18.4 10^{-3}	12	34.3 10^{-4}	47.1 10^{-4}	105.9	✅
294	6	22.1 10^{-3}	14.4	41.1 10^{-4}	56.5 10^{-4}	88.24	⊗

4.2.2 Effect of DC Electric field

Here, we discuss the mixing enhancement provided by the use of a DC electric field.For this purpose the 234mm long microchannel equipped with two platinum electrodes was considered. Several measurements were performed by using different voltages values from 0.4 to 4 Volts. We did not perform tests with a 2.4 flow rate ratio between the two reactant flow rates but the last line of Table 4.2shows the results with a ratio of 2 which is close. The temperature measurement is provided in Figure 4.8. It appears that the presence of a DC voltage between 1.5 and 4V was providing stable flows. However this DC voltage has generated two main problems. The first one is the formation of bubbles due to gas formation. We have attributed this phenomena to the water electrolysis. Indeed TiOCl$_2$ contains water :1 molecule of TiOCl$_2$ contain 7 molecules of H$_2$O. The second problem was the formation of Ti^{3+}at the positive electrode (anode), which can be observed by a characteristic purple color (Figure 4.7). This means that Ti^{4+} was reduced to Ti^{3+}. These two unwanted phenomena will negatively impact the final structure of TiDMF.
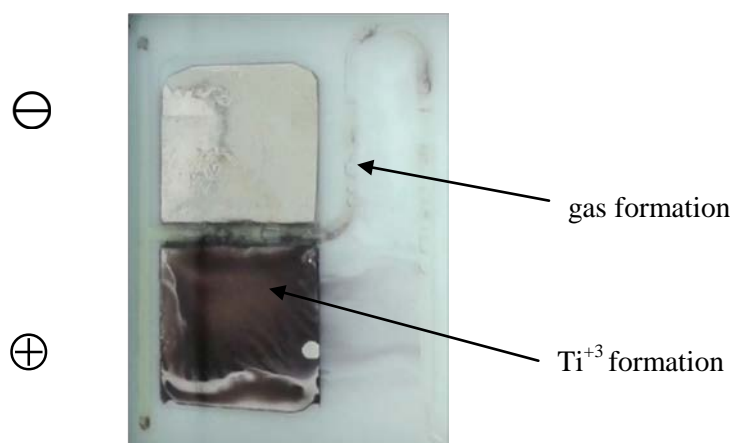

Figure 4.7: Formation of gas and Ti^{3+}observed during the use of a DC voltage between 1.5 and 4 V

Table 4.2: Mixing experiments using a DC electrical field (pre-diluted $TiOCl_2$ with 16.7% of DMF).

DMF/Ti Ratio	$TiOCl_2$ (diluted with 16.7% DMF)		DMF		Main channel velocity ($m\ s^{-1}$)	Residual time for 30 mL Volume (mn))	Voltage range (Volts) for **Unstable** flow (❌)	Voltage range for **Stable** Flow (✓)
	Inlet flow Rate (1) ($mL\ h^{-1}$)	Reynolds Number	Inlet Flow Rate (2) ($mL\ h^{-1}$)	Reynolds Number				
0.5	8	$29.4\ 10^{-3}$	4	$1.1\ 10^{-3}$	$33.2\ 10^{-4}$	150	0.4 to 3	4
1	4	$14.7\ 10^{-3}$	4	$1.1\ 10^{-3}$	$22.1\ 10^{-4}$	225	0.4 to 1	1.5 to 4
1.5	4	$14.7\ 10^{-3}$	6	$1.7\ 10^{-3}$	$27.7\ 10^{-4}$	180	0.4 to 1	1.5 to 4
2	4	$14.7\ 10^{-3}$	8	$2.3\ 10^{-3}$	$33.2\ 10^{-4}$	150	0.4 to 1	1.5 to 4

One have tried to investigate if changing the DMF/Ti ratio between the precursor $TiOCl_2$ +16.7%DMF and the solvent DMF could have an impact on the results. Figures 4.8, 4.9, 4.10 and4.11 show the IR images of the reaction in the microreactor for 0.5, 1, 1.5 and 2 DMF/Ti ratios. Figure 4.12 shows the corresponding temperature distributions along the microchannel for all the considered DMF/Ti ratios. Results are also presented in Table 4.2. It was observed from infrared images that by using voltage values from 0.4 to 1V, the flow was unstable and discontinuous. Voltages lower than 1 V are not affecting the mixing. Infact, the results were similar to these without electrical field. On the contrary, IR images using voltages between 1.5 and 4 V show the strong effect of the electrical field on the mixing. The flow becomes stable and the reaction is completing just after the electrodes in a very short distance.
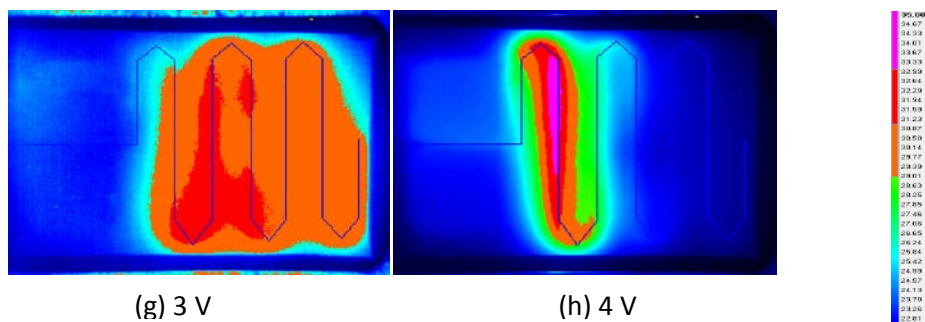

(a) 0.4 V

(b) 0.6 V

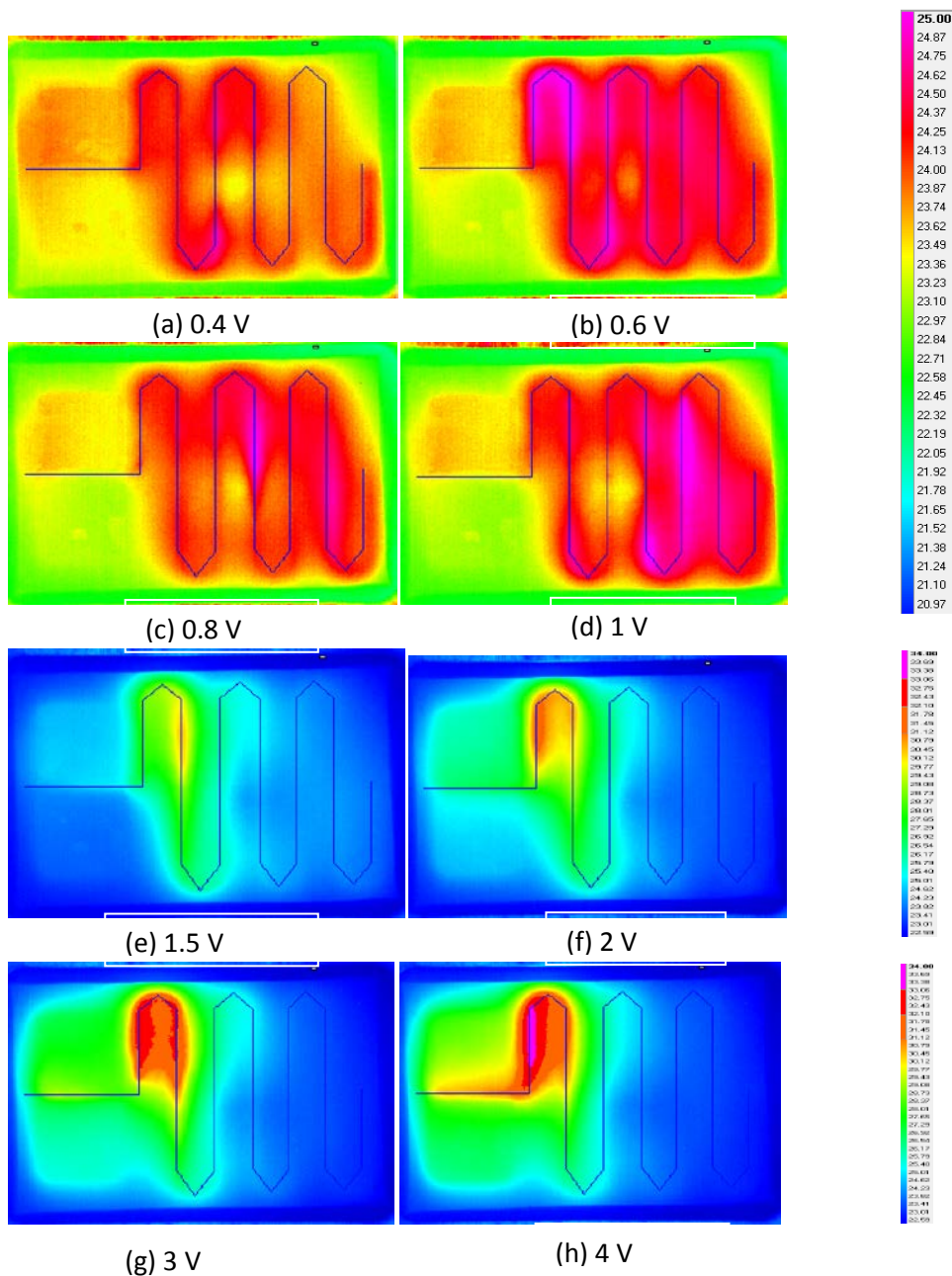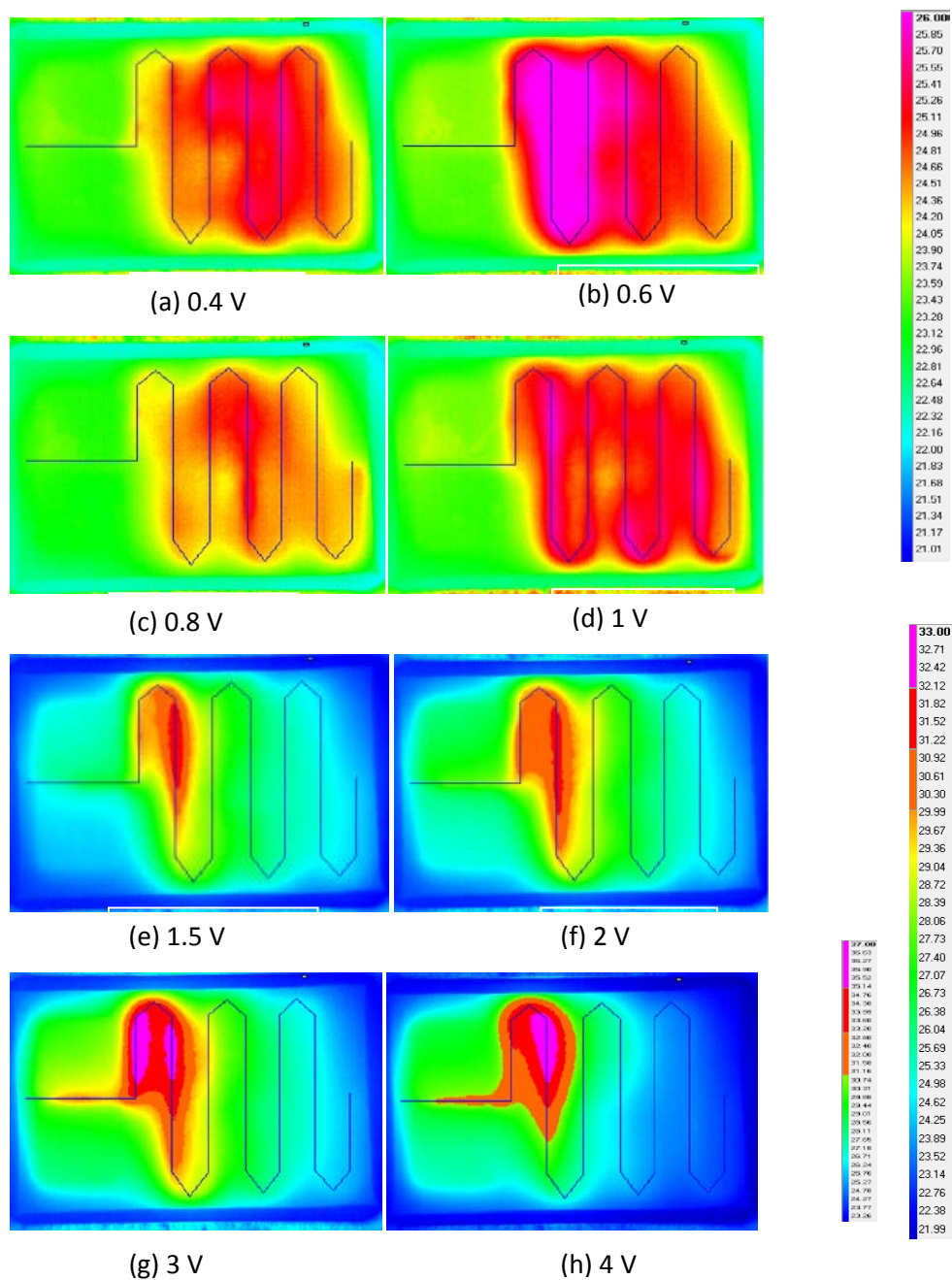(c) 0.8 V

(d) 1 V

(e) 1.5 V

(f) 2 V

(g) 3 V   (h) 4 V
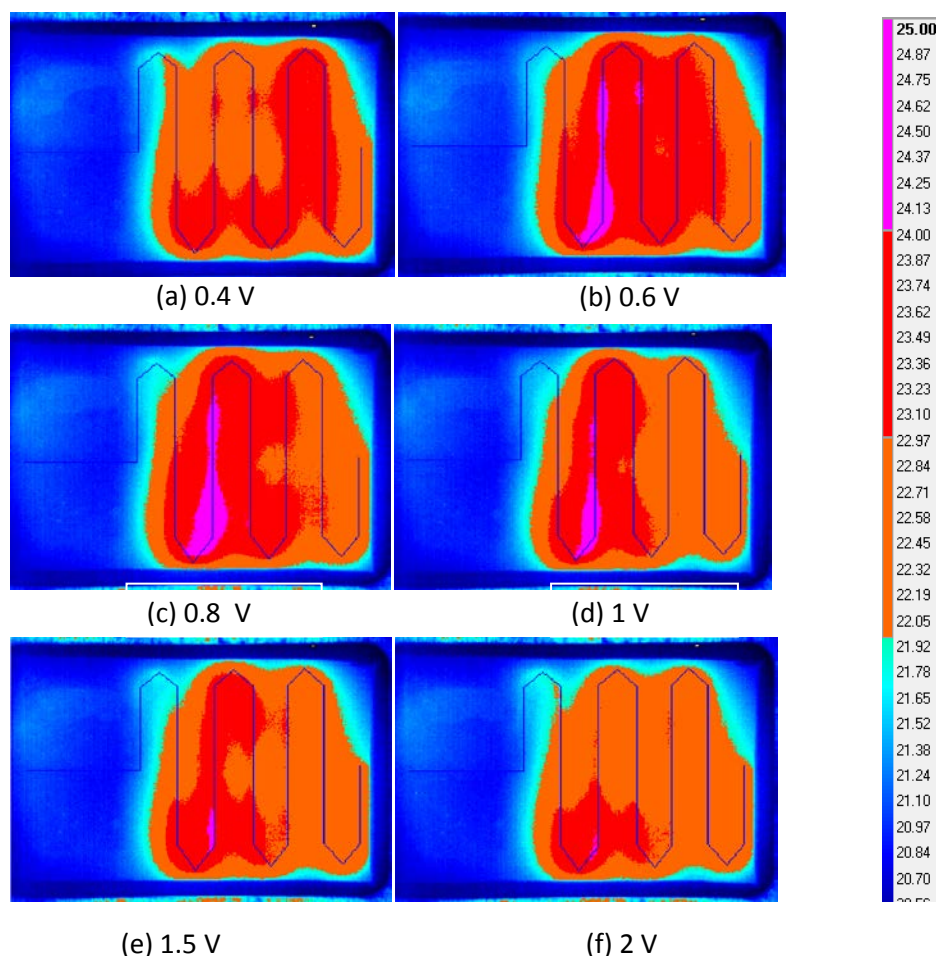
Figure 4.8: Infrared image of exothermic reaction inside the microreactor
($TiOCl_2$ + 16.7% DMF at 8 mL h^{-1} and DMF at 4 mL h^{-1}, DMF/Ti ratio=0.5)

(a) 0.4 V   (b) 0.6 V

(c) 0.8 V   (d) 1 V

(e) 1.5 V   (f) 2 V

(g) 3 V   (h) 4 V

Figure 4.9: Infrared image of exothermic reaction inside the microreactor
($TiOCl_2$+16.7% DMF at 4 mL h^{-1} and DMF at 4 mL h^{-1}, DMF/Ti ratio =1)

Figure 4.10: Infrared image of exothermic reaction inside the microreactor ($TiOCl_2$ + 16.7% DMF at 4 mL h^{-1} and DMF at 6 mL h^{-1}, DMF/Ti ratio =1.5)
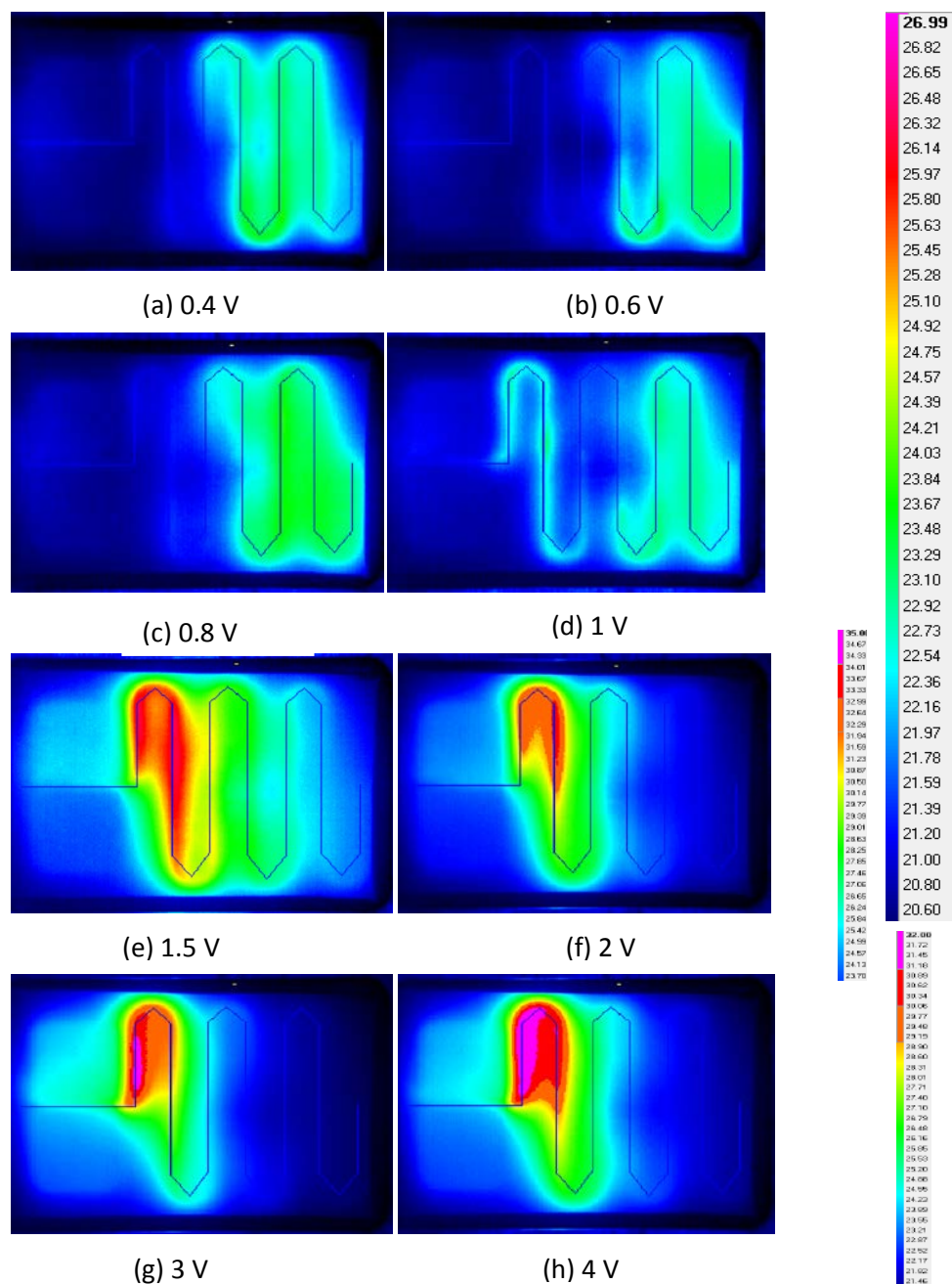
Figure 4.11: Infrared image of exothermic reaction inside the microreactor (TiOCl$_2$+ 16.7% DMF at 4 mL h^{-1}and DMF at 8 mL h^{-1}, DMF/Ti ratio =2)
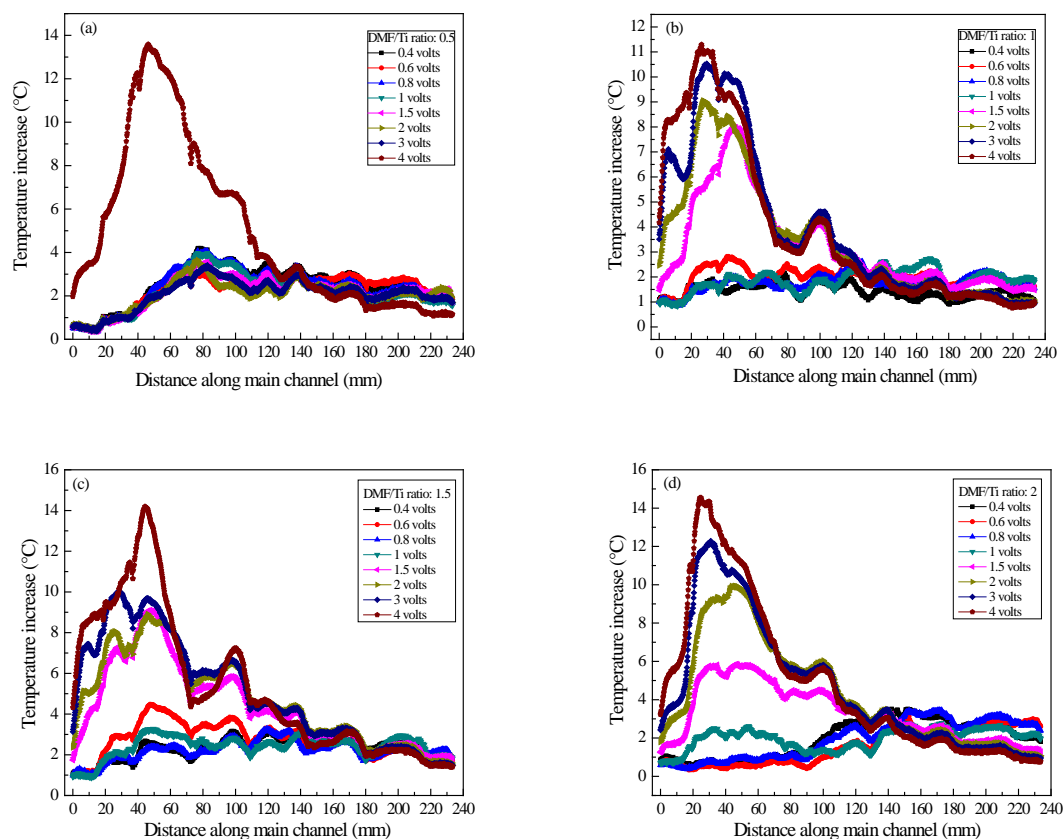
Figure 4.12: Temperature distributions in the 234mm long microreactor obtained with an electrical field and for DMF/Ti ratios equal to : (a) 0.5 (b) 1 (c) 1.5 and (d) 2
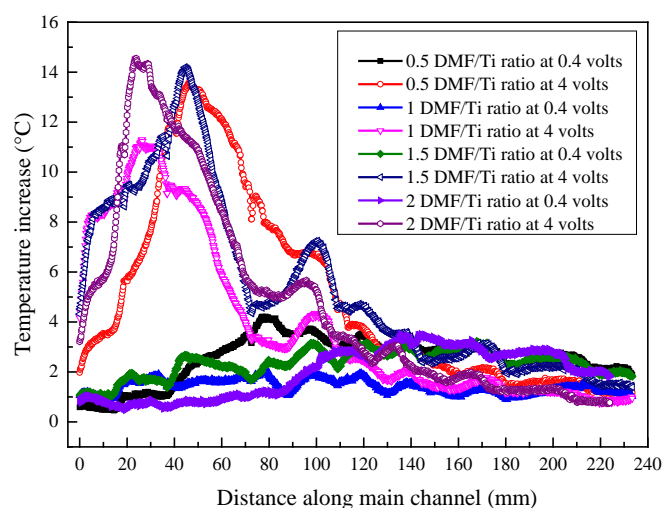

Figure 4.13: Temperature distribution in the 234mm long microreactor with a DC voltage of 0.4 and 4 V: ($TiOCl_2$ + 16.7% DMF and DMF with DMF/Ti ratios from 0.5 to 2)

Temperature distributions at the lower and higher voltages are compared in Figure 4.13as a function of the DMF/Ti ratio. A clear effect of the 4V voltage can be observed: with 0.4 V, the maximal temperature is about 4.5°C whereas with 4 V the temperature reaches 14.5°C.
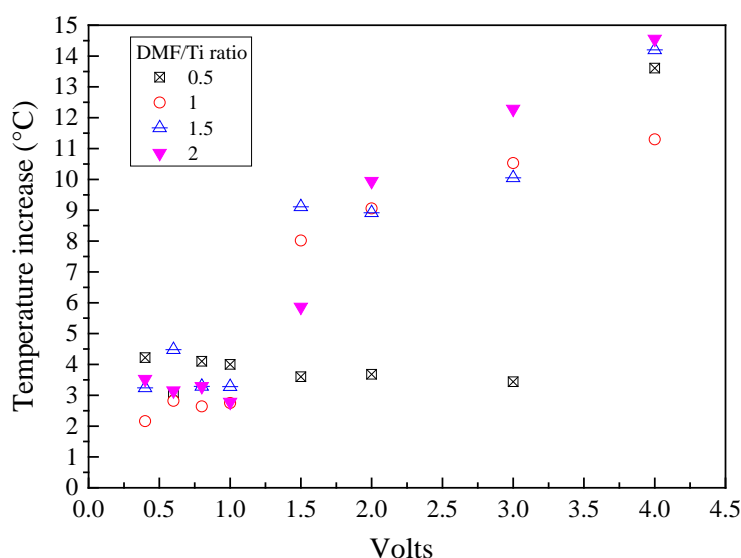

Figure 4.14: Maximum temperature recorded in the 234mm long microreactor during the mixing of $TiOCl_2$ + 16.7%DMF and DMF as function of the DC voltage and DMF/Ti ratios

Figure 4.14 shows the maximum temperature recorded for various DMF/Ti ratios and voltages. It can be seen that a better mixing takes place at higher DMF/Ti ratios (1, 1.5 and 2). However, as with DC voltage, water splitting and reduction of Ti^{4+} inTi^{3+} always occurs whatever the value of DMF/Ti ratio, one have also tested AC voltages. The results are reported in the next section.

4.2.3 Effect of AC electric field

In this section, the intensification of the mixing is performed by using an AC electric field. The idea is to use an adequate frequency whosevalue must be high enough in order to be much faster than the reaction kinetic of H_2O electrolysis. It's also important to find an adequate voltage to allow a better mixing.

4.2.3.1 Effect of flow rate on the mixing

Experiments were performed with the 214 mm long microreactor equipped with platinum electrodes and using the precursor $TiOCl_2$prediluted with 16.7% DMF. A large range of flow rate values were investigated keeping a 2.4 flow rate ratio between them. Figure 4.15 shows the IR images of the reaction in the microreactor for various flow rates, the AC voltage and frequency were kept equal to respectively 7 V AC and 1 MHz.
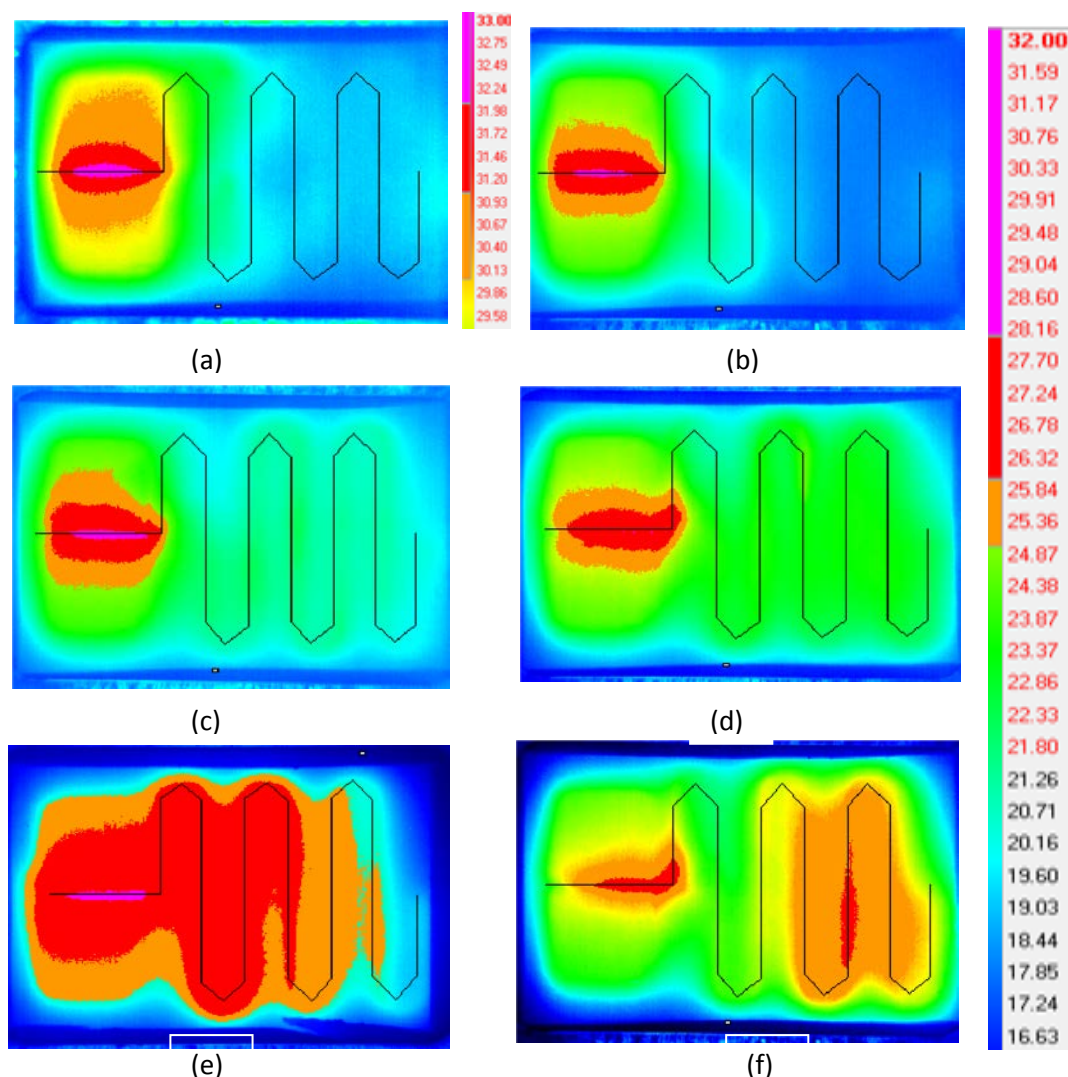
Figure 4.15: IR image of exothermic reaction inside the microreactor with a 7 V AC and 1 MHz AC voltage. Flow rates of precursor and DMF solvent:(a) 0.5 mL h^{-1} and 1.2 mL h^{-1} (b) 1 mL h^{-1} and 2.4 mL h^{-1} (c) 2 mL h^{-1}and 4.8 mL h^{-1} (d) 3 mL h^{-1} and 7.2 mL h^{-1} (e) 4 mL h^{-1} and 9.6 mL h^{-1} (f) 5 mL h^{-1} and 12 mL h^{-1}

Table 4.3:Experiments performed with pre-diluted TiOCl$_2$ with 16.7% of DMF (0.52 DMF/Ti) with an AC voltageof 7V AC and 1 MHz frequency.

TiOCl$_2$ (diluted with 16.7% DMF)		DMF		Main channel Velocity (m s^{-1})	Residual time for 30 mL Volume (minutes)	Stable Flow (✓) or unstable flow (✗)
Inlet flow Rate (1) (mL h^{-1})	Reynolds Number	Inlet flow Rate (2) (mL h^{-1})	Reynolds Number			
0.5	1.84 10^{-3}	1.2	0.34 10^{-3}	4.71 10^{-4}	1058.82	✓
1	3.68 10^{-3}	2.4	0.69 10^{-3}	9.42 10^{-4}	529.41	✓
2	7.37 10^{-3}	4.8	1.37 10^{-3}	18.8 10^{-4}	264.71	✓
3	11.1 10^{-3}	7.2	2.06 10^{-3}	28.2 10^{-4}	176.47	✓
4	14.7 10^{-3}	9.6	2.74 10^{-3}	37.6 10^{-4}	132.35	✗
5	18.4 10^{-3}	12.0	3.43 10^{-3}	47.1 10^{-4}	105.88	✗

It was observed from infrared images that the flow was fully stable for lower flow rates in the range of 0.5 to 3 mLh^{-1} for TiOCl$_2$+16.7% DMF and 1.2 to 7.2 mL h^{-1} for DMF. In fact for this low flowrate range, the reaction mainly takes place between the two electrodesand no thermal signature of the reaction is observed afterwards in the microchannel. On the contrary for higher flowrates, more than 3 mLh^{-1} for TiOCl$_2$+16.7% DMF and 7.2mL h^{-1} for DMF, the mixing was not sufficient to have the completion of the reaction between electrodes.Therefore temperature increases are reduced between the two electrodes and the reaction still occurs after the electrodes where the flow appears to be unstable.

These observations can also be inferred from Figure 4.16which shows the temperature distribution along the microchannel for the same measurements.Indeed between the two electrodes, the maximum temperature reaches 11.6°C for a low flow rate (1 mL h^{-1}) and 6.6°C for a high flow rate (4 mL h^{-1}).
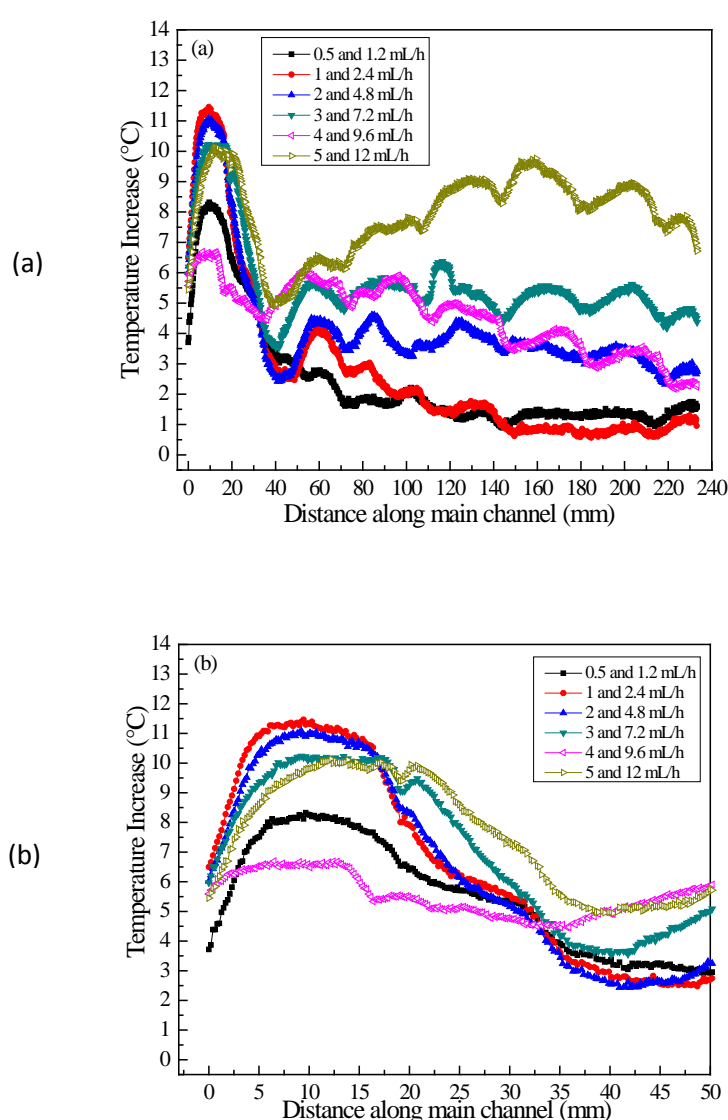
(a)

(b)

Figure 4.16: Temperature distribution in the 234mm long microreactor:mixing of the (TiOCl$_2$ + 16.7% of DMF) and DMF (with electrodes) with a 7 V AC and 1 MHz AC voltage (a) Full length of the channel (b) Zoom close to the electrodes;

4.2.3.2 Joule effect

As an electric field is used to activate the mixing, there is some heat produced by Joule effect. It is interesting to compare this contribution to the exothermal effect of the nanoparticle synthesis reaction. In the following, we have computed the power generated by Joule effect and the one produced by the reaction.

The "root mean square" value V_{rms} of an AC voltage is the value of a continuous voltage that will produce the same calorific effects (dissipated power) inside an electrical resistance. It is well known that for a a sinusoidal signal, the V_{rms} value can be obtained by divided the peak value of the AC voltage by $\sqrt{2}$:

Let's now calculate the electrical resistance of the fluid cell between the two electrodes as shown inFigure 4.17.
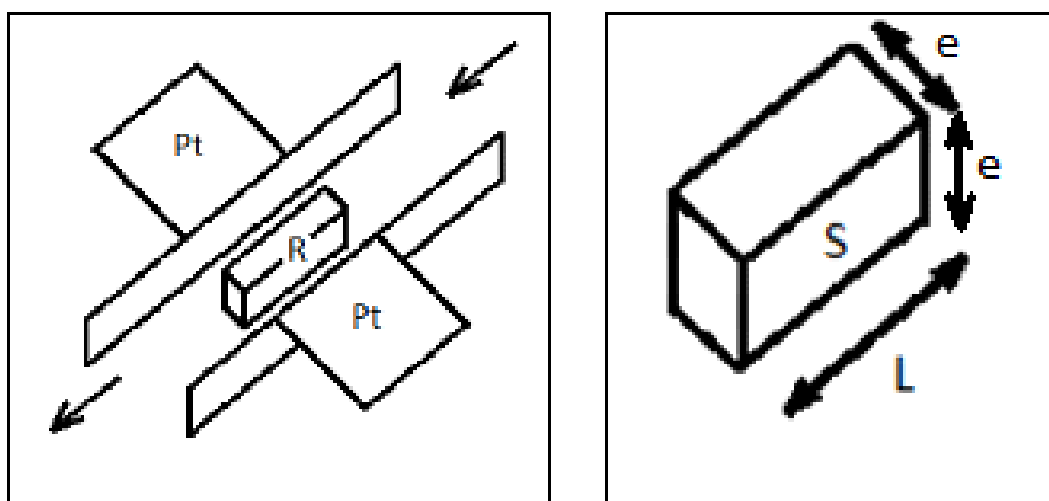

Figure 4.17: Fluid cell between electrodes interpreted as a resistance

The resistance R of the fluid cell is defined as: $R = \sigma^{-1} e S^{-1}$ where$\sigma$is thefluid electrical conductivity, e is the length of the gap between the two electrodes, and S=e*L is the section of the electrodes inside the microchannel. For the computation; the following values were considered:

σ= 2$\Omega^{-1}m^{-1}$ for TiOCl$_2$with DMF (data from previous work [2])
e = 1mm
L = 14mm (length of the electrodes)

Therefore the fluid cell has a resistance value of R = 397 Ω and applying Ohm's law, the electrical power dissipated in the fluid cell is:

$$P = \frac{V^2}{R} = \frac{7^2}{397} = \mathbf{1372\ mW}$$

This value has to be compared with the one of the synthesis reaction. Previously in section 3.4.2(Figure 3.15), the total heat fluxes measured using a Peltier cell (i.e. without electric field) were about 390 mW and 1000 mW for pure $TiOCl_2$ with flow rates of respectively 10.2 and 27.2 mL h^{-1}(sum of both inlet flow rates), as shown in Table 3.4. For $TiOCl_2$ with 15% DMF the values were even less 210 mW and 530mW for flowrates of respectively 10.2 and 27.2 mL h^{-1}(sum of both inlet flow rates). Therefore the heat provided by Joule effect with the active mixing is not negligible compared to the one provided by the reaction. The AC Voltage doesnot only provide a better mixing but also changes the thermal conditions of the reaction (i.e. increased temperature).

4.2.3.3 Effect of Frequency on mixing

Frequency value is very important, if this value is too low, it could have no effect on the mixing and it could also involve water electrolysis and production of Ti^{3+} as happened with DC electric field procedure. Various frequency values were tested by keeping a constant voltage of 7 VAC. First frequency value was 100 Hz then it was increased to 500Hz and then to 1MHz in order to avoid the water electrolysis phenomena.

Figured 4.15, 4.18 and 4.19 show the IR images of the reaction in the microreactor for various frequencies of the AC voltage and for various flow rates. Table 4.4 showsthe main results. Although, it can be seen from the IR images that change of frequencies are not causing that much difference in the stability of the flow but it was observed during experiments that lower frequency (0.1 MHz and 0.5 MHz) causes water electrolysis which can affect the end product. It was also noticed that at the higher flow rates (4 and 9.6 mL h^{-1}), the reaction takes place after passing the electrodes (Figures 4.15 e, 4.18 c and 4.19 c) showing that the flow is unstable.

Figure 4.20 shows the temperature distributions along the microchannel. One can see a clear effect of the frequency. Higher temperature peaks are obtained with the 1MHz frequency.

Table 4.4:Experiments performed withTiOCl$_2$ +16.7% DMF and DMF using an AC voltage of 7V AC and various frequencies

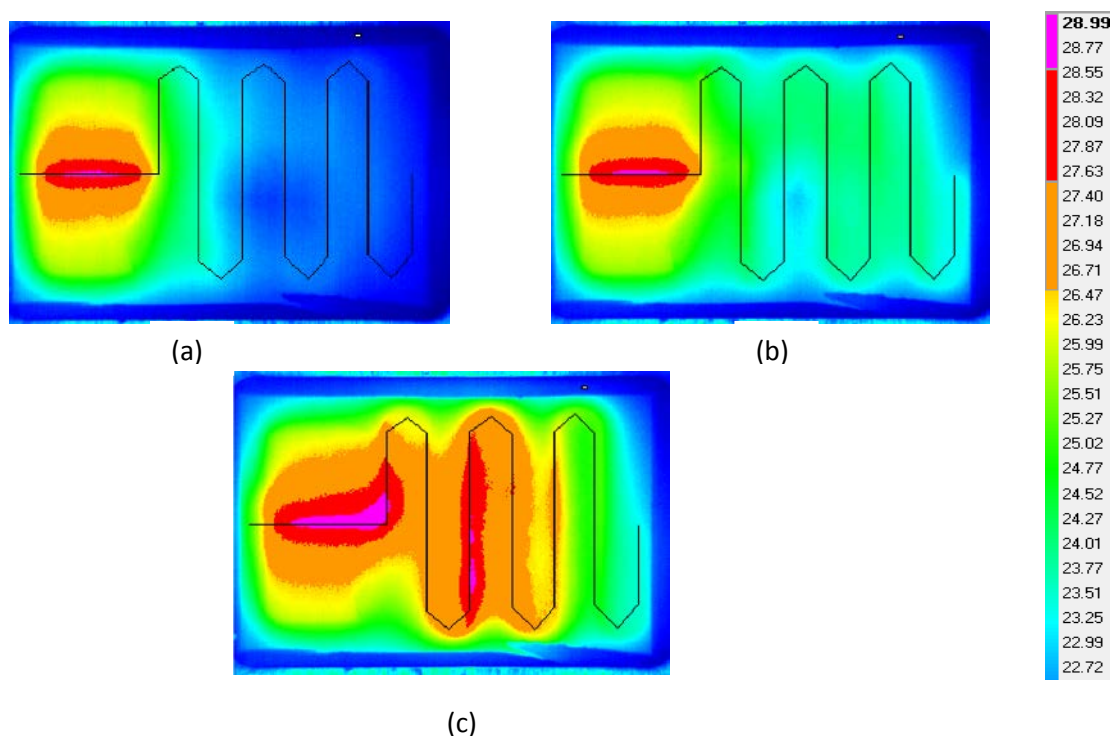| Frequency (MHz)	TiOCl$_2$ +16.7% DMF	DMF	Stable Flow (✓) or unstable flow (✗)	Comment
	Inlet flow Rate (1) (mL h^{-1})	Inlet flow Rate (2)(mL h^{-1})		
0.1	1	2.4	✓	Water electrolysis
	2	4.8	✓	Water electrolysis
	4	9.6	✗	Water electrolysis
0.5	1	2.4	✓	Water electrolysis
	2	4.8	✓	Water electrolysis
	4	9.6	✗	Water electrolysis
1	1	2.4	✓	No Water electrolysis
	2	4.8	✓	No Water electrolysis
	4	9.6	✗	No Water electrolysis

Figure 4.18: IR image of exothermic reaction with an AC voltage of 7 V AC and a 0.1 MHz frequency. ($TiOCl_2$ +17% DMF and DMF with the respective flow rates equal to (a) 1 mL h^{-1} and 2.4 mL h^{-1} (b) 2 mL h^{-1} and 4.8 mL h^{-1} (c) 4 mL h^{-1} and 9.6 mL h^{-1})
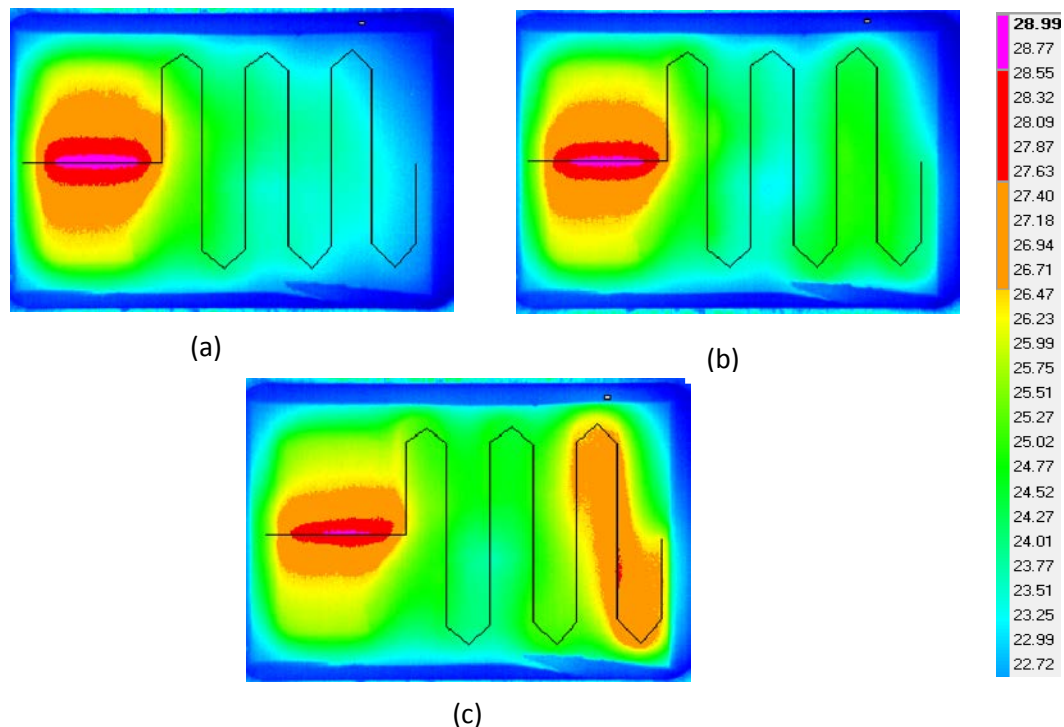

Figure 4.19: IR image of exothermic reaction with an AC voltage of 7 V AC and a 0.5 MHz frequency ($TiOCl_2$ +17% DMF and DMF with the respective flow rates equal to (a) 1 mL h^{-1} and 2.4 mL h^{-1} (b) 2 mL h^{-1} and 4.8 mL h^{-1} (c) 4 mL h^{-1} and 9.6 mL h^{-1})
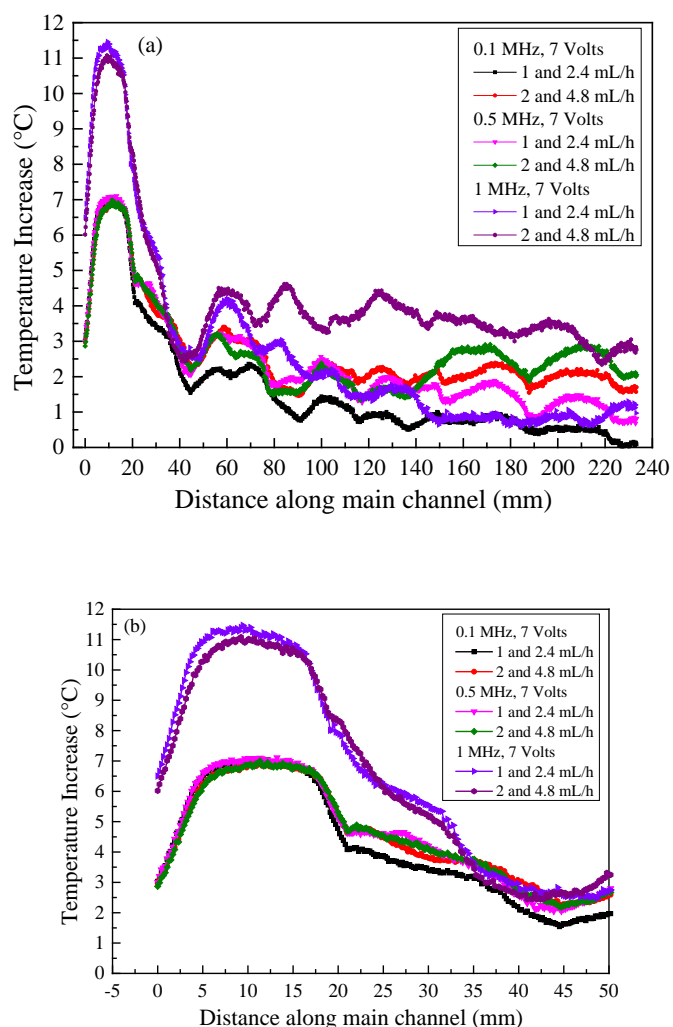
Figure 4.20: Effect of frequency on the temperature distribution in the 234mm long microreactor: (TiOCl$_2$ + 16.7% DMF and DMF) :(a) Full length of the channel, (b) Zoom close to the electrodes

4.2.3.4 Effect of Voltages on the mixing

Various values of AC voltages were tested while keeping the frequency constant. Infrared images are presented in Figure 4.21 and temperature distributions along the microchannel in Figure 4.22. The decrease of the voltage from 7 to 5 V AC has reduced the temperature increase probably due to a lower Joule effect. In addition as shown in Figure 4.21 (b) with 5V AC and flowrate of 2 and 4.8 mL h^{-1}, the reaction was not fully achieved between the two electrodes resulting in a discontinuous and unstable flow afterwards.
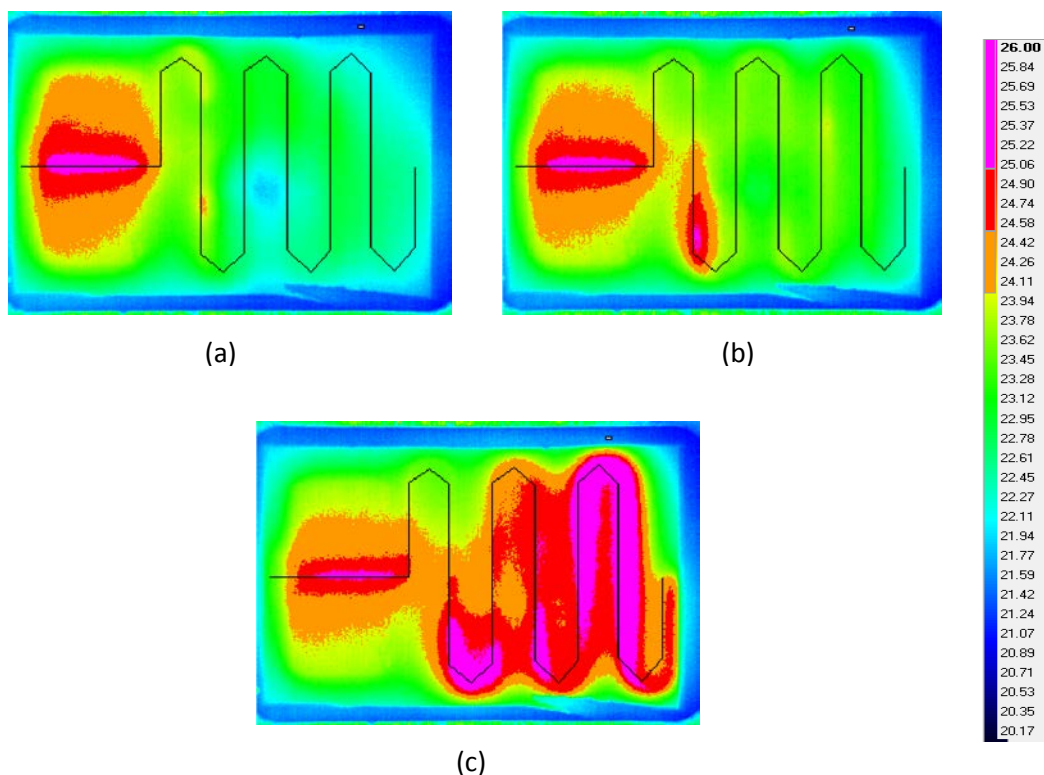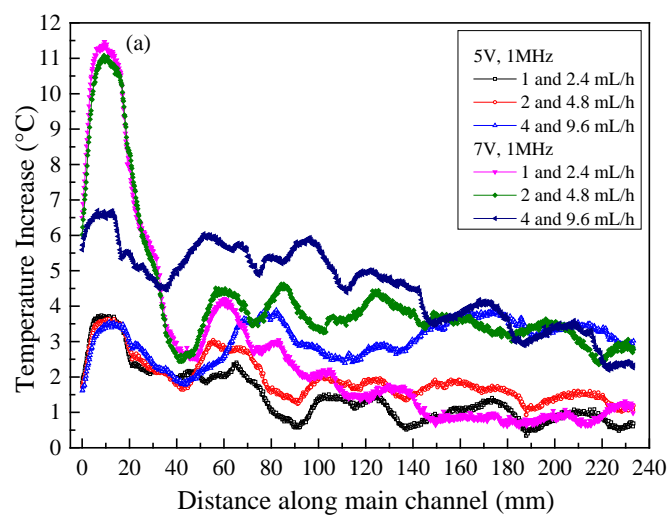
Figure 4.21: IR image of exothermic reaction with an AC voltage of 5 V AC and a 1 MHz frequency (TiOCl$_2$ + 16.7% DMF and DMF with flow rates respectively of (a) 1 mL h^{-1}and 2.4 mL h^{-1} (b) 2 mL h^{-1}and 4.8 mL h^{-1} (c) 4 mL h^{-1} and 9.6 mL h^{-1})
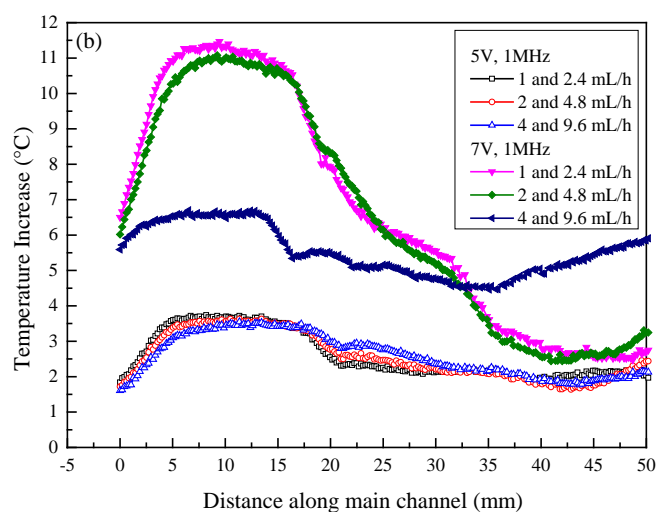
Figure 4.22: Effect of AC voltages on the temperature distribution in the 234mm long microreactor (TiOCl$_2$ + 16.7% DMF and DMF), 1MHz frequency: (a) Full length of the channel (b) Zoom close to the electrodes

Figure 4.23 presents the different peaks of temperature showing that they are reduced from 8-12 °C to 3.5-4°C when shifting from 7 V AC to 5 V AC.
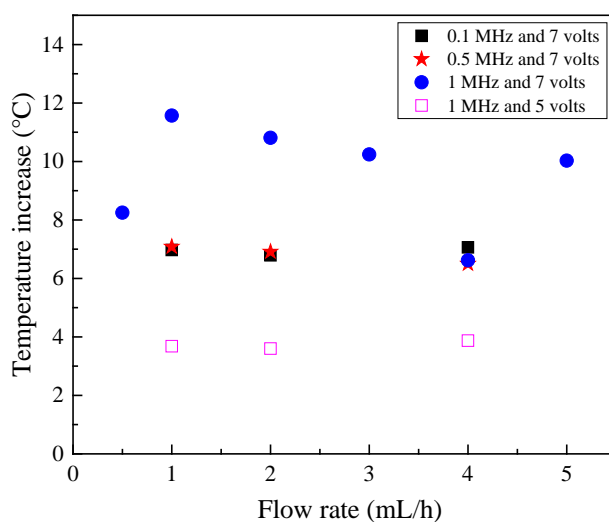

Figure 4.23: Maximum temperature recorded in the 234mm long microreactor(TiOCl$_2$ + 16.7% of DMF and DMF)

4.3 Pure Solution

As the previous experiments have shown that the mixing of prediluted $TiOCl_2$ could be enhanced without involving water hydrolysis by using a 7V AC and 1MHz frequency AC Voltage, it is of great interest to see what happens if we used the pure $TiOCl_2$ solution.

In this section, results are presented for pure $TiOCl_2$ and DMF injected into the 234mm long microreactorwith a large range of flowrate (0.5 to 5mL h^{-1} for $TiOCl_2$ and 1.2 to 12mL h^{-1} for DMF).A 7 V AC voltage with a 1 MHz frequency was used. Infrared measurements are presented in Figure 4.24 and observations on the flow in Table 4.5.

Table 4.5: Experiments performed with pure $TiOCl_2$ and DMF with a 7 V AC voltage and a 1 MHz frequency

Pure $TiOCl_2$		DMF		Main channel Velocity (m s^{-1})	Residual time for 30 mL Volume (minutes)	Stable Flow (✅) or unstable flow (❌)
Inlet flow Rate (1) (mL h^{-1})	Reynolds Number	Inlet flow Rate (2) (mL h^{-1})	Reynolds Number			
0.5	$3.0 \ 10^{-3}$	1.2	$0.34 \ 10^{-3}$	$4.71 \ 10^{-4}$	1058.82	✅
1	$6.0 \ 10^{-3}$	2.4	$0.69 \ 10^{-3}$	$9.42 \ 10^{-4}$	529.41	✅
1.5	$9.0 \ 10^{-3}$	3.6	$1.03 \ 10^{-3}$	$14.1 \ 10^{-4}$	352.94	✅
2	$12.0 \ 10^{-3}$	4.8	$1.37 \ 10^{-3}$	$18.8 \ 10^{-4}$	264.71	✅
3	$18.0 \ 10^{-3}$	7.2	$2.06 \ 10^{-3}$	$28.2 \ 10^{-4}$	176.47	❌
5	$30.0 \ 10^{-3}$	12	$3.43 \ 10^{-3}$	$47.1 \ 10^{-4}$	105.88	❌

It was observed from infrared images that the reaction was achieved between the electrodes only forlowflow rates between 0.5 and 2mL h^{-1} for pure $TiOCl_2$ and 1.2 to 4.8mL $h^{-1}$for DMF. For higher flow rates, the reaction has appeared further along the microchannel and the flow of reactants was no more stable as shown in Figure 4.24 e and f.
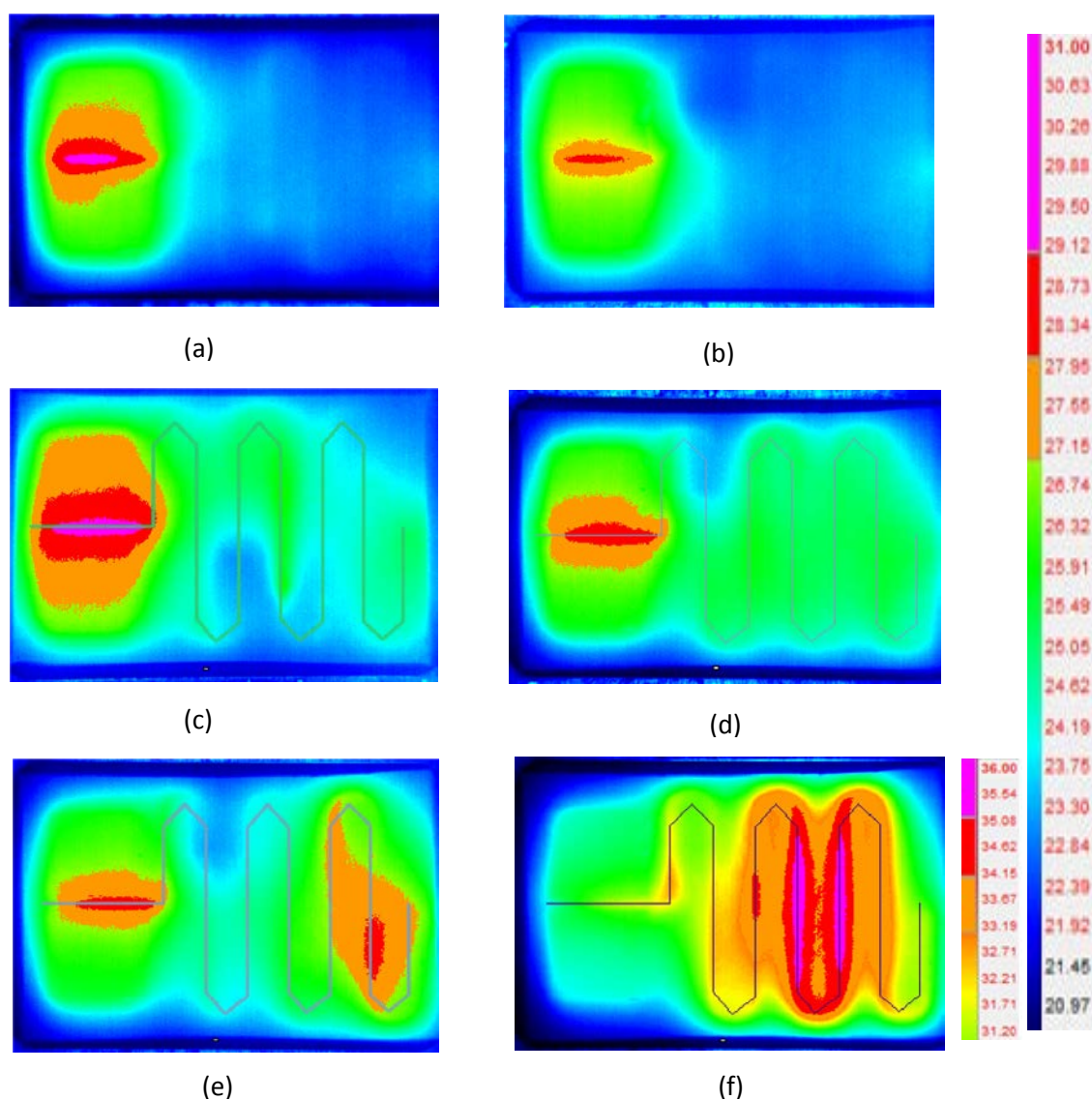
Figure 4.24: Infrared image of exothermic reaction inside the microreactorwith an AC voltage of 7V AC and a 1 MHz frequency (pure $TiOCl_2$ and DMF with flowrates respectively of : (a) 0.5 mL h^{-1} and 1.2 mL h^{-1} (b) 1 mL h^{-1} and 2.4 mL h^{-1} (c) 1.5 mL h^{-1} and 3.6 mL h^{-1} (d) 2 mL h^{-1} and 4.8 mL h^{-1} (e) 3 mL h^{-1} and 7.2 mL h^{-1} (f) 5 mL h^{-1} and 12 mL h^{-1})

Figure 4.25 shows the temperature distribution along the microchannel. For the two experiments with higher flow rates, one can observed temperature increase along the main microchannel after passing electrodes.
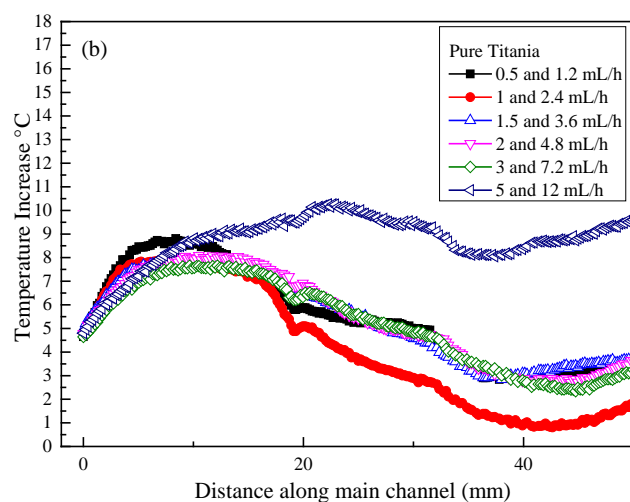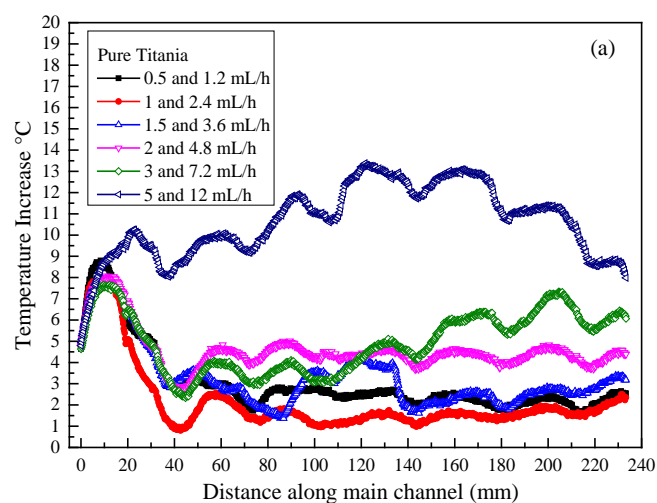
Figure 4.25: Temperature distribution in the 234mm long microreactor with a 7V AC Voltage and a 1 MHz frequency (pure $TiOCl_2$ and DMF) :(a) Full length of the channel (b) Zoom close to the electrodes,

4.4 Conclusion

In this 4th chapter, much longer microchannels (294 and 234mm long) were used. Without electric field, the flow with both reactants $TiOCL_2$ +16.7 % DMF and DMF was more stable than that was observed with shorter microchannel (32mm).

The activation of the electric field between two platinum electrodes located just after the inletshasenhancedthe mixing and therefore accelerated the nanoparticle synthesis reaction. In fact the electric fielddestabilizes the interface between the two reactive fluids. However, operating conditions to supply the electric field have to be appropriate.

Using a DC electric field, flows became stable for voltage from 1.5 to 4 V but one have noticedthe existence of the gas formation caused by water electrolysis and formation of Ti^{3+}. These problems which are detrimental for TiO_2 nanoparticle production were overcome by using an AC electric field. Frequencies of 0.1 and 0.5 MHz with a 5V voltage figured out to be too small. Finally, a 1MHz frequency and a 7V AC voltage appeared to be appropriate to avoid water electrolysisand formation of Ti^{3+} while providing enough mixing. Those results were obtained for $TiOCl_2$prediluted with 16.7%DMF. For pure $TiOCl_2$, the operating conditions 7 V AC voltage and 1 MHz frequency have also allowed the mixing enhancement without the occurrence of water electrolysis and Ti^{3+}. For prediluted or pure $TiOCl_2$ the flow rate should not exceed 2 mLh^{-1} since due to excessive velocity the reaction is not achieved while the reactive fluids is crossing the gap between the two electrodes. Otherwise the use of an electric field for mixing enhancement has induced changes in the thermal conditions inside the microreactorsince a significant heat flux compare to the one provided by the reaction is produced by Joule effect.

Next chapter will be dedicated to the analysis of the solutions collected at the outlet of the microchannel during each experiment.

References:

[1]   A. O. E. Moctar, N. Aubry, and J. Batton, "Electro-hydrodynamic micro-fluidic mixer," *Lab. Chip*, vol. 3, no. 4, pp. 273–280, 2003.

[2]   G. Guignard, "Vers la réalisation d'un prototype de photo-batterie à base de sols-gels d'oxyde de titane photosensibles.," Université de Nantes, 2014.

Chapter 5

**Sols characterization
by DLS and Raman scattering**

5.1 Size distribution by DLS

In the following, the word size is used instead of hydrodynamic diameter since we estimated in Chapter 2 that the Debye length is less than 0.2 nm. Size of nanoparticles and size distribution of nanoparticles were analysed by using Malvern Zeta Sizer Nano ZS, described in section 2.4.1.Despite the viscosity of samples increases with time due to approach of the sol to gel transition, the solvent in which the particles are suspended remains DMF, therefore we decided to keep the viscosity of DMF in the DLS data treatments, as mentioned in Chapter 2.To assess the precision on size, the standard deviation from the DLS fit was also plotted.Samples were prepared from the TiDMF sols at the end of mixing in the microreactor as explained in section 2.4.1.2.

5.1.1 Nanoparticles produced using Y-shape short microchannel (Pre-mixed Solution)

In this section, we further analysed the sols produced using Y-shape microreactor at various flow rates range for pre-diluted $TiOCl_2$ with 16.7% of DMF (4-7 mLh^{-1}) and for DMF (9.6-16.8 mL h^{-1}) at 2.4 flow rate ratio, as discussed in section 3.2.2.

5.1.1.1 Sols quality and polydispersity analysis

To check the quality of the data, as explained in section 2.4.1.1. (iii). Intercept values of the autocorrelation function of each sample was plotted in Figure 5.1. If intercept value is greater than 0.9 then the measurement is correct and if it is between 0.6 and 0.9 then the system is good and values lower than 0.6 measurement is considered as a bad measurement. Figure 5.1 shows that all the samples tested are having intercept values between 0.81 and 0.95 (y-axis) and at various days (x axis) which shows that all our samples are having good quality to do analysis.
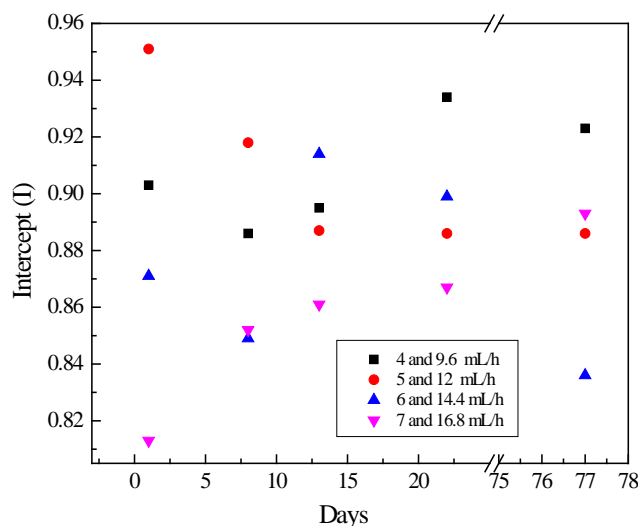

Figure 5.1: Intercept at various days to check the quality of the samples.
Flow rates: 4mL h^{-1} and 9.6 mL h^{-1} (■), 5mL h^{-1} and 12mLh^{-1}, (●), 6 mL h^{-1} and 14.4mL h^{-1} (▲), 7 mL h^{-1} and 16.8 mL h^{-1} (▼)

Second thing for size distribution analysis is to check whether our samples are having narrow or broad distribution. In order to check the size distribution, polydispersity index (PDI) were evaluated during DLS analysis for each sample at various days and plotted in Figure 5.2. If PDI is greater than 0.7 then size distribution is broad and samples are not suitable for DLS analysis. It was found from Figure 5.2 that for high flow rates, the PDI is large indicating that the sols exhibit multiple size distributions, however the latter are getting narrower (below 0.7) as time passes more consistently at lower flow rates (4 and 9.6 mL h^{-1} and 5 and 12 mL h^{-1}).
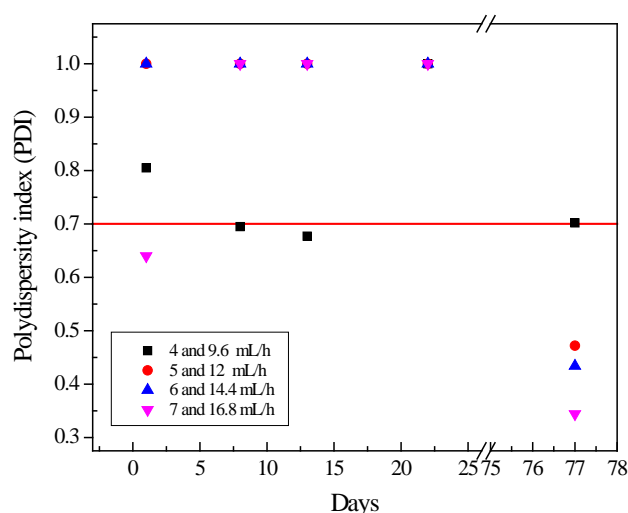

Figure 5.2: Polydispersity index (PDI) at various days.
Flow rates: 4mL h^{-1} and 9.6 mL h^{-1} (■), 5mL h^{-1} and 12mLh^{-1}, (●), 6 mL h^{-1} and 14.4mL h^{-1} (▲), 7 mL h^{-1} and 16.8 mL h^{-1} (▼)

5.1.1.2 Effect of time on NPs

To study the effect of time on nanoparticles size, a 20mL of TiDMF volume sol was stored in cells for each flow rate mentioned above. DLS analysis was performed for each sample at various days (day 1, day 8, day 22 and day 77) till sol becomes gel. We let the sol-gel transition to occur at room temperature.

Correlogram (Figure 5.3)shows that as time passes then correlation function decays more quickly than previous days which indicate that size of nanoparticles are getting smaller before transforming into gel. Similarly, auto-correlation fit is getting better as time passes (see Figure 5.4).

It was revealed from analysis that size distribution and size of nanoparticles remains constant from day 8 till day 22 for lower flow rates (4 and 9.6, 5 and 12 and 6 and 14.6 mL h^{-1}) (between 9 – 10.7nm) then suddenly increases before sol to gel transition. While size of nanoparticles increases with time for higher flow rates (7 and 16.8 mL h^{-1}) and continuously increasing till occurrence of the sol to gel transition, as demonstrated in Figure 5.5 and Figure 5.6. In Figure 5.5, x-axis indicates size distribution of nanoparticles and y-axis indicates the quantity of nanoparticles in terms of volume percentage. In Figure 5.6, x-axis indicates days and y-axis indicates size of nanoparticles. Sizes of the nanoparticles were found to lye

between 5 nm-40 nm size for 5 and 12 mL h^{-1} on different days.Taking into account the standard deviation, we can conclude that the size does not evolve for 22 days.
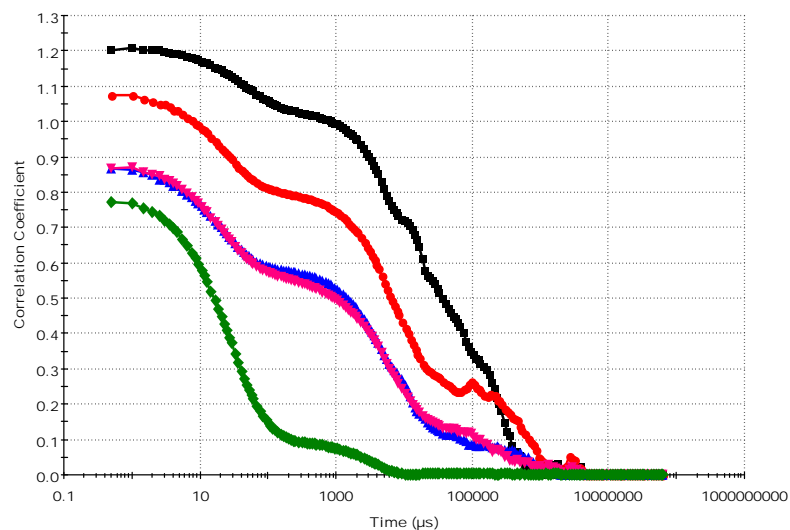

Figure 5.3: Correlogram at various days (Day 1(━■━), Day 8(━●━), Day 13(━▲━), Day 22 (━▼━) and Day 77 (━◆━))
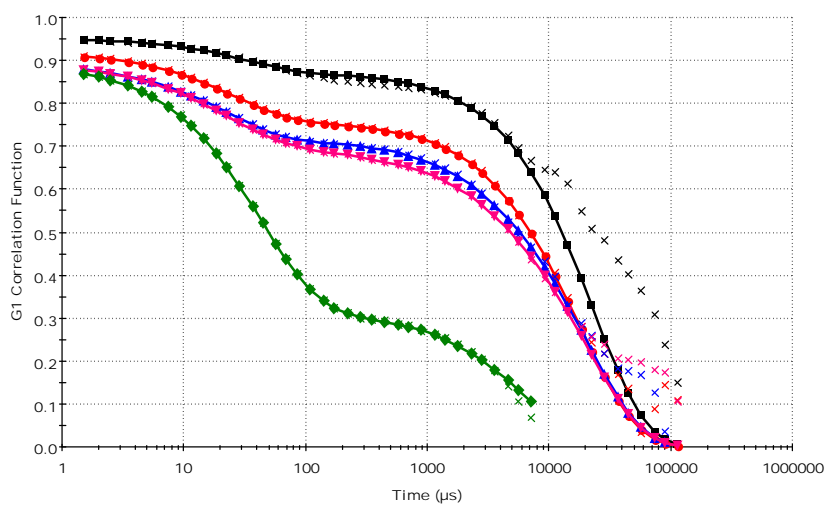Flow rate: 5 and 12 mL h^{-1}

Figure 5.4:Auto-correlation function fit at various days (Day 1(━■━), Day 8(━●━), Day 13(━▲━), Day 22 (━▼━) and Day 77 (━◆━))
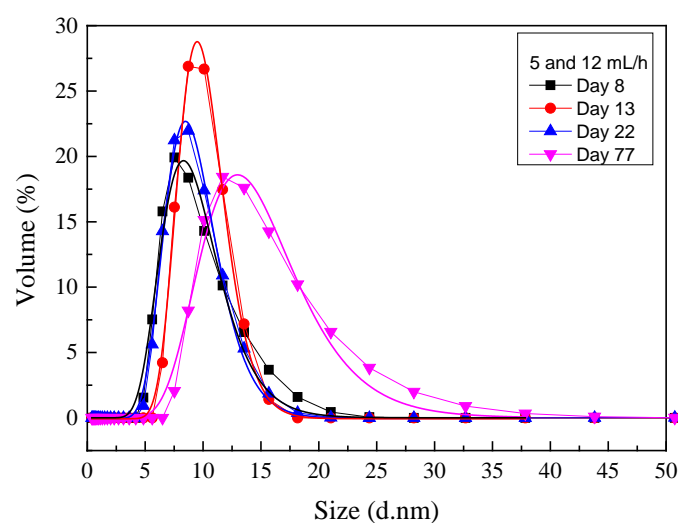Filled symbols (Fitted data) and Cross symbols (Experimental data)
Flow rate: 5 and 12 mL h^{-1}

Figure 5.5: Size distribution of nanoparticles at 5mL h^{-1} and 12mLh^{-1} flow rate. Day 8(■), Day 13 (●), Day 22 (▲), Day 77(▼)
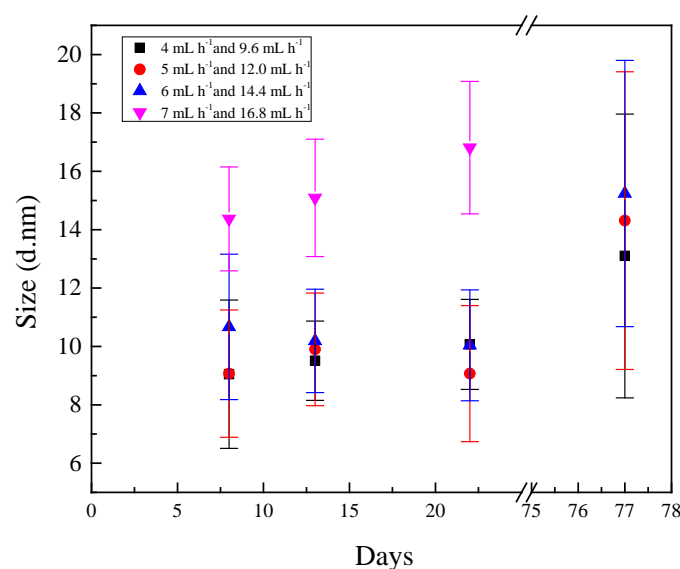

Figure 5.6: Size of nanoparticles at various days and various flow rates. Flow rates: 4 and 9.6 mL h^{-1} (■), 5and 12mLh^{-1}, (●), 6 and 14.4mL h^{-1} (▲), 7 and 16.8 mL h^{-1} (▼)

5.1.1.3 Effect of flow rate on NPs

To study the effect of flow rate on the nanoparticles size and distribution, various sols were prepared by using four different flow rates for pre-diluted TiOCl$_2$ (4, 5, 6 and 7 mLh^{-1}) and for DMF (9.6, 12, 14.4 and16.8 mL h^{-1}) at 2.4 flow rate ratio. Initially, freshly TiDMF prepared sols which is entirely in liquid state were analysed.

Correlogram (Figure 5.3) shows the existence of very large particles as correlation function decays very slowlyon day 1 for 5 and 12 mLh^{-1}. Normally, correlation function decays quickly for small particles because small particles move quickly as explained in section 2.4.1.The auto-correlation function is not fitted properly for day 1 especially after 100

μs (Figure 5.4) indicating the presence of large particles that are not accounted for at all in the size distribution. So, it is very difficult to comment on the result for day 1.

Figure 5.7 (a) shows the size distribution of nanoparticles on day 1 with effect of different flow rates, x-axis indicates the size of the nanoparticles and the y-axis indicates the quantity of nanoparticles in terms of volume percentage. It was revealed from size distribution analysis that sols contain polydisperse nanoparticles (different size of nanoparticles). Size distribution is also very poor at day 1 with wider distribution (PDI > 0.7) and very few points to define the size distribution indicating that it is meaningless.

Therefore, samples were re-tested for DLS after waiting for few days on day 8, shown in Figure 5.7 (b). At day 8, the size distribution of nanoparticles (in volume distribution) is much narrower with enough points for defining size distribution.It can be seen in Figure 5.3 that on day 8, correlation function also decays more quickly than day 1. While Figure 5.7 (c) shows the size distribution of nanoparticles in terms of intensity at day 8. One can see in Figure 5.7 (c) existence of large particles or dust particles at the end of the x-axis. These particles represents very small amount of sols which can be ignored.
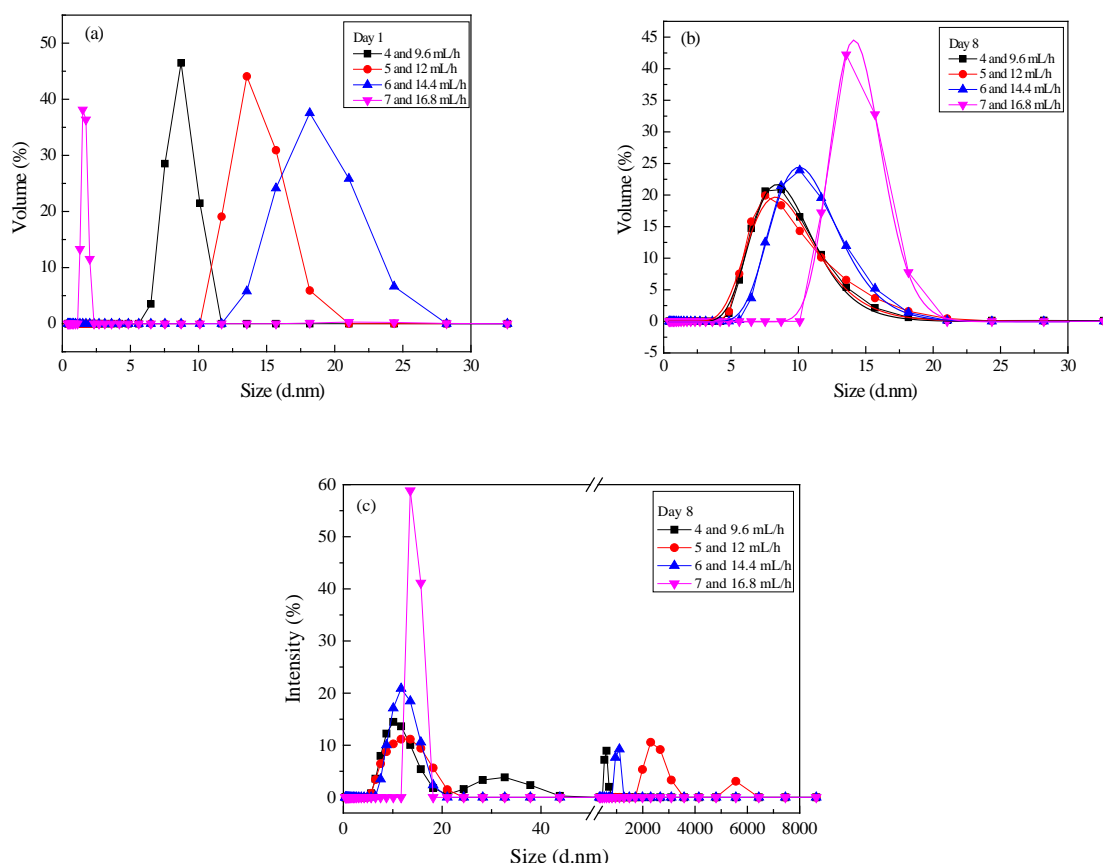

Figure 5.7: Size distribution of nanoparticles (a) Volume distribution at Day 1 (b) Volume distribution at Day 8 (c) Intensity distribution on Day 8
Flow rates: 4mL h^{-1} and 9.6 mL h^{-1} (—■—), 5mL h^{-1} and 12mLh^{-1}, (—●—), 6 mL h^{-1} and 14.4mL h^{-1} (—▲—), 7 mL h^{-1} and 16.8 mL h^{-1} (—▼—)

It was compared from the volume distribution graphs at day 8 (Figure 5.7 (b)) and size of nanoparticles at various days with effect of different flow rates (Figure 5.6) that size of

nanoparticles increases with increase of flow rates. Later, it was also noticed that size of nanoparticles increases at various other days also (day 13, 22 and 77) before transforming into gel, demonstrated in Figure 5.7 (b) and Figure 5.6. It can be seen in Figure 5.7 (b) and Figure 5.6 that size of nanoparticles (y-axis) increases at various days (x-axis).

5.1.2 Nanoparticles produced using longer microchannel

5.1.2.1 Without electric field (Pre-mixed Solution)

In this section, we further analysed the sols produced using 234mm longmicroreactor at various flow rates range for pre-diluted $TiOCl_2$with 16.7% of DMF (1-5 mLh^{-1}) and for DMF (2.4-12 mL h^{-1}) at 2.4 flow rate ratio, as discussed in section 4.2.1.

5.1.2.1.a Sols quality and polydispersity analysis

In order to check the quality of the data, intercept values of each sample were plotted in Figure 5.8. Figure 5.8 shows that all the samples (filtered) tested are having intercept values between 0.76 and 0.91 at various days which shows that all measurements are of good quality. Even non-filtered sols are having good quality for DLS analysis (Intercept values between 0.63 and 0.95).
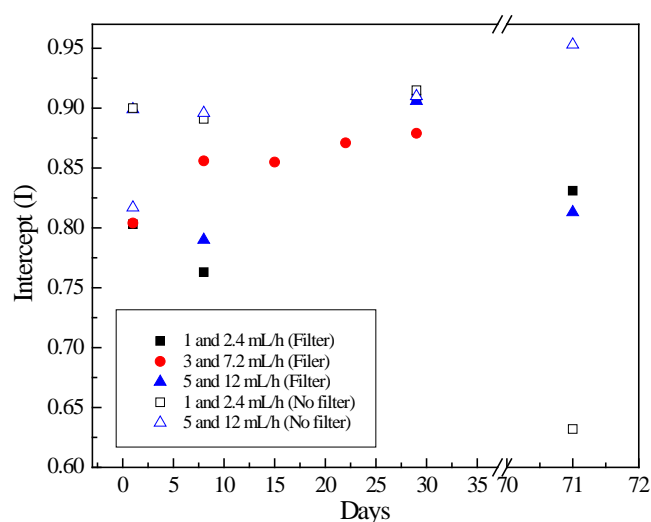

Figure 5.8: Intercept values at various days to check the quality of the samples.
Flow rates: 1 and 2.4 mL h^{-1} (Filtered (■) and Non filtered (□)), 3 and 7.2 mLh^{-1} (—●—), 5and 12mLh^{-1}(Filtered (▲) and Non filtered (△))

Figure 5.9: Polydispersity index (PDI) at various days.
Flow rates: 1 and 2.4 mL h^{-1} (Filter (■) and No filter (□)), 3 and 7.2 mLh^{-1} (─●─),
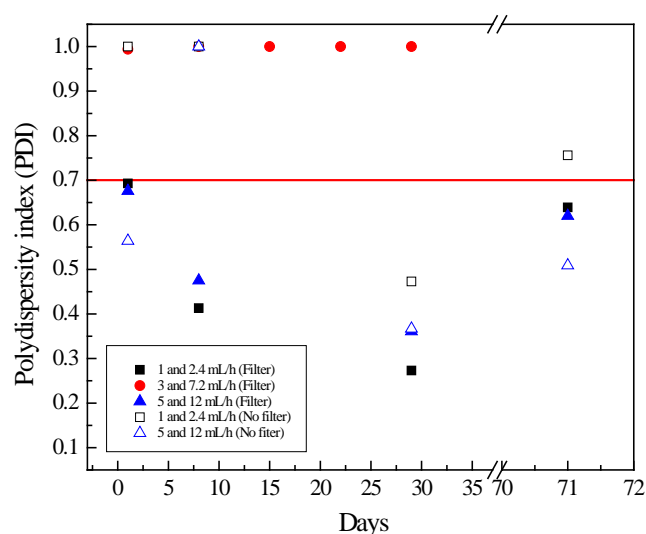5and 12mLh^{-1}(Filter (▲) and No filter (△))

For the size distribution analysis, polydispersity index (PDI) were evaluated during DLS analysis for each sample (filtered and non-filtered) at various days and plotted in Figure 5.9. Figure 5.9 revealed that size distributions for nanoparticles(filtered sols and non-filtered sols) are getting narrower (PDI<0.7) as time passes more consistently at very low flow rate (1 and 2.4 mL h^{-1}) and at very high flow rate (5 and 12 mL h^{-1}) then suddenly getting broader size distribution before transforming into gel. It can be noticed that filtered samples are having much narrower size distribution as compared to non-filtered samples at any day. So, it is better to do filtration for each sol as it is giving better size distribution values (PDI<0.7).

5.1.2.1.b Effect of filtration on the sols

In order to check the effect of filtration, two samples were selected. They were prepared for different flow rates (1 and 2.4mL h^{-1}) and (5 and 12 mL h^{-1}). Filtration of solswere performed as explained in section 2.4.1.2. Both the samples (Filtered and non-filtered) were analysed under DLS technique for the size distribution at different days.

It was noticed that filtration process avoids the dust and large particles in the sol as shown in correlogram (Figure 5.10) and auto-correlation fit (Figure 5.11).
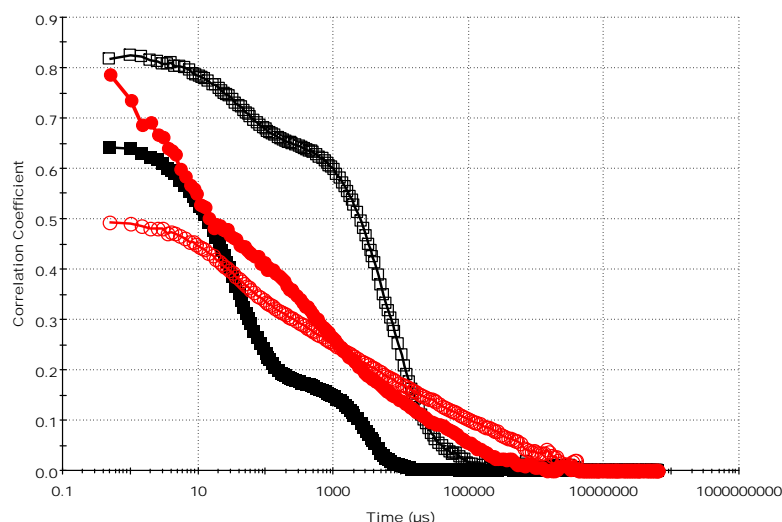
Figure 5.10: Correlogram at days (Day 1(─■─), Day 77 (─●─)
Filled symbols (Filtered) and Hollow symbols (Non filtered)
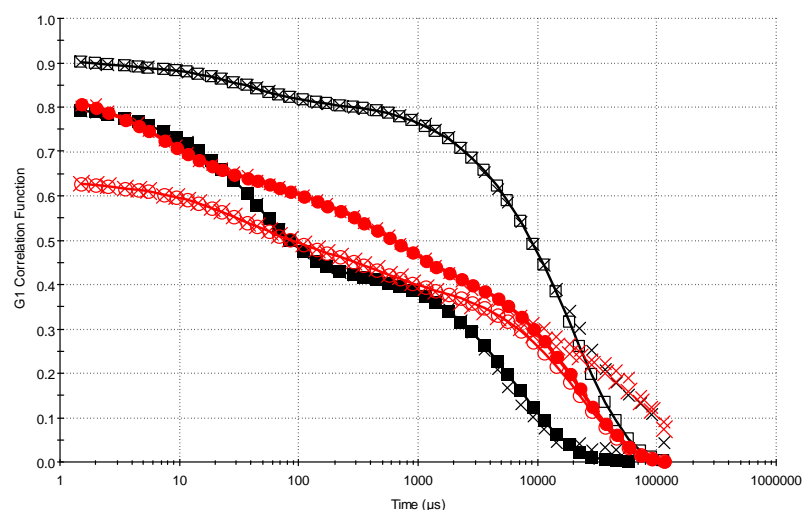Flow rate: 1 and 2.4 mL h^{-1}

Figure 5.11: Auto-correlation function fit at various Day 1(─■─), Day 77 (─●─)
Filled and Hollow symbols (Fitted data) and Cross symbols (Experimental data)
Flow rate: 1 and 2.4 mL h^{-1}

It can be seen in the Figure 5.10 that filtered sol correlogram decays more quickly as compared to without filtering, which shows the existence of large particles in the sol. While auto-correlation fit of total decay time (Figure 5.11) revealed the existence of large particles at the end which is not properly fitted for non-filtered sol. In without filtering, small and large particles are mixed and large particles scattered more light in DLS.

Figure 5.12 shows size of nanoparticles and it can be seen in the Figure 5.12 that filtration is not hugely causing difference in the size of nanoparticles at the initial days. However, it was already noticed in intensity size distribution (previously noticed in Figure 5.7(c)) that large and dust particles are creating various different peaks in the intensity distribution, so sometimes it is difficult to get real size of nanoparticles without filtration process.
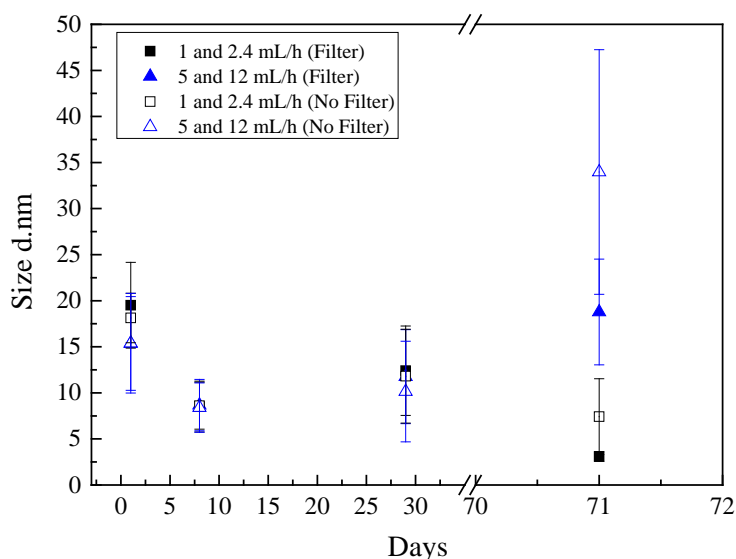
Figure 5.12: Effect of filtration on the sols at various days.
Flow rates: 1 and 2.4 mL h^{-1} (Filtered (■) and Non filtered (□)) and 5and 12mLh^{-1}(Filtered (▲) and Non filtered (△))

In general, as time passes then size of nanoparticles is decreasing then suddenly increasing till filtered sols become gel. But for non-filtered sols, as time passes size of nanoparticles decreases then increases quickly with big difference. This difference can be caused by the dust or large particles or agglomeration process of large particles. So filtration is required for each experiment to avoid this dust and large particles from the sols. Therefore, we kept filtered sols samples for further analysis.

5.1.2.1.c Effect of time on NPs

To study the effect of time on nanoparticles size, a 20mL of TiDMF volume sol was stored in cuvettes for each flow rate mentioned above. DLS analysis was performed for each sample at various days (day 1, day 8, day 15, day 22, day 29 and day 71) till sol becomes gel. We let the sol-gel transition to occur at room temperature.

Correlograms (Figure 5.13 and Figure 5.14) show that as time passes then correlation function decays more quickly than previous days, which indicates that size of nanoparticles are getting smaller before transforming into gel. However, it was noticed that after long period (day 71) correlogram starts decaying more slowly, which indicates the size of nanoparticles are increasing before transforming into gel. Similarly, auto-correlation fit is getting better fitting as time passes (see Figure 5.15 and Figure 5.16).

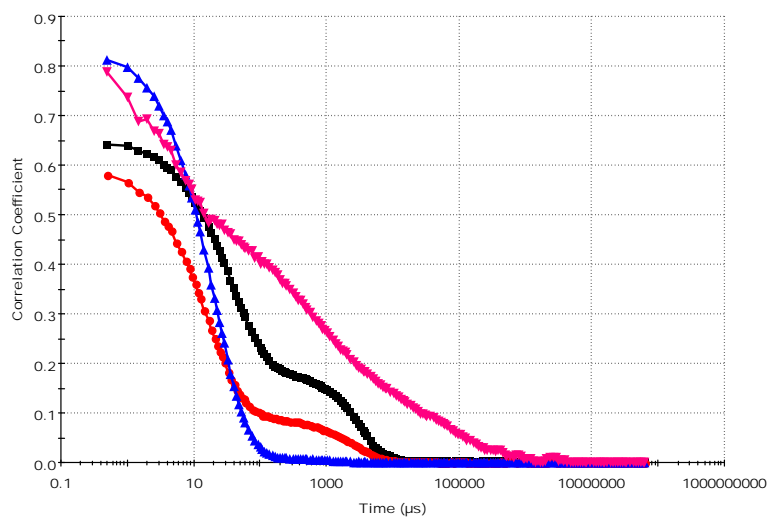Figure 5.13: Correlogram at various days (Day 1 (━■━), Day 8 (━●━), Day 29 (━▲━) and Day 71 (━▼━))
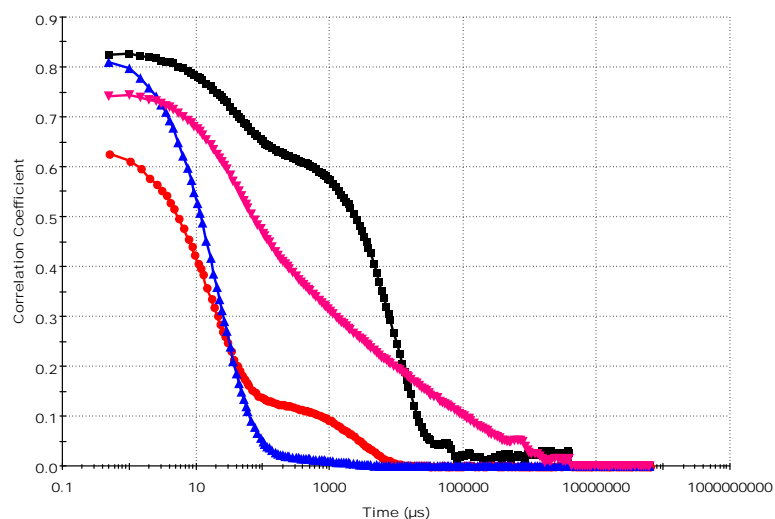Flow rate: 1 and 2.4 mL h^{-1}

Figure 5.14: Correlogram at various days (Day 1 (━■━), Day 8 (━●━), Day 29 (━▲━) and Day 71 (━▼━))
Flow rate: 5 and 12 mL h^{-1}

Figure 5.15: Auto-correlation function fit at various days (Day 1(■), Day 8(●), Day 13(▲), Day 22 (▼) and Day 77 (◆))
Filled symbols (Fitted data) and Cross symbols (Experimental data)
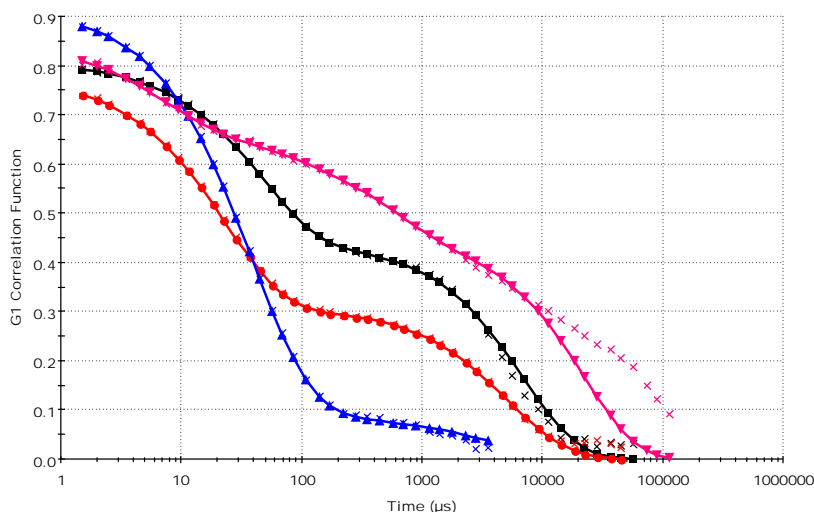Flow rate: 1 and 2.4 mL h^{-1}
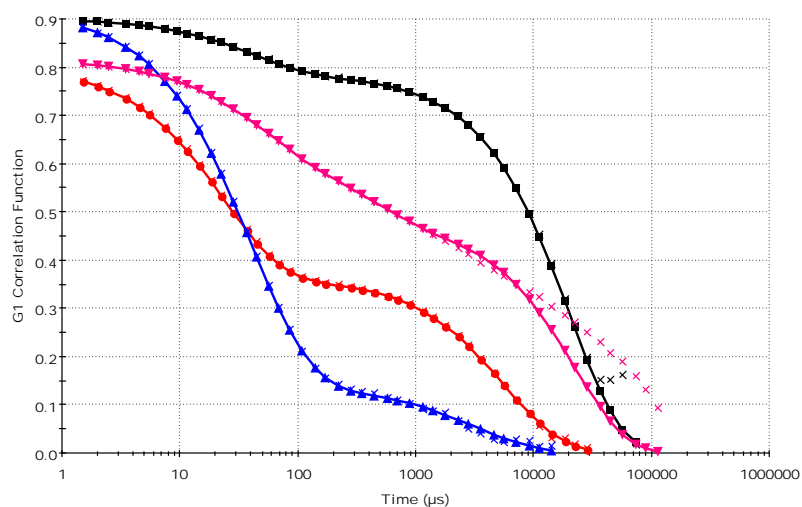
Figure 5.16: Auto-correlation function fit at various days (Day 1(■), Day 8(●), Day 13(▲), Day 22 (▼) and Day 77 (◆))
Filled symbols (Fitted data) and Cross symbols (Experimental data)
Flow rate: 5 and 12 mLh^{-1}

It was revealed from analysis that size distribution and size of nanoparticles decreases as time passes and remain in equilibrium size between 8.5nm – 15.6nm from day 8 till day 29 after that suddenly increases before transforming into gel, as demonstrated in Figure 5.17 and Figure 5.18. One can see in Figure 5.18 that at lower flow rates (1 and 2.4 mL h^{-1} and 3 and 7.2 mL h^{-1}) size continuously decreasing for long time then suddenly increases again before sol to gel transition. While at higher flow rates (5 and 12mLh^{-1}) size decreases for not long time as compared to lower flow rates. May be at higher flow rates both reactants are not staying in the channel for enough time to have good mixing/reaction which results in the rapid

agglomeration process.Size of the nanoparticles were deduced to be between 3nm-38nm and 4nm-45nm size for minimum flow rate tested (1 and 2.4 mL h^{-1}) and maximum flow rate tested (5 and 12 mLh^{-1}) respectively on different days, see Figure 5.17.
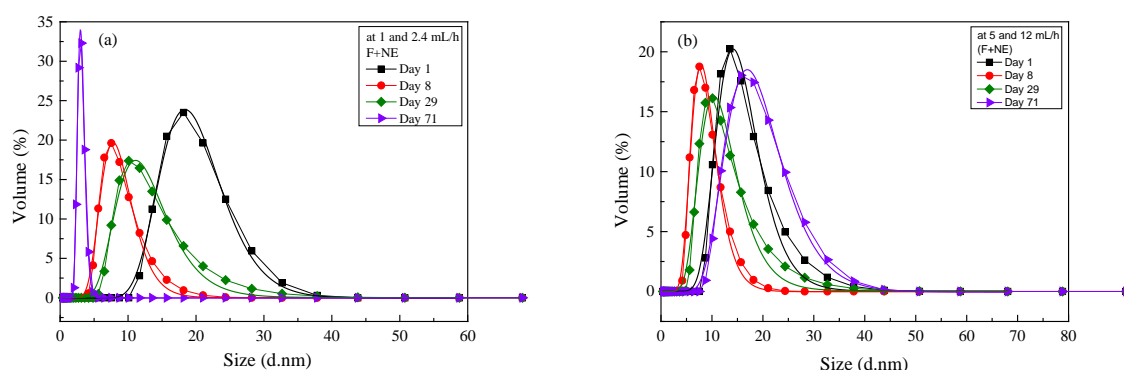
Figure 5.17: Size distribution of nanoparticles at flow rates (a) 1and 2.4 mLh^{-1} (b) 5and 12mLh^{-1} flow rate. Day 1 (■), Day 8 (●), Day 22 (◆), Day 71(▶)
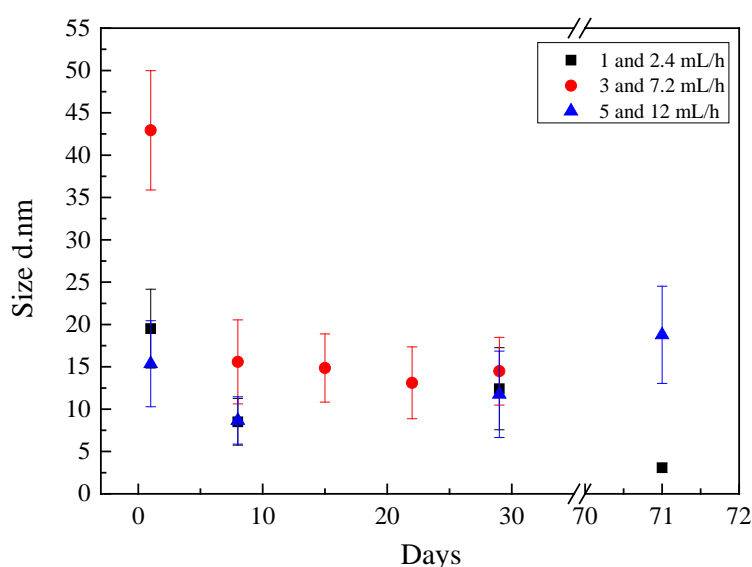
Figure 5.18: Size of nanoparticles at various days and various flow rates (without electrodes).
Flow rates: Flow rates: 1 and 2.4 mL h^{-1} (■), 3 and 7.2 mLh^{-1} (●), and 5 and 12 mL h^{-1} (▲)

5.1.2.1.dEffect of flow rate on NPs

To study the effect of flow rate on the nanoparticles various sols were prepared by using three different flow rates for pre-diluted TiOCl$_2$ (1, 3 and 5 mLh^{-1}) and for DMF (2.4, 7.2, and 12 mL h^{-1}) at 2.4 flow rate ratio. On the same time, we are also noticing the effect of using longer microchannel on the nanoparticles.Initially, freshly TiDMF prepared sols were analysed.

Correlogram (Figure 5.19) shows the results of increasing the size of nanoparticles with increase of flow rate. As one can see in Figure 5.19 that as flow rate increases from 1 and

2.4 mL h^{-1} to 5 and 12 mL h^{-1} then correlation function decays more slowly which indicates the size increment.

When correlation function exponentially fitted with total decay time (Figure 5.20) then it shows the existence of large particles which are not properly fitted in larger decay time while at lower flow rate it is nicely fitted.
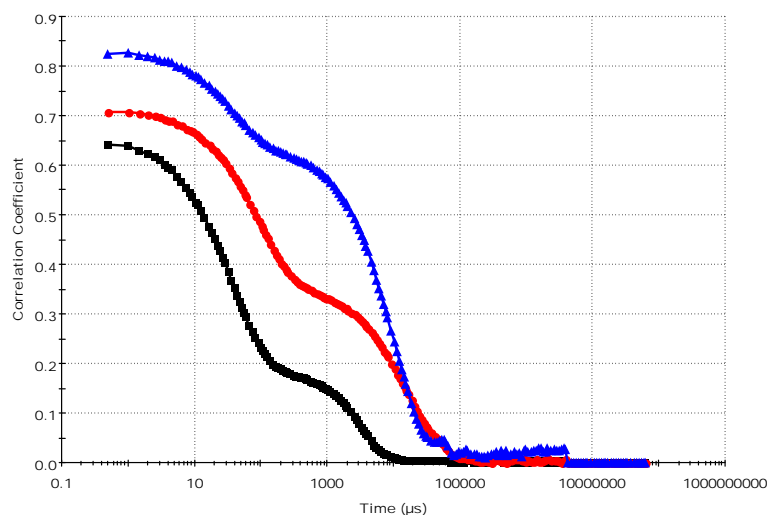
Figure 5.19: Correlogram at various flow rates on day 1
Flow rates: (1 and 2.4 mL h^{-1} (─■─), 3 and 7.2 mL h^{-1} (─●─) and 5 and 12 mL h^{-1} (
─▲─))
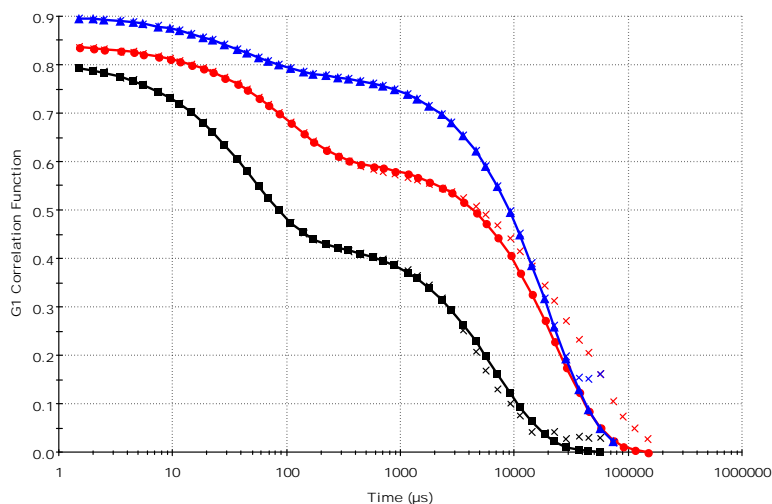
Figure 5.20: Auto-correlation function fit at various flow rates on day 1
Flow rates: (1 and 2.4 mL h^{-1} (─■─), 3 and 7.2 mL h^{-1} (─●─) and 5 and 12 mL h^{-1} (
─▲─))
Filled symbols (Fitted data) and Cross symbols (Experimental data)

Figure 5.21 shows the size distribution of nanoparticles on day 1 with effect of different flow rates, x-axis indicates the size of the nanoparticles and y-axis indicates the

quantity of nanoparticles in terms of volume percentage (Figure 5.21 (a)) and in terms of intensity distribution (Figure 5.21 (b)).

As we have discussed in section 5.1.1.2 that TiDMF sols prepared on day 1 are having very poor size distribution with PDI>0.7. There are not enough points to define size distribution peak. But here we noticed very fine narrow size distribution on very first day by using various flow rates, see Figure 5.21 (a). These results indicates that nanoparticles size distributions are better defined when we are using longer microchannel. May be in 32 mm long Y-shape microchannel both reactants are not staying in the channel for enough time to have good mixing/reaction which results in the very poor size distribution on day 1.It was revealed from volume distribution graph (Figure 5.21 (a)) of fresh TiDMF sol on day 1 and size of nanoparticles at various days with effect of different flow rates (Figure 5.18) that size of nanoparticles are increasing with increase of flow rate. Later, it was also noticed that size of nanoparticles increases at various other days also (day 8, 29 and 71) before transforming into gel.
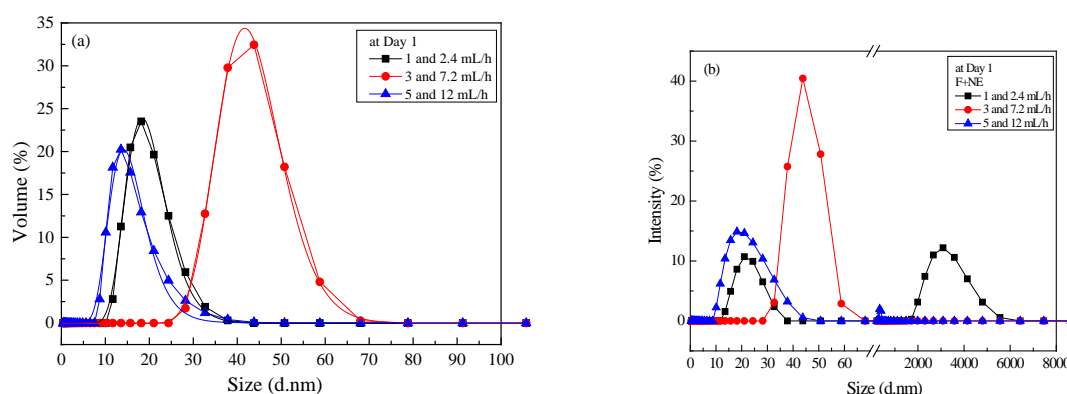
Figure 5.21: Size distribution of nanoparticle at Day 1 (a) Volume distribution (b) Intensity distribution
Flow rates: 1and 2.4 mL h^{-1} (■), 3 and 7.2mLh^{-1}, (●) and 5and 12 mL h^{-1} (▲)

It was concluded from the results that longer microchannel is recommended for mixing as it is providing better size distribution (narrow size distribution and enough points to define the size distribution) than the short microchannel. Even average size of nanoparticles is almost same but just the distribution is much more better (in terms of volume and intensity distributions) when using longer microchannel. May be in short microchannel reaction is not fully completed and it affects the overall size distributions.

5.1.2.2 With electric field

5.1.2.2.a Pre-mixed Solution

In this section, we further analysed the sols produced using 234mm longmicroreactorby applying to electrodes a voltage of 7 VAC and 1 MHz frequency at various flow rates range for pre-diluted TiOCl$_2$with 16.7% of DMF (0.5-5 mLh^{-1}) and for DMF (1.2-12 mL h^{-1}) at 2.4 flow rate ratio, as discussed in section 4.2.3.1.

i. Sols quality and polydispersity analysis

In order to check the quality of the data, intercept values of each samples were plotted in Figure 5.22. Figure 5.22 shows that all the samples (filtered) tested are having intercept values between 0.66 and 0.95 at various days, which shows that measurements are of good quality. Even non-filtered samples are having good quality for DLS analysis (Intercept values between 0.67 and 0.93).
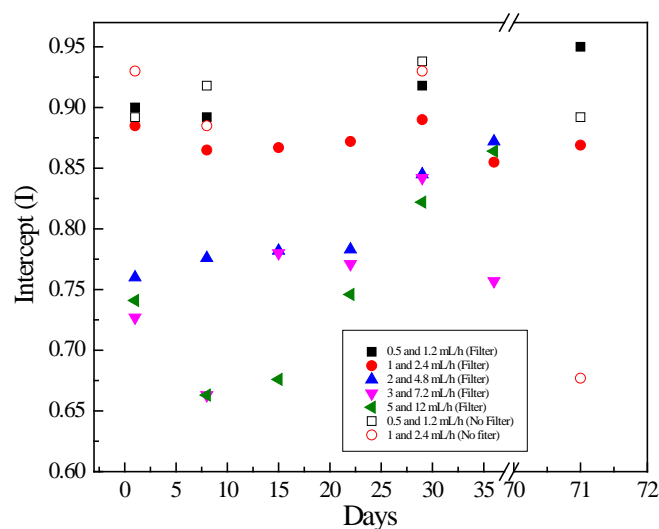
Figure 5.22: Intercept at various days to check the quality of the samples.
Flow rates: 0.5 and 1.2 mL h^{-1} (Filter (■) and No filter (□)), 1 and 2.4mLh^{-1} (Filter (●) and No filter (○)),2 and 4.8 mLh^{-1} (▲), 3 and 7.2 mL h^{-1} (▼), 5 and 12 mL h^{-1} (◀).
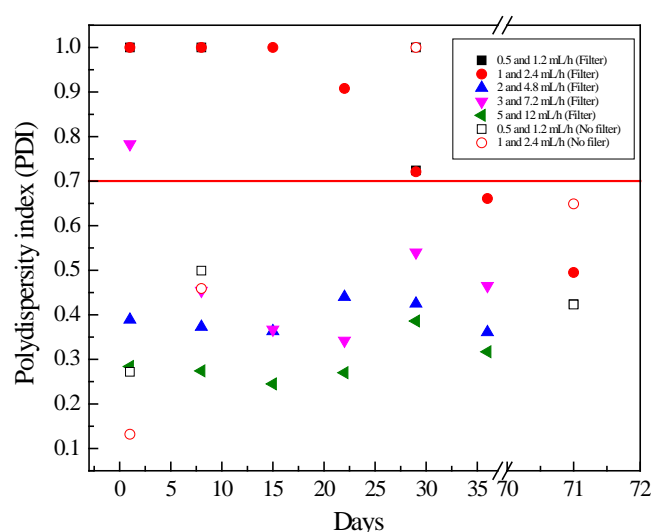

Figure 5.23: Polydispersity index (PDI) at various days.
Flow rates: 0.5 and 1.2 mL h^{-1} (Filter (■) and No filter (□)), 1 and 2.4 mL h^{-1} (Filter (●) and No filter (○)), 2 and 4.8 mL h^{-1} (▲), 3 and 7.2 mL h^{-1} (▼), 5 and 12 mL h^{-1} (◀).

For the size distribution analysis, polydispersity index (PDI) were evaluated during DLS analysis for each sample (filtered and non-filtered) at various days and plotted in Figure 5.23. Figure 5.18 revealed that size distributions for nanoparticles(filtered sols and non-filtered sols) are having PDI<0.7 for flow rates higher than 2 and 4.8 mL h^{-1}which indicates that the size distribution is better. While at lower flow rates (<2 and 4.8 mL h^{-1}) PDI<0.7 values are achieved after day 30, which means that the size distribution is better after day 30.

It can be noticed also that filtered samples are having much narrow size distribution as compared to non-filtered samples after day 30, as filtered PDI values are much lower than non filtered PDI values.

ii. Effect of Filtration on NPs

In order to check the effect of filtration, one sample was selected (1 and 2.4 mLh^{-1}) for which the reaction is finishing inside the electrode area with a better mixing, from Table 4.3, as described in section 4.2.3.1. Both the samples (Filtered and non-filtered) at 1 and 2.4mL h^{-1} flow rates were analysed under DLS technique for the size distribution at different days.

It was noticed that filtration process avoids the dust and large particles in the sol as shown in correlogram (Figure 5.24) and auto-correlation fit (Figure 5.25). It can be seen in the Figure 5.24 that filtered sol correlogram decays exponentially more quickly as compared to without filtered sol, which shows the existence of large particles in the sol. While auto-correlation fit at larger decay time (Figure 5.25) revealed the existence of large particles. It would be same reason as in without filtered sol, small and large particles are mixed and large particles scattering more light in DLS.
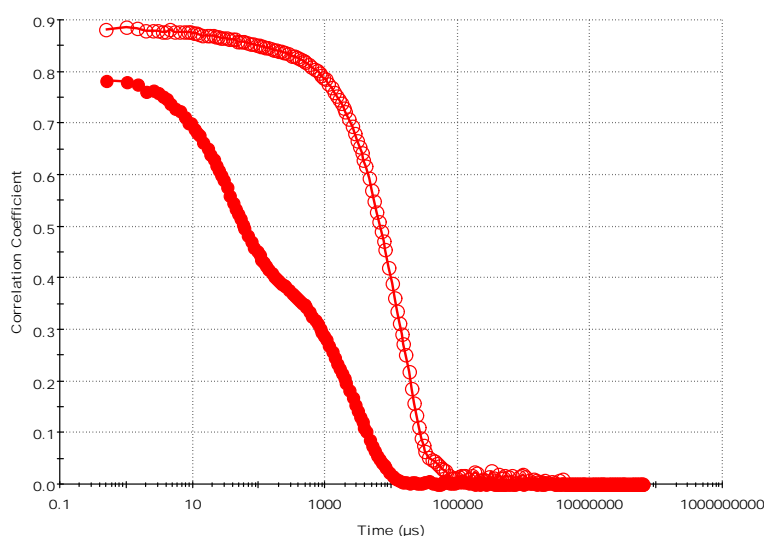
Figure 5.24: Correlogram at day 1 at 1 and 2.4 mL h^{-1} flow rate
Filled symbols (Filtered) and Hollow symbols (Non filtered)
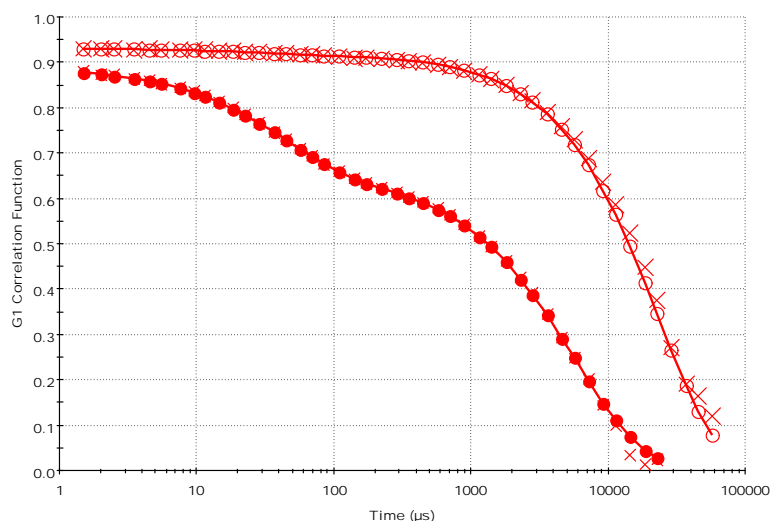
Figure 5.25: Auto-correlation function fit at day 1 at 1 and 2.4 mL h^{-1} flow rate
Filled and Hollow symbols (Fitted data) and Cross symbols (Experimental data)

Figure 5.26 shows size of nanoparticles of two different samples (filtered and non-filtered) on various days. It can be seen in the Figure 5.26 that filtration is not hugely causing difference again in the size of nanoparticles at the initial day when we use electrodes.

It was also noticed that large and dust particles are creating various different peaks in the intensity distribution, as shown in Figure 5.33 (b), so sometimes it is difficult to get real size of nanoparticles without filtration process. That is why we concluded that it is very necessary to do filtration to avoid dust and large particles even we are using electrodes or not, as without filtering, agglomerates may quickly occur as compared to filtered sol.
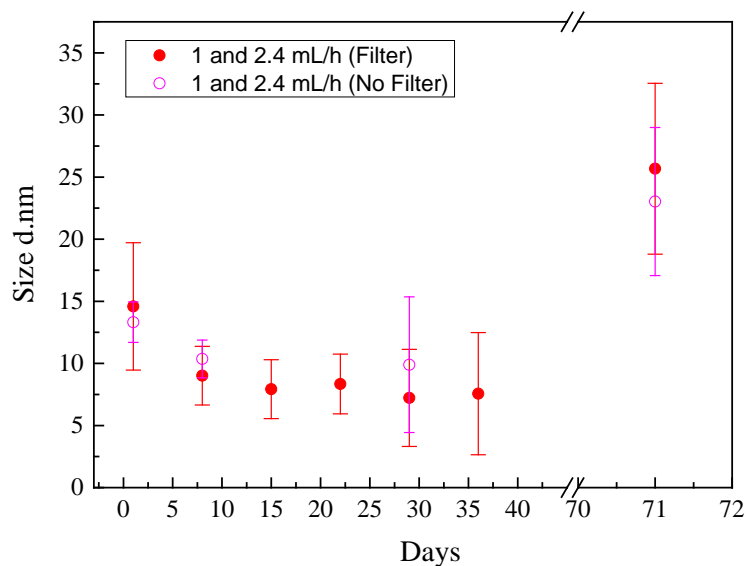
Figure 5.26: Effect of filtration on the sols (with electrodes) at various days.
Flow rates: 1 and 2.4 mL h^{-1} (Filtered (●) and Non filtered (○))

iv. Effect of time on NPs

To study the effect of time on the nanoparticles, DLS analysis was performed for each sample at various days (day 1, day 8, day 15, day 22, day 29, day 36 and day 71) till sol becomes gel.

Correlogram (Figure 5.27) shows that as time passes then correlation function decays more quickly than previous days which indicate that size of nanoparticles are getting smaller before transforming into gel. However, it was noticed that after long period (day 71) correlogram starts decaying more slowly, which indicates the size of nanoparticles are increasing before sol to gel transition. Similarly, auto-correlation function fit is getting better fitted as time passes (see Figure 5.22).
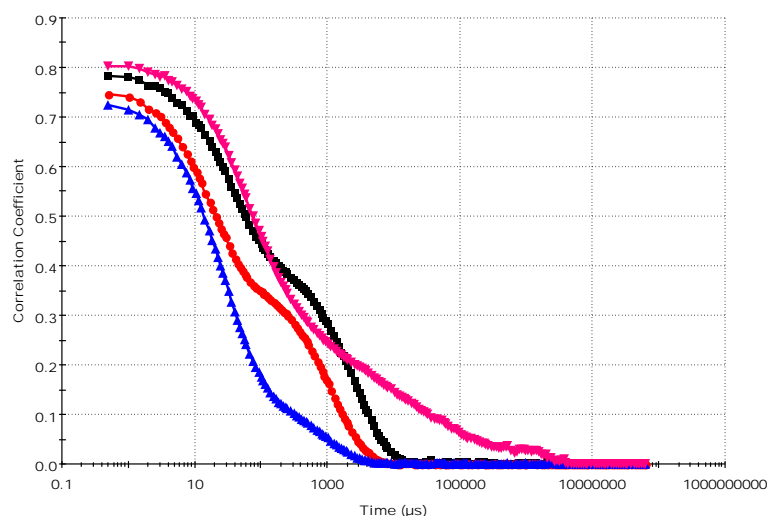
Figure 5.27: Correlogram at various days (Day 1 (▬■▬), Day 15 (▬●▬), Day 36 (▬▲▬) and Day 71 (▬▼▬))
Flow rate: 1 and 2.4 mL h^{-1}
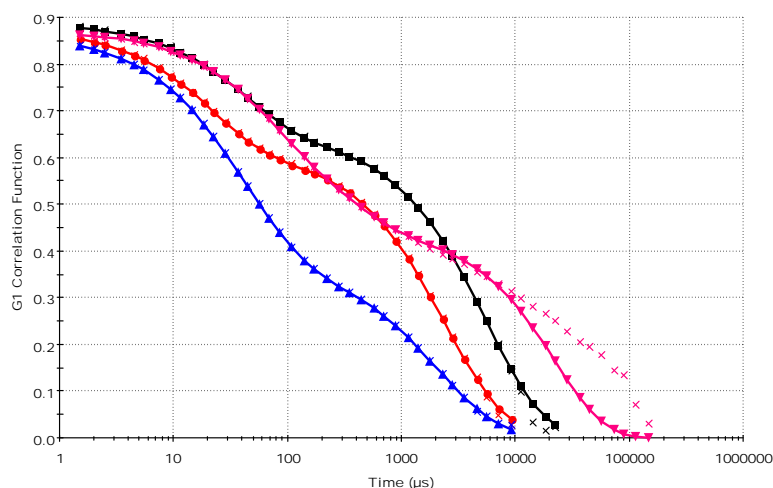
Figure 5.28: Auto-correlation function fit at various days (Day 1 (▬■▬), Day 15 (▬●▬), Day 36 (▬▲▬) and Day 71 (▬▼▬))
Filled symbols (Fitted data) and Cross symbols (Experimental data)
Flow rate: 1 and 2.4 mL h^{-1}

It was revealed from analysis that size distribution and size of nanoparticles decreases as time passes and becomes constant from day 8 till day 36 between size 6.5 nm- 11.9 nm and then suddenly increases before transforming into gel, as demonstrated in Figure 5.29 and Figure 5.30. One can see in Figure 5.30 that size continuously decreasing for long time then suddenly increases before sols to gels transformations. The reason which we noticed for size of nanoparticles decreasing and come in constant state then increasing before transforming into gel, can be existence of small bubbles or large particles in the sols. Fresh TiDMF sols collected from the microchannel have some fine bubbles due to mixing flow, later collected sols stirred for 2 to 3 minutes, which also creates some bubbles in the sols. Even filtration process also creates some fine bubbles. However, as time passes sedimentation process may take place (as we are leaving the sols undisturbed), these bubbles and large particles are not interacting anymore with the laser beam, and they are not measured (but still present at the bottom of solution). We also get better size distribution as time passes (in other words more sedimentation process takes place) before sol to gel transformation, see Figure 5.29. Size of the nanoparticles were recorded between 3nm-50nm for flow rate tested (1 and 2.4 mL h^{-1}) on different days, see Figure 5.29.
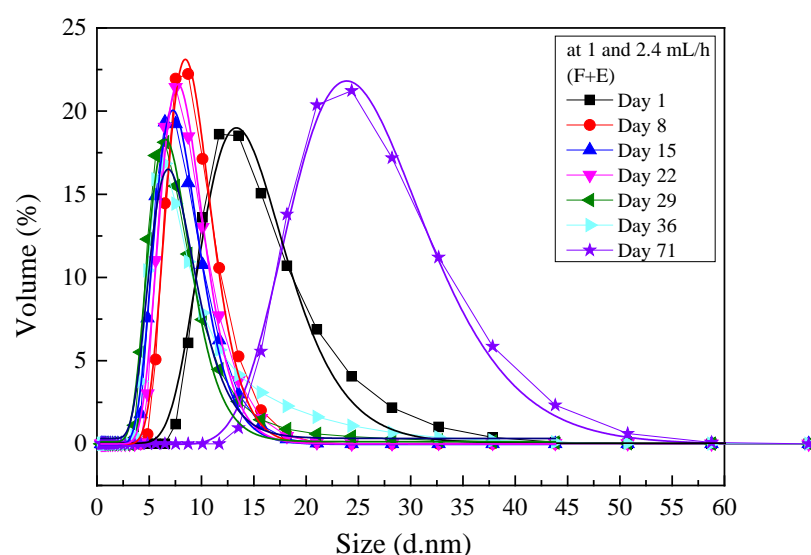
Figure 5.29: Size distribution of nanoparticles 1and 2.4 mLh^{-1} flow rate. Day 1 (—■—), Day 8 (—●—), Day 15 (—▲—), Day 22 (—▼—), Day 29 (—◄—), Day 36 (—►—), Day 71 (—★—)
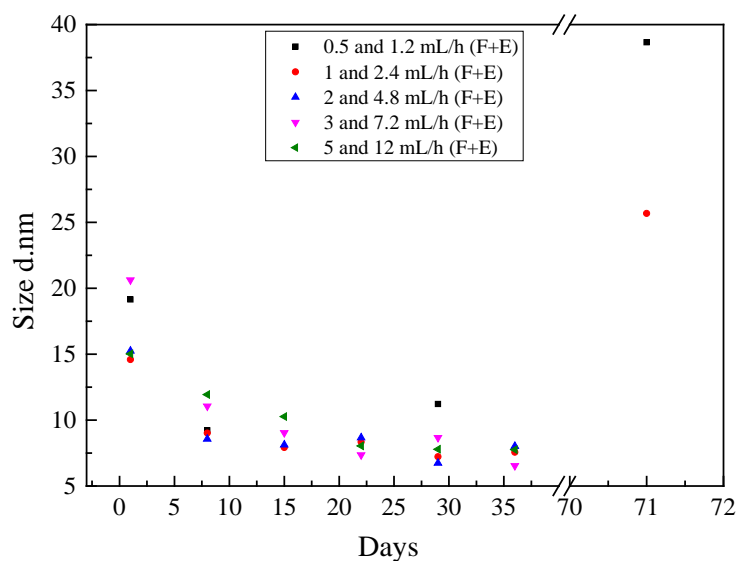
Figure 5.30: Size of nanoparticles at various days and various flow rates.
Flow rates: 0.5 and 1.2 mL h^{-1} (■), 1 and 2.4 mLh^{-1}, (●), 2 and 4.8 mL h^{-1} (▲), 3 and 7.2 mL h^{-1} (▼), 5 and 12 mL h^{-1}(◀)

iii. Effect of flow rate on NPs

To study the effect of flow rate on the nanoparticles, various sols were prepared by using five different flow rates for pre-diluted TiOCl$_2$ (0.5,1,2,3 and 5 mLh^{-1}) and for DMF (1.2, 2.4, 7.2, and 12 mL h^{-1}) at 2.4 flow rate ratio, on the same time to improve mixing,an electric field was applied via electrodes. So we are also noticing the effect of an applied electrid field at various flow rates on the nanoparticles.Initially, freshly TiDMFprepared sols were analysed.

Correlogram and auto-correlation fit (Figure 5.31 and Figure 5.32) show that there is not huge effect of flow rate on the nanoparticles on day 1.
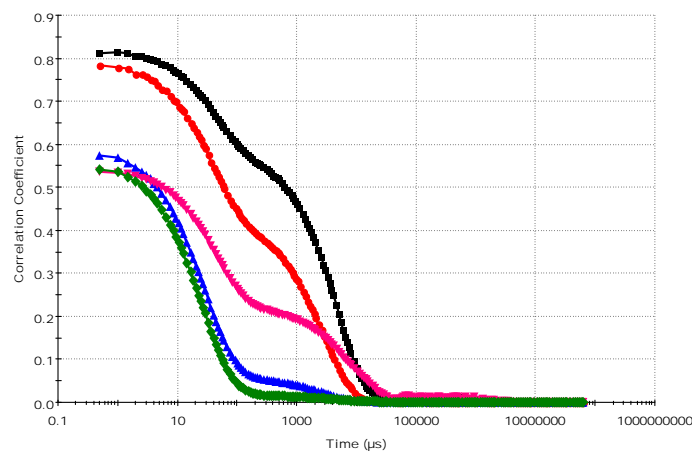
Figure 5.31: Correlogram at various flow rates on day 1
Flow rates: (0.5 and 1.2 mL h^{-1} (─■─), 1 and 2.4 mL h^{-1} (─●─), 2 and 4.8 mL h^{-1} (─▲─), 3 mL h^{-1} and 7.2 mL h^{-1} (─▼─) and 5 mL h^{-1} and 12 mL h^{-1} (─◆─))
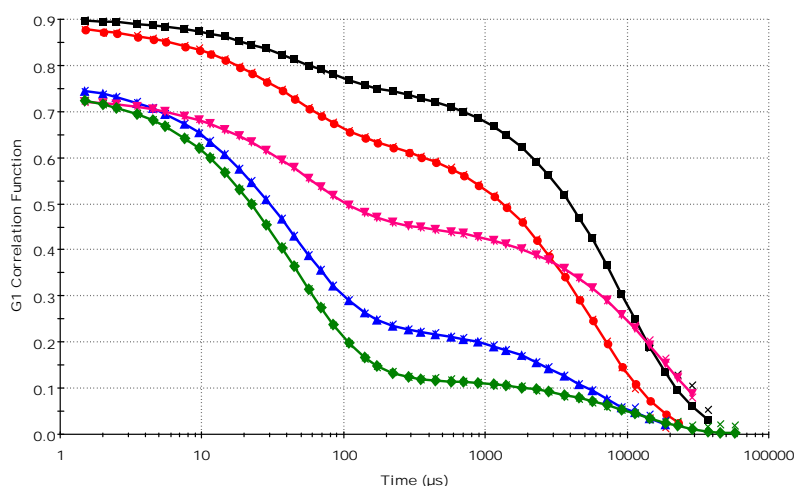
Figure 5.32: Auto-correlation function fit at various flow rates on day 1
Flow rates: (0.5 and 1.2 mL h^{-1} (─■─), 1 and 2.4 mL h^{-1} (─●─), 2 and 4.8 mL h^{-1} (
─▲─), 3 mL h^{-1} and 7.2 mL h^{-1} (─▼─) and 5 mL h^{-1} and 12 mL h^{-1} (─◆─))
Filled symbols (Fitted data) and Cross symbols (Experimental data)

Figure 5.33 shows the intensity and volume size distribution of nanoparticles on day 1 with effect of different flow rates. It was revealed from volume distribution graph of fresh TiDMF sol on day 1 (Figure 5.33(a)) and sizes of nanoparticles at various days (Figure 5.30) that size of nanoparticles are little bit increasing with increase of flow rates before transforming into gel, difference can be noticed while comparing lowest and highest flow rates at various days.One can see in Figure 5.33(a) that increase or decrease of flow rates are not hugelyaffecting size of nanoparticles at initial days but lower flow rates are important to use so that the reaction finishes inside the electrodes area which can be useful for better size distribution.
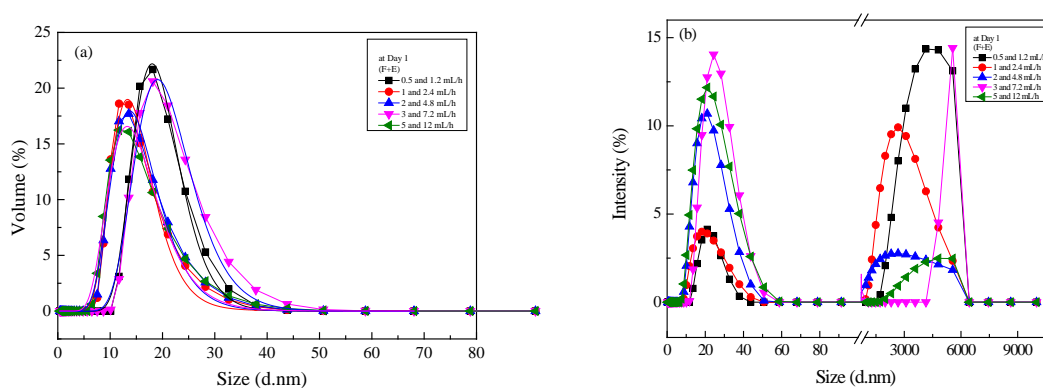
Figure 5.33: Size distribution of nanoparticles at Day 1 (a) Volume distribution (b) Intensity distribution
Flow rates: 0.5 and 1.2 mL h^{-1} (─■─), 1 and 2.4 mL h^{-1} (─●─), 2 and 4.8 mL h^{-1} (─▲─), 3 and 7.2 mL h^{-1} (─▼─), 5 and 12 mL h^{-1} (─◀─).

These results indicate that nanoparticles size distributions are better when we are using longer microchannel with electrodes, in comparison of using no electrodes as discussed in section 5.1.2.1.c.Previously in section 4.2.3.1, it was concluded that electrodes are providing better mixing and stable flows. So, here we have seen those stable flows are leading to better size distribution. Even at higher flow rates (when the flow is unstable) when reaction is not fully finishing inside the electrodes area the size distribution is also better (enough points to define the distribution). One more advantage of using electrodes is that almost all the PDI values are less than 0.7 which means the size distribution is narrower with enough points to plot the well defined size distribution. When we used same microchannel with electrodes avoiding the unstable flows and improper mixing, the size distribution is improved. Using electrodes not only controls the size distribution but it also tunes the size of nanoparticles, as demonstrated in Figure 5.34. Figure 5.34 shows the effect of using electrodes and no electrodes. It can be seen in this Figure 5.34 that size of nanoparticles are smaller when electrodes are used for better mixing as compared to without electrodes. Providing proper mixing and stable flows in the channel can provide better size distribution (narrow size distribution and well defined size distribution), small and fine nanoparticles.
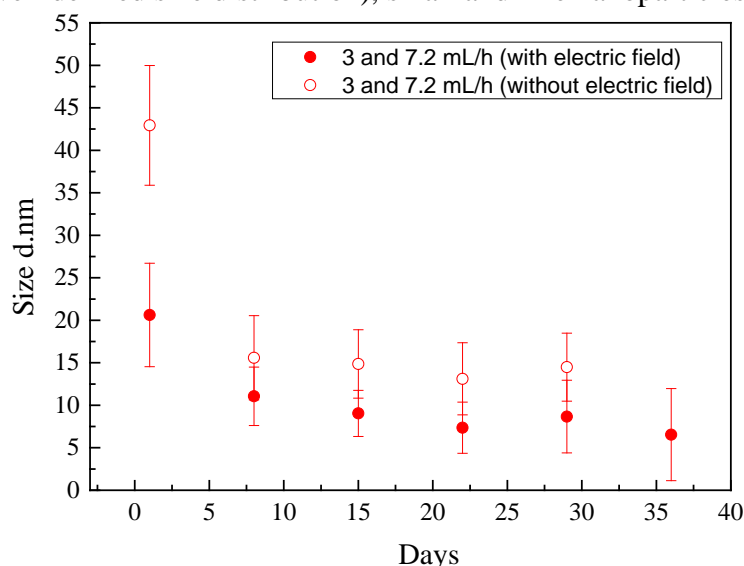
Figure 5.34: Comparison of using electrodes mixing samples v/s without using electrodes mixing samples

Flow rates: 3 and 7.2 mL h^{-1} (with electric field (●) and without electric field (○))

5.1.2.2.b Pure TiOCl$_2$ solution

In this section, we further analysed the sols produced using 234mm long microreactor by activating electrodes at voltage 7 VAC and 1 MHz frequency at various flow rates range for pure TiOCl$_2$ (0.5-5 mLh^{-1}) and for DMF (1.2-12 mL h^{-1}) at 2.4 flow rate ratio, as discussed in section 4.3.

i. Sols quality and polydispersity quality.

In order to check the quality of the data, intercept values of each sample were plotted in Figure 5.35. Figure 5.35 shows that all the samples (filtered) tested are having intercept values between 0.71 and 0.93 at various days which shows that all measurements are of good quality. Non-filtered results are also of good quality (Intercept values between 0.81 and 0.94).
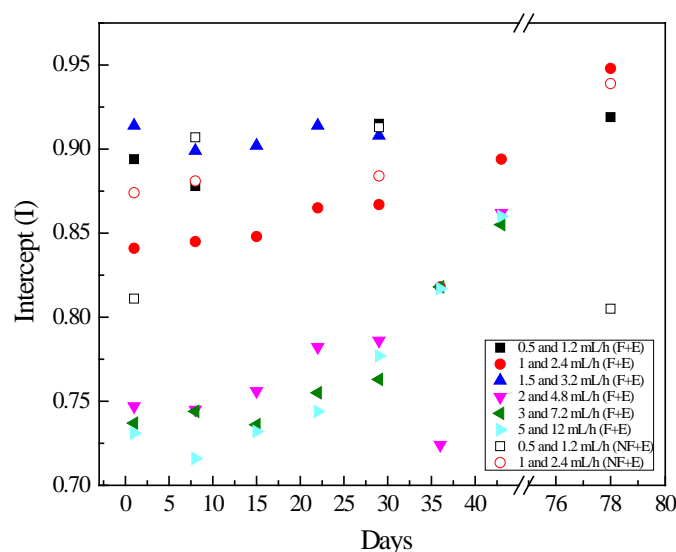
Figure 5.35: Intercept at various days to check the quality of the samples.
Flow rates: 0.5 and 1.2 mL h^{-1} (Filter (■) and No filter (□)), 1 and 2.4 mL h^{-1} (Filter (●) and No filter (○)), 1.5 and 3.2 mL h^{-1} (▲), 2 and 4.8 mL h^{-1} (▼), 3 and 7.2 mL h^{-1} (◄), 5and 12mLh^{-1} (►)
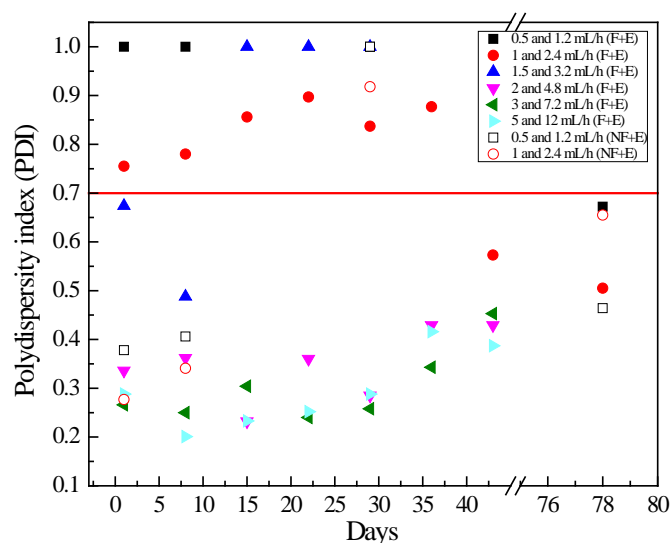
Figure 5.36: Polydispersity index (PDI) at various days.
Flow rates: 0.5 and 1.2 mL h^{-1} (Filter (■) and No filter (□)), 1 and 2.4 mL h^{-1} (Filter (●) and No filter (○)), 1.5 and 3.2 mL h^{-1} (▲), 2 and 4.8 mL h^{-1} (▼), 3 and 7.2 mL h^{-1} (◄), 5and 12mLh^{-1} (►)

PDI values are plotted in Figure 5.36 for the analysis of size distribution; Figure 5.36 revealed that size distributions for nanoparticles (filtered sols and non-filtered sols) are having PDI<0.7 for higher flow rates (>2 and 4.8 mL h^{-1}), which shows the size distribution is good. While for lower flow rates (<2 and 4.8 mL h^{-1}), PDI values are getting lower than 0.7 after day 43.

ii. Effect of Filtration on NPs

In order to check the effect of filtration on the sols, one sample was selected (1 and 2.4 mL h^{-1}) in which reaction is finishing inside the electrodes area with a better mixing, from Table 4.5, as described in section 4.3. Both samples (Filtered and non-filtered) were analysed under DLS technique at different days.

It was noticed that filtration process avoids the dust and large particles in the sols as shown in correlogram (Figure 5.37) and auto-correlation fit (Figure 5.38). It can be seen in the Figure 5.37 that filtered sol correlogram decays more quickly as compared to without filtering, which shows the existence of large particles in the sol. While auto-correlation fit of total decay time (Figure 5.38) revealed the existence of large particles at the end, which are not properly fitted for non-filtered sols.
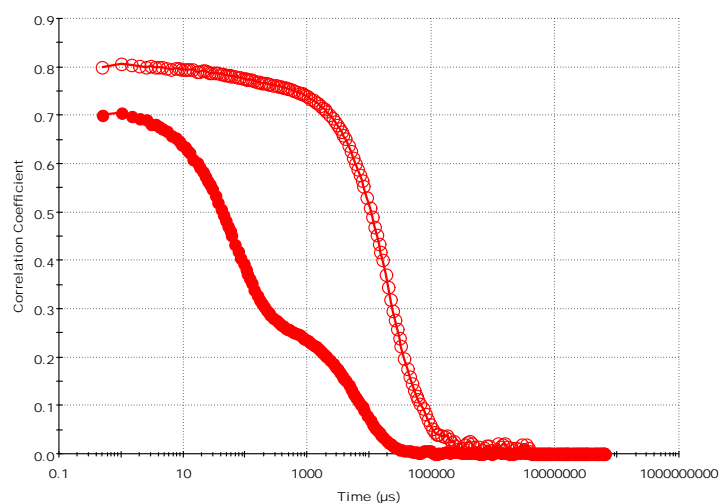
Figure 5.37: Correlogram at day 1 at 1 and 2.4 mL h^{-1} flow rate
Filled symbols (Filtered) and Hollow symbols (Non filtered)
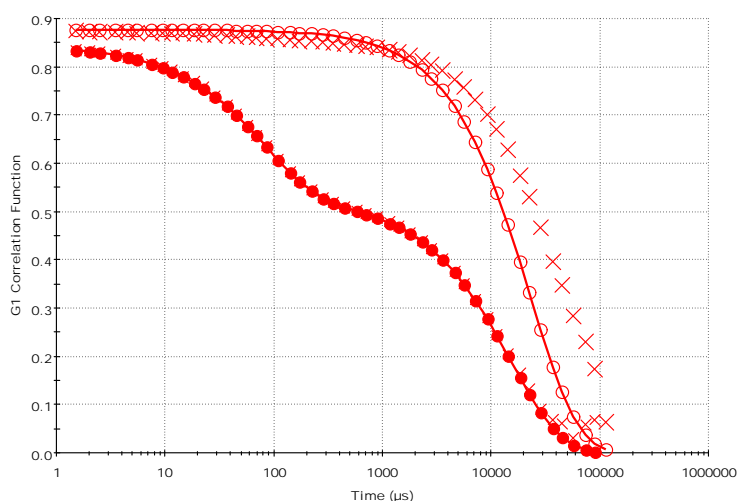
Figure 5.38: Auto-correlation function fit at day 1 at 1 and 2.4 mL h^{-1} flow rate
Filled and Hollow symbols (Fitted data) and Cross symbols (Experimental data)

It can be seen in the Figure 5.39 that filtration is causing change in the size of nanoparticles at initial day 1 and day 8. This change can be due to presence of large particles in the sample which are scattering more light and small particles are not detecting by DLS. However, after sedimentation process, size of nanoparticles are almost same in filtered and non-filtered sols.

It was also noticed in intensity size distribution that large and dust particles are creating various different peaks, as shown in Figure 5.44 (b). So, sometimes it is difficult to get real size of nanoparticles without filtration process. That is why we concluded that it is very necessary to do filtration of the sol to avoid dust and large particles even we are using electrodes or not with dilution or not.
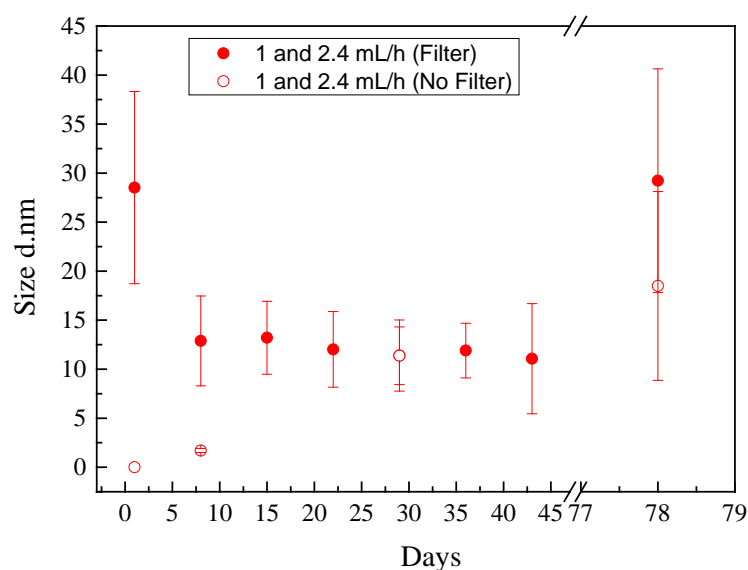
Figure 5.39: Effect of filtration on the sols at various days.
Flow rates: 1 and 2.4 mL h^{-1} (Filter (●) and No filter (○))

iii. Effect of time on NPs

To study the effect of time on nanoparticles size, DLS analysis was performed for each sample at various days (day 1, day 8, day 15, day 22, day 29, day 36, day 43 and day 78) till sol becomes gel at room temperature.

Correlogram (Figure 5.40) shows that as time passes then the signal decays more quickly than previous days which indicates that size of nanoparticles are getting smaller before transforming into gel. Similarly, auto-correlation fit is getting better fitting as time passes (see Figure 5.41). But, it was noticed that after long period (day 78) correlogram starts decaying more slowly, which indicates the size of nanoparticles are increasing before transforming into gel.
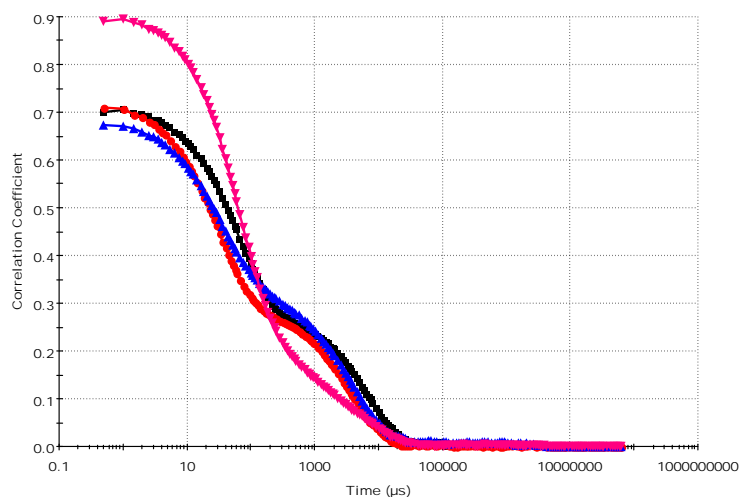
Figure 5.40: Correlogram at various days (Day 1 (—■—), Day 8 (—●—), Day 36 (—▲—) and Day 78 (—▼—))
Flow rate: 1 and 2.4 mL h^{-1}
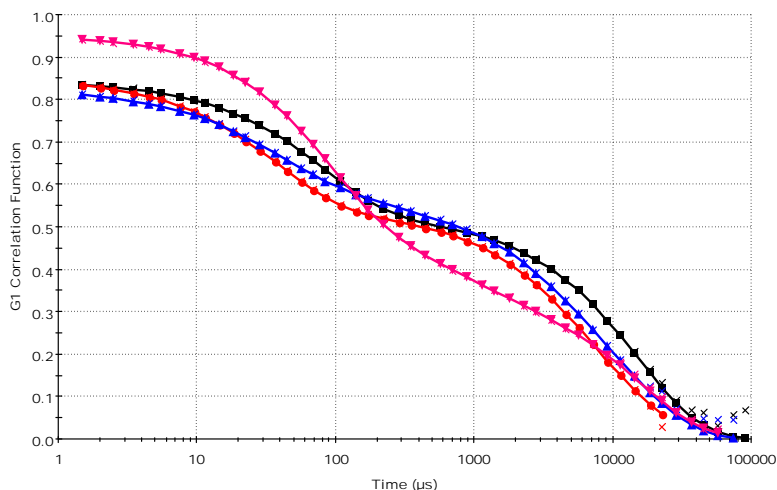
Figure 5.41: Auto-correlation function fit at various days (Day 1 (—■—), Day 8 (—●—), Day 36 (—▲—) and Day 78 (—▼—))
Filled symbols (Fitted data) and Cross symbols (Experimental data)
Flow rate: 1 and 2.4 mL h^{-1}

It was revealed from DLS analysis that size distribution and size of nanoparticles decreases as time passes and becomes constant from day 8 till day 43 between size 8.7 nm-15.2 nm and then suddenly increases before transforming into gel as plotted in Figure 5.42 (b) and Figure 5.43. Figure 5.43 shows that size of nanoparticles are continuously decreasing (from day 1 to day 8) due to sedimentation process and then suddenly increases before transformation of the sol into gel.Size of the nanoparticles were recorded between 5nm-70nm for flow rate tested (1 and 2.4 mL h^{-1}) on different days, see Figure 5.42 (a).
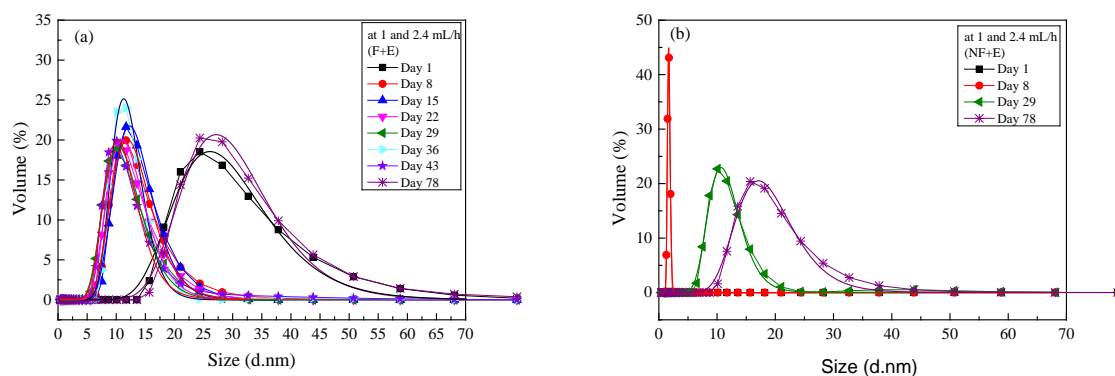
Figure 5.42: Size distribution of nanoparticles for 1 and 2.4 mLh^{-1} flow rate.
(a) Filter sol (b) Non filtered sol
Day 1 (■), Day 8 (●), Day 15 (▲), Day 22 (▼), Day 29 (◄), Day 36 (►), Day 43 (★), Day 78 (✳)
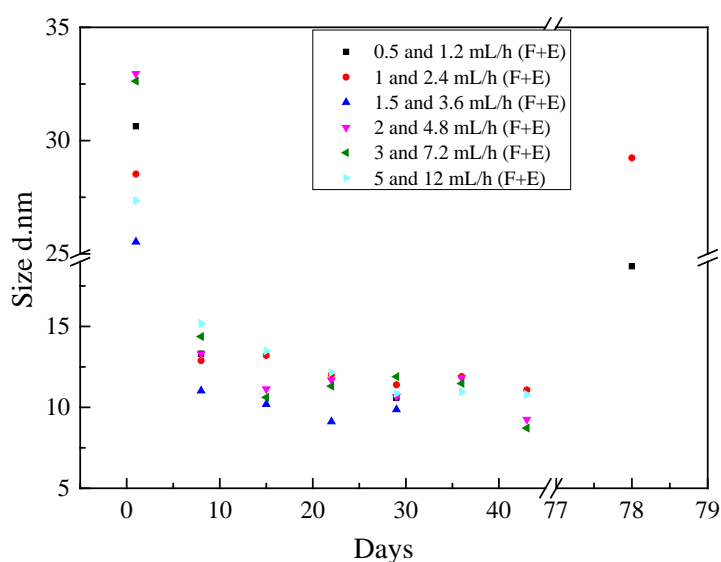
Figure 5.43: Size of nanoparticles at various days and various flow rates.
Flow rates: 0.5 and 1.2 mL h^{-1} (■), 1 and 2.4 mL h^{-1} (●), 1.5 and 3.2 mL h^{-1} (▲), 2 and 4.8 mL h^{-1} (▼), 3 and 7.2 mL h^{-1} (◄), 5 and 12 mL h^{-1} (►)

iv. Effect of flow rate on NPs

To study the effect of flow rate on the nanoparticles various sols were prepared by using six different flow rates for pure $TiOCl_2$ (0.5, 1, 1.5, 2,3 and 5 mLh^{-1}) and for DMF (1.2, 2.4, 3.6, 7.2, and 12 mL h^{-1}) at 2.4 flow rate ratio, on the same time to improve mixing, an electric field was applied via electrodes. Therefore, we are also noticing the effect of an applied electric field at various flow rates on the nanoparticles.Initially, freshly TiDMF prepared sols were analysed for size distribution.

Figure 5.44 shows the intensity and volume size distribution of nanoparticles on day 1 with effect of different flow rates.

Previously in section 4.3, it was concluded that electrodes are providing better mixing and stable flows. So, here we observed those stable flows are leading to have better size distribution. Even at higher flow rates (unstable flows) reaction is not fully finishing inside the electrodes area but size distribution is also better at higher flow rates. One more advantage of using electrodes is that almost all the PDI values are less than 0.7 which means that the size distribution narrow with enough points to define the peak.

It was revealed from volume distribution graph (Figure 5.44) fresh TiDMF sol on day 1 and and size of nanoparticles at various days with effect of different flow rates (Figure 5.43) that size of nanoparticles are a little bit increasing with increase of flow rates before transforming into gel, difference can be noticed while comparing lower and higher flow rates at various days. One can see in Figure 5.43 that increase or decrease of flow rates are not hugely affecting size of nanoparticles but lower flow rates are important to use so reaction finishes inside the electrodes area which can be useful for better size distribution.
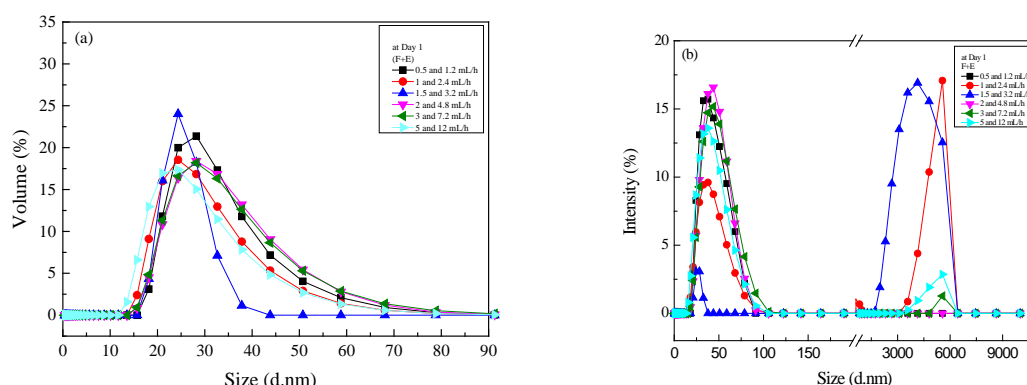
Figure 5.44: Size distribution of nanoparticles at Day 1 (a) Volume distribution (b) Intensity distribution
Flow rates: 0.5 and 1.2 mL h^{-1} (▬■▬), 1 and 2.4 mLh^{-1}(▬●▬), 1.5 and 3.2 mL h^{-1} (▬▲▬), 2 and 4.8 mL h^{-1} (▬▼▬), 3 and 7.2 mL h^{-1} (▬◄▬), 5 and 12 mL h^{-1} (▬►▬)

Effect of 16.7% DMF dilution and pure solution on the size of nanoparticles were also studied by DLS. Figure 5.45 shows the size of nanoparticles at various flow rates for pure and diluted with 16.7% of DMF. It was revealed by DLS analysis that dilution control the size and size distribution of nanoparticles. Smaller nanoparticles can be produced on the same flow rates by diluting the solution.
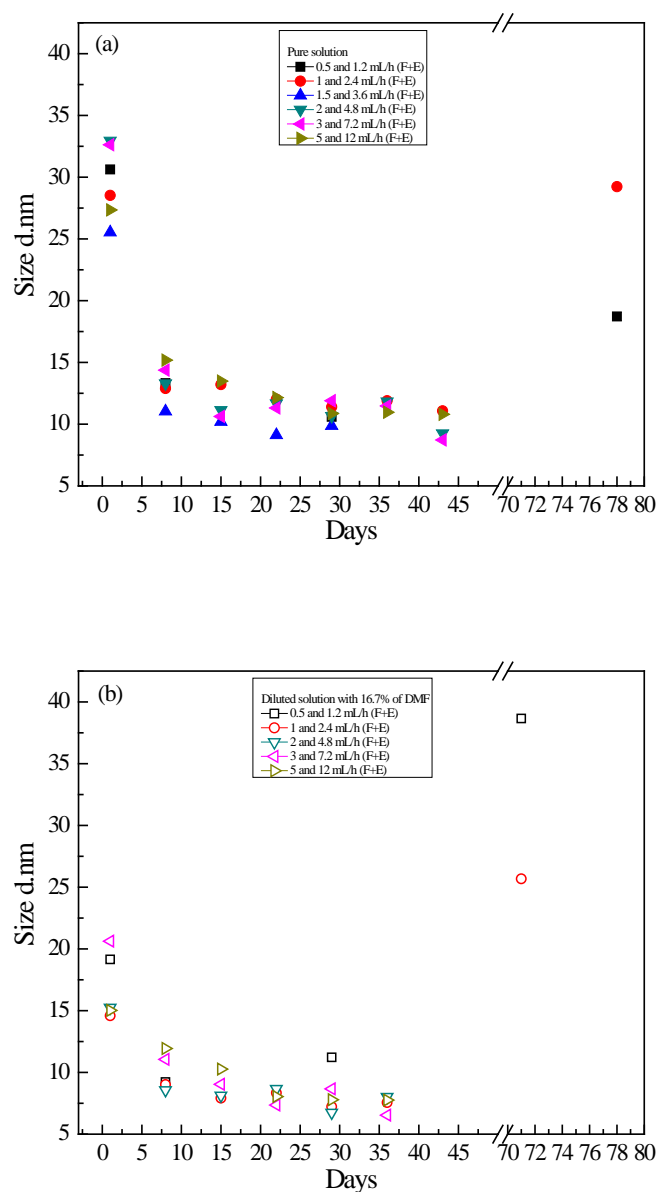
Figure 5.45: Effect of using pure solution and diluted solution with 16.7% of DMF for mixing on the nanoparticles size

5.1.3 Summary

It is not necessary to use the viscosity of the mixture for the DLS analysis, because that is the viscosity of the particles and the colloids. We need the viscosity of the medium in which colloids are moving that is why we keep the viscosity of the DMF which is dispersant. Filtration is recommended to avoid the dust and large particles. Use of longer microchannel is advantageous for producing narrower size distribution and small nanoparticles. While, active mixing through electric field not only improves mixing but it also provides the better narrower size distribution and small nanoparticles. Lower flow rates are recommended so the reaction completes inside the channel, which ultimately control the size distribution. Diluting

the $TiOCl_2$ solution with 16.7% of DMF gives the small nanoparticles and better size distribution than using pure solution.

5.2 Hydrolysis advancement monitored by Raman

FT Raman scattering is used to study the chemical composition and complexion of the organic part as a function of time. Kinetics of DMF hydrolysis in theTiDMF sols was analysed by Bruker MultiRAM FT-Raman Spectrometer (laser wavelength of 1064nm), described in section 2.4.2.1. Samples were stored and analysed in glass vials at the end of mixing from microreactor. All the spectra were decomposed and fitted in CASA XPS [1] to collect the area for various peaks, as explained in section 2.4.2.2.

DMF is known to be hydrolyzed as methanoic acid and dimethylammonium chloride (DMACl) with time according to reaction (equation 1) [2]. From the hydrolysis rate, it is then possible to obtain the number of DMF consumed per titanium, according to the overall equation of the polycondensation reaction. The progress of this reaction can be monitored by Raman diffusion in the 850-900 cm^{-1} range. Taking into account the stoichiometry of the titanium oxy-chloride, 3.4 DMACl molecules per Ti are expected to be detected, at the equilibrium.

$$TiOCl_2.1,4HCl.7H_2O + x(CH_3)_2NCHO \longrightarrow \text{« } TiO_2,zH_2O \text{ polymer »} +$$
$$y(CH_3)_2NH_2Cl + yHCOOH + (x-y)(CH_3)_2NCHO + (3,4-y)HCl + (7-y-z)H_2O \longrightarrow$$ Equation (1)
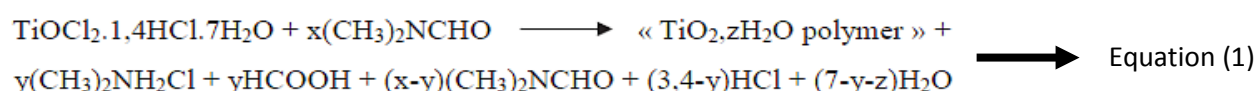
As explained previously in section 2.2.2 that one of the way to follow the hydrolysis of DMF to DMACl is to focus the study of the Raman spectra on the vibrating bands at 863 cm^{-1} ($v_s(C'_2N)$ of DMF) and 891 cm^{-1} ($v_s(CN)$ofDMA^+) [3]. We used pure $TiOCl_2$and 16.7% diluted $TiOCl_2$for our experiments. So, it is necessary to get an evaluation of the sensitivity factor for the different concentrations linking the concentration in one species to the area of one of its band. For various concentrations sensitivity factors were estimated by Solene Béchu in her thesis[4], as explained in section 2.4.2.2. Sensitivity factors are gathered in Table 5.1 for both concentrations.

Table 5.1. Sensitivity factor of both concentrations studied.

Solution	[DMF] mol L^{-1}	J890 DMA mol L^{-1}	J866 DMF mol L^{-1}	J660DMF mol L^{-1}
PureTiOCl$_2$	9.46	0.108	0.101	0.086
Pre-dilutedTiOCl$_2$ (with 16.7% of DMF)	9.81	0.104	0.099	0.084

5.2.1 Y-shape short microchannel (Pre-mixed Solution)

In this section, we further analysed the sols produced using Y-shape microreactor at various flow rates range for pre-diluted $TiOCl_2$with 16.7% of DMF (4-7 mLh^{-1}) and for DMF (9.6-16.8 mL h^{-1}) at 2.4 flow rate ratio, as discussed in section 3.2.2. All the freshly TiDMF

sols obtained immediately after mixing were transparent and homogeneous but their evolution with time differed according to the titanium concentration
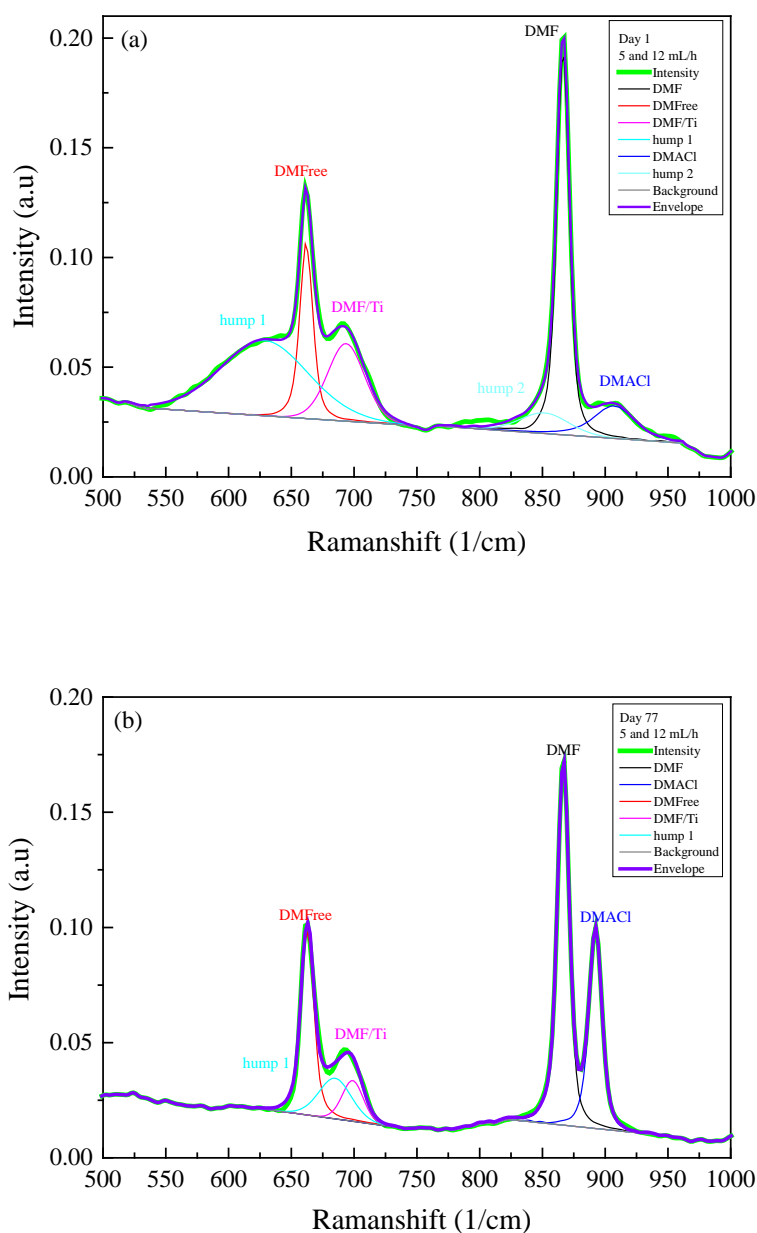
Figure 5.46: Fitted Raman spectra peaks at 5 mL h^{-1} (TiOCl$_2$ + 16.7% of DMF) and 12 mL h^{-1} (DMF) at (a) Day 1 and (b) Day 77

The Raman spectra of freshly TiDMF sols on day 1 and 77 days old TiDMF are presented in Figure 5.46. Raman spectra also provide information regarding complexation of Ti^{4+} by DMF through the oxygen of the molecule, mainly in the region between 500-750 cm^{-1} where two peaks are identified. First band at $663\,cm^{-1}$ corresponds to the bending $\delta(O = C - N)$ free DMF. Second broad band located at $692\,cm^{-1}$ corresponds to the deformation of DMFs linked to Ti (IV). Figure 5.46 is showing the evolution of the vibrational bands $\nu_s(C'_2N)$ of DMF at $866\,cm^{-1}$ and $\nu_s(CN)$ of dimethylammonium, at

$891 cm^{-1}$[3,5]. Moreover, free DMF at $663 cm^{-1}$, DMF linked with Titanium $\delta(O = CN)$ at $\sim$ $692 cm^{-1}$[6] are also monitored and also different humps appeared in spectra.

DMF hydrolysis results are presented in Figure 5.47. Figure 5.47 illustrates the number of molecules/Ti as a function of time. As time passes and DMF hydrolysis reaction takes place, we observe an increase in DMACl area and correlative decrease in DMF area, as demonstrated in Figure 5.46.

It is important to notice that the DMACl appears from day 2 to onwards as shown in Figure 5.47 from 1.5 up to 2.5 molecules per Ti (it is supposed to reach 3.4 at equilibrium). Here we noticed DMACl value starts from 1.5 that means simple microchannel accelerated the hydrolysis process. While DMF is correlatively decreasing from 6.4 up to 5.3 till occurrence of the gel. After 2 months, among both DMF, the hydrolysis mainly affects linked DMF evolving from 4.3 per Ti to 3 whereas free DMF remains almost constant and equal to 2 DMF per Ti indicating that this reaction mainly takes place in the vicinity of the inorganic part *i.e.* at the very surface of the nanoparticles.
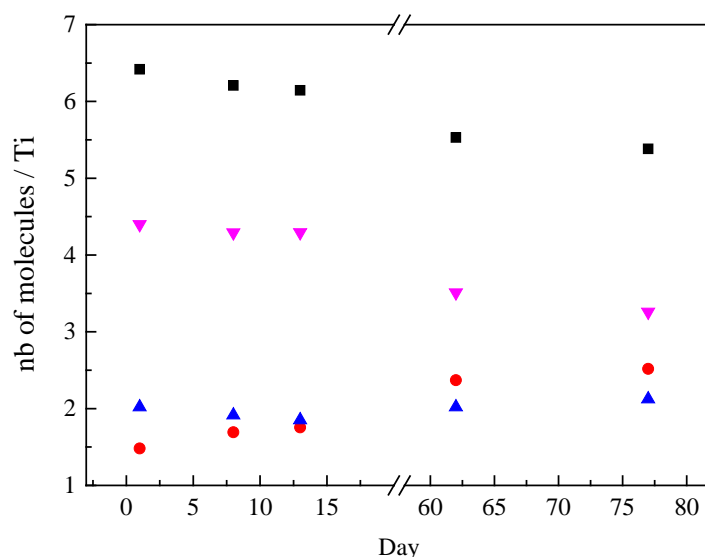
Figure 5.47: number of molecules / Ti as a function of time at 5 mL h^{-1} (TiOCl$_2$ + 16.7 % DMF) and DMF at 12 mL h^{-1}
DMF/Ti (■), DMA/Ti (●), Free DMF/Ti (▲), Linked DMF/Ti (▼)

5.2.2 Longer microchannel (with electric field)

5.2.2.1 Pre-mixed Solution

Initially, effect of filtration and electrodes were analysed on the sols. One sample was selected of flow rate and 2.4 mL h^{-1}. Both samples filtered and non-filtered with electrodes and without electrodes were analysed by Raman technique. It was revealed during analysis that there is not huge effect of filtration on the band areas (Figure 5.48 (a) and Figure 5.48 (b)) and hydrolysis rate Figure 5.49.
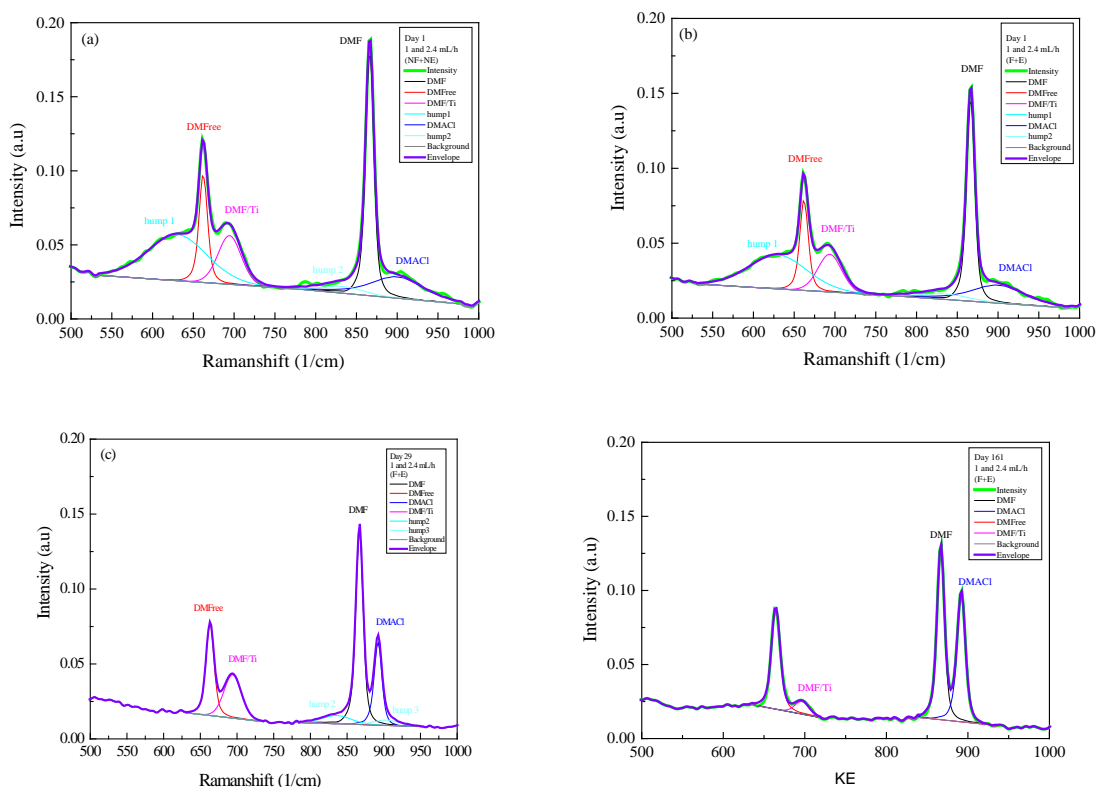
Figure 5.48: Raman spectra for 1 and 2.4 mL h^{-1} flow rate at (a) Day 1 (Non-filtered and without electrodes) (b) Day 1 (Filtered and with electrodes) (c) Day 29 (Filtered and with electrodes) (d) Day 161 (Filtered and with electrodes)

After that we analysed the effect of time on the sol. As already mentioned the Raman spectra of freshly TiDMF sols of flow rate (1 and 2.4 mL h^{-1}) on day 1 till 161 days old TiDMF are presented in Figure 5.48. One can see as time passes and DMF hydrolysis reaction takes place, the increase in DMACl area and decrease in DMF areas, as shown in Figure 5.48.

Results of DMF hydrolysis are presented in Figure 5.49. Figure 5.49 illustrates the number of molecules/Ti as a function of time. It is important to notice that the DMACl appears from day 2 to onwards as shown in Figure 5.49 from 2.8 up to 3.4 molecules per Ti while DMF is correlatively decreasing from 5.1 down to 4.45. DMACl reaches to its limit of 3.4 at day 161. Among both DMF, the hydrolysis mainly affects the DMF bounded to Titanium cation whereas free DMF remains almost constant indicating that again this reaction mainly takes place at the very surface of the nanoparticles.
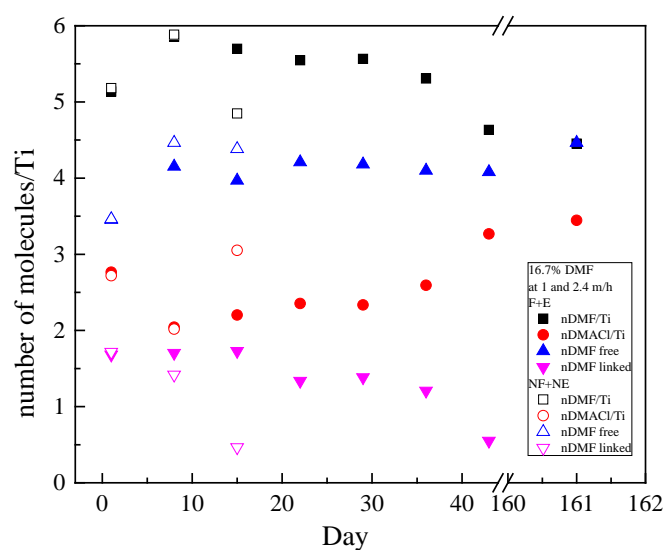
Figure 5.49: nb of molecules / Ti as a function of time at(1 and 2.4 mL h^{-1})
DMF/Ti(Filter with electrodes (■) and No filter and without electrodes (□)),
DMA/Ti(Filter with electrodes (●) and No filter and without electrodes (○) ,Free
DMF/Ti(Filter with electrodes (▲) and No filter and without electrodes (△)),Linked
DMF/Ti(Filter with electrodes (▼) and No filter and without electrodes (▽)),

To study the effect of short microchannel (without electrodes) and long microchannel (with and without electrodes). Sols of flow rate 5 and 12 mL h^{-1} were collected at the end of each microchannel for analysis. All three samples were analysed by Raman spectroscopy of same flow rate at Y shape channel, longer channel with electrodes and longer channel without electrodes. Raman spectra are presented in Figure 5.50. Results revealed that electrodes are not affecting the hydrolysis rate as both results are almost the same for DMACl on day 1 (~2.9), DMF on day 1 (~5.0). But, it was revealed that using longer microchannel accelerates the number of DMACl per Ti 2.9 versus 1.5 on day 1 in shorter channel.
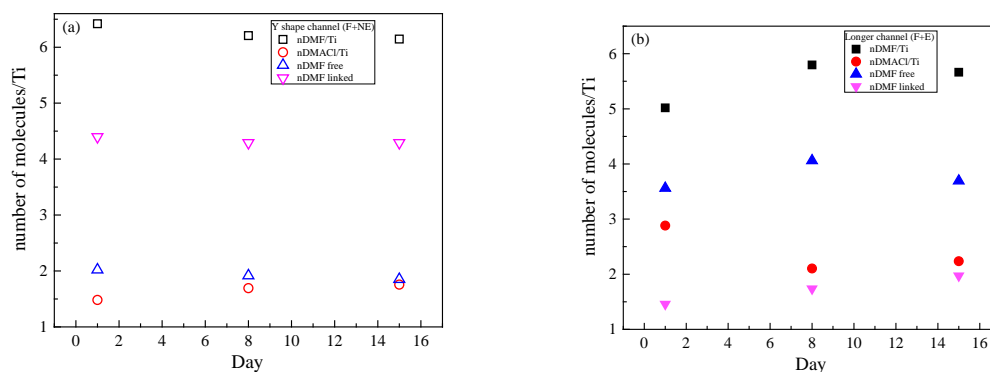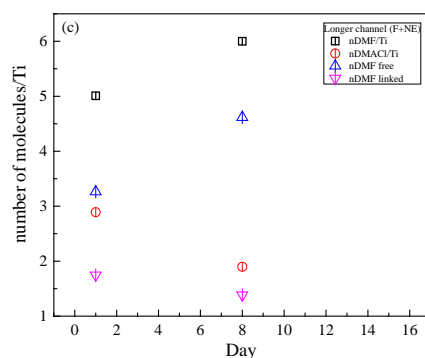
Figure 5.50. Effect of using Y shape microchannel and longer channel (with and without electrodes) on DMF hydrolysis for (5 and 12 mL h^{-1}) flow rates at Day 1 (a) for Y shape microchannel (b) Longer microchannel with electrodes (c) Longer microchannel without electrodes

Results of DMF hydrolysis are presented in Figure 5.42. Figure 5.42 illustrates the number of molecules/Ti as a function of time. One can see as time passes and hydrolysis takes place then DMF peak is reducing from 4.95 to 2.7 and DMACl peak keeps increasing from 1.2 upto 3.4, at day 168 as explained in section 5.2. Among both DMF, the hydrolysis mainly affects the DMF bounded to Titanium cation, evolving from 1.9 to 1.1 per Ti whereas free DMF remains almost constant indicating that this reaction mainly takes place at the very surface of the nanoparticles.
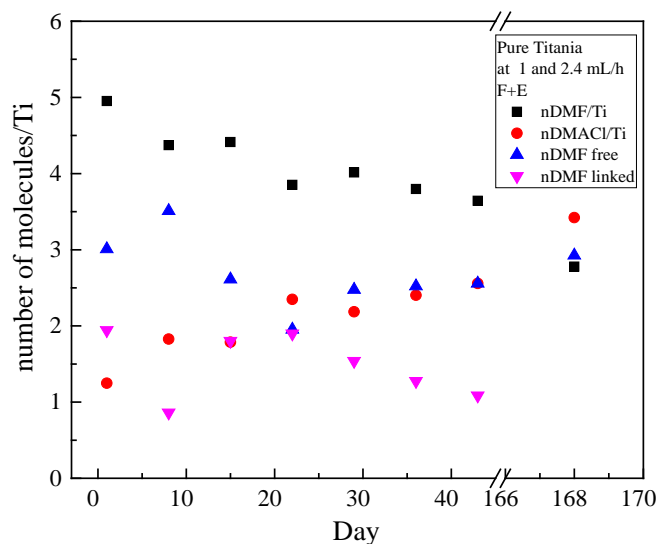
Figure 5.51: nb of molecules / Ti as a function of time at(1 and 2.4 mL h^{-1}) DMF/Ti (■), DMA/Ti (●), Free DMF/Ti (▲), Linked DMF/Ti (▼)

To study the effect of 16.7% DMF dilution and pure solution on the DMF hydrolysis, one common flow rate 1 and 2.4 mL h^{-1} was selected for comparison. Figure 5.52 shows the Raman spectra of pure and 16.7% DMF diluted solution at 1 and 2.4 mL h^{-1} flow rate.

DMF hydrolysis are presented in Figure 5.52. Results revealed that dilution increases the hydrolysis rate. DMACl is reaching to 3.4 DMF/Ti more quickly than for pure solution.
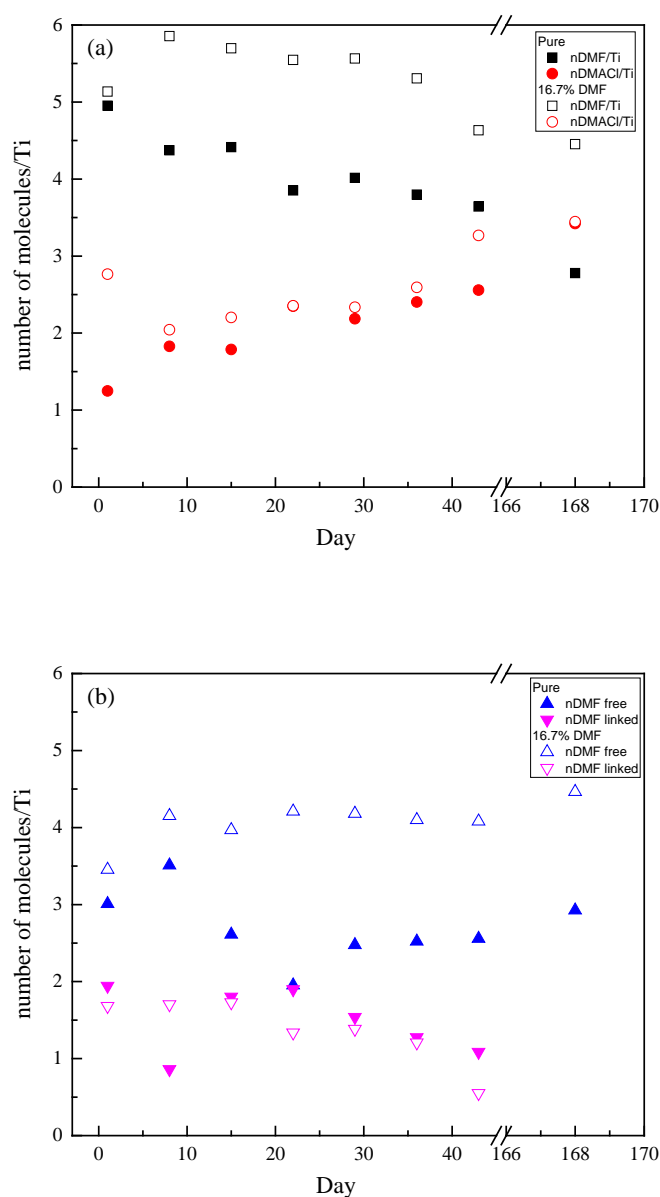
Figure 5.52: Fitted Raman spectra peaks for (1 and 2.4 mL h^{-1}) flow rate at Day 1 for Pure and diluted solution. (a) Representation of DMF/Ti and DMACl/Ti (b) Representation of DMFree/Ti and DMF linked
DMF/Ti(Pure(■) and diluted with 16.7% DMF (□)), DMA/Ti (Pure (●) and diluted with 16.7% DMF (○), Free DMF/Ti (Pure (▲) and diluted with 16.7% DMF (△)), Linked DMF/Ti (Pure (▼) and diluted with 16.7% DMF (▽)

5.3 Discussion:

The aim of this chapter was to investigate the size distribution of nanoparticles in microreactor and exploit the thermal conditions generated during mixing to accelerate the hydrolysis of DMF. Actually, the usual method involves the mixing of the reactants in the closed vessel at 0°C and controlling the advancement of the reaction by drying at 70°C for several 23 hours or for several months at room temperature. Even though both methods can be used for the production of Ti-based nanoparticles, they are strikingly different in many ways. For example, miroreactors are providing a better control of the thermal is one step. Whereas, in batch technique, two steps are required to control the synthesis. Another difference is the size of the nanoparticles. Table 5.2 shows the size of nanoparticles produced in microreactors (during stable period for size of nanoparticles) and batch process. It is interested to notice that even simple Y shape microchannel is producing smaller nanoparticles with narrow size distribution between 9 - 17 nm. While increasing the length of the channel seems to improve mixing and reaction, as it gives more narrow size distribution with small nanoparticles between 3 - 8 nm. Apart from that, application of electric field and pre-dilution of the $TiOCl_2$ solution not only improved the mixing but provides better size distribution and small nanoparticles between 6.5 - 11 nm. On the other hand in batch technique, particles with size of 15-30 nm and around 10 nm were achieved in various conditions [4,7] .

Table 5.2: Comparison of size/size distribution of nanoparticles produced in microreactor (our work) and batch technique ([4,7])

| Microreactor							
Reactants	Channel length (mm)	Electrodes	Size distribution of NPs (nm)	On flow rate (mL h⁻¹)	Overall Size of NPs (nm)	Stable period for size of NPs (days)	Overall flow rate range for TiOCl₂ (mL h⁻¹)
Pre-diluted(TiOCl₂)	32	No	5 - 40	5	9 -17	day 8 – day 22	4 – 7
	234		3 - 38	1	9 – 16	day 8 – day 29	1 - 5
			4 - 45	5			
		Yes	3 - 50	1	6.5 – 11	day 8 – day 36	0.5 - 5
Pure (TiOCl₂)		Yes	5 - 70	1	9 – 13	day 8 – day 43	
Batch Technique							
Reactants	Conditions			Overall Size of NPs (nm)		Ref:	
Pure (TiOCl₂)	70°C for 24 hours/ at room temperature for several months			15 – 30		Bechu PhD thesis [4]	
Pure (TiOCl₂)				~10		Cottineau et al.[7]	

Table 5.3: Comparison of hydrolysis advancement in microreactor and batch technique

				nDMF/Ti				nDMACl/Ti				nDMF free				nDMF linked			
Microreactor																			
Reactants	Channel length (mm)	Electrodes																	
Pre-diluted(TiOCl$_2$)	32		Day	1	13	62	77	1	13	62	77	1	13	62	77	1	13	62	77
			Results	6.4	6.1	5.5	5.4	1.5	1.7	2.4	2.5	2.0	1.85	2.0	2.1	4.4	4.3	3.5	3.3
	234	No	Day	1	8	-	-	1	8	-	-	1	8	-	-	1	8	-	-
			Results	5	6	-	-	2.9	1.9			3.3	4.6	-	-	1.7	1.4	-	-
		Yes	Day	1	29	43	161	1	29	43	161	1	29	43	161	1	29	43	161
			Results	5.1	5.5	4.6	4.4	2.8	2.3	3.2	3.4	3.4	4.1	4.0	4.5	1.7	1.3	0.5	-
Pure		Yes	Day	1	29	43	168	1	29	43	168	1	29	43	168	1	29	43	168
			Results	4.9	4.0	3.6	2.8	1.2	2.2	2.5	3.4	3.0	2.5	2.6	2.9	1.9	1.5	1.1	_

			nDMF/Ti		nDMACl/Ti		nDMF free		nDMF linked	
Batch Technique[4,7]										
Reactants		Conditions	Starting value	Ending value	Starting value	Ending value	Starting value	Ending value	Starting value	Ending value
Pure (TiOCl$_2$)		70°C for 24 hours/ at room temperature for several months	6.4	3	0	3.4	3.6	3.1	2.8	0.1

Two periods can be distinguished in the time evolution: before one month and after. Actually, for one month for all the conditions tested, it can be noted that the chemical composition does not significantly evolve. We can consider that during this period, the sol could be used to be processed by spin-coating, for instance to produce thin films in a reproducible manner. In Table 5.3 are gathered the characteristic features of the different sols from day 1 to onwards.Same than the mechanism already observed, the hydrolysis seems to affect first both kinds of DMF, linked and free whereas during the polycondensation of the framework, linked DMF are preferentially hydrolised. Part of them are also released in the solvent as we can infer from the slight increase in free DMF at longer time.

One can also see in the Table 5.3 that the number of molecules are not same at the start. Use of simple microchannel is advantageous to provide one step process and accelerates the hydrolysis process. Application of electric field (electrodes) allows an active mixing and a heat dissipation by Joule effect which still accelerates more the hydrolysis process, as it was already demonstrated in Cottineau i.e heating at 70°C accelerates the hydrolysis as compared to room temperature [7].

5.4 Conclusion

In 5th Chapter, size distribution of nanoparticles by using DLS technique and DMF hydrolysis advancement by using Raman spectroscopy were demonstrated. All the samples prepared, described in Chapter 3 (Samples prepared using Y shape microchannel) and Chapter 4 (samples prepared using longer microchannel with and without electrodes) are analysed here for DLS and Raman spectroscopy. The analysis of the nanoparticles size distribution using DLS has shown an effect of flow rates and of sample ageing for Y shape short channel and longer microchannel (with and without electrodes). DLS results shows that size of nanoparticles decreases with time (from day 1 till day 8) then remains in constant (depends on the flow rate, microchannel length and mixing process) and suddenly increases before transforming into gel. While increase in flow rate is causing increase in size of nanoparticles. Diluted solutions results the better size distribution.

Raman spectroscopy results revealed the acceleration of hydrolysis when simple Y shape microchannel is used. In batch technique, hydrolysis was done by drying at 70°C for several hours or several days at room temperature. Importance of electric field was also noticed in Raman spectroscopies results. The use of an AC electric field allows an active mixing and a heat dissipation by Joule effect. These combined phenomena accelerate the nanoparticle synthesis reaction which is continuously achieved in a short distance. Size distribution of nanoparticles with active mixing is much better without electrodes.

References:

[1]   "Neal Fairley. Copyright© 2005 Casa Software Ltd; 2005." .

[2]   T. Cottineau *et al.*, "Photosensitive Titanium Oxo-polymers: Synthesis and Structural Characterization," *Chem. Mater.*, vol. 20, no. 4, pp. 1421–1430, février 2008.

[3]   T. Cottineau, M. Richard-Plouet, J.-Y. Mevellec, and L. Brohan, "Hydrolysis and Complexation of N,N-Dimethylformamide in New Nanostructurated Titanium Oxide Hybrid Organic–Inorganic Sols and Gel," *J. Phys. Chem. C*, vol. 115, no. 25, pp. 12269–12274, juin 2011.

[4]   S. Bécho, "Etude et caractérisation de couches minces photosensibles organique-inorganique à base de titane pour la conversation de l'energie solaire," Institut des Matériaux Jean Rouxel, Nantes, Nantes, 2017.

[5]   A.-F. B. Hélène Terrisse, "Monodispersed titanium oxide nanoparticles in N,N-dimethylformamide: water solutions," *J. Sol-Gel Sci. Technol.*, vol. 67, no. 2, 2013.

[6]   P. Combelas, M. Costes, and C. Garrigou-Lagrange, "Protonation du N,N-diméthylformamide: étude par spectrométries vibrationnelle et électronique," *Can. J. Chem.*, vol. 53, no. 3, pp. 442–447, février 1975.

[7]   T. Cottineau, "Sols et gels photosensibles à base d'oxyde de titane pour applications photovoltaïques," Thèse de doctorat, École doctorale chimie biologie, Université de Nantes, France, 2007.

Chapter 6

Conclusion and perspectives

6.1 Conclusion

In the past recent years, one of the major use of Ti- based nanoparticles is for the solar energy conversion in photovoltaic cells. Higher efficiency of the conversion is provided by the high surface to volume ratio of these nanoparticles. The modus operandi of their production process is of great importance to obtain particles with nano metric sizes with a narrow distribution. Nowadays, their synthesis is often performed using sol – gel technique since it allows an easy and inexpensive production of thin films for photovoltaic applications. Among the different conditions of synthesis, sol-gel techniques afford low-cost alternative as compared to other processes involving deposition under vacuum or annealing. The control of the network polycondensation at moderate temperatures indeed leads to tunable nano-objects with enhanced properties due to the large surface to volume ratio. Here the sols are obtained by the hydrolysis of $TiOCl_2 \bullet 1.4\ HCl \bullet 7H_2O$ in the presence of N,N-dimethylformamide, (denoted $TiOCl_2$ and DMF, respectively).

In our work, nanoparticle production using microreactor was tested. It is an interesting alternative to the traditional batch technique for sol synthesis since such production process is continuous and the small size of the microchannels, typically with diameter less than 1 mm, provides a better temperature control of the reactive fluids. Moreover, an original way was used to observe the sol synthesis in microreactors: its thermal signature was followed by infrared thermography thanks to its high exothermic effect. It has revealed the presence of discontinuous and pulsating flows inside the microreactor, detrimental for the control of the nanoparticle production process. The dilution of the $TiOCl_2$ by mean of several solvents such as water, 1-propanol, 1,2-propanediol and 1-octanol did not improve the stability of the flows. Better results were obtained for 2-propanol with many flow rates for $TiOCl_2$ (1.5 to 12 mL h^{-1}), flow rate for DMF being 2.4 higher for stoichiometric purpose. Finally another solution was preferred avoiding additional complexity in the composition of the final product: The $TiOCl_2$ precursor was pre-diluted directly with the other reactive fluid; i.e. DMF. Effect of flow rates from 4 to 8 mLh^{-1} for pre-diluted $TiOCl_2$ with a 2.4 rate ratio for DMF flow rates was investigated. In addition, several DMF concentrations for the pre-dilution of the precursor were tested and finally a pre-dilution ratio with a 16.7% vol. amount of DMF was retained for further development in our work.

Microreactors implemented with a Peltier cell is asmart alternative to the use of calorimeters for the measurement of the sol synthesis enthalpy. This technique was developed improving the knowledge of the Ti based nanoparticles synthesis. As expected the enthalpy decreases while increasing the pre-dilution rate of $TiOCl_2$ with DMF. Indeed for pure $TiOCl_2$, the $\mathit{\Delta H}$ value was found equal to 10.08 kJ mol^{-1}, and for $TiOCl_2$ pre-diluted with 15% volume of DMF, $\mathit{\Delta H}$ value decreases to 7 kJ mol^{-1}.

One of the drawback of using microreactor is the lack of mixing provided by the laminar behavior of the flow inside the small microchannels. Therefore to avoid long microchannel and large pressure drop, it is of great interest to find a way to intensify mixing. To the best of our knowledge, there is no example of mixing intensification by electric field for Ti-based nanoparticles production. Using platinum electrodes, an electric field was implemented just after the fluid inlets inside the microreactorin order to destabilize the interface between the two reactive fluids. Such mixing process was found very efficient, this being possible thanks to the contrast between the dielectric constants of the $TiOCl_2$ precursor and DMF solvent. During our tests, the synthesis mainly occurs inside the gap between the two electrodes, no thermal effect was observed afterwards. Clearly this mixing process has enhanced the mixing and accelerated the nanoparticle synthesis reaction which is fully

realized within a very short distance. However appropriate conditions for the electric field have to be chosen in order to avoid parasitic effects.

With the application of a DC electric fieldwith voltage from 1.5 to 4 V, the flow inside the reactor was found quite stable but at the same time,a bleu coloration was noticed due to water splitting and formation of Ti^{3+}. These unwanted phenomena were also observed for AC voltage with frequencies of 0.1 and 0.5 MHz. They could be avoided by increasing the frequency up to 1 MHz and with a 7V AC voltage. With the latter conditions, tests were conducted with pure $TiOCl_2$ showing successful mixing and Ti-based nanoparticles synthesis. Beside electric conditions, a large range of flow rate was scanned for both reactive fluids. It was found that using our microreactor with a 1 x 1mm^2 cross section and pre-diluted or pure $TiOCl_2$, the precursor flow rate should not exceed 2 mL h^{-1} since due to excessive velocity the synthesis   is not achieved while the reactive fluids is crossing the gap between the two electrodes.

The use of an electric field has induced a supplementary thermal effect (Joule effect) which in term of heat flux value was found to be superior to the one provided by the exothermal effect of the synthesis. However, in our case, only a small temperature increase was observed (about 3 to 4°C) probably due to the heat diffusion in platinum electrodes which acts as a thermal fin therefore moderating the temperature increase.

The analysis of the $TiOCl_2$ nanoparticles size distribution using diffusion light scattering has shown an effect of flow rates and of sample ageing. Indeed the size of nanoparticles was increasing with increase of inlet flow rates. In addition the size of nanoparticles was found decreasing with time then suddenly increasing before transforming into gel.

Size of nanoparticles were recorded between 5 nm-45 nm for 5 and 12 mL h^{-1} inlet flow rates for respectively the precursor and the solvent in microreactor without active mixing. Using an AC electric field (7V AC, 1MHz)a small increase of the nanoparticles size was detected 5 nm-50 nm for prediluted $TiOCl_2$ with 16.7% vol. DMF and 5 to 70 nm for pure $TiOCl_2$, this being obtained with smaller inlet flow rate values (respectively 1 and 2 mL h^{-1}).

Finally, Raman spectroscopy results have shown that simple Y shape microchannel has accelerated the hydrolysis rate while in batch technique hydrolysis was achieved by drying at 70°C for several hours or several days at room temperature. One more interesting advantage was noticed:the active mixing using an electric field has not only improved the mixing but also accelerated the hydrolysis rate.

6.2 Perspectives

There are few further developments that can be done on the basis of the knowledge gained during this thesis.

- Computational fluid dynamics (CFD) can be used to simulate flow behavior inside our microreactor. In fact, some work has been already performed showing that the viscosity contrast between precursor and solvent was not responsible for the pulsations and lack of stability of the flows. But more work has to be done including also the energy equation in order to take into account thermal effects.

- Platinum electrodes can be replaced by thin film TiN electrodes. In that case, no fin effect would occur involving much higher temperature increase between electrodes and acceleration of the synthesis may occur.

-Another interesting way to improve the mixing in microreactors is by acoustic waves.First step is to design a horseshoe shape inside the microchannel. When fluid will pass over horseshoe then an air bubble will be caught in the horseshoe because of streams of the fluids. Excitation of the bubble at various frequencies through piezoelectric transducer or manually can provide a quick and homogenous mixing [1,2,3]. This acoustic bubble mixer is sometimes claimed as the best mixer [4]. This type of mixing also termed as best for high viscosity fluids (21.2-95.9 mPa s) with high flow rates [2,4].

References:

[1]   S. Wang, X. Huang, and C. Yang, "Mixing enhancement for high viscous fluids in a microfluidic chamber," *Lab. Chip*, vol. 11, no. 12, pp. 2081–2087, Jun. 2011.

[2]   K. Ward and Z. H. Fan, "Mixing in microfluidic devices and enhancement methods," *J. Micromechanics Microengineering Struct. Devices Syst.*, vol. 25, no. 9, Sep. 2015.

[3]   R. H. Liu, J. Yang, M. Z. Pindera, M. Athavale, and P. Grodzinski, "Bubble-induced acoustic micromixing," *Lab. Chip*, vol. 2, no. 3, pp. 151–157, 2002.

[4]   A. Ozcelik *et al.*, "An acoustofluidic micromixer via bubble inception and cavitation from microchannel sidewalls," *Anal. Chem.*, vol. 86, no. 10, pp. 5083–5088, May 2014.

ANNEX

1. Titanium history, importance, research on titanium

Titanium was discovered in 1791 by English chemist William Gregar (1761-1817). Four years later it was rediscovered by German chemist Martin Heinrich Klaproth (1743-1817). Klaproth suggested this name Titanium after the "Titans" which means the sons of the Earth goddess according to Greek mythology [1]. Titanium is 9th abundant element on the earth and very handy and useful material for energy storage/conversion. TiO_2 has unique merits such as very high refractive index (anatase n =2.48-2.56; brookite n=2.58-2.70; rutile n=2.6-2.89)[2], non-toxicity, easy handling, low cost, biocompatibility, very resistive against chemical and photochemical erosion, very easy to synthesize specially by sol-gel technique [17,18,19], due to these several advantages there is lots of research going on this topic as show in Fig 1[6]. Annual production of TiO_2 is 4.5 million tones throughout the world by using two different industrial processes Sulphate routes and Chloride routes [7]. It is being used in many application such batteries.
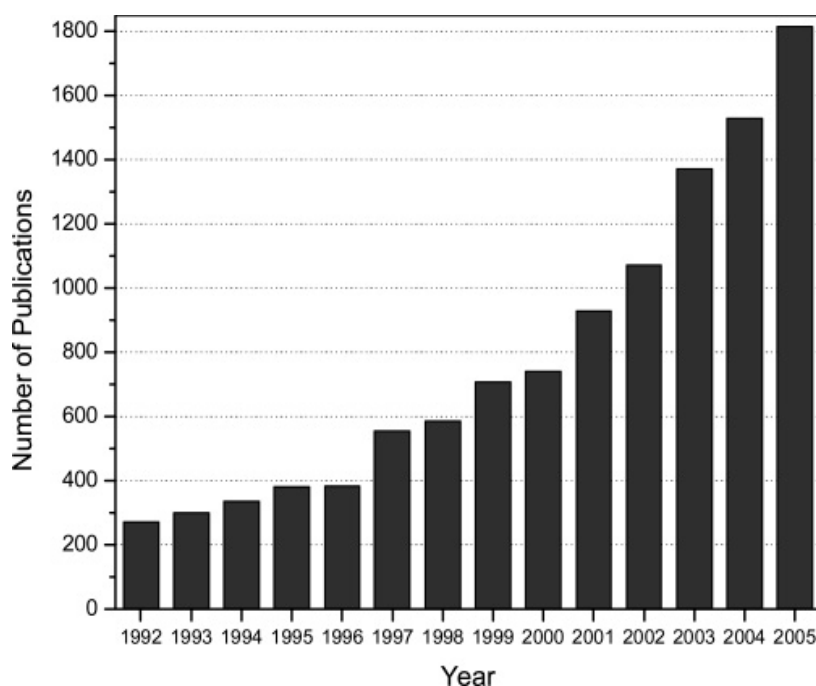

Fig 1: Annual number of publication on TiO_2[6]

2. Material for microreactors

Most often microreactors are designed according to the desired mixing and chemical reaction. Most commonly used materials for fabrication of microreactors are PMMA (Polymethyl methacrylate) [8], PDMS (Polydimethylsiloxane)[9], silicon [10], glass, ceramics, PTFE. Glass reactors are most chemically inert material but it's very difficult to handle [11]. Ceramic reactors are stable at high temperature and have good resistance against chemicals but their fabrication is very time consuming [12]. Silicon reactors are resistant to higher temperature and pressure but it's not compatible with bases[13]. PMMA is compatible with acid but it's vulnerable to other reagents. Polymers are the most cheapest material but

3. Various pumps for injections systems

The reactor is usually composed of injection system, tubing and mixer. Injection system can be mechanical or non mechanical pumps. In mechanical pumps piston movement is used to control the flow rates. Common mechanical pumps are syringe pump, peristaltic pump, high performance liquid chromatography (HPLC) pump as show in Figure 2.
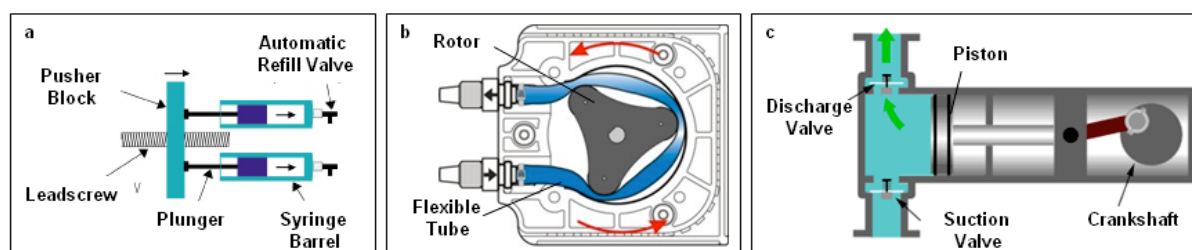
Figure 2: Various types of mechanical pumps (a) Syringe pump (b) Peristaltic pump (c) HPLC pump[14].

Syringe pumps are infusion pumps which store liquid in syringes and deliver the liquid by pushing the plunger in forward direction by means of motor. In peristaltic pump rotor compresses the flexible tube to deliver the liquid. In HPLC pumps, small pistons are used to displace the volume of the liquid into the tubing. Mixing in microreactor can be passive and active. Passive mixing is achieved only by molecular diffusion which active mixing required external source to mix the fluids like electric, pneumatic, mechanical vibration etc.

4. Selection of best microchannel from research

Ammar [4] has studied four passive mixing geometries in his thesis (a) right angle intersection, (b) ''Y'' intersection, (c) "T'' intersection, and (d) arrowhead intersection. He has shown in his results that the best mixing occurs between two miscible liquids in T type michrochannel and arrowhead microchannel at Reynolds number between 0.8 – 2 [15]. While Valery *et al*. suggested Y type microchannel for best mixing between two identical liquids at Reynolds number between 10 – 0.01[16].
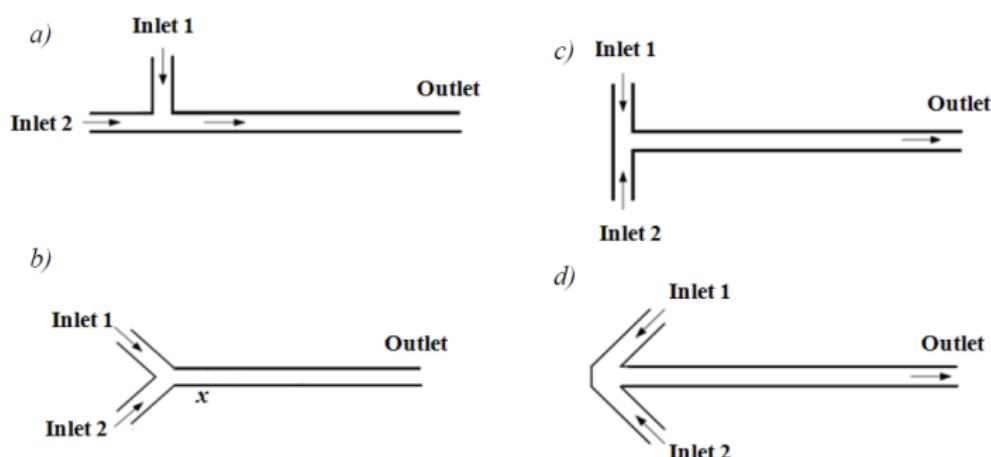
Table 1: Various Size measurement techniques and their size range.

Technique	Sample type	Size
Dynamic Light Scattering (DLS)	Emulsion or suspension (diluted)	1-1000 nm
X-Ray diffraction (XRD)	Powder	1 - 100 nm
Nanoparticle tracking analysis (NTA)	Emulsion or suspension	30 - 1000 nm
Acoustic attenuation spectrometry (AAS)	Emulsion or suspension	10 - 1000 µm
Transmission electron microscope (TEM)	Powder	0.05 nm - larger
Scanning electron microscope (SEM)	Powder	1 nm - larger

5. N-Dimethylformamide Safety data sheet and information

DASITGROUP | **CARLO ERBA** REAGENTS

Safety data sheet
according to 1907/2006/EC, Article 31

SECTION 1: Identification of the substance/mixture and of the company/undertaking

· *1.1 Product identifier*
· *Molecular formula:* $C_3 H_7 N O$
· *Structure formula:* $H C O - N - (C H_3)_2$
· *Trade name:* <u>*N,N-Dimethylformamide*</u>
· *MSDS number:* CH0019
· *CAS Number:*
68-12-2

· *EC number:*
200-679-5
· *Index number:*
616-001-00-X
· *Registration number* 01-2119475605-32
· *1.2 Relevant identified uses of the substance or mixture and uses advised against*
No further relevant information available.
· *Sector of Use*
SU3 Industrial uses: Uses of substances as such or in preparations at industrial sites
SU10 Formulation [mixing] of preparations and/or re-packaging (excluding alloys)
SU9 Manufacture of fine chemicals
SU24 Scientific research and development
· *Product category*
PC0 Other
PC19 Intermediate
PC20 Products such as ph-regulators, flocculants, precipitants, neutralisation agents
PC21 Laboratory chemicals
PC29 Pharmaceuticals
PC39 Cosmetics, personal care products
PC40 Extraction agents
· *Process category*
PROC5 Mixing or blending in batch processes for formulation of preparations and articles (multistage and/ or significant contact)
PROC8a Transfer of substance or preparation (charging/discharging) from/to vessels/large containers at non-dedicated facilities
PROC8b Transfer of substance or preparation (charging/discharging) from/to vessels/large containers at dedicated facilities
PROC1 Use in closed process, no likelihood of exposure
PROC2 Use in closed, continuous process with occasional controlled exposure
PROC3 Use in closed batch process (synthesis or formulation)
PROC4 Use in batch and other process (synthesis) where opportunity for exposure arises
PROC9 Transfer of substance or preparation into small containers (dedicated filling line, including weighing)
PROC15 Use as laboratory reagent
· *Environmental release category*
ERC2 Formulation of preparations
ERC6a Industrial use resulting in manufacture of another substance (use of intermediates)
ERC4 Industrial use of processing aids in processes and products, not becoming part of articles
ERC1 Manufacture of substances
· *Application of the substance / the mixture* Chemical products for laboratory

· *1.3 Details of the supplier of the safety data sheet*
· *Manufacturer/Supplier:*

GB

165

(Contd. of page 1)

CARLO ERBA REAGENTS
Chaussée du Vexin
Parc d'Affaires des Portes - BP616
27106 VAL DE REUIL Cedex
Téléphone: +02 32 09 20 00
Télécopie: +02 32 09 20 20
· **Further information obtainable from:**
Q.A / Normative
email:MSDS_CER-SDS@cer.dgroup.it
· **1.4 Emergency telephone number:**
France (ORFILA 24h/24) - Tel : +33 (0)1 45 42 59 59
Ireland - Tel : 00 353 1 8092568 - 00 353 1 8379964 (24h/24)
EU Tel : 112

SECTION 2: Hazards identification

· **2.1 Classification of the substance or mixture**
· **Classification according to Regulation (EC) No 1272/2008**

 GHS02 flame

Flam. Liq. 3   H226   Flammable liquid and vapour.

 GHS08 health hazard

Repr. 1B   H360D May damage the unborn child.

 GHS07

Acute Tox. 4   H312   Harmful in contact with skin.
Acute Tox. 4   H332   Harmful if inhaled.
Eye Irrit. 2   H319   Causes serious eye irritation.

· **Classification according to Directive 67/548/EEC or Directive 1999/45/EC**

 T; Toxic
Repr. Cat. 2
R61:   May cause harm to the unborn child.

 Xn; Harmful

R20/21:   Harmful by inhalation and in contact with skin.

 Xi; Irritant

R36:   Irritating to eyes.
· **Information concerning particular hazards for human and environment:**
The product has to be labelled due to the calculation procedure of the "General Classification guideline for
Substances of the EU", DIR. 67/548/EC, in the latest valid version, and of the "General Classification
guideline for Preparations of the EU", DIR. 99/45/EC, in the latest valid version.

Trade name: N,N-Dimethylformamide

(Contd. of page 2)

· **Classification system:**
The product has to be labelled due to the calculation procedure of the "General Classification guideline for Substances of the EU", DIR. 67/548/EC, in the latest valid version.

· **2.2 Label elements**
· **Labelling according to Regulation (EC) No 1272/2008**
The substance is classified and labelled according to the CLP regulation.
· **Hazard pictograms**

GHS02   GHS07   GHS08

· **Signal word** Danger
· **Hazard statements**
H226   Flammable liquid and vapour.
H312+H332 Harmful in contact with skin or if inhaled.
H319   Causes serious eye irritation.
H360D   May damage the unborn child.
· **Precautionary statements**
P210   Keep away from heat/sparks/open flames/hot surfaces. - No smoking.
P241   Use explosion-proof electrical/ventilating/lighting/equipment.
P264   Wash thoroughly after handling.
P303+P361+P353 IF ON SKIN (or hair): Remove/Take off immediately all contaminated clothing. Rinse skin with water/shower.
P304+P340   IF INHALED: Remove victim to fresh air and keep at rest in a position comfortable for breathing.
P305+P351+P338 IF IN EYES: Rinse cautiously with water for several minutes. Remove contact lenses, if present and easy to do. Continue rinsing.
P403+P235   Store in a well-ventilated place. Keep cool.
· **Additional information:**
Restricted to professional users.
· **2.3 Other hazards -**
· **Results of PBT and vPvB assessment**
· **PBT:** Not applicable.
· **vPvB:** Not applicable.

SECTION 9: Physical and chemical properties

· **9.1 Information on basic physical and chemical properties**
   Molecular weight   73.1 g
· **Appearance:**
   Form: Fluid
   Colour: Colourless
· **Odour:**   Amine-like
· **Odour threshold:**   Not determined.

· **pH-value (200 g/l) at 20 °C:**   7

· **Change in condition**
   Melting point/Melting range: -61 °C
   Boiling point/Boiling range: 152.5-153.5 °C
· **Flash point:**   58 °C
· **Flammability (solid, gaseous):**   Not applicable.

CARLO ERBA REAGENTS

DASIT GROUP

Safety data sheet
according to 1907/2006/EC, Article 31

Printing date 22.01.2015   Version number 2   Revision: 22.01.2015

Trade name: N,N-Dimethylformamide

· Ignition temperature:	440 °C
· Decomposition temperature:	Not determined.
· Self-igniting:	Not determined.
· Danger of explosion:	Not determined.
· Explosion limits:	
Lower:	2.2 Vol %
Upper:	16 Vol %
· Vapour pressure at 20 °C:	3.5 hPa
· Density at 20 °C:	0.95 g/cm³
· Relative density	Not determined.
· Vapour density	Not determined.
· Evaporation rate	Not determined.
· Solubility in / Miscibility with	
water:	Fully miscible.
· organic solvents:	Soluble in many organic solvents.

· **Partition coefficient (n-octanol/water):** Not determined.
· **Viscosity:**
   Dynamic at 20 °C: 0.802 mPas
   Kinematic: Not determined.
· **9.2 Other information**   No further relevant information available.

SECTION 10: Stability and reactivity

· **10.1 Reactivity** See 10.3
· **10.2 Chemical stability**
· **Thermal decomposition / conditions to be avoided:** No decomposition if used according to specifications.
· **10.3 Possibility of hazardous reactions** Reacts with strong alkali.
· **10.4 Conditions to avoid** No further relevant information available.
· **10.5 Incompatible materials:** No further relevant information available.
· **10.6 Hazardous decomposition products:**
Carbon monoxide, Carbon dioxide.
Nitrogen oxides (NOx)

6. TiOCl$_2$ Safety data sheet and information

CRISTAL Global كريستل العالمية

Titanium Oxychloride

PRODUCT DATA SHEET

Description: Titanium Oxychloride (indicative chemical formula TiOCl$_2$,xHCl,yH$_2$O) is a clear yellow liquid, which is sometimes also called "aqueous solution of titanium tetrachloride".

Key Features:
- Equivalent TiCl$_4$ content: ≥ 50 % to ≥ 60 %
- Specific gravity : ≥ 1490 to ≥ 1580 kg/m^3
- CAS N°. 13780-39-7
- EINECS N°. 237-430-5

Applications: Titanium Oxychloride is used in the manufacture of:
- Pearlescent pigments
- Ceramics, electronics
- Titanium dioxides

Typical Properties:
- TiO$_2$ equivalent :   ≥ 333 to ≥ 400 g/l
- pH :   ≤ 1

Caution
- Dangerous material
- Strongly acidic liquid
- Refer to the Safety Data Sheet

Safety and Regulatory information: For Safety, Storage, Handling, Labeling and Transportation guidelines as well as for Chemical Inventory status, Regulatory status and Classification refer to the Safety Data Sheet.

CRISTAL ◇ كريستل
Global العالمية

Material Safety Data Sheet

1. PRODUCT AND COMPANY IDENTIFICATION

Product Name   Titanium Oxychloride

UN-No   UN3264

Synonyms   Aqueous solution of Titanium Tetrachloride (TiCl4)

Recommended use   Manufacturing of titanium dioxides, pearlescent pigments, catalysers.

Other Information   e-mail contact: cldemille@cristalglobal.com

Manufactured by   Millennium Inorganic Chemicals
                               20 Wight Avenue, Suite 100
                               Hunt Valley, MD 21030

Company Switchboard Number 1 (410) 229-4400

Emergency Telephone Number Chemtrec 1-800-424-9300

2. HAZARDS IDENTIFICATION

Emergency Overview

Yellow viscous, acid liquid having a penetrating odor. Highly irritating or corrosive to eyes, respiratory tract and skin. Non-flammable.

Appearance Yellow	**Physical State** Viscous liquid	**Odor** Irritating

OSHA Regulatory Status   This product is considered hazardous under the criteria of the U.S. Federal OSHA Hazard Communication Standard (29 CFR 1910.1200).

Potential Health Effects

Acute Toxicity

    Skin   Liquid and vapors are corrosive to skin, resulting in irritation and burns. Frequent contact with aqueous solutions of hydrochloric acid may lead to dermatitis.

    Inhalation   Corrosive to respiratory system. Pre-existing respiratory problems may become aggravated upon exposure.

    Ingestion   Corrosion of mucous membranes, esophagus, stomach may occur. Symptoms may include nausea, vomiting, intense thirst, and diarrhea.

Chronic Effects   Repeated exposure to titanium oxychloride or its hydrolysis products incidental to proper industrial handling is not expected to cause any significant adverse health effects, however, excessive exposure can cause lung damage. This product is not considered a potential carcinogen by NTP, OSHA, ACGIH, IARC, or California Proposition 65.

9. PHYSICAL AND CHEMICAL PROPERTIES

Appearance	Yellow	Odor	Irritating
Physical State	Viscous liquid	pH	< 1 (Product as is)
Flash Point	Not applicable	Autoignition Temperature	No information available
Boiling Point/Boiling Range	59 °C @ 50%	Melting Point/Range	> 35 °C (Decomposition temperature)
Freezing Point	-45 °C (Crystallization)		
		Flammability Limits in Air	Not applicable
Explosion Limits	No information available		
Specific Gravity	1.46 g/cm³	Water Solubility	Miscible with water
Solubility	Insoluble product or at best very slightly soluble in hexane, cyclohexane, heptane, trichloroethylene, carbon tetrachloride.	Evaporation Rate	1.8 ml/100 ml/24 hrs: 2.16 ml/in2 (Butyl Acetate = 1)
Vapor Pressure	147 mm Hg @ 25°C	Vapor Density	1.15 (air=1)
VOC Content(%)	~ 75%		

References:

[1]   "21 - Titanium, Zirconium and Hafnium," in *Chemistry of the Elements (Second Edition)*, Oxford: Butterworth-Heinemann, 1997, pp. 954–975.

[2]   G. V. Samsonov, *The Oxide handbook*, 2d ed. New York: IFI/Plenum, 1982.

[3]   R. Doong and H. Shih, "Array-based titanium dioxide biosensors for ratiometric determination of glucose, glutamate and urea," *Biosens. Bioelectron.*, vol. 25, no. 6, pp. 1439–1446, Feb. 2010.

[4]   P. Pookmanee and S. Phanichphant, "Titanium dioxide powder prepared by a sol-gel method," *J. Ceram. Process. Res.*, vol. 10, no. 2, Apr. 2009.

[5]   D. Zhang, G. Li, H. Wang, K. M. Chan, and J. C. Yu, "Biocompatible Anatase Single-Crystal Photocatalysts with Tunable Percentage of Reactive Facets," *Cryst. Growth Des.*, vol. 10, no. 3, pp. 1130–1137, Mar. 2010.

[6]   T. L. Thompson and J. T. Yates, "Surface science studies of the photoactivation of TiO2--new photochemical processes," *Chem. Rev.*, vol. 106, no. 10, pp. 4428–4453, Oct. 2006.

[7]   G. S. McNulty, "Production of titanium dioxide," 2008.

[8]   Z. Wu, N.-T. Nguyen, and X. Huang, "Nonlinear diffusive mixing in microchannels: theory and experiments," *J. Micromechanics Microengineering*, vol. 14, no. 4, p. 604, 2004.

[9]   A. Houssein, G. Bertrand, A. OULD EL MOCTAR, and P. HASSAN, "Heat-transfer analysis and improved mixing in multifunctional microreactor using sapphire window and infrared thermography (PDF Download Available)," *ResearchGate*.

[10]   A. E. Kamholz, B. H. Weigl, B. A. Finlayson, and P. Yager, "Quantitative Analysis of Molecular Interaction in a Microfluidic Channel: The T-Sensor," *Anal. Chem.*, vol. 71, no. 23, pp. 5340–5347, décembre 1999.

[11]   Y. Kikutani, A. Hibara, K. Uchiyama, H. Hisamoto, M. Tokeshi, and T. Kitamori, "Pile-up glass microreactor," *Lab Chip*, vol. 2, no. 4, pp. 193–196, Nov. 2002.

[12]   R. Knitter, D. Göhring, P. Risthaus, and J. Haußelt, "Microfabrication of ceramic microreactors," *Microsyst. Technol.*, vol. 7, no. 3, pp. 85–90, Oct. 2001.

[13]   E. R. Murphy, T. Inoue, H. R. Sahoo, N. Zaborenko, and K. F. Jensen, "Solder-based chip-to-tube and chip-to-chip packaging for microfluidic devices," *Lab Chip*, vol. 7, no. 10, pp. 1309–1314, Sep. 2007.

[14]   P. Laurino, "Photochemical transformations in continuous flow devices," 2011.

[15]   H. Ammar, A. Ould el Moctar, B. Garnier, and H. Peerhossaini, "Flow Pulsation and Geometry Effects on Mixing of Two Miscible Fluids in Microchannels," *J. Fluids Eng.*, vol. 136, no. 12, pp. 121101-121101–9, Sep. 2014.

[16]   V. Rudyak and A. Minakov, "Modeling and Optimization of Y-Type Micromixers," *Micromachines*, vol. 5, no. 4, pp. 886–912, Oct. 2014.

UNIVERSITE BRETAGNE LOIRE

UNIVERSITÉ DE NANTES

Thèse de Doctorat

Sikandar Ali CHANNA

Synthèse en microréacteur de nanoparticules à base de titane

Synthesis of Ti-based nanoparticles in continuous flow microreactors

Résumé

Des nanoparticules à basede titane dispersées dans des sols ou des gels avec une distribution de taille étroite permettent l'exacerbation des propriétés photochimiques de films photosensibles. Utilisés comme absorbeurs solaires dans les photobatteries, ils permettraient la conversion et le stockage de l'énergie solairesous forme électrochimique. Dans ce travail, ces matériaux nanostructurés ont été produits par l'hydrolyse de $TiOCl_2, 1.4HCl, 7H_2O$ dans du N, N-diméthylformamide (DMF),à l'intérieur d'un microréacteur afin d'assurer un meilleur contrôle en température et de confiner les fluides. En fonction du temps de vieillissement ou par étuvage, cette hydrolyse conduit à l'obtention de sols et de gels constitués de nanoparticules dispersées dans le solvant. La signature thermique de l'hydrolyse du $TiOCl_2$en microréacteur observée par caméra infrarouge montre des instabilités de l'écoulement préjudiciables au contrôle de la taille des nanoparticules. Ceproblème a été finalement résolu par la pré-dilution de $TiOCl_2$ avec du DMF. Par ailleurs, l'usage d'un procédé actif de mélange(champ électrique) a permis d'accélérer la réaction d'hydrolysedu $TiOCl_2$pré-dilué ou pur pour certaines valeurs des conditions opératoires par ex. 7 VAC, 1MHz et ceci sans constater d'effets parasites (électrolyse de l'eau et formation d'ions Ti^{3+}). Finalement,les nanoparticules produites ont été analysées en utilisant la technique de diffusion dynamique de la lumière. Une taille moyenne de nanoparticules s'étendant de 5 à 50 nma été obtenueavec du $TiOCl_2$ pré-dilué, celle-ci dépendant de la vitesse d'écoulement, de l'âge des échantillons etde laprésence ou non de champ électrique.

Mots clés
Nanoparticules à base de titane, microréacteur, caméra infrarouge, intensification de mélange, diffusion dynamique de la lumière, diffusion Raman

Abstract

Ti-based nanoparticles dispersed in solutions or gels with narrow size distribution may constitute innovative materials as absorbers in new devices such as photobatteries, allowing conversion and electrochemical storage of solar energy. In our work, these nanostructured materials were produced inside a microreactor by hydrolysis of $TiOCl_2$ stabilized in aqueous HCl solution reacting with N,N-dimethylformamide (DMF). The use of a microreactor aims at providing a better temperature control and also a confinement of the reactive fluids. The thermal signature of the hydrolysis of $TiOCl_2$ recorded by an infrared camera shows flow instabilities detrimental to the control of nanoparticle sizes. This problem was solved by the pre-dilution of $TiOCl_2$ with DMF in the following proportion 0.52 DMF/Ti (16.7% vol. DMF).Otherwise, the use of an active mixing process based on an electric field implemented inside the microreactor has clearly shown the acceleration of the hydrolysis of $TiOCl_2$without generating parasitic effects(water splitting,formation of Ti^{3+}ions), if operating conditions are adequately chosen (for ex. 7 V AC and 1 MHz). Finally, using Dynamic Light Scattering, an average size of nanoparticles ranging from 5 to 50 nm for pre-diluted $TiOCl_2$ with 16.7% vol. DMFwas obtained depending on flow rates, ageing of samples and implementation or not of an AC electric field.

Key Words
Ti-based nanoparticles, microreactor, infrared camera, mixing intensification, dynamic light scattering, Raman scattering

L'Université Bretagne Loire